



Cortical Morphology and MRI Signal Intensity Analysis in Paediatric Epilepsy

Sophie Adler

Supervisor: Prof. T. Baldeweg
Prof. J.H. Cross
Dr. D.W. Carmichael

Developmental Neurosciences
Great Ormond Street Institute of Child Health
University College London

This dissertation is submitted for the degree of
Doctor of Philosophy

December 2017

“The problem of neurology is to understand man himself.”

Wilder Penfield

Declaration

I, Sophie Adler, confirm that the work presented in this thesis is my own. Where information has been derived from other sources, I confirm that this has been indicated in the thesis.

The work presented in this thesis reflects the contributions of a team of researchers including colleagues from the Developmental Neurosciences Programme, Great Ormond Street Institute of Child Health as well as close collaborators from the Brain Mapping Unit, University of Cambridge and the NeuroImaging of Epilepsy Laboratory, Montreal Neurological Institute. My individual contribution for the scientific studies included in this thesis is outlined below.

The work presented in chapter's 2 and 3 were part of a collaboration between Great Ormond Street Institute of Child Health and the Brain Mapping Unit, University of Cambridge. The development of features, such as "Local Cortical Deformation" and the "Doughnut Method", as well as machine learning algorithms for the detection of focal cortical dysplasia were completed in complete collaboration with Konrad Wagstyl, PhD Student, University of Cambridge. I was responsible for transfer, conversion and processing of the imaging data from the GOSH clinical PACs system. I have created scripts for batch processing of data, statistical analysis and machine learning. I performed all statistical analyses and produced all the figures and graphical presentation of the data shown in these chapters. All results and interpretations were presented by myself and were developed based on discussions with colleagues and at regular supervision meetings.

The work presented in chapter 4 was completed whilst on a fellowship at the Montreal Neurological Institute. The data was collected by Neda Bernasconi, Principal Investigator, and initial pre-processing of the struc-

tural and functional MRI data was performed by Benoit Caldairou, Post Doctoral Researcher. I performed all data analyses, statistical analyses and produced all the figures and graphical presentation of the data shown in this chapter. All results and interpretations were presented by myself and were developed based on discussions with colleagues and at regular supervision meetings.

The structural MRI scans of the paediatric controls used in chapters 2, 3 and 5 were collected by Gemma Northam as part of her PhD. Mallory Blackman, MSc student assisted with the manual editing of cortical reconstructions of the paediatric TLE data used in chapter 5.

Sophie Adler
December 2017

Acknowledgements

Research is always a team endeavour and this thesis would not have been possible without many people. First and foremost, I would like to thank Torsten Baldeweg, for his endless ideas, enthusiasm and constant support. He challenged me to become a better scientist and provided a perfect role model of how to guide and motivate a team of researchers. Secondly, Helen Cross, for investing time and effort into my professional development. I can only aspire to become such an inspirational doctor. Thirdly, David Carmichael, who provided additional direction, stimulating discussion and constructive feedback. It has been a privilege to be part of the Developmental Neurosciences Programme at the UCL GOSH Institute of Child Health. As well as meeting great colleagues and friends, I have been exposed to presentations of cutting edge paediatric research from around the world. I am also very grateful to Neda and Andrea Bernasconi and Boris Bernhardt, my adopted supervisors in Montreal. They introduced me to state-of-the-art structural MRI techniques in the world of adult epilepsy and welcomed me into their team.

I also wish to acknowledge all of my collaborators: in particular, Roxana Gunny, from GOSH, who taught me the mysteries of how to spot subtle brain malformations on MRI; all those working in the NeuroImaging of Epilepsy Laboratory, particularly Benoit Caldairou who preprocessed the data for chapter 4 and Seok-Jun Hong, whose work inspired mine and who is always happy to help solve my endless coding problems; Paul Fletcher and Lisa Ronan, my undergraduate supervisors from University of Cambridge, who are inspiring scientists and I am fortunate to still collaborate with.

I am also grateful to the Rosetrees Trust for generously funding my PhD and for the UCL Charlotte and Yule Bogue Research Fellowships,

Acknowledgements

which enabled me to spend a year at the Montreal Neurological Institute.

Finally, I am fortunate to have wonderful friends and family to support me. In particular, I am deeply grateful to my parents, Rachel and Steve, and siblings, Lena and Jack, for their love and for always encouraging me in my medical and scientific studies. And to Konrad, my partner in life and research, without you none of this would have been possible.

Abstract

Epilepsy encompasses a great variety of aetiologies, and as such is not a single disease but a group of diseases characterised by unprovoked seizures. The primary aim of the work presented in this thesis was to use multi-modal structural imaging to improve understanding of epilepsy related brain pathology, both the epileptogenic lesions themselves and extra-lesional pathology, in order to improve pre-surgical planning in medication-resistant epilepsy and improve understanding of the underlying pathogenic mechanisms.

The work focuses on 2 epilepsy aetiologies: focal cortical dysplasia (FCD) (chapters 2 and 3) and mesial temporal lobe epilepsy (chapters 4 & 5). Chapter 2 of this thesis develops surface-based, structural MRI post-processing techniques that can be applied to clinical T1 and FLAIR images to complement current MRI-based diagnosis of focal cortical dysplasias. Chapter 3 uses the features developed in Chapter 2 within a machine learning framework to automatically detect FCDs, obtaining 73% sensitivity using a neural network. Chapter 4 develops an in vivo method to explore neocortical gliosis in adults with TLE, while Chapter 5 applies this method to a paediatric cohort. Finally, the concluding chapter discusses contributions, main limitations and outlines options for future research.

Table of contents

Declaration	4
Acknowledgements	5
Abstract	7
List of figures	13
List of tables	15
List of Abbreviations	16
Publications associated with this thesis	18
Conference posters and talks related to this thesis	19
Awards	21
1 An introduction to the analysis of paediatric epilepsies with structural magnetic resonance imaging	23
1.1 Paediatric Epilepsies: clinical overview	23
1.1.1 Definition & Prevalence	23
1.1.2 Epileptic Seizures	23
1.1.3 Treatment	26
1.1.4 Aetiologies	27
1.1.5 Clinical Neuroimaging	39
1.2 Whole-brain Structural MRI Analysis	40
1.2.1 Voxel-based techniques	40
1.2.2 Surface-based techniques	43
1.3 Structural and Functional Cortical Networks	46
1.3.1 Resting-state functional connectivity	46
1.3.2 Cortical thickness covariance	49
1.4 Machine Learning	49

1.4.1	Neural Networks	51
1.5	Thesis Objectives	51
2	Quantification of surface-based lesion characteristics in focal cortical dysplasias	53
2.1	Introduction	53
2.2	Materials & Methods	56
2.2.1	Participants	56
2.2.2	MR Imaging	57
2.2.3	Cortical Reconstruction	57
2.2.4	Lesion Masks	58
2.2.5	Measures of Morphological / Intensity Features	58
2.2.6	"Doughnut" Method	59
2.2.7	Local Cortical Deformation	60
2.2.8	Normalisation of Features	60
2.2.9	Registration to Template Space	61
2.2.10	Statistical Analysis	62
2.3	Results	63
2.3.1	Demographics	63
2.3.2	Individual Assessment of Quantitative Surface-based Features	67
2.3.3	Group-level Lesion Characteristics	71
2.4	Discussion	74
3	Automated detection of focal cortical dysplasias in paediatric epilepsy	80
3.1	Introduction	80
3.2	Materials & Methods	82
3.2.1	Participants & MR Imaging	82
3.2.2	Cortical Reconstructions & Lesion Masks	82
3.2.3	Established Surface-based Measures	82
3.2.4	Novel Surface-based Measures	83
3.2.5	Normalisation of Features	83
3.2.6	Interhemispheric Asymmetry	83
3.2.7	Statistical Analysis	84
3.3	Results	88
3.3.1	Demographics	88
3.3.2	Assessment of Novel Surface-based Feature Maps	88
3.3.3	Establishing the Parameters for the Classifier	89

3.3.4	Classification Including Novel Features vs. Classification Using Established Features	90
3.3.5	Local Cortical Deformation vs Local Gyrfication Index	92
3.4	Discussion	92
3.5	Conclusions	96
4	FLAIR Hyperintensity in Adults with Temporal Lobe Epilepsy	98
4.1	Introduction	98
4.2	Materials & Methods	99
4.2.1	Participants	99
4.2.2	Imaging	101
4.2.3	Image Processing	102
4.2.4	Statistical Analysis	103
4.3	Results	106
4.3.1	Relationship between T2R and FLAIR signal intensity	106
4.3.2	Whole-brain mapping of FLAIR signal intensity in TLE	106
4.3.3	Relation to whole-brain topography of cortical thickness	108
4.3.4	Relation to hippocampal covariance networks	110
4.3.5	Relation to clinical variables	112
4.4	Discussion	112
5	Multimodal surface-based imaging in paediatric temporal lobe epilepsy	116
5.1	Introduction	116
5.2	Materials & Methods	117
5.2.1	Participants	117
5.2.2	Neurodevelopment/Cognition	118
5.2.3	MR Imaging	118
5.2.4	Hippocampal Segmentation	118
5.2.5	Cortical Reconstruction	119
5.2.6	Neocortical Morphological/Intensity Features	120
5.2.7	Statistical Analysis	120
5.3	Results	122
5.3.1	Demographics	122
5.3.2	Hippocampal Changes	124

5.3.3	Topography of Neocortical Changes	125
5.3.4	Relation to Clinical Variables	128
5.4	Discussion	128
6	Overall Discussion	132
6.1	Introduction	132
6.2	Lesional pathology	133
6.2.1	Main Findings	133
6.3	Extra-lesional pathology	135
6.3.1	Main Findings	135
6.4	Neurobiological and Clinical Implications	136
6.4.1	Paediatric FCD	136
6.4.2	TLE in adults	137
6.4.3	Paediatric TLE	138
6.5	Limitations	139
6.5.1	Clinically acquired paediatric data	139
6.5.2	Histopathology	139
6.5.3	Technical limitations	140
6.5.4	Accounting for cortical morphometry	140
6.6	Future perspectives	140
6.6.1	FCD	141
6.6.2	TLE	143
	References	145
	Supplementary Material A Towards In Vivo Focal Cortical Dysplasia Phenotyping Using Quantitative MRI	175
A.1	Abstract	175
A.2	Histopathology of focal cortical dysplasia	179
A.3	Genetics of the focal cortical dysplasias	182
A.4	Radiological identifiers of focal cortical dysplasias	183
A.5	Computational Anatomy	185
A.6	Quantitative MRI (qMRI)	185
A.7	Quantitative MRI in focal cortical dysplasia detection	191
A.8	Combinations of qMRI and morphometry measures in FCD	192
A.9	Conclusions and future directions	193
	Supplementary Material B Morphology-corrected metabolic pattern learning: Application to drug-resistant epilepsy	195
B.1	Abstract	195

B.2	Introduction	196
B.3	Materials & Methods	197
B.3.1	Surface-registration of PET	197
B.3.2	Surface-based preprocessing	197
B.3.3	Group-level statistical inference	198
B.3.4	Individualised assessment based on supervised learning	198
B.4	Experiments and Results	199
B.4.1	Subjects	199
B.4.2	PET acquisition	199
B.4.3	MRI acquisition	200
B.4.4	PET-MRI processing	200
B.5	Results	201
B.5.1	Group-level results	201
B.5.2	Individualised assessments.	201
B.6	Discussion and Conclusion	202

List of figures

1.1	Histopathology of FCDs	29
1.2	Radiological features of FCDs	31
1.3	Histopathology of HS	37
1.4	Radiological features of HS	38
1.5	Metabolic divergence of FLE and TLE	41
1.6	Voxel-based morphology	41
1.7	Surface-based techniques	45
1.8	Structural and functional cortical networks	48
1.9	Structure of Neural Networks	52
2.1	"Doughnut" Method	60
2.2	Local Cortical Deformation	61
2.3	Surface Feature Maps	68
2.4	Individual Feature Profiles	69
2.5	"Doughnut" Features	72
2.6	Group Feature Profiles	73
3.1	Overview of classifier	86
3.2	Receiver operator characteristics and AUC for classifiers	90
3.3	Examples of top cluster output in 5 patients with FCD	91
3.4	Local Cortical Deformation vs Local Gyrfication Index	92
4.1	Relationship between hippocampal T2R and FLAIR signal intensity	106
4.2	Hippocampal FLAIR signal intensity	107
4.3	Topography of neocortical FLAIR increases and cortical atrophy in TLE relative to controls	108
4.4	Regions of FLAIR hyperintensity in TLE	109
4.5	Bootstrap reproducibility	110
4.6	Relationship between FLAIR signal and hippocampal networks.	111

4.7 FLAIR covariance using AAL regions as seeds	112
4.8 Relationship between neocortical FLAIR signal intensity and febrile convulsions.	113
5.1 Hippocampal atrophy and FLAIR signal intensity	119
5.2 Hippocampal Asymmetries	125
5.3 Whole-brain analysis	127
5.4 FLAIR hyperintensity in paediatric HS	128
A.1 Relationship between histological features, biophysical prop- erties, MR images and quantitative neuroimaging.	178
A.2 Computational and quantitative MRI features used by Hong et al.,	193
B.1 Surface sampling of FDG-PET with MRI-informed mor- phology correction	198
B.2 Metabolic divergence of epilepsy syndromes	201
B.3 Individual Classification	202

List of tables

1.1	ILAE 2017 Classification of Seizures	25
1.2	Paediatric Epilepsy Surgery Aetiologies	28
1.3	Characteristics of FCD lesion subtypes.	34
2.1	Paediatric FCD: Demographic & Clinical Information	65
2.2	Individual lesion characteristics	66
2.3	Group lesion characteristics	73
3.1	Automated detection of paediatric FCDs	89
4.1	Adult TLE Demographic & Clinical Information	101
4.2	Effect sizes in clusters of findings	109
5.1	Paediatric TLE patient demographics	123
5.2	Paediatric control demographics	124

List of Abbreviations

AED	Anti-epileptic drug
AUC	Area under the curve
CSF	Cerebrospinal fluid
DTI	Diffusion Tensor Imaging
EEG	Electroencephalography
EZ	Epileptogenic zone
FCD	Focal cortical dysplasia
FLAIR	Fluid Attenuated Inversion Recovery
FLE	Frontal lobe epilepsy
fMRI	Functional magnetic resonance imaging
GM	Grey matter
HS	Hippocampal sclerosis
ILAE	International League Against Epilepsy
LCD	Local cortical deformation
LGI	Local gyrification index
MRI	Magnetic resonance imaging
NN	Neural network
PET	Positron emission tomography
ROC	Receiver operating characteristics

List of Abbreviations

T1w	T1-weighted
TLE	Temporal lobe epilepsy
VBM	Voxel-based morphology
WM	White matter

Publications associated with this thesis

Adler, S*, Wagstyl, K*, Gunny, R., Ronan, L., Carmichael, D., Cross, J. H., Fletcher, P. C., Baldeweg, T. (2016). Novel surface features for automated detection of focal cortical dysplasias in paediatric epilepsy. *NeuroImage: Clinical*, 18:27. <http://doi.org/10.1016/j.nicl.2016.12.030>

Adler, S*, Lorio, S*, Jacques, T. C., Benova, B., Gunny, R., Cross, J. H., Baldeweg, T., Carmichael, D. W. (2017). Towards In Vivo Focal Cortical Dysplasia Phenotyping Using Quantitative MRI. *NeuroImage: Clinical*, <http://doi.org/10.1016/j.nicl.2017.04.017>

Adler, S., Liu, M., Gill, R., Fadaie, F., Hong, S.J., Caldairou, B., Baldeweg, T., Cross, J. H., Bernasconi, A., Bernhardt, B. C*, Bernasconi, N*. Topographic principles of cortical FLAIR signal in temporal lobe epilepsy (*under review*)

Adler, S., Hong, S.J., Caldairou, B., Soucy, J. P., Baldeweg, T., Bernasconi, A., Bernasconi, N., Bernhardt, B. C. Morphology-corrected metabolic pattern learning: Application to drug-resistant epilepsy (*in prep*)

Northam, G., **Adler, S.**, Eschmann, K., Chong, W, K., Cowan, F, M., Baldeweg, T. Persistent repetition impairment after neonatal injury to the dorsal language stream: a developmental variant of conduction aphasia?(*in prep*)

Conference posters and talks related to this thesis

Talks / Lectures

“Structural imaging of lesional and extra-lesional pathology in epilepsy”, Feindel Brain Imaging Lecture, Montreal Neurological Institute, Canada, 2017

“Cortical FLAIR signal in TLE”, Epilepsy Day, Montreal Neurological Institute, Canada, 2017

Cortical Development Lecture, MSc/PG Diploma in Paediatric Neuropsychology, Module 5 - Infant and neurodevelopmental assessment, Great Ormond Street Institute of Child Health, 2017

“FLAIR hyperintensity in Paediatric TLE: Topographic principles & clinical / cognitive correlates”, Young Epilepsy Annual Conference, UK, 2017

“In vivo mapping of gliosis in temporal lobe epilepsy using FLAIR intensity analysis”, Organisation for Human Brain Mapping, Geneva, Switzerland, 2016

“Increased gliosis within hippocampal network in TLE”, Young Epilepsy Annual Conference, UK, 2016

Cortical Development Lecture, MSc / Postgraduate Diploma in Clinical and Applied Paediatric Neuropsychology, Great Ormond Street Institute of Child Health, 2016

“Automated FCD detection in paediatric epilepsy”, Brain Mapping Unit, University of Cambridge, UK, 2016

"Doughnut Method: Identifying FCDs", Young Epilepsy Annual Conference, UK, 2015

Cortical Development Lecture, MSc / Postgraduate Diploma in Clinical and Applied Paediatric Neuropsychology, Great Ormond Street Institute of Child Health, 2015

Poster Presentations

"FLAIR Hyperintensity in Paediatric TLE: Topographic principles, clinical and cognitive correlates", Organisation for Human Brain Mapping, Vancouver, Canada, 2017

"Automated FCD detection in paediatric epilepsy", Organisation for Human Brain Mapping, Vancouver, Canada, 2017

"In-vivo mapping of gliosis in temporal lobe epilepsy using FLAIR intensity analysis", Great Ormond Street Institute of Child Health Poster Competition, London, 2016

"Metabolic Divergence of focal epilepsy syndromes", American Epilepsy Society, Houston, Texas, USA, 2016

"Whole-brain mapping of gliosis in temporal lobe epilepsy using FLAIR", American Epilepsy Society, Houston, Texas, USA, 2016

"Metabolic Divergence of focal epilepsy syndromes", Canadian League Against Epilepsy, Quebec City, Canada, 2016

"In-vivo mapping of gliosis in temporal lobe epilepsy using FLAIR intensity analysis", Organisation for Human Brain Mapping, Geneva, Switzerland, 2016

"Doughnut method: Automated lesion detection in paediatric epilepsy using relative cortical structure", Organisation for Human Brain Mapping, Hawaii, USA, 2015

"Doughnut method: Automated lesion detection in paediatric epilepsy using relative cortical structure", Great Ormond Street Institute of Child Health Poster Competition, London, 2015

Awards

Rosetrees Trust Scholarship, 2014-2017

Young Investigator Award provided by the American Epilepsy Society (AES), Houston, Texas, USA, 2016, \$1200 USD

Commendation, Developmental Neurosciences category Great Ormond Street Institute of Child Health Poster Competition, London, 2016

Charlotte and Yule Bogue Fellowship Award to spend 6 months at the Montreal Neurological Institute, 2016, £4,169

Merit Abstract Award provided by the Organization of Human Brain Mapping, , Geneva, Switzerland, 2016, \$2000 USD

Charlotte and Yule Bogue Fellowship Award to spend 4 months at the Montreal Neurological Institute, 2015, £4,000

2nd Prize, Developmental Neurosciences category, Great Ormond Street Institute of Child Health Poster Competition, London, 2015

Conference Travel Awards

Guarantors of Brain, 2017, £1000

UCL GOS ICH Travel Award, 2017, £350

Astor Foundation Travel Bursary, 2016, £500

Chapter 1

An introduction to the analysis of paediatric epilepsies with structural magnetic resonance imaging

1.1 Paediatric Epilepsies: clinical overview

1.1.1 Definition & Prevalence

Over 65 million people worldwide are estimated to suffer from epilepsy (Ngugi et al., 2010), making it one of the most common chronic neurological diseases affecting around 1% of the general population. Similarly, the prevalence in the paediatric population is also around 1% (Russ et al., 2012). The International League Against Epilepsy (ILAE) consider epilepsy to be a disease of the brain defined by either two unprovoked seizures over 24 hours apart; one unprovoked seizure and an over 60% chance of further seizures in the next 10 years; or an epilepsy syndrome diagnosis (Fisher et al., 2014).

1.1.2 Epileptic Seizures

An epileptic seizure is defined as “a transient occurrence of signs and/or symptoms due to abnormal, excessive or synchronous neuronal activity in the brain” (Fisher et al., 2014). Seizure incidence across the lifespan peaks during infancy and childhood (Rakhade and Jensen, 2009). These seizures can be generalized, i.e. involving bilaterally distributed networks,

1.1 Paediatric Epilepsies: clinical overview

or focal, i.e. contained within one hemisphere and either localized to a discrete area of the brain or involving a more disparate network (Berg et al., 2010), or the onset zone may be unknown. Seizures can either occur with or without impaired awareness. During a seizure with retained awareness, the patient is aware of self and environment, even if they are unable to respond. Whereas, during a seizure with impaired awareness, a child is unable to respond to external stimuli and has abnormal responsiveness and awareness during the episode and its recall (Bancaud et al., 1981).

The recent ILAE seizure classification (Fisher et al. (2017), Table 1.1) subcategorises focal, generalised and unknown onset seizures into motor-onset or nonmotor-onset, where seizures are categorised by the first evident sign or symptom. If a seizure does not fall into another category or there is insufficient information, it is unclassified. Seizure type is extremely heterogeneous (Table:1.1), and furthermore, many paediatric epilepsy patients will have multiple seizure types, such as tonic-clonic seizures which are characterized by rigidity and uncontrolled jerking, myoclonic seizures where are there brief shock-like jerks of muscles or absence seizures which involve staring spells where there is a brief loss and then return of consciousness.

Table 1.1 ILAE 2017 Classification of Seizures

Focal Onset	Generalized Onset	Unknown Onset						
<table border="1"> <tr> <td data-bbox="531 1883 608 1989">Aware</td> <td data-bbox="531 1733 608 1883">Impaired Awareness</td> </tr> </table>	Aware	Impaired Awareness	<table border="1"> <tr> <td data-bbox="531 1559 608 1664">Motor</td> <td data-bbox="531 1379 956 1559">Nonmotor (absence)</td> </tr> </table>	Motor	Nonmotor (absence)	<table border="1"> <tr> <td data-bbox="531 1189 608 1339">Motor</td> <td data-bbox="531 1055 715 1189">Nonmotor</td> </tr> </table>	Motor	Nonmotor
Aware	Impaired Awareness							
Motor	Nonmotor (absence)							
Motor	Nonmotor							
<table border="1"> <tr> <td data-bbox="619 1794 695 1989">Motor Onset</td> <td data-bbox="619 1711 1037 1794">Nonmotor Onset</td> </tr> </table>	Motor Onset	Nonmotor Onset	<ul style="list-style-type: none"> tonic-clonic clonic tonic myoclonic myoclonic-tonic-clonic myoclonic-atonic atonic epileptic spasms 	<ul style="list-style-type: none"> tonic-clonic epileptic spasms behavior arrest 				
Motor Onset	Nonmotor Onset							
<ul style="list-style-type: none"> automatisms atonic² clonic epileptic spasms² hyperkinetic myoclonic tonic 	<ul style="list-style-type: none"> typical atypical myoclonic eyelid myoclonia 	<p>Unclassified³</p>						
<p>focal to bilateral tonic-clonic</p>								

Adapted from Fisher et al. (2017)

1.1.3 Treatment

Anti-epileptic drugs (AEDs) are the mainstay treatment for children with epilepsy. They are a heterogeneous group of medications including membrane stabilisers, GABA mimetics, drugs reducing neurotransmitter release, as well as calcium channel blockers and NMDA receptor channel blockers (Howard et al., 2011). The precise relationship between the mechanisms of action of these drugs and the anti-seizure clinical effects are not fully understood. Yet, most patient's seizures are effectively managed with careful drug treatment.

However, studies have found that up to 1/3 of patients continue to have regular seizures despite treatment with anti-epileptic medication (Kwan and Brodie, 2001; Kwan et al., 2011). Drug resistant epilepsy is defined as when two adequately chosen and tolerated anti-epileptic medications fail to achieve seizure freedom (Kwan et al., 2010). For many paediatric patients, growing up with poorly controlled epilepsy is associated with developmental arrest, cognitive impairment, behavioural comorbidities and poor academic achievement (Berg et al., 2008; Cormack et al., 2007; Hermann et al., 2006a; Huttenlocher and Hapke, 1990; MacAllister and Schaffer, 2007; Nickels et al., 2012; Parkinson, 2002). Structural brain abnormalities are a significant cause of drug-resistant epilepsy (Cormack et al., 2005; Hermann et al., 2010) and early intervention is crucial as these problems progress and can be augmented by longer duration of epilepsy (Hermann et al., 2006b), on-going seizures (Vingerhoets, 2006) and anti-epileptic drugs (AEDs) (Bjørnaes et al., 2001; Ijff and Aldenkamp, 2013).

Non-pharmacological approaches are required in these drug-resistant children. Surgery to remove the epileptic region is an option in focal onset epilepsy, as it is a possible epilepsy cure or can reduce seizure frequency and the need for AEDs. Importantly, improvements in cognition, behaviour and quality of life have been reported following epilepsy surgery (Ryvlin et al., 2014; Skirrow et al., 2011, 2015). However, surgical outcomes are better when the structural abnormality can be visualised on MRI (Télez-Zenteno et al., 2010), as this allows accurate planning of the location and extent of the surgery by the neurosurgeon and multidisciplinary team. Identification of structural abnormalities is not always achieved as lesions can be subtle and missed on visual inspection by radiologists. Further

methods for structural assessment of MRI scans are thus required to help characterise pre-surgical structural changes.

1.1.4 Aetiologies

Genetic, structural or metabolic causes can underlie epilepsy or the aetiology can be currently unknown (Berg et al., 2010). According to the 2004 ILAE survey, which included 413 children, the four most prevalent aetiologies in paediatric epilepsy surgery patients are cortical dysplasia (42.4%), tumour (19.1%), atrophy or stroke (not including Rasmussen’s syndrome) (9.9%) and hippocampal sclerosis (6.5%) (Harvey et al., 2008) (see Table 1.2).

During my PhD, I have focused on investigating alterations in cortical morphometry and intracortical tissue composition in children with focal cortical dysplasia (FCD), the most common cause of medication-resistant epilepsy in children, and another structural cause of paediatric epilepsy, hippocampal sclerosis.

FCD

Focal Cortical Dysplasias (FCDs) are malformations of cortical development that are highly epileptogenic. In fact, the dysplastic cortex has been shown to have intrinsic epileptogenicity (Palmini et al., 1995). In the ILAE survey mentioned previously, lobar or focal cortical dysplasias accounted for 59% of cortical dysplasias (Harvey et al., 2008) and are the leading aetiology in children undergoing resective surgery for drug-resistant epilepsy. The lesions can be located anywhere in the neocortex and are extremely variable in size. Seizures can begin at any age and the semiology is highly dependent on the location.

Histopathology of FCD

Focal cortical dysplasia (FCD) encompasses a broad spectrum of histopathological abnormalities. The first detailed descriptions of FCDs were provided by Taylor and colleagues in 1971 (Taylor et al., 1971). Several classification schemes have since been proposed to categorize the spectrum of histopathological changes observed in FCD. The scheme by Palmini and colleagues (Palmini et al., 2004) distinguishes lesions with cortical

1.1 Paediatric Epilepsies: clinical overview

Table 1.2 Paediatric Epilepsy Surgery Aetiologies

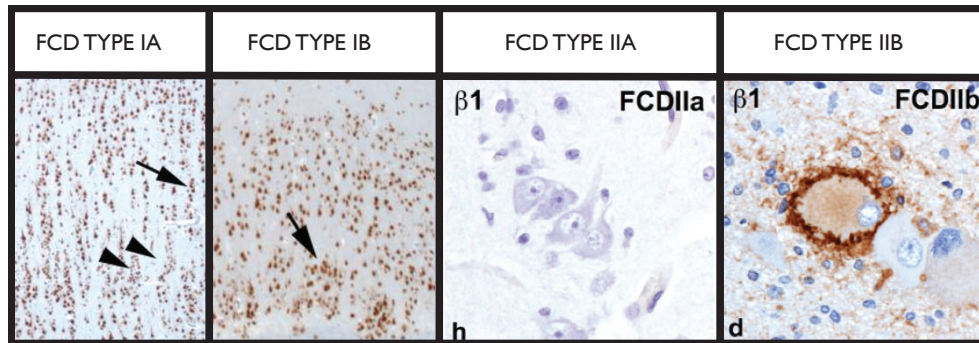
Aetiology in descending order of frequency for paediatric epilepsy surgery patients (n=413)

1. Cortical dysplasia ^a	42.4% (<i>n</i> = 175)
(a) Hemimegalencephaly	10% (<i>n</i> = 17)
(b) Hemispheric CD	12% (<i>n</i> = 21)
(c) Multilobar CD	19% (<i>n</i> = 34)
(d) Lobar / focal	59% (<i>n</i> = 103)
2. Tumour	19.1% (<i>n</i> = 79)
(a) DNET	29% (<i>n</i> = 23)
(b) Ganglioma	28% (<i>n</i> = 22)
(c) Other tumour	43% (<i>n</i> = 34)
3. Atrophy / stroke (not Rasmussen)	9.9% (<i>n</i> = 41)
(a) Stroke	44% (<i>n</i> = 18)
(b) Unspecific atrophy	49% (<i>n</i> = 20)
(c) Trauma	7% (<i>n</i> = 3)
4. Hippocampal sclerosis ^b	6.5% (<i>n</i> = 27)
5. Gliosis / normal pathology	6.3% (<i>n</i> = 26)
6. Tuberous sclerosis complex	5.1% (<i>n</i> = 21)
7. Hypothalamic hamartoma	3.6% (<i>n</i> = 15)
8. Sturge-Weber	2.9% (<i>n</i> = 12)
9. Rasmussen syndrome	2.7% (<i>n</i> = 11)
10. Vascular (not Sturge-Weber)	1.5% (<i>n</i> = 6)

Aetiology frequency in paediatric epilepsy surgery patients from the 2004 ILAE survey. Adapted from (Harvey et al., 2008).

architectural changes only (cortical dyslamination, clustering of neurons, and heterotopic neurons in the white matter) (Palmini Ia), from lesions with giant or immature neurons (Palmini Ib). More severe lesions with dysmorphic neurons are classified as Palmini IIa, while lesions with balloon cells correspond to Palmini IIb. The newer classification scheme, provided by the international league against epilepsy (ILAE) (Blümcke et al., 2010) is a three-tiered classification system. According to the ILAE, FCD type I has abnormal radial and/or tangential lamination, FCD type II is associated with aberrant cytology and FCD type III occurs alongside another lesion, e.g. hippocampal sclerosis (see Figure 1.1).

Fig. 1.1 Histopathology of FCDs



Adapted from (Blümcke et al., 2010). FCD Type Ia - radial dyslamination, abundant microcolumns composed of more than 8 neurons are visible. FCD Type Ib - tangential dyslamination, no cortical layers visible. FCD Type IIa - dysmorphic neurons present. FCD Type IIb - balloon cells within cortical mantle.

FCD ILAE Type I

FCD type I are isolated lesions in the neocortex that are characterised by either radial (type IA) or tangential (type IB) cortical dyslamination or a mixture of both (type IC).

FCD ILAE Type Ia

In FCD type IA the radial cortical dyslamination arises due to an increased frequency of microcolumns and increased numbers of neurons within these microcolumns. A “microcolumn” occurs when at least 8 neurons are aligned in a vertical orientation within the cortex. During cortical development, radial units form that consist of cells that originate from several progenitor stem cells, share the same birthplace, migrate along the same pathway and reside in the cortex within the same ontogenetic column (Rakic, 1988). Microcolumns resemble these ontogenetic columns. The micro-columnar organization in FCD type IA is most prominent within layer 3. Furthermore, the grey-white matter boundary is usually less easily defined due to increased numbers of heterotopic neurons. There may also be cellular abnormalities such as immature small diameter neurones, hypertrophic pyramidal neurones positioned outside layer 5 or normal neurones with disoriented dendrites (Blümcke et al., 2010). These malformations of cortical development arise due to aberrant radial migration and maturation of neurones.

FCD ILAE Type Ib

In FCD type IB the normal 6-layered composition of the cortex is disrupted. There may be no identifiable layers in the neocortex or disruptions may be restricted to abnormal layering of layer 2, layer 4, or both. These lesions are also normally characterised by a less well-demarcated grey-white matter boundary and cellular abnormalities similar to type IA (Blümcke et al., 2010).

FCD ILAE Type II

Focal cortical dysplasia type II is characterised by disrupted cortical lamination and specific cytologic abnormalities, where FCD Type IIa has dysmorphic neurons without balloon cells whereas FCD Type IIb has both dysmorphic neurons and balloon cells (Blümcke et al., 2010).

FCD ILAE Type IIa

FCD type IIa features cortical dyslamination and dysmorphic neurons. These neurons with enlarged diameters and enlarged nuclei can be distributed in any layer within the cortical mantle or in the underlying white matter. There is usually blurring of the grey-white matter junction and increased heterotopic neurons in white matter.

FCD ILAE Type IIb

The balloon cells that are characteristic of FCD type IIB have large bodies, eosinophilic cytoplasm, which lacks Nissl substance, and often have multiple nuclei. These cells can be located in any layer of the cortex or in the underlying white matter. FCD type IIB always demonstrate cortical dyslamination and blurring of the grey-white matter boundary. Often these lesions have reduced myelin in the subcortical white matter (Blümcke et al., 2010).

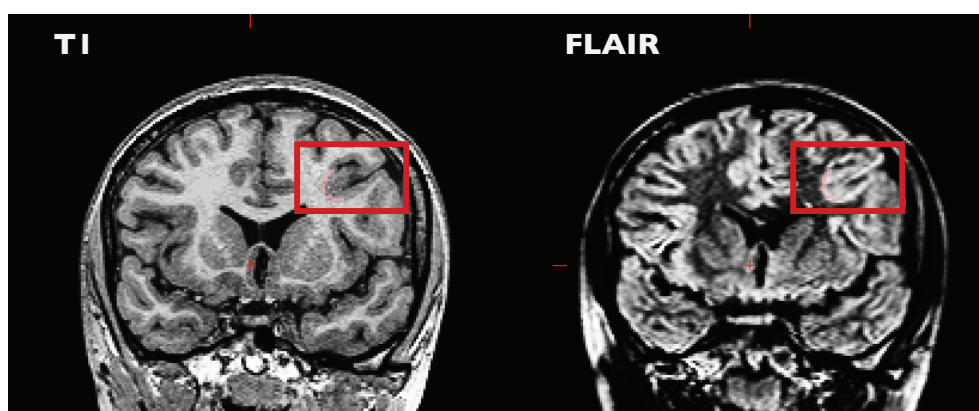
FCD ILAE Type III

These focal cortical dysplasias are characterised by cortical lamination abnormalities associated with a principal lesion. This lesion is hippocampal sclerosis in Type IIIa, a tumour in Type IIIb, a vascular malformation in IIIc and in Type IIId it is any other lesion acquired during development. The lesions are normally adjacent to or affect the same cortical lobe as the FCD.

Radiological features of FCD

Radiologically, on T1w structural MRI scans, FCDs may be characterised by abnormal cortical thickness, blurring of the grey-white matter boundary and abnormal gyral-sulcal structure. On T2w/FLAIR imaging, FCDs may exhibit increased signal intensity and FCD type IIB can demonstrate the transmantle sign, a hyperintense signal extending from the ventricle to the cortex (Barkovich et al., 1997; Wang et al., 2013).

Fig. 1.2 Radiological features of FCDs



Example FCD: small bottom of sulcus FCD on T1w MRI (left), FLAIR hyperintensity visible on FLAIR MRI (right).

It is important to note that FCDs can be subtle and are often missed by standard radiological analysis (Besson et al., 2008b). Furthermore, it is difficult to subtype FCDs based on radiological features. A study by Kim and colleagues (Kim et al., 2012) investigated whether radiologically identified MRI features could differentiate FCD type I and II. The MRI abnormalities they analysed included cortical thickness, blurring of the grey-white matter junction, increased cortical or subcortical signal on the T2-weighted FLAIR images, presence of the transmantle sign, and localized cortical thinning or atrophy. They also investigated whether the presence of a mass or cyst-like appearance could differentiate histological subtypes, as there have been previous reports that these have been observed in FCD patients. They found that most MRI features were unable to differentiate FCD type I and II, except the transmantle sign, which was specific to type IIB.

1.1 Paediatric Epilepsies: clinical overview

The ability to detect and phenotype lesions into histological subtypes is of paramount importance in providing accurate and detailed pre-surgical planning. First, surgical outcomes are highly dependent on MRI visualisation of the FCD (Téllez-Zenteno et al., 2010). Second, FCD type I and type IIA have poorer post-surgical outcomes than type IIB (Tassi et al., 2002). The difference in surgical outcome between type I and IIA and type IIB may be explained by the fact that FCD type I and IIA are often more subtle and their boundaries are more difficult to discern (Blümcke et al., 2010; Hong et al., 2015; Tassi et al., 2002). Third, the epileptogenicity of FCDs is related to their histopathological subtype (Boonyapisit et al., 2003; Tassi et al., 2002, 2010). Increasing the ability to detect and subtype FCDs is therefore useful for surgery planning, improving surgical outcome, and to more accurately advise the patient and their family of likely post-surgical outcome. Chapter 2 of this thesis explores using surface-based techniques to improve the detection of FCDs in paediatric epilepsy. A review on the potential for using quantitative MRI for FCD subtyping *in vivo* is included in the supplementary material.

Genetics of FCD

In recent years, much evidence has cumulated for the common genetic origin of focal epilepsy with FCD (Baulac et al., 2015), with causative pathogenic variants present in the germ line of rare familial cases (see Table 1.3). An interesting example is the DEPDC5 gene involved both in pathogenesis of a typical genetic epilepsy syndrome (familial focal epilepsy with variable foci - FFEVF) and of FCD (Baulac et al., 2015). DEPDC5 codes for a subunit of GATOR1 complex, an upstream regulator of the mTORC1 protein. In addition, pathogenic variants in the DEPDC5 gene have been identified in a case of hemimegalencephaly with the histological pattern of FCD IIA (Mirzaa et al., 2016). Furthermore, a study of familial cases of histologically confirmed FCD IIA identified germ line pathogenic variants in NPRL3 gene, another mTOR regulator (Sim et al., 2016).

The mTOR pathway has generated great interest in the field of genetic research of various malformations of cortical development, FCD being among them. Indeed, the histological pattern of FCD IIB lesions is identical or closely resembles that of cortical tubers in tuberous sclerosis complex (TSC) and hemimegalencephaly (Majores et al., 2005). Therefore, it has been hypothesised that, given their similarities, these lesions

1.1 Paediatric Epilepsies: clinical overview

might share a common genetic background. Since pathogenic variants in TSC1 and TSC2 genes have long been known to cause TSC, they have also been studied in FCD lesions, and pathogenic variants of TSC1 gene discovered in FCD IIB brain tissue samples (Becker et al., 2002). Furthermore, interesting allelic variants of TSC2 gene have been observed in FCD IIA samples (Majores et al., 2005), contributing to the evidence for involvement of TSC1 and TSC2 genes, both upstream inhibitors of mTOR signalling. In contrast to these findings, no clear causative pathogenic variants were found for either TSC1 or TSC2 genes in brain tissue samples from a different cohort of FCD patients (Gumbinger et al., 2009). Somatic mutations of mTOR gene itself were discovered in FCD IIA (Lim et al., 2015; Mirzaa et al., 2016) and FCD IIB (Lim et al., 2015) samples.

Located further upstream of the complex PI3K-AKT-mTOR pathway, the AKT3 and PI3KCA genes contribute to mTOR signalling, and these are primarily involved in severe cortical malformations associated with complex megalencephaly and hemimegalencephaly syndromes (Rivière et al., 2012). As previously mentioned, these malformations may share similar histological features with FCD, and we might expect similar genetic background underlying their formation; indeed, a somatic mutation in PI3KCA was detected in an FCD IIA brain tissue sample (Jansen et al., 2015). In addition, a somatic missense variant in exon 8 of PTEN was described in an FCD IIB sample (Schick et al., 2006). Furthermore, a chromosomal rearrangement in the region encompassing the AKT3 gene was identified in the brain tissue sample of a dysplastic frontal lobe, showing the histological pattern of FCD IB (Conti et al., 2015).

The aforementioned examples point to the complex interplay between many signalling molecules involved mostly, but not exclusively, in the mTOR pathway. Further study of these molecules and their interactions is warranted in order to understand the complex genetic background of formation of FCD.

The intriguing possibility is that the interplay between genetic background and the formation of the cortex may provide defining features that can be measured in vivo using structural MRI, in particular using novel quantitative MRI parameters.

Table 1.3 Characteristics of FCD lesion subtypes.

Lesion Subtype	Histology	Genetics	Radiological features
FCD I (A&B)	FCD IA: radial cortical dyslamination (Blumcke et al., 2011)	<ul style="list-style-type: none"> Variants in DEPDC5 (Baulac et al., 2015) FCD IB: chromosomal rearrangement in AKT3 (Conti et al., 2015) 	<ul style="list-style-type: none"> Cortical thinning Grey/white matter blurring Signal abnormalities on T1w/T2w imaging (Blumcke et al., 2011; Kabat and Król, 2012; Kim et al., 2012; Krsek et al., 2008) Lobar hypoplasia
	FCD IB: tangential cortical dyslamination (Blumcke et al., 2011)		
FCD IIA	Dysmorphic neurons (Blumcke et al., 2011)	<ul style="list-style-type: none"> Variants in NPRL3 (Sim et al., 2016) Variants in DEPDC5 (Mirzaa et al., 2016) Variants of TSC2 (Majores et al., 2005) Mutations of mTOR (Lim et al., 2015; Mirzaa et al., 2016) Mutation in PI3KCA (Jansen et al., 2015) 	<ul style="list-style-type: none"> Cortical thickening Grey/white matter blurring Signal abnormalities on T1w/T2w imaging (Kabat and Król, 2012; Krsek et al., 2008) Abnormal gyrification
	Dysmorphic neurons and balloon cells (Blumcke et al., 2011)		
FCD IIB	Dysmorphic neurons and balloon cells (Blumcke et al., 2011)	<ul style="list-style-type: none"> Variants of TSC1 (Becker et al., 2002) Mutations of mTOR (Lim et al., 2015; Mirzaa et al., 2016) Variant in exon 8 of PTEN (Weiskopf et al., 2013) 	<ul style="list-style-type: none"> Cortical thickening Grey/white matter blurring Signal abnormalities on T1w/T2w imaging Transmantle sign Abnormal gyrification (Kim et al., 2012; Mühlebner et al., 2011) (Barkovich et al., 1997)

The table summarises the histological, genetic and radiological features reported to characterise lesion types

Hippocampal Sclerosis

Hippocampal sclerosis (HS) is the most common epilepsy aetiology in adults (Engel, 1996) and the fourth leading cause of drug-resistant epilepsy in children (Harvey et al., 2008). The association of hippocampal sclerosis and temporal lobe epilepsy was first described by Wilhelm Sommer in 1880 (Sommer, 1880) based on a series of 90 post-mortem cases. The pathological findings described include neuronal loss in what is now known as CA1, as well as in the dentate gyrus and CA4 (Thom, 2009) and gliosis. However, although the histopathology of this aetiology is now well defined (see histopathology section below), the relationship between the underlying aetiology and the generation of seizures is still a source of debate. There is a known strong association between HS and a history of febrile convulsions - 30-50% of patients with mesial temporal sclerosis had febrile convulsions in childhood (Scott, 2014). This led to the hypothesis that an initial precipitating injury damages or alters the hippocampus, leading to the later development of HS. Alternatively, it has been suggested that an underlying hippocampal abnormality predisposes to both febrile convulsions and HS. Prospective studies reveal definitive hippocampal changes, including T2 hyperintensity, in the immediate aftermath following febrile status epilepticus in some children (Scott et al., 2002; Shinnar et al., 2012) and pre-existing mesial temporal sclerosis in others (Shinnar et al., 2012).

To date, not only is the cause of HS still unclear, but exactly how HS leads to the development of seizures remains unclear. It has been suggested that the epileptogenic process may be multifactorial involving neuronal and network dysfunction with studies implicating mossy fibre sprouting, interneuronal dysfunction, neuropeptide and neurotransmitters alterations (Thom, 2014). More recently, glial dysfunction and disruption of the blood brain barrier have emerged as other important mechanisms of epileptogenesis (Devinsky et al., 2013; Rakhade and Jensen, 2009; Vezzani, 2014; Wetherington et al., 2008).



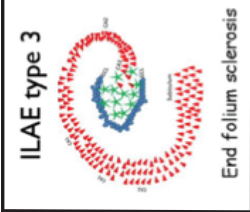
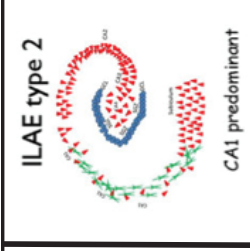
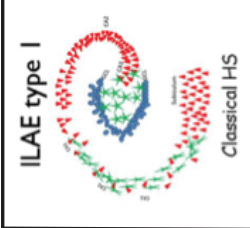
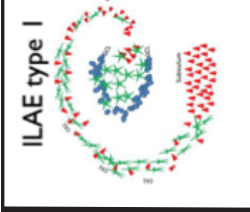
Unlike FCDs, temporal lobe epilepsy, due to hippocampal sclerosis, may demonstrate characteristic seizure semiology involving auras such as epigastric rising sensations and déjà vu, motor phenomena such as unilateral head deviation or facial contractions, behavioural arrest and oral automatisms. Seizure spread to the contralateral hemisphere can lead to altered consciousness, amnesia, motor automatisms, including tonic

posturing, and autonomic phenomena (Blair, 2012; Commission, 1989).

Histopathology of HS

HS is characterised by cell loss and gliosis in the hippocampus. However, the topography of these pathologies can be very variable across patients. The International League Against Epilepsy (ILAE) recently developed a classification system for HS ((Blümcke et al., 2013), Figure 1) where HS ILAE type I refers to severe neuronal cell loss and gliosis predominantly in CA1 and CA4 regions. HS ILAE type II involves cell loss and gliosis predominantly in CA1. In HS ILAE type III, the cell loss and gliosis is predominantly in CA4 whereas, in HS ILAE type IV there is gliosis only (see Figure 1.3).

Fig. 1.3 Histopathology of HS

<p>No HS</p>  <p>No HS</p>	<p>No neuronal loss and no gliosis</p>
<p>Gliosis only</p>  <p>End folium gliosis</p>	<p>Gliosis only (often involving the subgranular zone)</p>
<p>ILAE type 3</p>  <p>End folium sclerosis</p>	<p>Neuronal loss and gliosis in CA4 subfield (endplate/hilus)</p>
<p>ILAE type 2</p>  <p>CA1 predominant</p>	<p>Neuronal loss and gliosis predominant in CA1 subfield</p>
<p>ILAE type 1</p>  <p>Classical HS</p>	<p>Neuronal loss and gliosis in CA1 > CA4, CA3 with sparing of CA2</p>
<p>ILAE type 1</p> 	<p>Extensive neuronal loss (and gliosis) in all subfields including the dentate gyrus</p>

Adapted from (Thom, 2014)

1.1 Paediatric Epilepsies: clinical overview

However, it is important to note that there are also histopathological changes beyond the hippocampus. Postmortem studies indicate neuronal loss and gliosis is also present in a proportion of patients in the amygdala (Yilmazer-Hanke et al., 2000), entorhinal cortex (Du et al., 1993) and temporal neocortex (Thom et al., 2009). In fact, remote neocortical changes have also been documented, including both widespread atrophy and gliosis (Blanc et al., 2011; Margerison and Corsellis, 1966).

Radiological features of HS

Classical radiological features of hippocampal sclerosis include hippocampal atrophy on T1w imaging and T2 or FLAIR signal hyperintensity (Blümcke et al., 2013) (Figure 1.4). The reduced volume of the hippocampus on T1w imaging reflects neuronal loss (Bronen et al., 1991; Goubran et al., 2015) whereas the T2 or FLAIR hyperintensity is related to gliosis (Briellmann et al., 2002; Goubran et al., 2015).

Fig. 1.4 Radiological features of HS

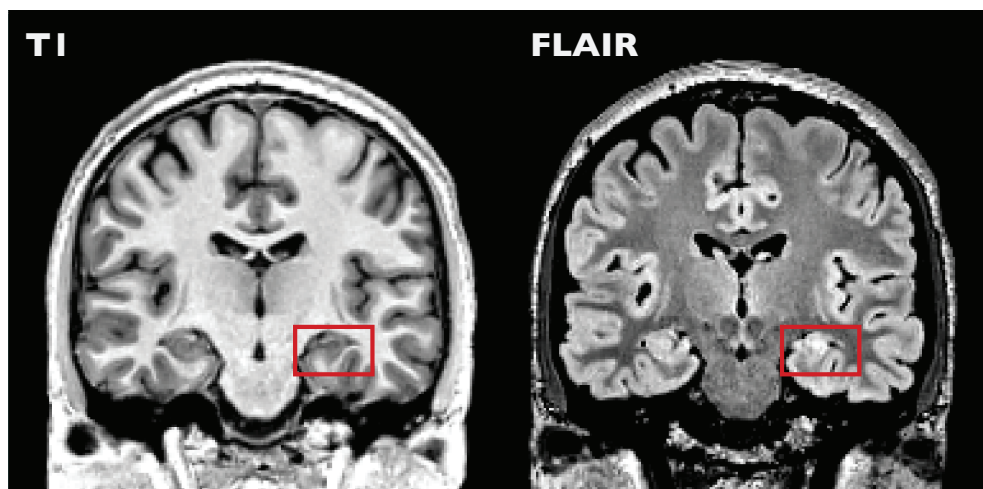


Figure: Radiological features of mTLE: hippocampal atrophy on T1w MRI (left), hippocampal hyperintensity on FLAIR MRI (right).

Genetics of HS

The genetic basis for HS remains largely unknown. However, there is some evidence for genetic involvement in this aetiology. As previously mentioned, there is a known association between febrile convulsions and HS. Furthermore, several rarer epilepsy syndromes, such as Dravet syndrome, which has febrile seizures as a defining feature, are caused by mutations in *SCN1A*. *SCN1A* encodes a sodium channel subunit. An

impressive genome-wide association study including 1018 people with mesial temporal lobe epilepsy with hippocampal sclerosis and 7552 control subjects as well as another large independent validation cohort found a significant association for HS with febrile seizures in part of the *SCN1A* gene (rs7587026) (Kasperaviciute et al., 2013). Interestingly, no association to rs7587026 was found in individuals with febrile seizures who did not develop epilepsy. This suggests the possible involvement of *SCN1A* in mTLE with febrile convulsions. One other gene that has been implicated is *GAL*, the galanin-encoding gene. Mutations in *GAL* were found in a pair of monozygotic twins with mTLE but no visible HS on MRI (Guipponi et al., 2015). However, in 582 patients with TLE, no mutations in *GAL* were found indicating that mutations in this gene are a very rare cause of TLE.

1.1.5 Clinical Neuroimaging

Role of structural MRI

In the presurgical evaluation of children with epilepsy, structural MRI scans are integral for lesion localisation and lateralisation, to help characterise the nature of the epileptogenic lesion, to establish the position of the focal lesion in relation to eloquent cortex as well as to exclude the presence of any abnormality on the contralateral hemisphere (Cross, 2002; Raybaud et al., 2006). High-resolution 3D MRI sequences providing T1 and T2 contrast are the initial scans used to detect epileptogenic lesions (Wehner and Lüders, 2008). Fluid Attenuated Inversion Recovery (FLAIR) sequences look similar to T2 weighted sequences except the signal from CSF is attenuated and appears dark. The sequence begins with an inversion recovery pulse of 180 degrees which is followed by a conventional spin echo after T1 recovery.

Diffusion tensor imaging (DTI), through sensitivity to the microscopic movement of water molecules (Johansen-Berg and Behrens, 2013), may also assist in the planning of resective surgeries (Widdess-Walsh et al., 2006). However, alterations in diffusivity in the region of the lesion are usually only visually appreciable ictally or in the immediate post-ictal period (Wehner and Lüders, 2008). Usually post-processing techniques are necessary to acquire useful information for the pre-surgical work-up of epilepsy patients. For example, DTI tractography can successfully recon-

struct the optic radiation and therefore be used as assess the proximity of the epileptogenic lesion to the optic tracts (Winston et al., 2011).

Other neuroimaging tools

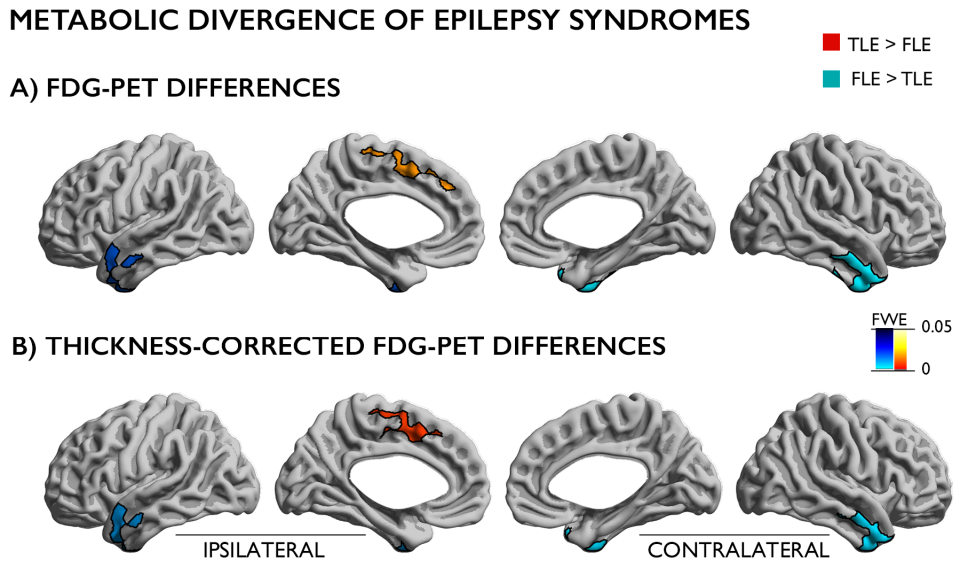
As well as structural MRI, other neuroimaging techniques are often appropriate and illuminating for individual patients. Positron emission tomography (PET) and single photon emission tomography (SPECT) are metabolic imaging techniques capable of visualising metabolic alterations of the brain in ictal and interictal states. These techniques may have localising value in MRI negative patients with underlying FCDs (Kudr et al., 2013; Salamon et al., 2008; Sun et al., 2015) or HS (Carne et al., 2004). Whole-brain, quantitative analysis of PET data also has the capability to dissociate anatomic areas of seizure onset (Adler et al., CLAE poster, Figure 1.5), i.e. to differentiate frontal lobe epilepsy due to FCDs from temporal lobe epilepsy due to HS. In addition, language and/or sensorimotor functional MRI is often helpful to non-invasively identify areas of eloquent cortex (Wehner and Lüders, 2008) in order to check at the individual level the possible functional sequelae of a proposed resection. Lastly EEG-fMRI, which identifies brain regions with fMRI changes associated with EEG events, can help better characterise and localise brain areas involved in interictal spike generation (Lemieux et al., 2001).

1.2 Whole-brain Structural MRI Analysis

1.2.1 Voxel-based techniques

Voxel-based morphometry (VBM) is a framework for neuroimaging analysis that measures differences in local concentrations of brain tissue per voxel (Ashburner and Friston, 2000). It has the advantage over volumetry, the manual delineation of regions of interest and subsequent calculation of the volume of tissue, that it is automated and therefore not affected by intra- or inter-rater variability. Furthermore, it can be applied to the whole-brain to detect changes in grey matter (GM), white matter (WM) or cerebro-spinal fluid (CSF) (Figure 1.6). Classically, two groups (e.g. patient vs control) are compared. However, VBM can also be used to compare an individual MRI scan to a control group. It has most

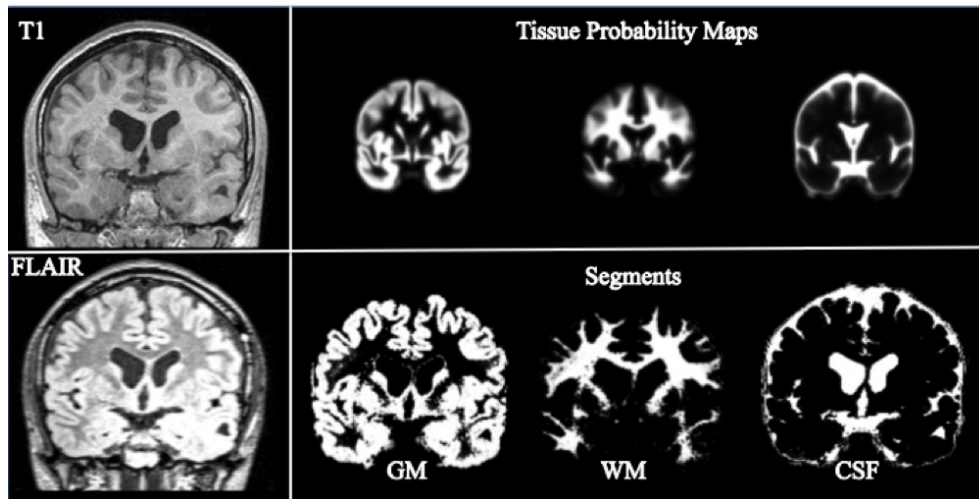
Fig. 1.5 Metabolic divergence of FLE and TLE



Metabolic divergence of epilepsy syndromes. FDG-PET differences (A) and cortical thickness corrected FDG-PET differences (B) between TLE and FLE patients. Findings were corrected for multiple comparisons at a family wise error level (FWE) of 0.05.

frequently been based on T1-weighted images, but has been applied to other sequences, such as T2-weighted / FLAIR.

Fig. 1.6 Voxel-based morphology



Segmentation of T1 and FLAIR using Tissue Probability Maps

Voxel-based techniques require voxel-to-voxel correspondence between subjects. This is achieved through non-linear image registration to a standard brain template. Once all images are co-registered, differences can be obtained by performing voxel-wise statistical tests.

Voxel-based techniques in FCD

In FCD, voxel-based studies have mainly focussed on lesion localisation. These studies involve comparing individual T1, T2 or FLAIR patient images against a group of healthy individuals. As FCD lesions may be characterised by signal hyperintensity in the grey matter on T1-weighted images or in the subcortical WM on T2/FLAIR images, voxel-based analysis of 3D T1-weighted (Colliot et al., 2006; Huppertz et al., 2005), T2-weighted (House et al., 2013) and FLAIR (Focke et al., 2009, 2008; Riney et al., 2006) images has been used to assist the detection of FCDs in individual patients with visually identified FCDs as well as patients with "cryptogenic" focal epilepsy.

The most influential voxel-based post-processing method used for FCD identification is the morphometric analysis programme (MAP) implemented in SPM, which identifies brain regions characterised by blurring of the grey-white junction, abnormal folding patterns, or abnormal cortical thickness (House et al., 2013; Huppertz et al., 2005; Wagner et al., 2011; Wang et al., 2015, 2013). This programme generates a number of 3D z-scored feature maps, where each voxel in an individual patient is compared to those from a cohort of healthy controls. Thus, areas that deviate from normal brain values have high z-scores and may indicate putative lesion locations. These maps include the junction map, sensitive to blurring of the grey-white matter boundary, the extension file which identifies areas of abnormal gyration and/or extension of the grey matter into the white matter and the thickness map which identifies areas of abnormal cortical thickness. This methodology has been applied successfully in adult cohorts to improve the visualisation of these lesions both in patients with visible lesions (Huppertz et al., 2005) and in MRI negative epilepsies (Wang et al., 2015). However, normalisation using a cohort of controls is more problematic in a paediatric cohort as children's brains are rapidly developing. For example, cortical thickness and surface area of the brain undergo an inverted U-shaped trajectory (Raznahan et al., 2011) and so comparing a 7 year old patient to a control group with a mean

age of 12, may result in areas being misidentified as abnormal purely due to the child being younger. As such, successful methodologies to identify subtle focal cortical dysplasias in children need careful consideration of developmental trajectories.

Voxel-based techniques in TLE

In adults, voxel-based morphology has revealed that grey matter pathology extends beyond the ipsilateral mesial temporal lobe structures involving subcortical structures such as the thalamus, midbrain, cerebellum, claustrum, globus pallidus, caudate nucleus and putamen and neocortical regions such as the occipital, parietal, cingulate, temporopolar and lateral temporal and dorsal frontal neocortices (see review: Keller and Roberts (2008)). This extra-hippocampal cortical atrophy has been related to duration of epilepsy (Bonilha et al., 2006; Keller et al., 2002) indicating the progressive nature of this pathology. In agreement with this, a study in children, found relatively limited GM loss, mainly involving ipsilateral temporal neocortex (Cormack et al., 2005).

Interpretation of VBM studies in epilepsy

VBM has provided a rapid, automated methodology in epilepsy to identify areas of potential brain pathology in epilepsy. However, there are a number of limitations to VBM studies. A change in grey matter density could be caused by a range of processes and thus the biological interpretation is difficult. A reduction in grey matter density could indicate atrophy or it could be due differences in cortical folding between the groups. In fact the sensitivity of VBM to detect changes may be hindered by differences in cortical folding across individuals. Furthermore smoothing, which is necessary to compensate for minor misalignment during nonlinear registration to a template space and to reduce noise, may average areas that are close in voxel-space (i.e. short euclidean distance) but much further apart across the cortical surface (i.e. long geodesic distance), creating partial volume effects.

1.2.2 Surface-based techniques

Surface-based approaches for analysis of the cortex, such as FreeSurfer, first create models of the grey-white matter boundary and the pial surface

(Figure 1.7). These surfaces have point-to-point correspondence, and can be used to calculate a range of anatomical measures at each point (vertex) across the cortical surface. These include cortical thickness, curvature, surface area and sulcal depth (Figure 1.7). Within FreeSurfer, it is possible to visualise these measures on the cortical surfaces. Furthermore, the surfaces can be inflated, to improve the visualisation of buried cortex and sulcal areas.

Individual surfaces can be registered to templates that have been created based on average folding patterns. This registration aligns cortical folding patterns, i.e. gyri and sulci, rather than image intensities, thus optimising inter-subject correspondence. Once individuals have been registered to a template space there is point-to-point correspondence between subject and group maps can be created. General linear models applied to surface-based data can test how a particular measure changes as a function of group membership (e.g. epilepsy or control).

Surface-based techniques in FCD

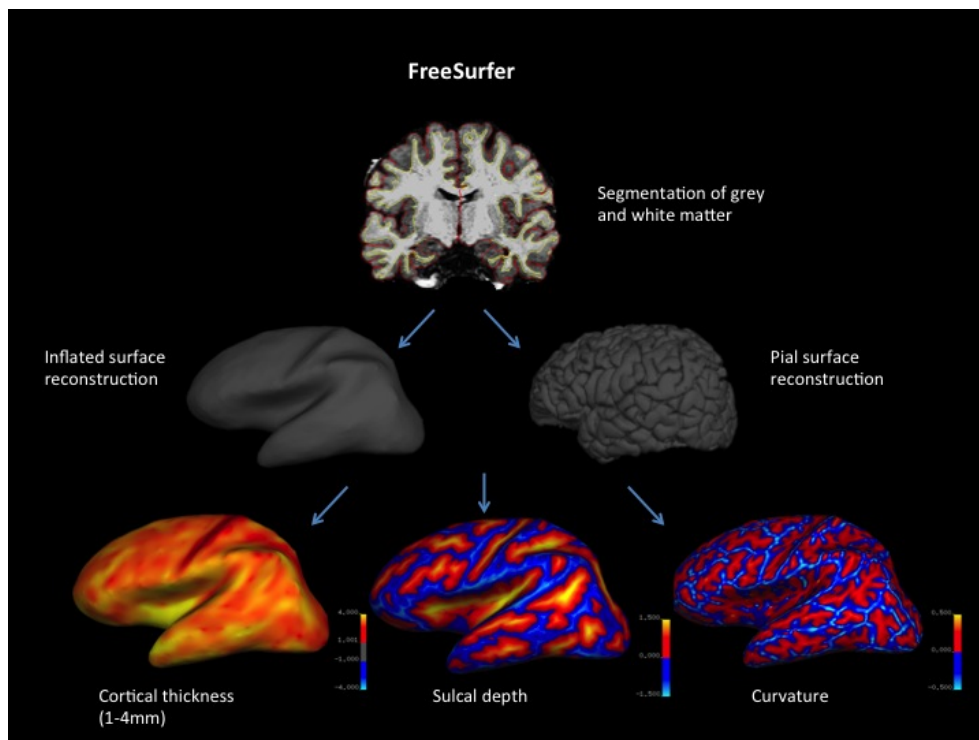
Within FCD research, surface-based analyses have been used to document lesion characteristics, with studies finding that FCDs have abnormal cortical thickness, intensity contrast at the grey-white matter boundary, curvature, sulcal depth and folding (Ahmed et al., 2015; Besson et al., 2008a,c; Hong et al., 2014; Thesen et al., 2011) and that quantitative structural abnormalities extend into the penumbra around the visible lesion (Hong et al., 2017a). Yet, there are differences in lesion characteristics between FCD subtypes (Hong et al., 2017a), with FCD type IIB lesions having abnormal morphology and intensity throughout the cortical mantle, whereas, type IIA lesions only have abnormal intensity and only close to the grey/white matter boundary.

By excluding lesional vertices, surface-based analysis has revealed that there are also extra-lesional structural abnormalities, cortical thickening in temporal and post-central neocortices, in FCD type II (Hong et al., 2016). Furthermore, whole-brain structural changes are dependent on the FCD subtype. For example, patients with FCD type I have multilobar cortical thinning, whereas patients with type II have cortical thickening in temporal and post-central neocortices (Hong et al., 2016). However,

the neuroimaging evidence base for extra-lesional pathology in FCD is currently limited to this one study and as such is very preliminary and requires replication.

Overall, surface-based techniques reveal extensive morphological and intensity abnormalities within lesional cortex and that morphological abnormalities extend beyond the visible dysplasia into perilesional cortex, as well as more diffuse whole-brain structural changes.

Fig. 1.7 Surface-based techniques



FreeSurfer is an example of a surface-based framework. 1. Segmentation of the grey and white matter. 2. Inflated and pial surface reconstructions. There is point-to-point correspondence between vertices on the two surfaces. 3. Examples of surface feature maps - curvature, sulcal depth and cortical thickness.

Surface-based techniques in TLE

In concordance with voxel-based studies, surface-based studies have consistently shown that adults with temporal lobe epilepsy have widespread cortical atrophy (Bernhardt et al., 2010, 2008; Keller et al., 2015; Lin

1.3 Structural and Functional Cortical Networks

et al., 2007; McDonald et al., 2008; Mueller et al., 2009), and that cortical thinning is progressive (Bernhardt et al., 2009b). Furthermore, network-based analyses using surface-based data support the notion of system-level structural compromise, with studies findings decoupling of the hippocampus (Bernhardt et al., 2016) and temporo-limbic neocortices (Liu et al., 2016) from default mode hubs in TLE. In healthy individuals the hippocampus is heavily connected to default mode hubs. Whereas in TLE, there is reduced connectivity between the anterior (dorsal medial prefrontal neocortex) and posterior (retrosplenial and posterior cingulate) default mode hubs and the hippocampus (Bernhardt et al., 2016).

Considerations when applying surface-based techniques to a paediatric population

The body of work presented in this thesis primarily uses surface-based frameworks to explore lesional and extra-lesional abnormalities in paediatric focal epilepsies. Surface-based analyses have advantages such as optimisation of inter-subject correspondence, mitigation of the effects of partial voluming, and the ability to integrate multiple modalities. However, analysis is restricted to the neocortex and therefore does not extend to subcortical structures.

1.3 Structural and Functional Cortical Networks

Recent years have witnessed a shift from the mapping of local grey matter properties to the study of inter-regional covariance of such properties, to describe brain networks in both normal and diseased conditions (Alexander-Bloch et al., 2014; Bernhardt et al., 2013a; Bullmore and Sporns, 2009; Evans, 2013). Crucially, several neuroimaging techniques have been brought forward to study different types of inter-regional relationships, offering complementary perspectives on large-scale cortico-cortical brain networks.

1.3.1 Resting-state functional connectivity

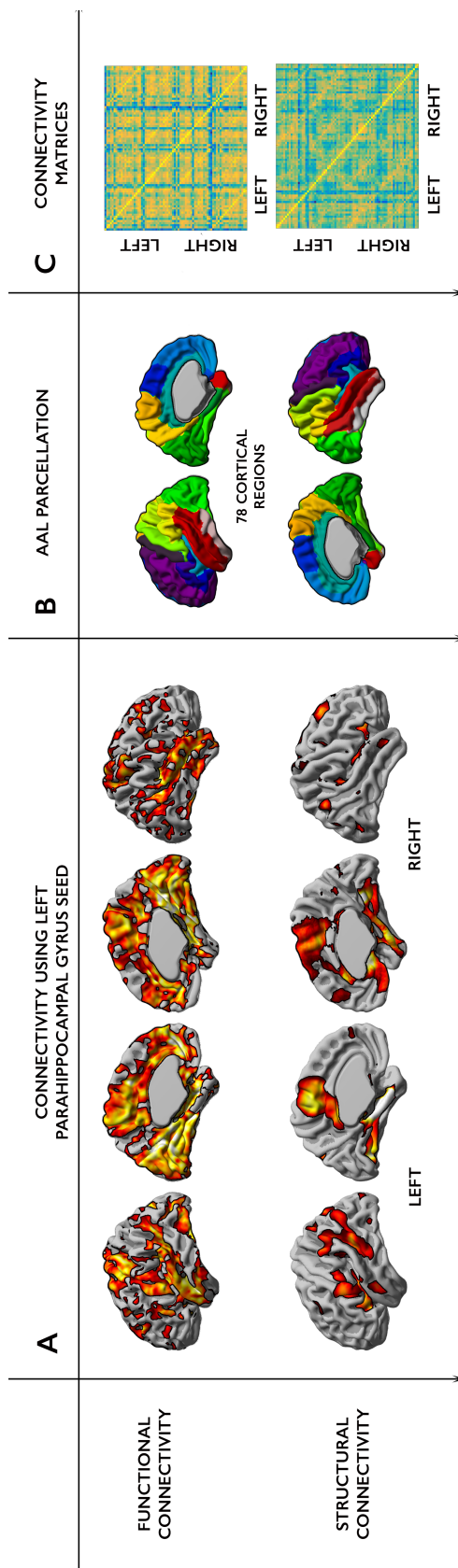
Resting state functional connectivity (rs-fMRI) has successfully identified intrinsic functional networks, such as the default mode, sensorimotor, visual, and executive networks (Damoiseaux et al., 2006). Seed-based

1.3 Structural and Functional Cortical Networks

functional connectivity involves the correlation of resting-state fMRI time series from one region of interest (ROI) or voxel or vertex with corresponding times series from other ROIs / voxels / vertices (Figure 1.8 A). Whereas, whole-brain connectivity matrices can be created by correlating the times series of every ROI / voxel / vertex with every other times series (Figure 1.8 C). High positive correlations between two cortical areas indicates functional interactions between these cortical areas. This methodological framework can be conducted at either the individual or group level.

In TLE, functional connectivity analyses of rs-fMRI signals have shown altered functional connectivity between the hippocampus and other temporal (Bettus et al., 2009) and extra-temporal (Voets et al., 2012) cortical regions. Studies of connectivity alterations in patients with focal cortical dysplasia are challenging to do for a number of reasons. First, the lesions can be located anywhere in the cortex and thus the networks affected are likely to differ depending on lesion location. Second, lesion's are very variable in terms of size and a large lesion may be located within multiple resting-state networks. Third, how a lesion affects the function of networks and other brain regions may differ depending on FCD subtype. As such, to date there have been little research on how FCDs affect the function of other brain regions or how they affect brain networks. One recent study, used a novel framework in order to circumvent the challenges raised earlier (Hong et al., 2017b). They subdivided the cortex into small parcels and investigated the functional connectivity of each of the parcels, finding three different categories of FCDs. The first category were characterised by reduced connectivity to both the functional network within which they were located as well as to other networks. FCDs in the second category had reduced connectivity within the functional network they were located but normal connectivity to other networks and the third group of FCDs had increased connectivity within the network they were located and to other networks. However, it has been found that functional connectivity in intrinsic connectivity networks is affected by interictal discharges (Shamshiri et al., 2016). It is thus possible that differences in interictal discharges underlie the functional connectivity differences found by Hong and colleagues.

Fig. 1.8 Structural and functional cortical networks



Cortical networks created on the basis of cortical thickness correlations and rs-fMRI connectivity. A) Parahippocampal connectivity using seed-based rs-fMRI (upper) and cortical thickness covariance (lower) in a sample of healthy controls. B) AAL parcellation into 78 cortical regions. C) Inter-regional rs-fMRI (upper) and cortical thickness (lower) correlation matrices. The value of the cell in row i and column j is given by the $\text{rs-fMRI} / \text{cortical thickness}$ correlation of areas i and j across all healthy subjects.

1.3.2 Cortical thickness covariance

Morphological covariance analysis, commonly based on cortical thickness correlations, has been used to reveal areas with synchronised maturational development (Alexander-Bloch et al., 2013; Bernhardt et al., 2008; Whitaker et al., 2016; Zielinski et al., 2010). It can only be conducted at the group level. Seed-based cortical thickness covariance involves the correlation of the cortical thickness values of the group from a particular ROI or vertex with the cortical thickness values of the group at every other ROI / vertex (Figure 1.8 A). Similar, to functional connectivity, whole-brain connectivity matrices can be created by correlating the cortical thickness values in every ROI / vertex with every other ROI or vertex (Figure 1.8 A). High cortical thickness correlations between two cortical areas indicates areas with similar developmental trajectories.

In temporal lobe epilepsy (TLE) patients, voxel-based studies investigating the covariation between hippocampal and extrahippocampal volume loss have demonstrated limbic network pathology that is dependent on the degree of mesiotemporal damage (Bonilha et al., 2007; Düzel et al., 2006). Similarly, a surface-based study that used the entorhinal cortex as a seed for cortical thickness covariance, also demonstrated alterations in limbic networks (Bernhardt et al., 2008).

As mentioned previously, there are significant challenges in conducting connectivity analyses in FCD cohorts. As a result, to the best of my knowledge, there have no structural connectivity studies using cortical thickness (morphological) covariance in FCD cohorts. As morphological covariance is conducted at the group rather than individual level, a study would have to group together lesions regardless of location or size and thus this framework would not be appropriate to explore the interesting questions such as "Does lesional cortex modulate the structure of other cortical areas?".

1.4 Machine Learning

Statistical machine learning methods can provide powerful tools for neuroimaging data analysis, particularly as they are able to model high-dimensional datasets, i.e. they can integrate multiple modalities and identify patterns in the data. Conventional statistics, such as the general

linear model, serve to test whether there is a difference between two groups (e.g. patient versus healthy control). To move from characterisation of group-level differences to individualised diagnosis or subgrouping requires the identification of the threshold of a measure above which an individual / data point is likely to fall into the disease group. In the most simple case, where one feature distinguishes patient from control (e.g. the case of microcephaly where a brain volume more than two standard deviations below the mean is diagnostic), a machine learning algorithm if trained on patient and control brain volumes, would seek to optimise the threshold to diagnose patients automatically. However, machine learning has the capability to handle much more complex data, such as to find interactions between multiple features that would be challenging or impossible for a human to match.

In order to do this, datasets are divided into training, validation and testing sets, where the training data is used to learn the pattern, the validation set is used to validate how correct the model is and the error is used to update the model, and finally the testing set is used to validate the final model. Once a machine-learning classifier has been trained and validated, the algorithm can be used to make individual predictions.

During training (or learning), a model is fitted and the parameters of the model are refined to allow the best prediction of the data. This is also called optimization, and during this procedure an equation (the cost function) is specified that measures how well the model fits. Cost functions calculate the mismatch between the predictions of the model and the desired output. Optimization involves finding the parameter values that minimise the cost function.

There are many different machine learning algorithms, but they can be broadly categorised into supervised and unsupervised learning methods. In neuroimaging, input features are usually image features (e.g. voxels, volumes, tracts or vertices) and the desired outputs are often binary (e.g. patient or control, left TLE or right TLE, lesion or not lesion). In supervised machine learning frameworks, such as support vector machines (SVMs) and artificial neural networks (NNs), the algorithm is given a set of input features and the desired outputs of the training set and aims to predict the correct output given the set of input features. Whereas, unsupervised learning occurs when the algorithm is only given input

features and no outputs and aims to find hidden patterns to cluster the data (e.g. principal component analysis (PCA) or k-means).

1.4.1 Neural Networks

Artificial neural networks (NNs) have a structure akin to biological neural networks. They consist of a set of "neurons" with connections between them, analogous to synapses. Each connection has a parameter called the weight and multiplies the signal from its input "neuron" by its weight (w). Each "neuron" sums up the signals from its input connections, modifies this value according to an activation function, then propagates this value through its outgoing connections to the next layer (Figure 1.9). The architecture of the neural network is highly flexible and can have a range of hidden layers. Finally, the output neuron(s) add up the incoming signals.

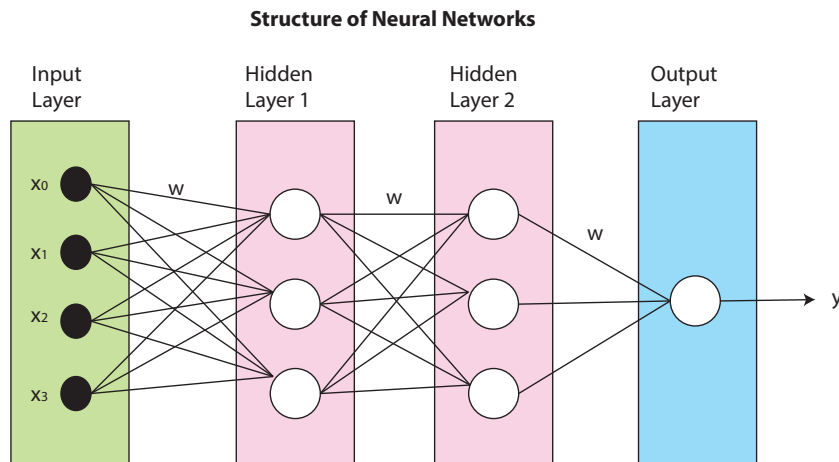
In epilepsy, applications of neural networks include the automated detection of epileptic activity in EEG recordings (Patnaik and Manyam, 2008) as well as to classification of EEG signals into inter-ictal, pre-ictal, ictal and post-ictal states (Costa et al., 2008).

1.5 Thesis Objectives

To date much of the work using surface-based frameworks to analyse cortical structure in patients with epilepsy has been conducted in adults. This work suggests that surface-based analysis may be able to quantify epilepsy related brain pathology in children; both the epileptogenic lesions themselves and extra-lesional pathology. However, owing to the particular differences between adult and paediatric brains it is unclear that current approaches are suitable or would yield similar results. This thesis focusses on characterising cortical morphology in lesional epilepsy. Borrowing some new developments from adult epilepsy, it aims to identify focal and network level changes in two common forms of paediatric epilepsy. The work is organised into 5 remaining chapters.

Chapters 2 and 3 focus on patients with focal cortical dysplasias. Chapter 2 develops surface-based, structural MRI post-processing techniques that can be applied to clinical T1 and FLAIR images to complement

Fig. 1.9 Structure of Neural Networks



A three layer neural network with four inputs (x_0, x_1, x_2, x_3), two hidden layers of 3 neurons each and one output layer. Each neuron is connected to all neurons in adjacent layers but not connected to neurons within the same layer. Neurons are represented by circles and connections or synapses are represented by straight lines. Each neuron applies an activation function to its input. Connections are weighted (w).

current MRI-based diagnosis of focal cortical dysplasias, whilst accounting for developmental differences between participants. These metrics are then used to create lesion profiles. Chapter 3 uses the features developed in Chapter 2 within a machine learning framework to automatically detect FCDs. Chapters 4 and 5 focus on patients with temporal lobe epilepsy. Chapter 4 develops an in vivo method to explore FLAIR signal intensity abnormalities in adults with TLE, while Chapter 5 applies this method to a paediatric cohort enabling multimodal surface-based imaging of paediatric TLE. Finally, the concluding chapter discusses contributions, main limitations and outlines options for future research.

Chapter 2

Quantification of surface-based lesion characteristics in focal cortical dysplasias

2.1 Introduction

As discussed in Chapter 1, focal cortical dysplasias (FCDs) are the most common cause of surgically remediable drug-resistant epilepsy in children (Harvey et al., 2008; Lerner et al., 2009). Early age of surgical intervention and complete resection of the dysplastic cortex are important predictors of good seizure outcome, cognitive development and quality of life (Chen et al., 2014). However, as surgical outcome is also dependent on pre-surgical lesion identification on MRI (Rowland et al., 2012; Téllez-Zenteno et al., 2010), the detection of these often elusive lesions is critical in the pre-surgical evaluation of paediatric patients.

Radiologically, FCDs have been associated, albeit inconsistently, with a range of features including local cortical thinning or thickening, blurring of the grey-white matter boundary, abnormal cortical folding patterns, altered signal intensity on FLAIR/T2-weighted MRI (including the trans-mantle sign in FCD Type IIB) and interhemispheric asymmetry in any of the above traits (Colombo et al., 2012, 2003; Leach et al., 2014a; Mellerio et al., 2012; Yagishita et al., 1997).

Between 22% and 58% of histopathologically confirmed cortical dysplasias are MRI negative (Leach et al., 2014b; Lerner et al., 2009), with ILAE Type I and IIa more frequently non-lesional on MRI (Radhakrish-

nan et al., 2016). Even lesional cortical dysplasias are often overlooked on initial radiological inspection (Radhakrishnan et al., 2016). The variable presentation of the radiological features, the fact that they are often small and subtle and the inherent subjectivity in human-eye diagnosis, means that they are easily missed on visual inspection by radiologists (Wagner et al., 2011). Despite improvements in prospective detection of FCDs with use of higher field strength MRI scanners (De Ciantis et al., 2016; Guerrini et al., 2015), the current ILAE classification scheme and after review of MR images in multidisciplinary team meetings (Radhakrishnan et al., 2016), there is a need for automated, quantitative FCD features that are objective and user-independent.

In adults, surface-based methodologies have been used to compare individual patients with known lesions to healthy controls (Besson et al., 2008a; Régis et al., 2011; Thesen et al., 2011). The study by Thesen and colleagues calculated clusters of abnormal cortical thickness, grey-white matter contrast, local gyrification index (LGI), sulcal depth, jacobian distance and curvature (Thesen et al., 2011). Using receiver operating characteristics (ROCs) they demonstrated that cortical thickness and grey-white matter intensity contrast have the most discriminatory ability between lesional and nonlesional cortex. Yet, the other features were also able to detect lesional cortex and no features could capture the extent of lesions. The study by Régis and colleagues found abnormal patterns of gyration in patients with cortical malformations (Régis et al., 2011). Although, folding abnormalities co-localized with the epileptogenic zone (EZ) in 75% of patients, they extended beyond the EZ in 66%. Lastly, the study by Besson and colleagues quantified sulcal depth and found that small FCDs are often positioned at the bottom of deep sulci (Besson et al., 2008a). Yet, to date automated surface-based methodologies have not been used to characterise FCDs within a paediatric cohort, despite the developmental nature of this pathology.

One main challenge to lesion profiling in a paediatric cohort compared to an adult cohort is that the brain is still rapidly developing. Although most brain development occurs prenatally, substantial brain changes still occur postnatally, especially during adolescence (Giedd et al., 1999). Post-natal cortical development is driven by local changes in dendritic length (Huttenlocher et al., 1997; Huttenlocher and Hapke, 1990), dendritic spine density (Travis et al., 2005), intracortical myelination, gliogenesis and

synaptogenesis (Hill et al., 2010). Neuroimaging studies in healthy populations attempting to capture this *in vivo* have revealed mixed results. Some work using the metric grey matter density (GMD) (Giedd et al., 1999, 1996; Gogtay et al., 2004; Mechelli et al., 2005) or cortical thickness (Raznahan et al., 2011; Shaw et al., 2008) have found that overall cortical development follows an "inverted-U" shaped trajectory that peaks during adolescence. Whereas, other studies find continuous cortical thinning (Gogtay et al., 2007; Zielinski et al., 2014). There is also evidence that some regions of the cortex age more rapidly than others (Fjell et al., 2009; Giedd et al., 1999; Gogtay et al., 2004; Shaw et al., 2008; Sowell et al., 2004; Toga et al., 2006) and that cortical development is sexually dimorphic (Giedd et al., 1996; Luders et al., 2006; Raznahan et al., 2010, 2011). A recent review of the cortical thickness maturation literature stated that at present it is not possible to conclude which cortical thickness maturation trajectory reported is "correct" (Walhovd et al., 2017). However, what can be concluded is that cortical thickness is not constant during development and that this must be accounted for when analysing neuroimaging data from a paediatric disease cohort.

This study aimed to quantify FCD lesion characteristics in a paediatric cohort to profile FCDs and identify features that may assist lesion delineation, whilst addressing the particular challenges of a paediatric cohort. To this end, structural measures and post-processing methods were applied to quantify a number of radiological identifiers of focal cortical dysplasias.

Established surface-based structural markers of FCD

Established surface-based structural markers are features that have been previously quantified to assist FCD lesion detection. It is important to note that these features have not been assessed in a paediatric cohort. They include cortical thickness, intensity contrast at the grey-white matter boundary, FLAIR signal intensity, curvature and sulcal depth. These features have normal developmental and regional differences which can obscure locally abnormal values within an FCD. To address this, per-vertex measures were normalised within subjects and then the values for each vertex were normalised relative to a group of healthy paediatric controls.

Novel surface-based structural markers of FCD

FCDs are characterised by focal changes in cortical structure and thus subtle lesions should be identifiable as local areas of abnormal cortical thickness and grey-white matter contrast. This study developed a new method, the "doughnut" method, to quantify these local changes. The "doughnut" method calculates the difference between an area of cortex and its surrounding annulus at each vertex, highlighting where these differences are greatest.

Noise and particularly motion artefacts are common problems in paediatric scans. Intrinsic curvature, a small-scale measure of cortical shape deformation, only requires an accurate pial surface and is unaffected by motion-related inaccuracies in the segmentation of the grey-white matter boundary. Furthermore, it is more sensitive to subtle cortical abnormalities than larger scale folding parameters measures such as LGI (Ronan and Fletcher, 2014). My collaborator, Konrad Wagstyl, developed a measure of local cortical deformation (LCD) based on the magnitude of intrinsic curvature surrounding each vertex (Ronan et al., 2011), as a more robust measure of cortical shape, which was calculated per-vertex in all participants.

Lesion profiling in paediatric FCD

In this study, ten surface-based features were computed - cortical thickness, grey-white matter intensity contrast, curvature, sulcal depth, grey and white matter FLAIR signal intensity, local gyrification index, LCD, and "doughnut" thickness and "doughnut" grey-white matter intensity contrast. All surface-based features were quantified in lesional cortex and compared to contralateral, homotopic healthy cortex both at the group and individual level to assess their discriminatory ability.

2.2 Materials & Methods

2.2.1 Participants

A retrospective cohort of 27 patients with radiologically defined FCD (mean age= 11.57 ± 3.96 , range=3.79 - 16.21 years, 10 females) who underwent 3D T1 and FLAIR imaging on the 1.5T MRI scanner at Great Ormond Street Hospital as part of their clinical workup were studied,

following permission by the hospital ethical review board. Cases were identified by searching the medical reports for a radiological diagnosis of FCD. Exclusion criteria were patients scanned using a different MRI scanner or protocol. The following information from the medical notes was gathered for all patients included in this study: age at epilepsy onset, duration of epilepsy, radiological report, current anticonvulsant medications and, where applicable, post-surgical histology. A control group of 28 term-born children with no history of any neurological diagnosis (mean age= 14.57 ± 3.06 , range=10.1 - 19.75 years, 11 females) were recruited by advertisement.

2.2.2 MR Imaging

All participants were scanned on a 1.5T Avanto MRI scanner (Siemens, Erlangen, Germany). Three-dimensional data sets were acquired using a T1-weighted 3D-FLASH sequence (TR = 11 ms, TE = 4.94 ms, FOV = 256x256mm, flip angle = 15° , voxel size = $1 \times 1 \times 1 \text{ mm}^3$) and T2-weighted FLAIR sequence (TR = 6000 ms, TE = 353 ms, TI = 2200 ms, FOV = 256x256 mm, flip angle = 15° , voxel size = $1 \times 1 \times 1 \text{ mm}^3$). Anonymised FLAIR and T1 volumetric scans were rated from one to five according to severity of motion artifact using the motion classification system described in Section 3.2.1.

2.2.3 Cortical Reconstruction

FreeSurfer software v5.3 (Dale et al., 1999; Fischl and Dale, 2000; Fischl et al., 1999) was used to generate the cortical reconstructions and to co-register the FLAIR scans to T1-weighted images. In outline, FreeSurfer firstly sub-samples the raw image data voxels to 1 mm^3 isotropic voxels. The data is then normalized for intensity and RF-bias field inhomogeneities are modeled and removed. The skull is then removed from all of the images using a skull-stripping algorithm (Ségonne et al., 2004). Subsequently, cerebral white matter is identified, and the hemispheres are separated, tessellated and deformed to create accurate smooth mesh representations of the grey-white matter interface and pial surface, with approximately 150,000 vertices per hemisphere. Within-subject registration of FLAIR scans to T1 images was performed using a boundary-based cost function; the white-matter boundary is mapped to the FLAIR image and the FLAIR intensity is sampled per-vertex either side of the boundary. The difference

in intensity between each pair of intensities is then used to calculate the cost function. All of the reconstructions were checked and any inaccuracies were manually corrected. Five participants were excluded from the patient cohort due to severe motion artefacts. There was no significant difference in age between the included and excluded participants (Mann-Whitney U: -1.53, $p=0.13$).

2.2.4 Lesion Masks

Manual lesion masks were created for the 22 participants, on axial slices of the volumetric scan. Lesions were identified combining information from T1 and FLAIR images, previous radiological reports, reports from multi-disciplinary team meetings as well as oversight from a consultant paediatric neuroradiologist. The lesion masks were then registered onto the cortical surface reconstructions.

2.2.5 Measures of Morphological / Intensity Features

FreeSurfer was used to calculate the established measures: cortical thickness, grey-white matter intensity contrast, curvature, sulcal depth and FLAIR intensity at each vertex of the 3D cortical reconstruction. Thickness was calculated as the mean minimum distance between each vertex on the pial and white matter surfaces and the opposing surface, generating a millimeter-scale measure of the thickness of the cortex. Further details of these methods are available in Fischl and Dale (2000).

Grey-white matter intensity contrast was calculated as the ratio of the grey matter signal intensity to the white matter signal intensity (Salat et al., 2009). The grey matter signal intensity was sampled at a distance of 30% of the cortical thickness above the grey-white matter boundary. The white matter signal intensity was sampled 1mm below the grey-white matter boundary. These are the FreeSurfer defaults. This measure is aiming to quantify the grey white contrast. 1mm inside the white matter is the minimum required to ensure that the voxel is entirely white matter, with no partial grey matter. Further than 1mm risks crossing into adjacent gyral cortex or sampling white matter that is increasingly unrelated to the vertex in question. Cortical thickness is generally 3mm but ranges from 1-5mm, so sampling at 1mm above the grey/white boundary would be sampling different aspects of cortical anatomy depending on

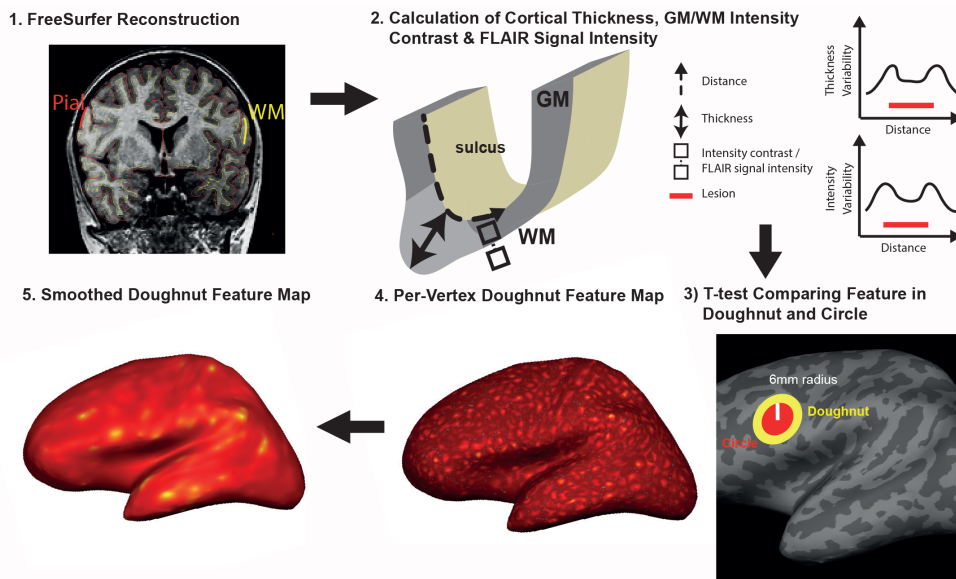
the area being sampled. Therefore, for intracortical sampling it is more biologically consistent to sample a proportional depth of 30%, which is 1mm within typical 3mm cortex. Lesions with blurring of the grey-white matter boundary are expected to have low grey-white matter intensity contrast values compared to healthy cortex.

FLAIR intensity was sampled at 50% of the cortical thickness and at -1mm below the grey-white matter boundary. A 50% intra-cortical depth was chosen to minimise partial volume effects. A 1mm subcortical depth was chosen to sample within the white matter and avoid sampling from adjacent grey matter in the case of narrow gyri. Mean curvature was measured at the grey-white matter boundary as $1/r$, where r is the radius of an inscribed circle and is equal to the mean of the principal curvatures k_1 and k_2 (Pienaar et al., 2008). The dot product of the movement vector of the cortical surface during inflation is used to calculate the sulcal depth. Shallow, gyral areas of the brain move inwards during inflation and have a negative value whereas, deep, sulcal areas move outwards and have a positive value.

2.2.6 "Doughnut" Method

A 6mm radius circle was centred on a vertex on the inflated surface (Figure 2.1). A surrounding "doughnut" of cortex of the same area (~ 113 mm²) was placed around it. The cortical thickness, grey-white matter intensity contrast or FLAIR signal intensity was measured within the circle and within the doughnut. A t-test was used to compare the thickness/grey-white matter intensity contrast in the circle and doughnut. This measurement was repeated per vertex over the inflated surface. "Doughnut" thickness and "doughnut" intensity contrast maps were created per participant using the log of the per-vertex, t-test p-values. "Doughnut" maps were smoothed using a 10mm FWHM Gaussian kernel, to remove noise while maintaining local specificity. A 6mm radius was used as it offered a balance between identifying local changes in thickness/intensity on a scale finer than gyral/sulcal changes, and insensitivity to motion artefact, a common problem when analysing paediatric MRI data (Reuter et al., 2015). The code is available from <https://github.com/kwagstyl/FCDDetection/>.

Fig. 2.1 "Doughnut" Method



Doughnut Method Pipeline. 1) Cortical reconstruction using FreeSurfer. Red = pial, yellow = white matter surface. 2) Per-vertex calculation of cortical thickness and grey-white matter intensity contrast (left). Hypothesised profiles of feature variability around lesion (right). 3) T-test comparing feature in 6mm radius circle and doughnut. 4) Per-vertex doughnut surface map. 5) Smoothed (10mm FWHM) doughnut feature map.

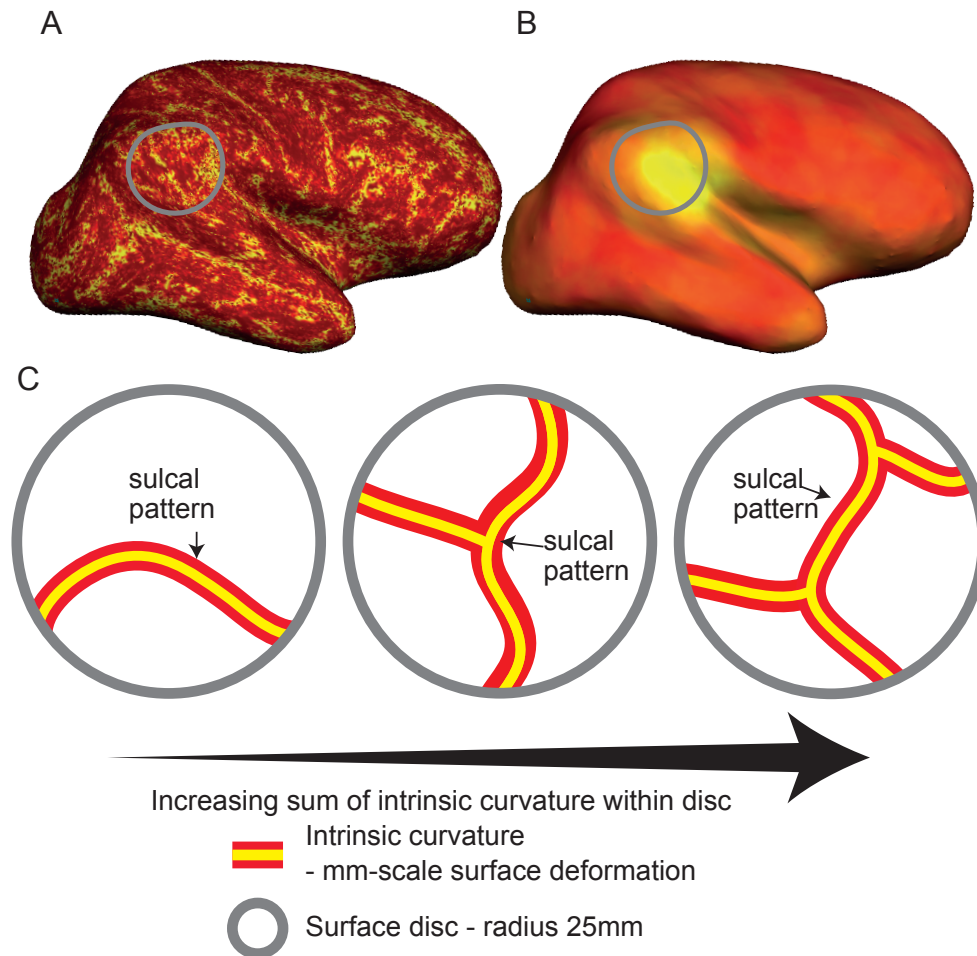
2.2.7 Local Cortical Deformation

Cortical deformation, also known as intrinsic or Gaussian curvature, was calculated at a mm scale across the pial surface (Ronan et al., 2011). As the product of the principal curvatures, k_1 and k_2 , it is extremely sensitive to local surface deformations, and particularly high in sulcal fundi. A 25mm radius ring was centred on a vertex and the sum of the intrinsic curvature within the ring was computed (Figure 2.2). This process was repeated per vertex across the cortical surface to create a measure of local cortical deformation. A 25mm ring was chosen as in normal folded cortex it captures approximately equal amounts of gyral and sulcal cortex, whether the central vertex is gyral or sulcal (Wagstyl et al., 2016). The code used is available from <https://github.com/kwagstyl/FCDDetection/>.

2.2.8 Normalisation of Features

The following features were smoothed using a 10mm FWHM Gaussian kernel - cortical thickness, grey-white matter intensity contrast and FLAIR signal intensity. In every individual, these features underwent two normalisation procedures. 1) Features were normalized using a within-subject

Fig. 2.2 Local Cortical Deformation



A) Surface overlay of per-vertex intrinsic curvature. The modulus of intrinsic curvature is summed within a 25mm disc (grey circle) to calculate per-vertex local cortical deformation (B). C) Local cortical deformation is increased either due to increased sulci fundi (i.e. more folds) or small-scale surface deformation.

z-scoring, that adjusts for inter-individual differences in the mean and standard deviation. 2) Features were normalised using a between-subject z-scoring, where each participant's per vertex feature was normalised by the mean and standard deviation in the population of healthy controls. This adjusts for inter-regional differences in the mean and standard deviation.

2.2.9 Registration to Template Space

Cortical thickness, grey-white matter intensity contrast, curvature, sulcal depth, local cortical deformation, local gyrification index, "doughnut" measures and FLAIR intensity samples, were registered to an average

space that has an identical number of vertices for each hemisphere (Greve et al., 2013). Lesion masks were registered to both the ipsi- and contra-lesional hemisphere of the average template space.

2.2.10 Statistical Analysis

Individual level analyses

Lesion size

To assess lesion size, the surface area of the lesion mask was calculated in each individual.

Morphometric and intensity features of FCDs

To assess the distribution of morphometric and intensity features in lesions in comparison to healthy cortex, kernel density plots were constructed. For each feature in individual lesions and in the lesion mask applied to the contra-lesional homotopic region, a kernel density plot was created in R (R Core Team, 2014) based on the values from 100 randomly selected vertices from within the mask.

Kernel density plots overcome the discreteness of a histogram by centring a smooth kernel function at each data point and can be applied to nonparametric data, i.e. data not normally distributed around the mean (Deng and Wickham, 2011). As such, they provide a superior method to visualise continuous data. They are used to estimate the probability density function of a random variable. Comparisons of lesional features with features in lesion masks applied to the contra-lesional cortex ensured that features were being compared with areas of cortex of the same size and from the same region of cortex as the individual lesions. The mean for the set of vertices within the lesion mask was calculated for each feature in each individual. This was repeated for the set of vertices within the lesion mask applied to the contra-lesional, homotopic hemisphere.

Finally, the prevalence of abnormal features (z score $> \pm 1.5$) in lesions was assessed to provide an objective index of which features are frequently abnormal in FCDs.

Group level analyses

Mean values of features in individual lesions and in the lesion mask applied to the contra-lesional homotopic region were calculated in MATLAB R2014a (The MathWorks, Natick, MA, U.S.A). Kernel density plots for each feature based on the mean values of features in individual lesions and in the lesion mask applied to the contra-lesional homotopic region were created in R (R Core Team, 2014). For each feature, Levene's test (Trujillo-Ortez and Hernandez-Walls, 2003) was used to check for differences in variance between the distribution of values in lesional versus homotopic regions. Mean, standard deviation (SD), skewness, and kurtosis of features were calculated in MATLAB in order to quantify the shape of the distribution of each feature within the lesion masks.

Assessment of demographics

Demographic variables between patients and controls were compared using a Mann-Whitney U test in SPSS version 22.

2.3 Results

2.3.1 Demographics

A total of 22 patients with a radiological diagnosis of FCD and 28 healthy controls were included. Demographic information for the patients is available in (Table 2.1). The sex of the control group was not significantly different to the FCD group (Mann-Whitney U: 431.50, $p=0.964$). However, the median age of the control group did differ significantly from the FCD group (Mann-Whitney U: 251.00, $p=0.005$). Based on the radiological reports the seizure focus was left-sided in 10 patients, right-sided in 12 patients. Lesion location was largely split between involving the temporal lobe (N=9) and the frontal lobe (N=8), with only 2 lesions in the parietal cortex, 1 in the occipital lobe and 2 multi-lobar. Individual FCD size was extremely variable with surface areas ranging from 2 to 96 cm² (Table 2.2). At the time of study, 11 out of 22 patients with a radiological diagnosis of FCD had undergone focal resections. Seven resections met a histopathological diagnosis of FCD Type IIB, one FCD Type IIA, two demonstrated focal neocortical gliosis only and one did not in fact have an FCD, but a focal ganglioglioma (WHO Grade I) was evident from histological examination. Interestingly, the quantitatively assessed lesional

features of the patient with a ganglioglioma did not stand out from the FCD cohort; i.e. it was not possible to differentiate the patient with a ganglioglioma from the rest of the FCD cohort. This is not unexpected given the molecular, histological (Crino, 2009), radiological (Castillo et al., 1990) and metabolic (Phi et al., 2010) similarities between these two pathologies. In particular, the MRI findings of gangliogliomas are non-specific (Zhang et al., 2008) and the radiological features, such as T2 hyperintensity, overlap those of FCD.

Table 2.1 Paediatric FCD: Demographic & Clinical Information

AGE	SEX	ONSET	DURATION	MRI	HEMI	AED	SURGERY	HISTOLOGY	ENGEL	
1	4.03	F	0.5	3.53	Peri-sylvian & temporal	R	LVT, VPA, CLB	y	Gliosid only	III
2	14.92	M	7	7.92	Inferior parietal	R	LVT, OXCZB, CLB	y	FCD type IIB	III
3	14.93	M	8	6.93	Inferior temporal sulcus *	L	OXCZB, LVT	y	FCD type IIB	Ia
4	9.06	M	2	7.06	Superior temporal sulcus	L	CBZ	y	FCD type IIB	Ia
5	14.31	F	2.5	11.81	Temporal pole	R	LVT, TPR	y	FCD type IIB	Ia
6	15.37	M	9	6.37	Middle temporal gyrus	R	CBZ, TPR	n		
7	13.58	F	0.67	12.91	Medial occipital lobe *	R	LVT	n		
8	9.04	M	1.92	7.12	Anterior temporal lobe	R	VPA, CBZ	y	Subpial gliosis	IV
9	3.79	M	3	0.79	Superior frontal sulcus	L	CLB, TPR, OXCZB, PNT	y	FCD type IIB	Ia
10	13.51	M	4	9.51	Temporal pole	R	LVTG, methylphenidate	n		
11	15.2	M	10	5.2	Anterior temporal pole	L	OXCZB, CLB	y	FCD type IIB	Ia
12	16.21	F	1	15.21	Mesial parietal **	L	CBZ	n		
13	14.77	F	6	8.77	Superior temporal gyrus	L	LVT, LTG	y	Ganglioglioma	Ia
14	14.21	F	0.67	13.54	Superior frontal sulcus	R	VPA, OXCZB, perampanel	y	FCD type IIA	Ia
15	5.49	M	0.5	4.99	Temporal lobe	R	VPA, LVT, LTG, prednisolone	n		
16	12.73	M	3	9.73	Middle frontal gyrus	L	OXCZB, CLB	y	FCD type IIB	Ia
17	11.8	F	3	8.8	Temporal, occipital, posterior parietal lobes	L	LTG, CLB, OXCZB	n		
18	8.18	M	1.5	6.68	Lateral orbital gyrus *	R	VPA, CBZ	n		
19	15.98	M	10	5.98	Precentral gyrus *	L	VPA, LVT, CBZ	n		
20	15.58	F	5	10.58	Inferior frontal lobe	R	VPA, LVT	n		
21	9.22	M	7	2.22	Superior frontal sulcus and precentral sulcus	R	VPA	n		
22	13.82	F	11	2.82	Precentral sulcus *	L	CBZ	n		

Age, onset, and duration are presented in years; MRI: lesion location on MRI report, * originally MRI -ve ** participant had dental braces during MRI scan; AED: current anti-convulsants: LVT = levetiracetam, CBZ = carbamazepine, OXCZB = oxcarbazepine, VPA = sodium valproate, CLB = clobazam, LTG = lamotrigine, TPR = topiramate, PNT = phenytoin; Engel: post-operative surgical outcome according to Engel classification (Engel, 1993), Ia = completely seizure free, III = worthwhile improvement, IV = no worthwhile improvement

Table 2.2 Individual lesion characteristics

Patient	Area	Thickness	GM/WM Intensity	LCD	LGI	Curvature	Sulcal Depth	GM FLAIR	WM FLAIR	Doughnut Thickness	Doughnut Intensity	Abnormal Features
1	95.66	-0.05	-1.52	1.55	1.59	0.06	0.46	-0.45	0.75	0.14	-0.09	3
2	38.7	-3.03	-1.98	2.60	0.37	0.35	0.08	-3.90	-1.24	0.40	0.24	4
3	2.66	0.26	-3.19	-0.21	0.33	0.21	0.25	-5.80	0.25	-0.27	0.31	2
4	31.42	-0.64	-0.59	1.91	0.12	-0.13	0.03	-2.62	-1.12	0.82	-0.24	2
5	20.07	-1.64	-1.64	1.75	2.63	-0.07	-0.11	-3.24	-0.58	0.40	0.91	5
6	17.02	-4.21	-5.44	2.26	0.48	0.09	-0.04	-4.05	-2.09	0.04	-0.64	5
7	24.23	0.29	-2.12	0.77	-0.06	0.00	-0.64	-3.49	-1.06	1.15	-0.27	2
8	34.24	-1.13	-1.71	1.28	0.47	0.10	0.55	-2.72	-1.36	-0.09	0.78	2
9	6.76	-0.04	-0.42	4.15	0.54	0.14	2.04	1.73	4.53	2.71	2.06	6
10	24.24	0.13	-0.74	0.18	0.87	0.07	-0.10	-1.92	-0.58	0.05	0.52	1
11	21.44	-0.46	-1.20	0.42	-0.03	-0.01	-0.23	-2.14	-0.75	-0.50	-0.51	1
12	13.76	1.77	-0.35	-1.45	-1.74	0.22	2.08	0.79	0.79	-0.71	-0.55	3
13	20.63	-1.82	-0.33	1.03	-1.03	0.21	-0.37	-2.64	1.51	-0.12	-0.02	3
14	13.54	0.34	-0.71	3.37	-0.29	0.17	0.79	0.33	0.75	0.64	0.53	1
15	39.2	-2.14	-3.86	0.74	-0.98	0.24	0.18	-2.92	-1.67	-0.14	0.68	4
16	4.18	3.31	-2.37	-1.00	-0.74	0.02	0.74	-0.71	5.47	4.52	3.19	5
17	16.84	-0.50	-1.38	1.38	0.40	0.03	0.04	-1.81	-1.13	0.22	0.29	2
18	3.98	0.64	-0.15	-0.84	-0.27	0.58	2.61	-0.13	-1.02	2.34	1.88	3
19	5.85	0.39	0.85	-1.90	2.30	-0.15	1.06	-0.09	0.72	1.29	-1.21	2
20	6.04	2.03	-1.05	-0.27	-1.39	0.03	-0.91	-3.45	-2.65	0.55	-0.53	3
21	13.63	-0.25	-1.78	-0.97	0.97	0.17	0.06	-2.54	0.95	0.56	-0.03	2
22	6.57	0.51	-0.03	-0.80	0.45	0.17	0.20	-0.46	2.78	1.98	-0.34	2
Prevalence		36%	50%	36%	18%	0%	14%	68%	32%	18%	14%	

Area = surface area of lesion in cm^2 ; The value of individual lesions features (cortical thickness, GM/WM intensity contrast, LCD, LGI, curvature, sulcal depth, GM & WM FLAIR signal intensities and "Doughnut" features) are calculated as the mean of the normalised values from the vertices within the lesion mask. Abnormal features = number of features with a mean z-score of $> \pm 1.5$. Prevalence = percentage of patients where feature is abnormal (z score $> \pm 1.5$)

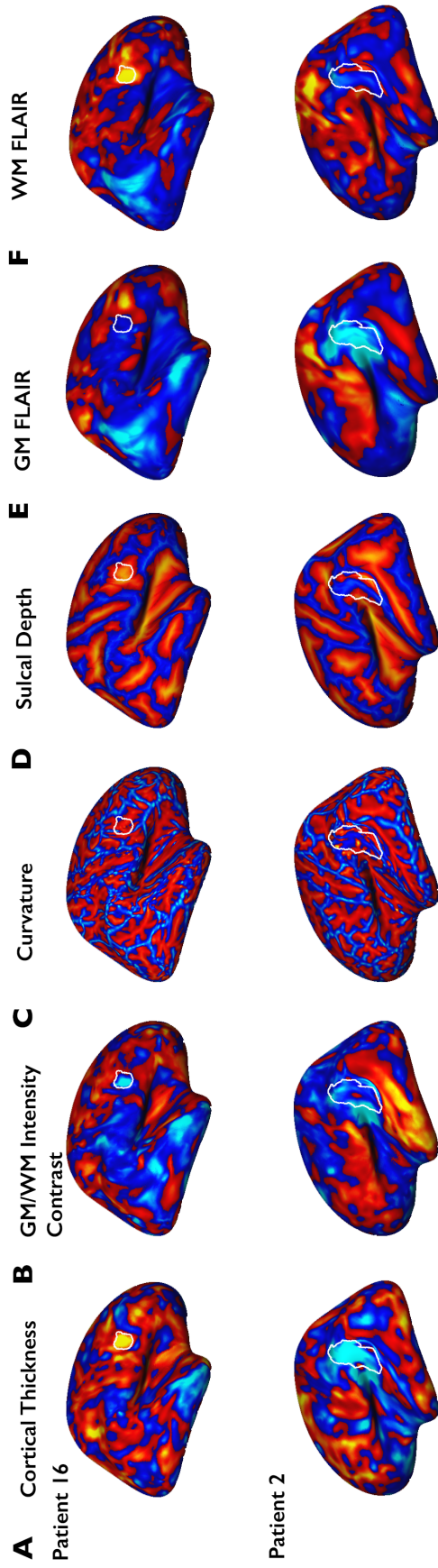
2.3.2 Individual Assessment of Quantitative Surface-based Features

Cortical thickness

Automated surface-based quantification of cortical thickness after intra- and inter-subject normalisation for two representative patients is demonstrated in Figure 2.3. Figure 2.3 A shows the cortical thickness findings in relation to the identified malformation, in Patient 16 and 2. Patient 16 has a small FCD (4 cm²) located in the middle frontal sulcus that is characterised by a focal area of cortical thickening. Following resective surgery, histopathological tissue analysis confirmed the diagnosis of FCD Type IIB. In contrast, patient 2 also has a histologically confirmed FCD Type IIB, yet their lesion is larger (31 cm²) and characterised by cortical thinning. Overall, qualitative analysis of cortical thickness maps viewed on cortical surface reconstructions indicates that FCDs are often characterised by abnormal cortical thickness but some lesions are characterised by cortical thickening and others by thinning.

Quantitative analysis revealed that 8/22 (36%) lesions have either abnormally high or low cortical thickness values (z score $> \pm 1.5$; Table 2.2). Individual kernel density plots demonstrate divergence between cortical thickness in lesion and homotopic region on contra-lesional hemisphere. Figure 2.4 shows kernel density plots of the ten features in three individuals, patient 3, 6 and 16. In patient 16, the kernel density plot (Figure 2.4) of cortical thickness is shifted to the right compared to the healthy homotopic region, indicating that the lesion is characterised by abnormally high cortical thickness as visually indicated in Figure 2.3. In contrast, patient 6 has a medium sized lesion (17 cm²) in the middle temporal gyrus, where the kernel density plot is shifted to the left compared to the healthy homotopic region (Figure 2.4), indicating that the lesion is characterised by abnormally low cortical thickness. In patient 3, who has a very small lesion (3 cm²) in the inferior temporal sulcus, the cortical thickness density plots of lesion and contra-lesional cortex are largely overlapping, suggesting that cortical thickness may not be a particularly distinguishing feature in this case.

Fig. 2.3 Surface Feature Maps



Surface feature maps in patients 2 and 16. Lesions are outlined in white.

Fig. 2.4 Individual Feature Profiles



Kernel density plots showing the distribution of lesional vertices in comparison to vertices from the homotopic area in patients 3, 6 and 16. Green = lesion profile. Pink = healthy homotopic cortex profile.

Grey-white matter intensity contrast

Visualisation of normalised grey-white matter intensity contrast maps overlaid on cortical surface reconstructions indicates that FCDs often demonstrate abnormally low grey-white matter intensity contrast indicative of the blurring at the cortical-subcortical interface (e.g. patient 16 Figure 2.3 B). However, visualisation of grey-white matter surface maps in other patients is less informative (e.g. patient 2, Figure 2.3 B).

Quantitative analysis reveals that abnormally low contrast at the grey-white matter boundary (z score $>\pm 1.5$; Table 2.2) is prevalent in 11 out of 22 cases (50%). This is further exemplified in the kernel density plots where the distribution of lesional vertices is shifted to more negative z scores. Representative plots of grey-white matter intensity contrast in three example patients are illustrated in Figure 2.4.

Curvature and sulcal depth

Surface-based curvature maps accurately identify gyri (curvature values > 0) and sulci (curvature values < 0) and therefore provide an accurate map of individual folding patterns. However, visual inspection of these curvature maps is unable to identify lesions (Figure 2.3 C) and no lesions have mean curvature values above or below a z score of 1.5 (Table 2.2). Similarly, the kernel density plots of lesional and homotopic area vertices are largely overlapping (Figure 2.4). However, visual inspection of individual maps of sulcal depth on cortical surface reconstructions reveals that a small proportion of lesions are characterised by abnormally high sulcal depth i.e. the lesions are positioned in deep sulci. However, these FCDs positioned in deep sulci tend to be small lesions and only represent 14% of the cohort (Table 2.2). Patient 16's FCD (Figure 2.3 D) is one example of a bottom of sulcus lesion. The kernel density plot of sulcal depth in the lesion of this patient (Figure 2.4) is shifted to the right compared to the plot of contra-lesional cortex.

Local Cortical Deformation and Local Gyrification Index

Local cortical deformation (LCD) is abnormal (z score $>\pm 1.5$; Table 2.2) within the lesion in 9 out of 22 cases (41%), whereas local gyrification index (LGI) is only abnormal in 4/22 lesions (18%) which are also characterised by abnormal LCD. Visual inspection of individual maps of LCD indicates that LCD is able to capture regions of abnormal cortical morphology characteristic of some FCDs (Figure 2.2) and appears to be more sensitive to folding changes than LGI. Individual kernel density plots substantiate this idea as although not all lesions are characterised by abnormal folding patterns, density plots of LCD in those that are can be more readily separated from contralateral health cortex than density plots of LGI (e.g. patient 6, figure 2.4).

GM and WM FLAIR Intensity

Visualisation of normalised grey and white matter FLAIR signal intensity maps (Figure 2.3 E/F) highlights that lesions can be characterised by abnormal T2 signal intensity. In patient 2, the FCD has high FLAIR signal intensity within the white matter, whereas, in patient 16, the FCD has low FLAIR signal intensity within the grey matter. The prevalence of abnormal (z score $>\pm 1.5$; Table 2.2) mean grey and white matter signal within the lesion is 68% and 32% respectively. Kernel density plots of normalised GM and WM signal intensity in individual patients demonstrate that lesions can be characterised by abnormally low or high FLAIR signal. For example, in patients 3 and 6 (Figure 2.4), the distribution of GM FLAIR signal is shifted to the left in the lesion compared to the distribution within healthy cortex, whereas, WM FLAIR signal is shifted to the right (i.e. FLAIR hyperintensities) in patient 3 and shifted to the left (i.e. FLAIR hypointensities) in patient 6.

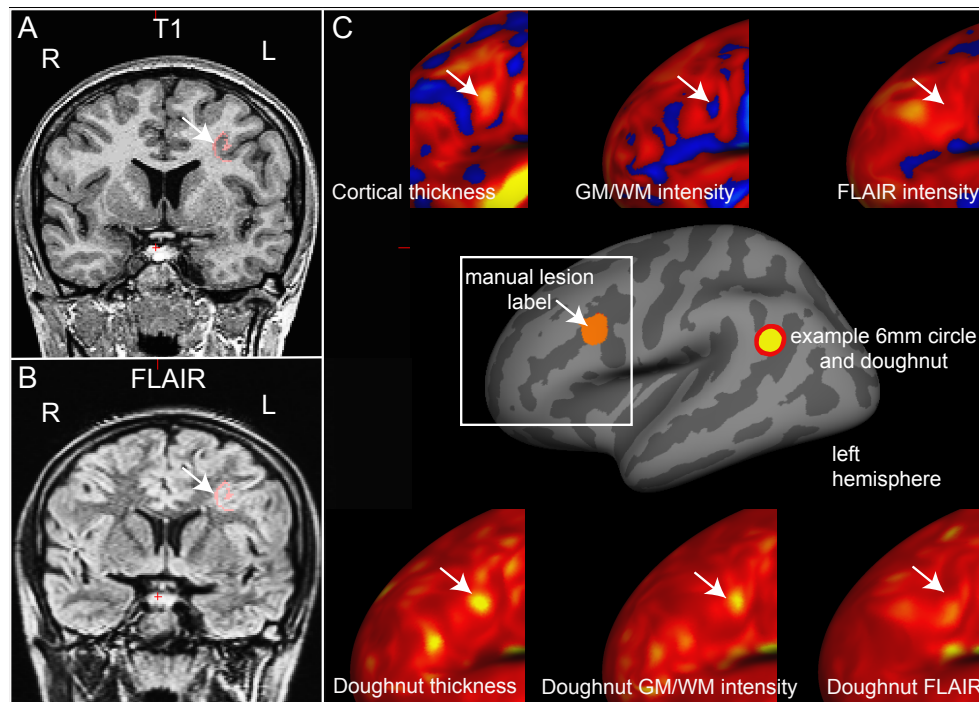
"Doughnut" thickness and intensity contrast

Qualitative analysis of the "doughnut" maps indicated that they may provide useful surface features for the detection of FCDs. By quantifying local changes in cortical thickness and grey-white matter intensity (Figure 2.5 (C)) this method highlighted locally abnormal areas of cortex. However, these metrics were judged to be sensitive but relatively unspecific. For example, in small lesions, the centre of the lesion was often identified, whereas in larger lesions, it is the lesion boundaries that were detected. As well as identifying the lesion as an area of high variability in cortical structure, the "doughnut" method did identify many other areas of high cortical variability, thus suggesting their limited use in univariate analyses and the need for their use in combination with other features. Mean doughnut thickness or intensity were only abnormal (z score $>\pm 1.5$; Table 2.2) in 18% and 14% of lesions respectively. Kernel density plots in patient 16 (Figure 2.4) illustrate an exemplar patient where doughnut profiles assist characterisation of the lesion.

2.3.3 Group-level Lesion Characteristics

Figure 2.6 shows the kernel density plots for each feature based on the mean values of features in individual lesions and in the lesion mask applied to the contra-lesional homotopic region. In contrast to the feature profiles

Fig. 2.5 "Doughnut" Features

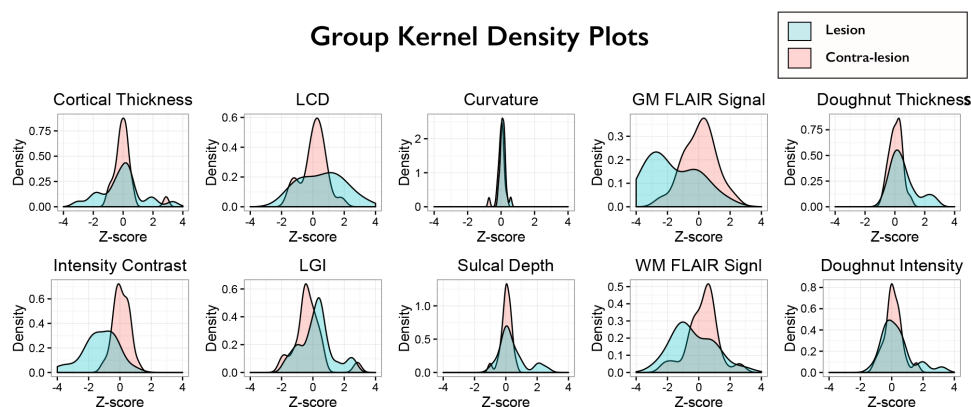


Example of "Doughnut" method feature maps in a patient with a left middle frontal sulcus FCD. A) T1 image B) FLAIR image - manual lesion label in pink, white arrow indicates lesion. C) Inflated surface view with manual lesion label (orange) and example of 6mm doughnut and circle. Upper panel - intra-subject normalised cortical thickness, grey-white matter contrast and FLAIR intensity (sampled at 50% cortical thickness) overlays around lesion area (white square). Lower panel - "doughnut" thickness, "doughnut" grey-white matter intensity and "doughnut" FLAIR (sampled at 50% cortical thickness). This lesion is characterised by a subtle increase in cortical thickness, though much less thick than the insula (bright yellow), subtle decrease in contrast at the grey-white matter boundary and no obvious FLAIR hyperintensity. "Doughnut" thickness and "doughnut" grey-white matter intensity contrast highlight lesion, in this particular example "doughnut" FLAIR is of less use. All surface measures also identify other areas of cortex with extreme values and must therefore be used in combination.

of homotopic, healthy cortices, which are normally distributed and centre around zero, feature profiles of lesions often have increased variance or skewed distributions. FLAIR signal intensity and grey-white matter intensity contrast profiles are negatively skewed indicating that overall lesions are characterised by reduced FLAIR signal intensity and blurring of the grey-white matter boundary. Lesional cortical thickness and LCD have increased variance (Levene's test $p < 0.05$), likely reflecting that some lesions are characterised by abnormally high values of cortical thickness and LCD and others by abnormally low values. Sulcal depth, doughnut thickness and doughnut intensity features have bimodal distributions

indicating a small proportion of lesions are characterised by increased sulcal depth or doughnut features. The profiles of curvature and LGI are less distinguishable from homotopic areas, indicating limited use in lesion profiling.

Fig. 2.6 Group Feature Profiles



Kernel density plots showing the distribution of mean feature values in lesional and homotopic cortices across the cohort of paediatric FCD patients. Green = lesion profile. Pink = healthy homotopic cortex profile.

Table 2.3 Group lesion characteristics

	Mean	STD	Skew	Kurtosis
Thickness	-0.28	1.65	-0.27	3.57
GM/WM Intensity	-1.44	1.40	-1.11	4.43
Curvature	0.11	0.16	0.85	4.44
Sulcal Depth	0.40	0.88	1.13	3.69
LCD	0.73	1.59	0.30	2.42
LGI	0.23	1.08	0.36	3.09
GM FLAIR Signal	-1.92	1.84	0.09	2.47
WM FLAIR Signal	0.13	2.03	1.20	3.95
Doughnut Thickness	0.73	1.22	1.60	5.36
Doughnut Intensity	0.32	1.01	1.24	4.40

Mean = mean of z scores, STD = standard deviation of z scores, Skew and Kurtosis of z scores within lesions.

Across individuals, the mean, standard deviation, skew and kurtosis of each feature within the lesion masks is available in Table 2.3. At the group-level, only FLAIR signal intensity in the grey matter has an abnormal mean (Z score $> \pm 1.5$), reflecting how consistently across the cohort FLAIR signal is decreased within the lesion. In different lesions

the values of cortical thickness, LCD, as well as FLAIR signal in grey and white matter are highly variable. This is reflected in the high standard deviations. Doughnut thickness has a positively skewed distribution, reflecting the subgroup of lesions where most vertices are characterised by increased variability in cortical thickness (i.e. small lesions that are characterised by increased cortical thickness).

2.4 Discussion

The radiological features of focal cortical dysplasias can be subtle and are overlooked in up to 40% of cases (Mellerio et al., 2012; Radhakrishnan et al., 2016). Whereas, automated, quantitative analysis of FCD features is objective and user-independent. In contrast to the feature profiles of homotopic, healthy cortices, which are normally distributed and centre around zero, feature profiles of lesions often have increased variance or have shifted or skewed distributions. At the group level, FLAIR signal intensity and grey-white matter intensity contrast profiles have shifted distributions; lesional cortical thickness and LCD have increased variance; whereas sulcal depth has a bimodal distribution indicating a small proportion of lesions are characterised by increased sulcal depth. At the individual level, lesions are extremely variable in terms of size, location and quantitative features. However, all lesions were characterised by at least one abnormal feature (z score $> \pm 1.5$). As such, surface-based morphometric and intensity analysis is able to capture characteristic radiological features of paediatric FCDs.

Thickness

Comparisons between histology- and MRI-based measures of cortical thickness generally show good correspondence (Fischl and Dale, 2000; Scholtens et al., 2015; Song et al., 2015). However, MRI-based morphological measures can be confounded by other microstructural changes, such as heavy cortical myelination in the motor cortex blurring the grey-white boundary and leading to underestimates of cortical thickness (Glasser and Van Essen, 2011; Scholtens et al., 2015). This is particularly problematic in FCDs where blurring is a characteristic abnormality (Blümcke et al., 2010). At the group level, cortical thickness was much more variable in lesional cortex than contra-lesional healthy cortex. This can be explained

by the fact that at the individual level some lesions were characterised by thin cortex and others by thick cortex. However, overall 36% of lesions have a mean cortical thickness that is abnormal (z score $> \pm 1.5$). Therefore, in accordance with the previous literature, cortical thickness is a useful feature for the detection of lesional cortex (Bernasconi et al., 2011). It is also important to note that anti-epileptic drugs (AEDs), such as sodium valproate, can produce atrophic changes (Pardoe et al., 2013). However, one would expect these effects to be generalized, global effects and not limited to the lesional cortex. Thus, the stringent intra-subject normalization should account for any global atrophic effects of AEDs. Thus, either because different FCD subtypes are characterised by either increased or decreased cortical thickness or due to difficulty segmenting grey and white matter in lesions due to intensity abnormalities, paediatric FCDs can be characterised by either high or low cortical thickness.

Grey-white matter intensity contrast

In accordance with a body of radiological literature (Bernasconi et al., 2011; Blümcke et al., 2010; Mühlebner et al., 2012) and automated computational anatomy studies in adults (Ahmed et al., 2015; Hong et al., 2014; Thesen et al., 2011), this study finds that paediatric FCDs are characterised by blurring at the interface between the grey and white matter. This is a relatively consistent finding occurring in 50% of the lesions. The histopathological underpinning of blurring may be related to demyelination, increased heterotopic neurons in the white matter, cortical dyslamination and reduced neuronal densities (Mühlebner et al., 2012).

Curvature and sulcal depth

Mean curvature, as the average of principal curvatures, provides a quantitative map of individual cortical folding patterns where convex areas reflect gyri and concave areas reflect sulci. At both the group and individual level, no large differences in curvature were found between lesional cortex and homotopic cortex on the contra-lesional hemisphere. Although this study indicates that curvature does not have discriminatory value in differentiating lesional from nonlesional vertices, this feature may still be useful within a multivariate framework as it provides information as to whether a vertex is from a gyrus or a sulcus. As gyri are thicker than sulci, this information may assist in revealing whether a thickness value

is abnormal in the context of the vertex's morphological position.

The bimodal distribution of sulcal depth highlights that some paediatric lesions, like adult FCDs (Besson et al., 2008a) are positioned at the bottom of deep sulci, but it is only a small proportion (14%). Unlike in adult studies, where the majority of FCDs are located in the frontal lobe, paediatric FCDs can be located anywhere in the cortex. Within this cohort they were largely split between frontal and temporal neocortices with only a few cases in parietal or occipital lobes.

Grey and white matter FLAIR intensity

At both the group and individual level, normalised FLAIR signal intensity sampled in the grey and white matter are features that assist with discriminating lesional from non-lesional cortex. Abnormal signal intensity both on T1 and FLAIR scans in FCD has been related to demyelination, which is associated with severe fibre loss and altered myelin sheaths, abnormal cells and sometimes oedema (Garbelli et al., 2011; Mühlebner et al., 2011; Zucca et al., 2016). Both T1 and FLAIR sequences, which are standard structural MRI scans acquired as part of an epilepsy protocol (Duncan et al., 2016), are able to delineate the brain anatomy but are not specific to tissue property variations. A change in image intensity can be caused by a range of underlying neurobiological tissue properties, such as water, myelin and iron content, taking place on the microstructural scale (Lorio et al., 2016; Weiskopf et al., 2013). Quantitative MRI (qMRI) parameters are specific to tissue structure and biophysical properties at the micrometre scale. These parameters are neuroimaging biomarkers for myelin, water and iron content (Bilgic et al., 2012; Deoni et al., 2015; Schweser et al., 2011), and may provide the MRI "fingerprints" (Ma et al., 2013) of brain tissue microstructure (Weiskopf et al., 2013). By linking brain tissue property changes with image intensity, qMRI may assist understanding of the neurobiological mechanisms underlying a change in morphometry. As such, future work replacing or adding sampling from qMRI sequences may assist FCD lesion profiling.

"Doughnut" method

The "doughnut" method introduced here created individual surface maps that were able to identify abnormal changes in cortical thickness and

grey-white matter boundary intensity across the cortex. Focal cortical dysplasias are often characterised by abnormal cortical thickness and blurring of the grey-white matter boundary. However, there are normal changes in cortical structure that might obscure these changes. For example sulci are thinner than gyri (Brodmann, 1909; von Economo and Koskinas, 1925) and small FCDs, characterised by cortical thickening, are often located at the bottom of sulci (Besson et al., 2008a). Thus, a lesion at the bottom of a sulcus, may be abnormally thick relative to the surrounding sulcal cortex and yet a measurement of absolute thickness might still fall within the normal range for the cortex. However, the "doughnut" method was specifically designed to obviate such difficulties by taking into account values of neighbouring vertices, to measure local changes. As such this method was sensitive to such subtle structural changes, that might be missed by solely considering values from isolated vertices, which has to date been the established approach (Ahmed et al., 2015; Hong et al., 2014). Importantly these "doughnut" maps could be calculated on any surface registered maps and could therefore be used to highlight local structural changes using a much wider range of measures or imaging modalities.

Although, at the group-level the bimodal and trimodal distribution of the kernel density plots in lesions might suggest that these measures are only abnormal in a small proportion of lesions, it is important to note that if these features are only picking up the borders of larger lesions, only vertices near the boundary of the lesion will have abnormal values. Thus, the mean lesional value calculated here may under represent the utility of these features within multivariate frameworks for lesion detection.

Local cortical deformation

Local cortical deformation (LCD) maps small-scale alterations in cortical shape. For example, it would differentiate a golf ball from a smooth sphere by being sensitive to the dimples in the golf ball's surface. As it is based on intrinsic curvature, a mm-scale metric of cortical deformation or differential expansion of the cortex, it is more sensitive to subtle shape abnormalities than LGI, a cm-scale measure (Ronan et al., 2011; Schaer et al., 2008). Differential growth is when one area of the cortex grows faster than another. Positive intrinsic curvature occurs when the centre of an area grows faster than the surrounding area and it results in a hump

shape. Negative curvature occurs when the surrounding area grows faster than the centre. It results in a saddle-like shape. The degree of positive or negative intrinsic curvature is dependent on the degree of differential growth. Thus, abnormal differential growth results in abnormal folding patterns and altered values of LCD. In this work, LCD is a sensitive metric to quantify folding abnormalities and to differentiate lesional from healthy cortex at the individual level. However, as FCDs can be characterised by either low or high LCD values, at the group level, this is reflected in the increased variance of the distribution rather than a left or right shift. The potential applicability of this metric is not limited to FCDs. LCD is likely to be helpful in the delineation of polymicrogyrias and other malformations of cortical development.

Local gyrification index

Local gyrification index is an established measure of folding that has been previously used to index maturation of cortical folding patterns (Li et al., 2014) and abnormal cortical folding in pathologies such as autism spectrum disorder (Ecker et al., 2016), schizophrenia (Palaniyappan and Liddle, 2012) as well as in adults with epilepsy (Thesen et al., 2011). However, as it is measured on a centimetre scale, it is a relatively crude measure that may only be sensitive to large-scale folding changes. This is reflected in the fact that alterations in LGI ($z > \pm 1.5$) were found in less lesions than LCD abnormalities. Furthermore, at a group level LGI was unable to differentiate healthy from lesional cortex. As LCD abnormalities were found in all the patients with LGI abnormalities and in four additional patients, LCD may be a more sensitive marker of folding abnormalities in FCDs.

Quantitative analysis of paediatric FCDs can capture characteristic radiological features like abnormal cortical thickness, grey-white matter blurring, signal abnormalities and irregular cortical folding patterns. However, individual lesions are variable and there is no single feature capable of always distinguishing these lesions. Furthermore, some features, such as cortical thickness, demonstrate no difference in mean value at the group level but increased variance due to some individual lesions being characterised by thin cortex and others by thick cortex. While the characterisation of lesions into thin and thick may be a computational error resulting from where the grey-white matter boundary is placed in

lesional cortex; surface-based analyses are still a very effective way to delineate lesions given the current limitations of volumetric approaches and small sizes. For further discussion of these issues, see discussion section of Chapter 3. Similar to radiologists, who have to use multiple MR modalities and features to accurately detect these subtle lesions, successful automated approaches for lesion detection and in vivo FCD subtyping will require nonlinear, multivariate approaches, such as the incorporation of multiple features into nonlinear machine-learning classifiers (see Chapter 3).

Chapter 3

Automated detection of focal cortical dysplasias in paediatric epilepsy

3.1 Introduction

To overcome the difficulty of radiological assessment of FCDs, automatic detection methods build a series of morphological measures into an identification algorithm to improve detection rate (Ahmed et al., 2015; Hong et al., 2014). For example, surface-based techniques may be used to calculate various measures such as cortical thickness (Fischl and Dale, 2000), signal intensity in the grey or white matter (Salat et al., 2009), local gyrification index (LGI) (Schaer et al., 2008), sulcal depth and curvature (Fischl et al., 2004) at each point on the cortical surface (henceforth vertices). These measures, when incorporated into machine learning frameworks, provide detection rates as high as 74% in adult cohorts (Hong et al., 2014). In comparison, other approaches such as voxel-based morphometry (VBM), while often providing high sensitivity to detect MRI visible lesions, usually require visual assessment of the output maps, thus they are not fully automated. Furthermore, they are less easily incorporated into multivariate frameworks meaning that multiple output maps have to be independently reviewed. The long-term aim of this work is the development of diagnostic decision aids that can be incorporated into clinical practice.

While progress has been made in improving the detection of FCDs in adults using structural neuroimaging techniques (Thesen et al., 2011;

Wang et al., 2015) and automated classifiers (Ahmed et al., 2015; Hong et al., 2014), automated lesion classification has not been attempted in a solely paediatric cohort despite this being a congenital condition (Chen et al., 2014). Therefore, an automated tool capable of improving the detection of FCD in the paediatric population would represent an important step in improving the quality and consistency of presurgical evaluation with implications for surgical outcome. However, owing to the particular differences between adult and paediatric brains it is unclear that current approaches are suitable or would yield similar results.

As mentioned in the previous chapter, applying automated lesion detection methods in a paediatric population raises a number of unique challenges. First, between the ages of one and 18 the cortex undergoes major structural changes including vast increases in brain size and surface area, cortical thickening and thinning (Giedd et al., 2015; Gogtay et al., 2004; Raznahan et al., 2011; Shaw et al., 2008), as well as changes in gyrification (Li et al., 2014) and myelination (Deoni et al., 2015; Whitaker et al., 2016), thus identifying focal abnormalities in cortical structure requires careful consideration of developmental trajectories. For example, an apparent thickening of cortex may not necessarily signify an abnormality for a given individual at a given age. Second, motion artefacts are more prevalent in paediatric imaging affecting the accuracy of established surface-based features (Ducharme et al., 2015). Sensitivity to detect FCDs may therefore be improved by novel features and post processing methods measuring different aspects of cortical structure.

My overall approach to develop a tool for automated FCD detection, which addresses the particular challenges of a paediatric cohort, was to optimise the ability to find and quantify each area of cortex in terms of how it differed from healthy cortex. As identified in Chapter 2, characteristics of individual FCD lesions are variable and thus successful approaches were likely to involve the incorporation of multiple features quantifying different radiological identifiers of FCDs. Furthermore, some metrics, such as the "Doughnut" measures, were judged to be sensitive but relatively unspecific, as they identified many other areas of high cortical variability, thus suggesting their limited use in univariate analyses and the need for their use in combination with other features.

To this end, the following surface-based metrics that have been established for FCD detection in adults were computed: cortical thickness, grey-white matter intensity contrast, FLAIR signal intensity, curvature and sulcal depth. Novel features developed in Chapter 2 were included as complementary metrics of surface morphology such as local cortical deformation as well as post-processing methods such as the "doughnut" method, which quantifies local variability in cortical morphometry / MRI signal intensity. Per-vertex inter-hemispheric asymmetry calculates the difference in a feature between the left and right hemispheres. Radiologists use hemispheric asymmetries as identifiers of abnormal areas of cortex. This novel post-processing method is an objective means to assess these inter-hemispheric differences.

The novel structural markers and post-processing methods - local cortical deformation, inter-hemispheric asymmetry and the "doughnuts" of structural measures - were then combined with the established surface-based metrics in a neural network trained to classify cortical regions into lesional and nonlesional vertices. Furthermore, I directly compared the novel measure of cortical shape, LCD, with the existing measure LGI.

3.2 Materials & Methods

3.2.1 Participants & MR Imaging

The same cohort of participants and MR scans were used as in Chapter 2. Anonymised FLAIR and T1 volumetric scans were rated from one to five according to severity of motion artefact. The following classification system was used: 1) no visible motion artefacts, 2) subtle artefacts visible, 3) mild ringing artefacts, 4) severe ringing artefacts and 5) adjacent gyri indistinguishable due to motion.

3.2.2 Cortical Reconstructions & Lesion Masks

The same manually corrected FreeSurfer cortical reconstructions and manually segmented lesion masks used in Chapter 2 were used.

3.2.3 Established Surface-based Measures

FreeSurfer was used to calculate the established measures: cortical thickness, grey-white matter intensity contrast, curvature, sulcal depth and

FLAIR intensity at each vertex of the 3D cortical reconstruction, more details are available in Chapter 2. Unlike in the previous chapter, FLAIR intensity was sampled more extensively - at the grey-white matter boundary as well as at 25%, 50% and 75% depths of the cortical thickness and at 0.5mm and 1mm below the grey-white matter boundary. This was because in chapter 2 FLAIR signal was the feature most consistently abnormal in lesions. Yet, lesions differed in whether the signal abnormality was in the GM or WM. By sampling the intensity more thoroughly throughout the cortical ribbon and underlying white matter, I aimed to increase the likelihood of capturing the signal alterations.

3.2.4 Novel Surface-based Measures

The doughnut method was applied (details in Chapter 2) to cortical thickness and grey-white matter intensity contrast. In addition, "doughnut" feature maps of FLAIR signal intensity at the grey-white matter boundary, 25%, 50% and 75% cortical depths and 0.5mm and 1mm below the grey-white matter boundary were calculated. "Doughnut" thickness, "doughnut" intensity contrast and the six "doughnut" FLAIR signal intensity maps were smoothed using a 10mm FWHM Gaussian kernel, to remove noise while maintaining local specificity. Local cortical deformation was calculated per vertex in each participant as per the methodology in Chapter 2.

3.2.5 Normalisation of Features

The following features were smoothed using a 10mm FWHM Gaussian kernel - cortical thickness, grey-white matter intensity contrast and FLAIR signal intensities. In every individual, features underwent intra- and inter-subject normalisation following the same procedure as in Section 2.2.8.

3.2.6 Interhemispheric Asymmetry

Cortical thickness, grey-white matter intensity contrast, local cortical deformation and FLAIR intensity samples, were registered to an average space that has an identical number of vertices for each hemisphere (Greve et al., 2013). The right hemisphere vertex values for each feature were subtracted from the left hemisphere values to create an asymmetry map. In the resulting asymmetry map, positive values indicated greater feature

values on the left hemisphere while negative indicated that the right hemisphere has a higher value for that vertex.

3.2.7 Statistical Analysis

Machine Learning Classification

The Neural Network Toolbox in MATLAB R2014a (The MathWorks, Natick, MA, U.S.A) was used to create a nonlinear classifier. An artificial neural network is a group of interconnected nodes, each of which represents an artificial neuron. It is a supervised, feedforward network that can be trained to recognise complex patterns. This network has one-way connections from input to output layers and via a layer of hidden nodes (Figure 1.9). Each node is activated by a differently weighted combination of features, which are optimised during the training phase. The outputs of the hidden nodes are then combined to determine whether the set of features of that a particular vertex resemble healthy (output value closer to zero) or lesional (closer to one) cortex.

There is no established procedure for choosing the structure of the neural network, i.e. how many hidden layers and how many nodes in each layer. A single hidden layer neural network was chosen as the classifier as they can be rapidly trained on large datasets, are flexible and incorporate the capabilities of support vector machines. Choosing the number of nodes is a balance between ensuring that you have enough nodes to represent all the complex combinations of features and the time and processing power required to train and test the neural network. Unless otherwise stated, the number of nodes in the network was determined through running a principal component analysis (PCA) on the input surface-based features in the control cohort, and using the number of components that explained over 99% of the variance.

Neural network classifiers were trained using surface based measures from vertices from each patient (Figure 3.1). For the full network the 28 input measures were - normalised cortical thickness, normalised grey-white matter intensity contrast, sulcal depth, mean curvature, the 6 normalised FLAIR intensity samples at different cortical depths, normalised LCD, "doughnut" thickness, "doughnut" intensity contrast, "doughnut" FLAIR intensity at different cortical depths as well as the normalised interhemispheric asymmetry measures of cortical thickness, grey-white matter

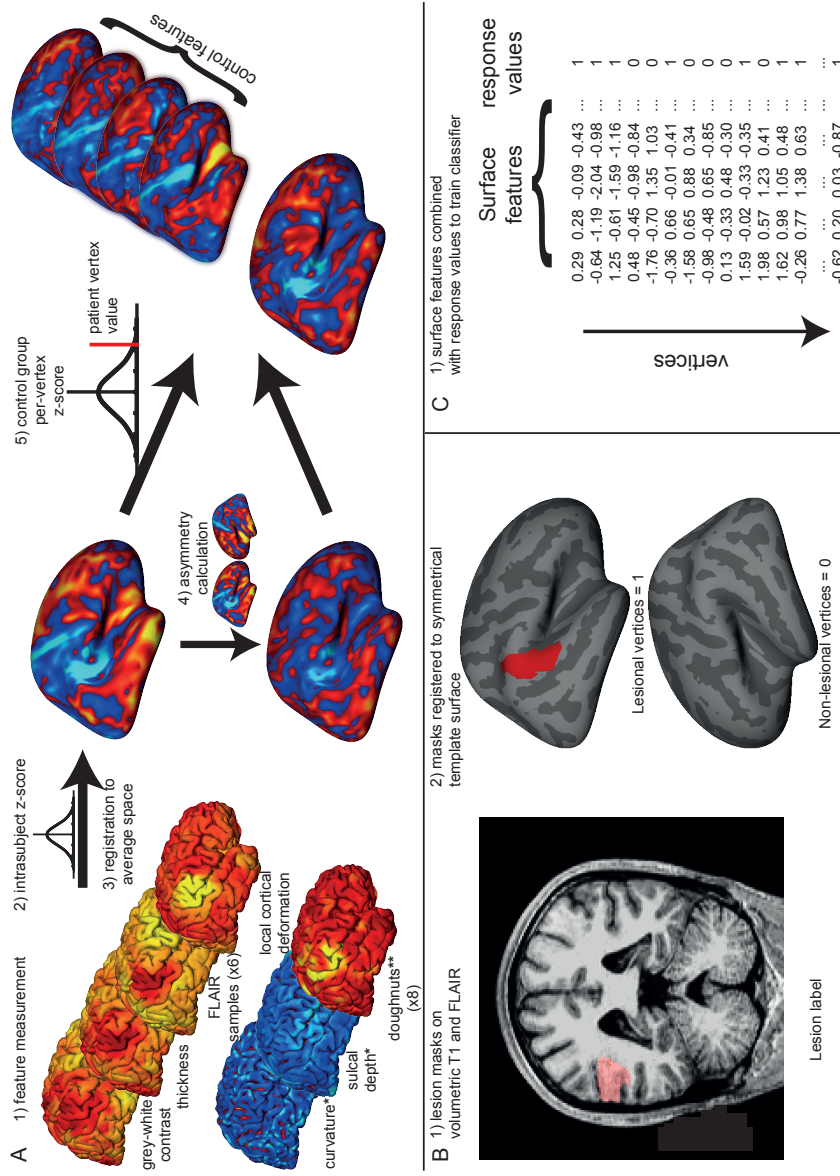
intensity contrast, the FLAIR intensity samples and local cortical deformation.

As neural networks are a black box and it is extremely difficult to know which features are being used to classify the data, separate neural networks were also trained using individual surface based features. This enabled an evaluation of the discriminatory value of specific individual features. As the activation function of each node is linear, for neural networks trained on individual features, 2 nodes were included in the hidden layer to enable sensitivity to both abnormally high and low values.

Each vertex in the training dataset was given one of two response values - lesional cortex or healthy cortex. Vertices from within each lesion mask were given a response value of one, while vertices from contralateral hemisphere of each patient were given the value zero, i.e. healthy cortex. Ipsilateral healthy vertices were disregarded from the training set to minimise the number of misclassified vertices; for example where lesions extend beyond what is visible through conventional radiological analysis. For testing the network the data were split in the following manner. For each patient, the neural network was trained using data from 21 patients and then tested on the 22nd patient. When training the network the data must be split into training and validation data, where 70% of the pooled vertices from all 21 patients are used for classifier training and 30% are used for validation. The validation data is used to evaluate the progress in training the model and to prevent the model from overfitting the training data. This can be detected when the training accuracy continues to increase but the validation accuracy falls. The trained network is then tested on the data from the previously unseen patient. Training, validation and testing was then repeated for each patient. This ensures when the networks are tested on a patient, they have not been trained with any of the data from that particular patient, mimicking how the network would be applied in clinical practice.

The full matrix of data input to the neural network and reference list of features is available from the University of Cambridge's online data repository <https://www.repository.cam.ac.uk/handle/1810/261717>.

Fig. 3.1 Overview of classifier



A) 1. Quantification of surface based features on each individual including established features - cortical thickness, FLAIR intensity (sampled at 6 cortical depths), grey-white contrast, curvature, sulcal depth - and novel features - "doughnut" method (for 6 FLAIR intensity samples, cortical thickness and grey-white contrast) and local cortical deformation (LCD). 2. Intra-subject normalisation (z-score). 3. Registration to the symmetrical template brain. 4. Per-vertex interhemispheric asymmetry calculations for each feature map. These serve to filter symmetrically extreme values such as thin primary sensory cortices. 5. Per-vertex normalisation by the controls of z-scored feature maps and asymmetry maps. These serve to filter common regional differences or asymmetries such as the planum temporale. * = feature undergoes steps 1, 2 and 5 only. ** = feature undergoes steps 1 and 2 only. B) 1. Volumetric lesion masks are manually segmented using T1 and FLAIR images. 2. Lesion masks are mapped to the surfaces and then to the symmetrical template brain. Lesional vertices are given a response value of 1, and contralateral non-lesional vertices are given a value of 0. C) 1. Neural network classifier is trained on surface based features and response values using leave one out cross-validation. Each row corresponds to a single vertex on one patient, each column to a surface based feature or the response variables.

Clustering

The output probability maps from the classifier are thresholded so that only the top 5% of vertices remain and surviving vertices are grouped into neighbour-connected clusters. The smallest clusters, below 200 vertices ($\sim 1\text{cm}^2$) were excluded as noise. The primary source of false positive findings are due to reconstruction errors, where a small group of vertices are placed in an incorrect position. These can arise from poor temporal lobe contrast, motion artefacts or kinks in the mesh surfaces. While it is possible for lesions to be smaller than 1cm, noise-induced abnormalities are far more common at this scale. Improvements in MR image quality and increased training data-size should in future alleviate the need to exclude these small clusters.

The cluster with the highest mean probability value is considered the putative lesion location. The automated lesion detection method is considered successful if this cluster overlaps the lesion mask. This final step is designed to always output one putative lesion location per test subject, as a radiological aid to FCD diagnosis. As a consequence, specificity cannot be calculated.

Evaluation of novel features

Surface based features were evaluated using two methods - receiver operator characteristics of individual surface-based features and sensitivity of classifiers containing combinations of features. To assess the discriminatory value of individual surface-based features receiver operator characteristics (ROC) and area under the curve (AUC) were calculated per vertex for the classifiers trained on each individual feature.

Evaluation of the full impact of these novel features was carried out by comparing the sensitivity of the classifier including novel features, to that of a classifier based on solely established surface-based features for FCD detection (normalised cortical thickness, normalised grey-white matter intensity contrast, sulcal depth, mean curvature and the 6 normalised FLAIR intensity samples). To evaluate whether local cortical deformation is a more sensitive marker of cortical folding complexity than local gyrification index, a subsequent analysis compared the sensitivity of the classifier with all novel features (including local cortical deformation) to

the sensitivity of a classifier replacing local cortical deformation with local gyrification index.

Assessment of demographics and movement artefact

Demographic variables between patients and controls, and motion ratings of FLAIR scans between detected and non-detected groups were compared using a Mann-Whitney U test in SPSS version 22.

3.3 Results

3.3.1 Demographics

Demographic information for the 22 patients with a radiological diagnosis of FCD who were included in this study is available in Chapter 2 (Table 2.1). Median subjective motion rating across all patients' FLAIR scans was 3 (range 1-5; Table 3.1).

3.3.2 Assessment of Novel Surface-based Feature Maps

For quantitative evaluation of individual established and novel features, receiver operating characteristics and area under the curve (AUC) were calculated using the output of a 2-node neural network classifier (to enable sensitivity for both abnormally high and low values) (Figure 3.2). Receiver operating characteristics are created by titrating the threshold placed on the output of the classifier and calculating the number of true positives and false positives. For example, when the output of the 2-node neural network classifier, which is a probability map, is thresholded at 0, all vertices will be identified and the TP and FP rates will both be 1 and this is plotted. This is then repeated at different thresholds.

These revealed that individually, all novel surface-based features add some discriminatory value ($AUC > 0.5$). Of the established features, FLAIR intensity appeared most discriminatory ($AUC = 0.83$) followed by GM- WM contrast ($AUC = 0.80$) and thickness ($AUC = 0.63$). Individual novel features all added some discriminatory value ($AUC > 0.5$) with FLAIR intensity asymmetry performing highest across all measures ($AUC = 0.87$). It is important to note that these statistics were calculated on a per-vertex basis, and therefore do not differentiate between when all lesions are partially detected and when entire lesions are either detected or

Table 3.1 Automated detection of paediatric FCDs

PATIENT	MRI	HEMI	MOTION	ARTEFACTS	DETECTED
1	Peri-sylvian & temporal	R		4	y
2	Inferior parietal	R		3	y
3	Inferior temporal sulcus *	L		2	y
4	Superior temporal sulcus	L		3	y
5	Temporal pole	R		1	y
6	Middle temporal gyrus	R		1	y
7	Medial occipital lobe *	R		2	y
8	Anterior temporal lobe	R		3	y
9	Superior frontal sulcus	L		3	y
10	Temporal pole	R		5	n
11	Anterior temporal pole	L		2	y
12	Mesial parietal **	L		5	n
13	Superior temporal gyrus	L		2	y
14	Superior frontal sulcus	R		3	y
15	Temporal lobe	R		3	y
16	Middle frontal gyrus	L		2	y
17	Temporal, occipital, posterior parietal lobes	L		2	y
18	Lateral orbital gyrus *	R		5	n
19	Precentral gyrus *	L		3	n
20	Inferior frontal lobe	R		2	y
21	Superior frontal sulcus and precentral sulcus	R		3	n
22	Precentral sulcus *	L		3	n

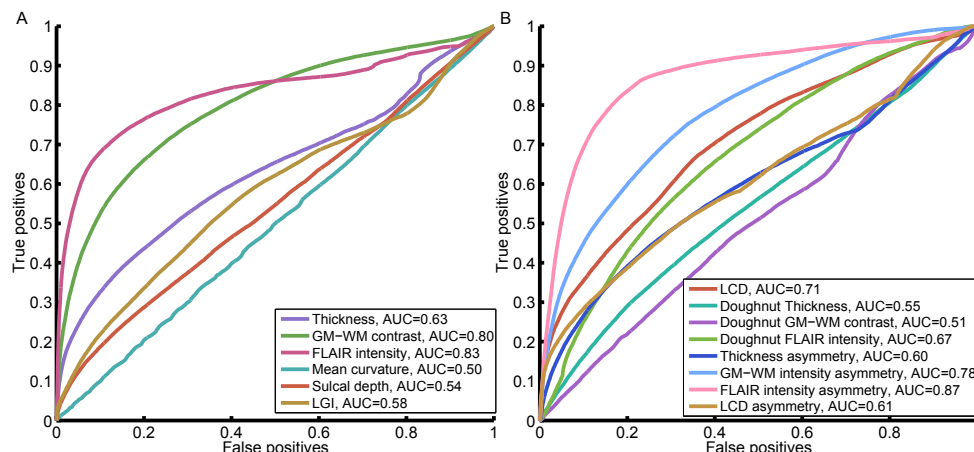
MRI: lesion location on MRI report, * originally MRI -ve ** participant had dental braces during MRI scan; Motion/Artefacts: ranking according to motion classification system; Detected: y = classifier detects lesion as primary cluster, n = lesion undetected.

undetected by specific metrics. Moreover, if there were any undiagnosed multifocal structural abnormalities outside of the radiological lesion mask, these would have appeared as false positives incorrectly reducing the AUC. Nevertheless, these results strongly suggested that classifiers might be improved by the incorporation of these novel features.

3.3.3 Establishing the Parameters for the Classifier

The principal component analysis using both novel and established features (No. of features = 28) in the control cohort revealed 11 principal components were required to explain over 99% of the variance compared to 6 when using solely established features (No. of features = 11). The neural network was therefore trained using the full 28 established and novel features with 11 nodes and 1 hidden layer. The sensitivity of the output of this classifier was then compared with classifiers trained using only

Fig. 3.2 Receiver operator characteristics and AUC for classifiers



Receiver operator characteristics and AUC for classifiers trained on individual established (A) and novel (B) features. Within established features, FLAIR signal intensity, cortical thickness and grey-white matter intensity contrast are most discriminatory of lesional vertices. Within novel features, interhemispheric FLAIR intensity asymmetry, grey-white matter contrast asymmetry and local cortical deformation are the most discriminatory of lesional vertices.

the 11 previously established surface features. Two classifiers were trained and tested, one with 6 nodes and the other with 11 nodes - to prevent systematic bias introduced by differing neural network parameters.

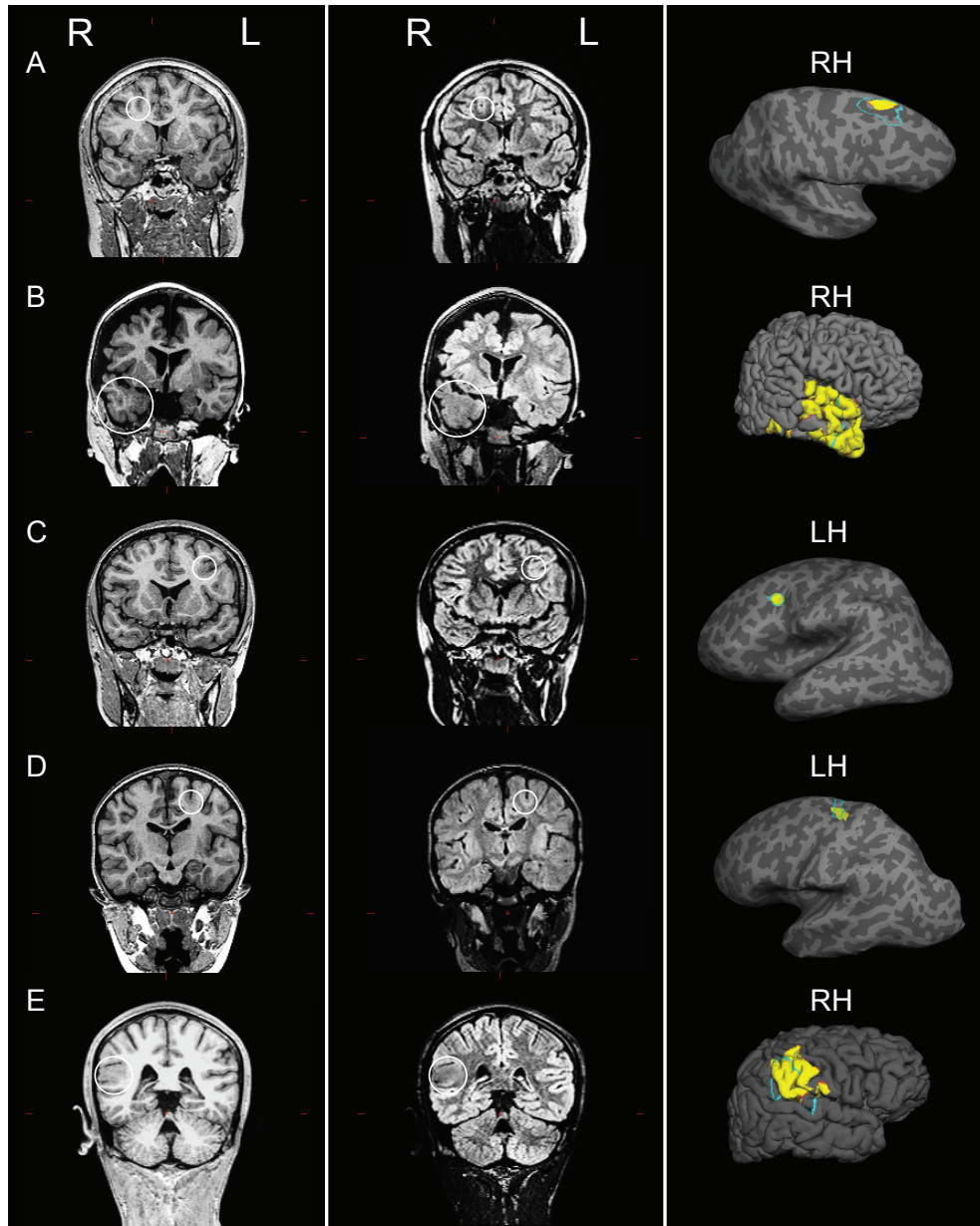
3.3.4 Classification Including Novel Features vs. Classification Using Established Features

The neural network involving novel and established features was able to detect 16 out of 22 FCDs (73%) as the putative lesion location (Figure 3.3). Out of the remaining 6 cases, the lesion in one patient was detected as the 4th cluster, and in 5 patients their lesions were not detected as one of the top 5 clusters. Further inspection of the scans of the 5 undetected patients revealed large motion artefacts particularly on the FLAIR images. The median anonymised motion rating of FLAIR images was 3 for the undetected patients in comparison to 2 in the detected patients (Mann-Whitney U: 12, $p < 0.019$), which may account for why they were missed. There was no significant age difference between detected and undetected patients (Mann-Whitney U: -0.48, $p = 0.63$).

In comparison, the neural network using only previously established surface features and 11 hidden nodes was only able to detect 12 out of

22 FCDs (55%) as the primary cluster, whilst with 6 hidden nodes (as established through a principal components analysis) was able to detect 13 out of 22 FCDs (59%), further evidence that inclusion of the novel features aided the detection of FCDs.

Fig. 3.3 Examples of top cluster output in 5 patients with FCD

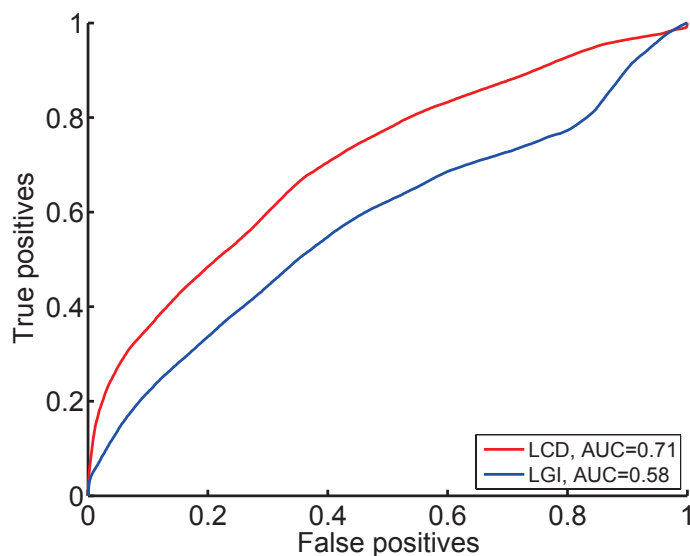


Examples of top cluster output in 5 patients with a radiological diagnosis of FCD. First column: T1-weighted images. Second column: FLAIR images. White circle on T1 and FLAIR images indicates lesion location. Third column: Top cluster of neural network classifier output (yellow) and manual lesion mask (light blue) viewed on pial surface, for large lesions, or inflated surface, for small lesions buried in sulci. For corresponding patient numbers in demographics table: A = 14, B = 15, C = 16, D = 9, E = 2.

3.3.5 Local Cortical Deformation vs Local Gyrfication Index

Measures of cortical shape, LCD and LGI, were directly compared both in terms of their individual discriminatory value and as inputs in the multivariate framework. In the AUC analysis of networks trained on a single feature, LCD (AUC = 0.71) performed much better than LGI (AUC = 0.58) (Figure 3.4). In the full classifier containing 28 features, including LGI instead of LCD (11 nodes), the neural network was only able to detect 12 out of 22 FCDs (55%) as the primary cluster, significantly lower than the sensitivity when including LCD (73%).

Fig. 3.4 Local Cortical Deformation vs Local Gyrfication Index



Receiver-operating characteristics and AUC comparing classifiers trained on local cortical deformation and local gyrfication index. Of the two measures of cortical folding, local cortical deformation is superior to local gyrfication index in discriminating lesional vertices from non-lesional vertices.

3.4 Discussion

The automated FCD algorithm proposed here successfully identified FCDs despite the challenges of a paediatric population. By identifying local changes (both by looking at local changes using the "doughnut" method, as well as utilising abnormal structural asymmetries), implementing subtle morphological markers (LCD) and normalising within each subject, between hemispheres and with a paediatric control group, this work

demonstrated that it is possible to detect FCDs with a sensitivity of 73%. Previous studies have demonstrated that surface-based structural MRI, coupled with automated computational techniques can detect FCDs in adult cohorts (Ahmed et al., 2015; Hong et al., 2014). This therefore represents a potentially significant advance in the treatment of paediatric epilepsy.

On visual inspection, FCDs are often most easily identified as an area of abnormal signal intensity on FLAIR and T1 scans. This is reflected in the fact that FLAIR signal intensity is the most discriminatory feature (AUC=0.83). However, FreeSurfer and other cortical segmentation algorithms rely on signal intensity contrast to segment the grey and white matter compartments. As such, segmentation of the grey-white matter boundary within lesional cortex is more complex than in healthy cortex, as even histologically there is blurring at the interface between gray and white matter. Sometimes the white matter reconstruction within the lesions are too superficial or too deep. Sampling FLAIR at multiple intra- and sub-cortical depths ensures that regardless of where the grey-white matter boundary has been segmented, the signal intensity abnormality will still be captured.

The "doughnut" method introduced in Chapter 2 identifies areas of increased variability in a feature across the cortex. As, focal cortical dysplasias are often characterised by abnormal cortical thickness, grey-white matter boundary intensity and FLAIR signal intensity compared to surrounding cortex, measuring local changes in these features may assist detection of these lesions. As "doughnut" maps can be calculated on any surface registered maps to highlight local structural changes, this work created "doughnut" maps based on cortical thickness, grey-white matter intensity contrast and FLAIR signal intensity, all of which demonstrated some ability to discriminate healthy from lesional vertices (AUC = 0.51 - 0.67).

Comparison of the ipsi- and contra-lesional hemispheres is an integral component of the radiological assessment of MRI scans. Interhemispheric registration of feature maps allowed for quantification of interhemispheric asymmetry of surface-based metrics at each vertex. These measures were of particular use in preventing normal anatomical variants from being considered abnormal. For example, the primary somatosensory cortex

is normally very thin. As it is thin bilaterally, although it falls in the extreme values for cortical thickness, the interhemispheric asymmetry values for this gyrus were around zero (see Figure 3.1). In contrast, the lesions were unilateral and therefore had abnormal unilateral cortical thickness values and abnormal asymmetry values. This served to filter healthy but symmetrical interregional variations, such as bilaterally thin and heavily myelinated primary sensory cortices (Lutti et al., 2014; Wagstyl et al., 2015) or regions showing differential but symmetrical developmental trajectories (Shaw et al., 2008). Importantly, commonly occurring interhemispheric asymmetries, such as the planum temporale (Geschwind and Levitsky, 1968), were subsequently filtered by normalising these asymmetry values with the control dataset. This approach for interhemispheric registration has obvious applications for detection of any unilateral abnormalities including other malformations of cortical development, strokes and tumours.

In this study, the novel folding measure LCD was directly compared to the more established measure LGI. As mentioned in Chapter 2, local cortical deformation (LCD) maps small-scale alterations in cortical shape and may be more sensitive to subtle shape abnormalities than LGI, a cm-scale measure (Ronan et al., 2011; Schaer et al., 2008). This was clearly demonstrated both through the increased AUC of a classifier trained on LCD compared to LGI, as well as the increased sensitivity of a classifier trained on the established and novel features that incorporated LCD, as opposed to LGI. It may therefore help to identify subtle shape changes in a wider range of disorders of cortical development (Ronan et al., 2012; Wagstyl et al., 2016).

Machine-learning algorithms have been previously applied to the problem of FCD detection in adults (Ahmed et al., 2015; Hong et al., 2014). These studies have similar sample sizes of 19 and 31 patients respectively and also trained their classifiers on surface-based data. They obtained lesion detection sensitivities of 74% (Hong et al., 2014) and 65% (when pooling the results from MRI-negative and MRI-positive patients) (Ahmed et al., 2015). Thus, despite the additional difficulties of paediatric data, through utilisation of the novel features developed in Chapter 2, the classifier is able to obtain similar sensitivity to the adult literature.

One previous study attempting automated paediatric FCD detection utilised a voxel-based technique (Riney et al., 2012). The study by Riney and colleagues only had a small cohort of MRI-positive FCDs (eight patients) but found VBM assessment of FLAIR MRI was able to detect 88% of them (Riney et al., 2012). However, in the cohort of cryptogenic FCD patients ($n = 14$), the VBM method detected an abnormal cluster in only 4 patients and this was only concordant with data from the pre-surgical investigations in 2 patients (14%). In these two patients, a visible abnormality was then seen on repeat inspection of the MRI scans. This study also conducted VBM assessment of T1 images, finding poorer ability to detect lesions using T1 data. Overall, this suggests that although this VBM method has good results when applied to FLAIR in overt FCD lesions, it performs poorly in subtle, cryptogenic cases. One advantage of the surface-based method proposed in this work is that it can incorporate multiple modalities, i.e. T1 and FLAIR. Furthermore, in the five patients in this study who were initially reported as MRI-negative we are able to detect 4 out of 5, an improvement on the voxel-based results.

This study advances automated FCD lesion characterisation and detection in a number of respects. First, previous work in adults has made use of voxel-based (Bernasconi et al., 2001; Colliot et al., 2006; Focke et al., 2008; House et al., 2013; Huppertz et al., 2005; Wagner et al., 2011; Wang et al., 2015) and surface-based structural features (Ahmed et al., 2015; Hong et al., 2014; Thesen et al., 2011) to which LCD could be a valuable addition particularly given its increased discriminatory value over the existing measure of shape, LGI. Second, combining features into multivariate classifiers has only been applied in adults (Ahmed et al., 2015; Hong et al., 2014). Data post-processing methods including the "doughnut" method, interhemispheric asymmetry and intra- and inter- subject normalisation were included to address specific problems in the paediatric population but may well aid lesion detection in adults. Third, studies in children have focused on voxel-based techniques (Riney et al., 2012), where individual maps can be sensitive but are less readily combined into a multivariate classification tool. Thus, novel structural features, data post-processing methods and incorporation of surface-based features into a neural network classifier furthers the detection of FCDs in epilepsy.

Although this study reports a lesion detection sensitivity of 73% in our cohort, certain challenges were unavoidable - excessive head motion

is a recognised problem causing artefacts (Ducharme et al., 2015), dental braces creating large artefacts, difficulty recruiting age matched controls for patients as young as 4 years old and 1.5T data. Indeed, the undetected lesions demonstrated relatively increased motion artefacts. The use of 1.5T data including some imperfect images, although a limitation does mean that the methods are likely to be effective on routine clinical data from any centre/MRI scanner. One final limitation, which is generally applicable to FCD detection studies, is the issue of multifocal lesions (Fauser et al., 2009). In some patients, multiple FCDs can be identified either presurgically, histologically or in post-surgical assessment when a patient continues to have seizures. However in this study radiological assessment of each patient only identified single lesions and patients had undergone resection of a single epileptogenic zone, thus we designed the classifier to identify only the single most likely FCD in a given subject. When investigating multifocal lesions in the form of extra-primary clusters, categorising abnormal tissue from image artefact without a gold standard method for their identification, remains a challenge. However, if multifocal lesions were heavily hypothesised within an individual, the classifier could be adapted to identify a set of abnormal clusters. Despite these challenges automated lesion detection in children was achievable. The novel surface measures developed here demonstrated substantial improvements in lesion detection in comparison to established features used in the adult literature. In future studies, classifier performance is likely to be improved by the use of larger, better quality datasets.

3.5 Conclusions

This work advocates development and incorporation of new surface-based measures for FCD detection, as well as re-emphasising the use of established surface-based measures and machine learning paradigms. These tools could be more generally applied in the detection of localised lesions such as polymicrogyria, gangliogliomas or dysembryoplastic neuroepithelial tumours (DNETs). Furthermore, improving the detection of FCDs in a paediatric cohort may assist in the selection, referral and subsequent pre-surgical evaluation of children with drug-resistant focal epilepsy by providing putative lesion locations that may aid conventional visual analysis by neuro-radiologists. Paediatric automated lesion detection, when considered alongside a patient’s detailed medical history and examination,

video-EEG, MEG, PET/SPECT and neuropsychological evaluation in multi-disciplinary team meetings, might enable earlier and more effective assessment for surgical intervention. For an individual, this could mean shorter duration of uncontrolled epilepsy, reduced anti-epileptic medication and their associated side effects and improvement in their cognitive outcome. To date the prediction algorithm has been trained and tested in a cohort with FCDs. It will be important to test these types of algorithms in mixed cohorts, e.g. patients with diagnoses of refractory focal epilepsy to see how they perform. To assist in this endeavour, all code used is freely available from <https://github.com/kwagstyl/FCDdetection/> and data matrices downloadable from the University of Cambridge's online data repository.

Future work developing machine-learning capabilities for FCD detection, such as deep convolutional neural networks, will require larger cohorts with more conservative cross-validation. Neural networks are excellent feature detectors and one day 3D volumetric convolutional neural networks might replace the extensive pre-processing and manual selection of surface-based features. However, these approaches would require huge amounts of training data, where each patient is an example rather than each vertex on the surface.

Chapter 4

FLAIR Hyperintensity in Adults with Temporal Lobe Epilepsy

The work presented in this chapter was completed while on a fellowship at the Montreal Neurological Institute under the supervision of Professor Andrea Bernasconi, Professor Neda Bernasconi and Professor Boris Bernhardt. The methodology and scientific approach learnt during this fellowship and used in this chapter is then applied to paediatric data in Chapter 5.

4.1 Introduction

Converging evidence from electro-clinical studies, histopathological assessments, and neuroimaging research emphasises a central role of the hippocampus in the pathophysiology of drug-resistant temporal lobe epilepsy (TLE). However, MRI-based studies have demonstrated that structural damage in this condition extends beyond the mesiotemporal lobe structures affecting grey and white matter systems (Bernhardt et al., 2013a; Engel et al., 2013). Diffusion MRI tractography has consistently shown microstructural alterations along efferent hippocampal pathways (Concha et al., 2005; Vaughan et al., 2016), with more marked effects proximal to the temporal lobe (Concha et al., 2012). Moreover, a close relationship has been demonstrated between hippocampal atrophy and diffusion anomalies in the superficial white matter immediately below temporo-limbic cortices (Liu et al., 2016). Conversely, controversy exists as to whether damage to the hippocampus or its efferents leads to

neocortical atrophy (Bernhardt et al., 2008; Mueller et al., 2009; Voets et al., 2012), suggesting that morphometry may not adequately capture this likely complex relationship.

Recent years have witnessed a shift from the mapping of grey matter morphology to the study of inter-regional covariance to describe fundamental aspects of brain organisation in normal and diseased conditions (Bernhardt et al., 2013a). While task-free functional MRI time-series correlation analysis has successfully identified intrinsic functional networks (Damoiseaux et al., 2006), morphological covariance, commonly based on cortical thickness correlations, has been used to reveal areas with synchronised maturational development (Alexander-Bloch et al., 2014). Previous studies have shown that signal intensity variations across the cortex, particularly based on T2-weighted imaging, may signify differences in architectonic organisation (Hirai et al., 2000; Schneider and Vergesslich, 2007).

This study proposes covariance analysis of signal intensity to identify areas with similar architecture, thereby providing an alternative methodology to probe grey matter tissue integrity and its relationship to hippocampal pathology. To this end, first cortical T2-weighted signal is mapped, based on fluid attenuated inversion recovery (FLAIR), in a consecutive cohort of adult TLE patients and healthy controls. Core to this approach was a surface-based analysis framework that optimises inter-subject correspondence, mitigates effects of partial voluming, and provides an integrated anatomical sampling scheme across modalities. The relation of whole-brain FLAIR signal to hippocampal networks derived from morphological covariance, intra-cortical intensity covariance, and resting-state functional MRI is then evaluated. Finally, the relationship between FLAIR intensity and clinical variables is assessed.

4.2 Materials & Methods

4.2.1 Participants

A consecutive cohort of 61 adult patients with unilateral drug-resistant TLE (31 LTLE, mean \pm SD age=34 \pm 9 years, range=18-53 years, 11 males; 30 RTLE, 34 \pm 9 years, 20-52 years, 15 males) and 38 age- and sex-matched healthy controls (30 \pm 7 years, 20-53 years, 21 male) investigated at the

Montreal Neurological Institute and Hospital were studied. Demographic and clinical data were obtained through interviews with patients and their relatives (Table 4.1). TLE diagnosis and lateralisation of the seizure focus were determined by a comprehensive evaluation; this involved a detailed history and neurological examination, the review of medical records, scalp video-EEG recordings, as well as MRI assessment in all patients. Clinical MRI evaluation revealed hippocampal atrophy and increased T2 signal intensity in 37/61 (61%). Quantitative analysis including volumetry and shape modeling revealed variable degrees of ipsi-lesional atrophy in all patients (Bernasconi, 2003; Bernhardt et al., 2013b). No patient had a mass lesion (malformations of cortical development, tumours, or vascular malformations), traumatic brain injury, or a history of encephalitis.

The comprehensive investigation recommended surgery as treatment to all patients; among them, 43 have undergone a selective amygdalo-hippocampectomy at the time of study. The surgeon's procedure of choice at the MNI is a selective amygdala-hippocampectomy, rather than the classical anterior temporal lobectomy. Studies comparing these two surgical options have been mixed with many individual studies showing equivalence between the procedures (Mansouri et al., 2014; Tanriverdi et al., 2008; Wang et al., 2016), whereas two meta-analyses indicate an improvement in seizure freedom for ATL versus SAH (Hu et al., 2013; Josephson et al., 2013) but concluded that a randomized control trial would be necessary to validate their findings. Histological analysis of the resected specimens (Blümcke et al., 2013) revealed neuronal cell loss and gliosis in both CA1 and CA4 subfields in 17 patients (ILAE HS Type-1), neuronal loss predominantly in CA1 in 6 (ILAE HS Type-2), neuronal loss predominantly in CA4 in 5 (ILAE HS Type-3), and only gliosis without detectable neuronal loss in 15. Post-operative seizure outcome was determined according to Engel's modified classification (Engel, 1993) after a mean \pm SD follow-up time of 52 \pm 21 months (range: 14-88 months). Among the 43 operated patients, 30 (70%) had Class-I outcome, 7 (16%) Class-II, 5 (12%) Class-III, and 1 (2%) Class-IV. Comparable rates of seizure-free patients were observed across ILAE HS subtypes: [Type-1: 14/16 (88%), Type-2: 4/6 (66%), Type-3: 5/5 (100%), chi-squared: $P = 0.36$], while rates were lower in patients with isolated gliosis [6/15 (40%), chi-squared: $P = 0.01$]. Among the 18 non-operated patients, nine are currently awaiting surgery and nine delayed it for personal reasons.

The Ethics Committee of the Montreal Neurological Institute and Hospital approved the study and written informed consent was obtained from all participants.

Table 4.1 Adult TLE Demographic & Clinical Information

	AGE	MEN	ONSET	DURATION	FC	SURGERY	HS	ENGEL I
LTLE (n=31)	35 ± 9 (18 - 53)	11	18 ± 10 (4 - 40)	16 ± 10 (2 - 45)	7	19	12	13 (68%)
RTLE (n=30)	34 ± 9 (20 - 52)	15	14 ± 9 (1 - 30)	20 ± 11 (3 - 41)	12	24	16	17 (71%)
Controls (n=38)	30 ± 7 (20 - 53)	21	NA	NA	NA	NA	NA	NA

Age, age at seizure onset, and duration of epilepsy are presented in mean±SD (year range). FC = febrile convulsions; HS = hippocampal sclerosis on histopathology (remaining patients had gliosis only); ENGEL I= seizure free, i.e. Class I postsurgical outcome in Engel’s classification; NA = not applicable.

4.2.2 Imaging

Multimodal 3T MRI data were obtained on a Siemens TimTrio (Siemens Healthcare, Erlangen, Germany), equipped with a 32-channel head coil. The following scan sequences were acquired: 3D T1-weighted (T1w) magnetization-prepared rapid gradient echo (TR=2300 ms, TE=2.98 ms, TI=900 ms, FA=9°, FOV = 256x256mm², matrix=256x256, 176 sagittal slices, voxel size=1x1x1 mm³), fluid-attenuated inversion recovery images (FLAIR; TR=5000 ms, TE=389 ms, TI=1800 ms, FA=120°, FOC=207x207mm², matrix=230x230, 173 sagittal slices, voxel size=0.9x0.9x0.9 mm³) and 2D echo-planar resting-state fMRI (rs-fMRI, TR=2020 ms, TE=30 ms, flip angle=90°, matrix size=64x64, FOV=256x256 mm², 34 slices, voxel resolution=4.0x4.0x4.0 mm³, 150 volumes). For the latter, participants were instructed to keep their eyes closed while remaining awake. To minimize signal loss and distortion affecting orbitofrontal and mesiotemporal regions, slices were tilted in an oblique coronal orientation. In a subset of participants (29 TLE/19 controls), T2 relaxometry (T2R) (TSE; TR=12750ms, TE=14ms, 123ms, TI=2805.9ms, FA=130°, FOV=256x256mm², 34 oblique slices tilted at a -29° from coronal orientation, matrix=256x256, voxel size=1x1x3mm³) data were available, acquired along the entire hippocampal long axis.

4.2.3 Image Processing

T1w and FLAIR images underwent correction for intensity inhomogeneity and intensity normalization (Sled et al., 1998). After T1w images were linearly registered to the MNI152 symmetric template (Fonov et al., 2009), FLAIR images were linearly co-registered to them. T1w data were classified into white matter (WM), grey matter (GM), and cerebro-spinal fluid (CSF). Using the Constrained Laplacian Anatomic Segmentation using Proximity (CLASP) algorithm, models of the inner (GM-WM) and outer (GM-CSF) cortical surfaces were generated and cortical thickness was measured across 81,924 corresponding surface points (henceforth, vertices) (Kim et al., 2005). Surface extraction was visually verified and corrected if necessary. The pial and GM-WM surfaces have the same number of vertices and a straight line, the t-link, can connect corresponding vertices on the two surfaces. Cortical thickness was calculated as the straight line between corresponding points on the inner and outer surface and blurred using a smoothing kernel of 20mm FWHM (Lerch and Evans, 2005).

To examine intracortical signal intensity, 3 equidistant surfaces were positioned between the GM-CSF and GM-WM at 25%, 50%, and 75% cortical thickness (Hong et al., 2015) guided by a straight line providing vertex correspondence across these surfaces. Voxel-wise FLAIR intensity measures were normalized by the mode of the FLAIR intensity histogram and the intensity at the GM-WM boundary (Hong et al., 2015, 2014). Normalized intensities were mapped to the nearest vertex of each intracortical surface. Notably, intensities were not sampled on the outermost (i.e., GM-CSF) surface to avoid CSF contamination. At remaining surfaces, intensities were corrected for residual CSF partial volume effects (PVE_{CSF}) using a methodology used in a previous study by the Bernasconi group (Hong et al., 2015; Shafee et al., 2015). This involves the estimation of GM and CSF partial volume effects on T1w and FLAIR scans (Tohka et al., 2004) and the interpolation of these values onto the 3 intra-cortical surfaces. Then, the relative intensity (RI) of the GM is calculated by solving the following equation:

$$RI = PVE_{GM} \times I_{GM(vi)} + PVE_{CSF(vi)} \times I_{CSF(vi)}$$

where I_{GM} and I_{CSF} are the relative intensities of the GM and CSF. $I_{CSF(vi)}$ was computed by averaging neighbouring voxels (within a radius

of 10mm of the voxel of interest) with PVE_{CSF} equal to 1. Data were blurred with a surface-based Gaussian diffusion kernel, with a full-width-at-half-maximum of 20mm. Finally, at each vertex, I averaged normalized intensities across the 3 intra-cortical surfaces to create average cortical T1w and FLAIR signal intensities per vertex.

The hippocampus was segmented automatically with a recently developed SurfPatch algorithm (Caldairou et al., 2016), combining a surface-based processing with patch intensity similarity measures shown to achieve excellent accuracy in healthy individuals and TLE patients. Mean normalized FLAIR signal intensity was calculated within hippocampal labels.

For T2 relaxometry, a dual-echo method was used where two T2 images were acquired at two different echo times. This has been previously deemed to be comparable to a 16-echo method (Duncan et al., 1996). Single-exponential-decay equations were fitted to the T2 imaging data obtained in each pixel, and then T2 relaxation times were calculated for each pixel. A map was then constructed in which pixel intensity corresponded to the calculated T2 relaxation time. T2 relaxation times were calculated in microseconds. A threshold of 20 was applied to attenuate background noise. T2 relaxometry (T2R) data processing involved registration to native T1w data. Automated hippocampal segmentations were eroded by two voxels and T2R signal intensity was sampled within these eroded labels. This was to ensure that hippocampal T2R signal was not contaminated by CSF. Average T2R signal was calculated within hippocampal labels.

Preprocessing of resting-state fMRI was carried out in native functional space using the DPARSF toolbox for Matlab (Chao-Gan and Yu-Feng, 2010). The first 5 volumes from each time-series were removed to ensure magnetization equilibrium, and slice-timing and motion correction were performed. Prior to connectivity analysis, the effects of head motion, white matter signal, and CSF signal were corrected for and the time series was band-pass filtered to 0.01-0.08 Hz (Chao-Gan and Yu-Feng, 2010).

4.2.4 Statistical Analysis

Analyses were performed using SurfStat (<http://www.math.mcgill.ca/keith/surfstat/>) for Matlab (Worsley et al., 2009). Patients were analysed

relative to the epileptogenic hemisphere (i.e., ipsi- and contralateral to the seizure focus). To control for hemispheric asymmetry, features (intensity, cortical thickness) were z-normalized at each vertex with respect to the corresponding distribution in controls (i.e., each patient's right/left feature was expressed as a z-score with respect to right/left values in controls).

a) Relationship between T2R and FLAIR signal intensity. To ensure that there is a tight coupling between T2R and FLAIR data, T2R intensity asymmetry was correlated with FLAIR intensity asymmetry in the hippocampi in 30 patients and 20 controls for which T2R data was available. As FLAIR is not a quantitative scan, it was more appropriate to compare asymmetry values between T2R and FLAIR than actual values. Asymmetry was calculated as follows:

$$Asymmetry = (L - R)/(L + R)$$

b) Mapping FLAIR signal intensity. Cortical FLAIR signal intensity was compared between patients and controls using vertex-wise Student's t-tests. In clusters of findings, average effect sizes were computed using the Cohen's d metric both over the average relative signal intensity across the 3 intra-cortical surfaces (positioned at 25%, 50% and 75% cortical depths) and also individually in each of the intra-cortical surfaces. Each intra-cortical surface has point-to-point correspondence and has 4,0962 vertices per hemisphere. A one-way ANOVA with correction for multiple comparisons was used to assess difference in effect sizes across the three intra-cortical surfaces. For individual analysis, in clusters of findings, we assessed the number of patients with FLAIR z-scores >1.5 relative to controls, to provide an estimate of how prevalent neocortical FLAIR abnormalities are within unilateral TLE patients. To rule out possible effects of morphology, using linear regression, the effects of cortical thickness were estimated at each vertex, and then the group-level FLAIR comparisons were repeated after statistically controlling for vertex-wise cortical thickness. This tested if FLAIR changes co-localised with atrophy (cortical thickness changes). To test how generalisability of group-level FLAIR findings, bootstrap reproducibility analyses were performed. Cortical FLAIR signal intensity comparisons between TLE and controls were repeated across 1000 comparisons of groups that were randomly resampled with replacement. If one was to choose a random subset of 30 from the 61 patients, there would be $61!/(30!)(31!)$ different sets of patients. This is

equal to $2e+17$. Thus, 1000 replications using random subsets of patients and controls is supported by the data.

c) Relationship to hippocampal networks. Hippocampal networks were generated in controls based on resting-state functional connectivity and morphological covariance similar to previous studies by the Bernasconi group (Bernhardt et al., 2016, 2009a, 2008).

Functional connectivity. In brief, we calculated Pearson’s correlation coefficient between the average left hippocampal time-series and the time-series of each neocortical vertex in each control. A Fisher r-to-z transformation was applied to render the correlation coefficients more normally distributed.

Morphological covariance. To calculate morphological covariance, we correlated the volume of the left hippocampus with cortical thickness at each vertex in the group of controls (Evans, 2013). Vertices that covary with hippocampal morphology will have higher correlation values across the group.

FLAIR intensity covariance. To also generate networks based on intensity covariance (Eickhoff et al., 2005), mean normalized FLAIR intensity of the left hippocampal labels was correlated with the neocortical intensities at each vertex in the group of controls.

To establish whether the overall pattern of FLAIR between-group difference can be predicted by the topography of hippocampal networks, the t-statistic map of the analysis in a) was correlated with the three different hippocampal network maps across all neocortical vertices. To ensure findings were related to hippocampal networks rather than due to anatomical proximity to the hippocampus, the network analysis was repeated after regressing out geodesic distance (i.e., the shortest distance across the surface) from the hippocampus to each neocortical vertex (Dijkstra, 1959; Ecker et al., 2013). This was necessary as the ipsi-lateral temporal lobe is strongly connected to the hippocampus. Yet, any FLAIR signal anomalies in temporal neocortex could have arisen from tangential spread across the cortex rather than due to functional, morphological or FLAIR signal intensity covariance.

d) Relation to clinical variables. Using surface-wide linear models, correlations between FLAIR intensity and the following clinical factors - history of febrile convulsions, age at seizure onset, duration of epilepsy,

and post-operative seizure outcome, were assessed.

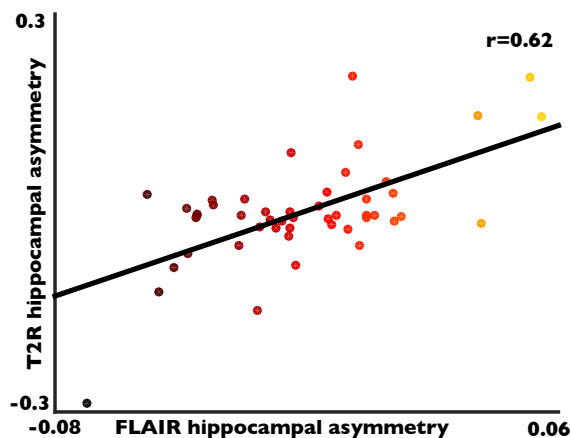
e) Correction for multiple comparisons. Surface-based findings were corrected using random field theory for non-isotropic images (Worsley et al., 1999), controlling the family-wise error (FWE) to be below $P_{\text{FWE}} < 0.05$.

4.3 Results

4.3.1 Relationship between T2R and FLAIR signal intensity

Hippocampal FLAIR and T2R signal intensity asymmetries were significantly correlated (Figure 4.1; $r=0.62$, $p<0.001$) supporting the idea that FLAIR and T2 relaxometry signals are sensitive to similar cytoarchitectural properties.

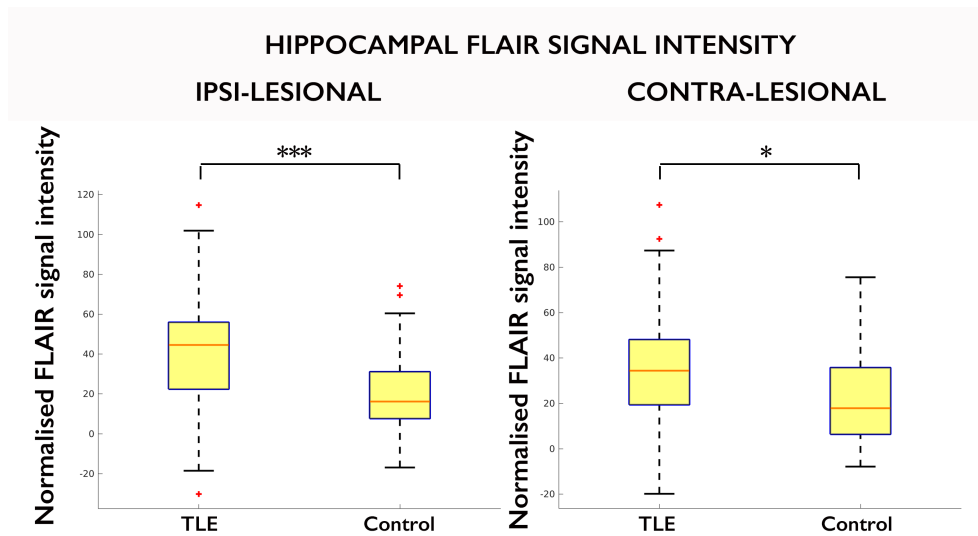
Fig. 4.1 Relationship between hippocampal T2R and FLAIR signal intensity



4.3.2 Whole-brain mapping of FLAIR signal intensity in TLE

Compared to controls, hippocampal FLAIR intensity increases in patients were observed bilaterally (ipsi-lesional: $t=3.99$, $p<0.001$; contra-lesional: $t=2.25$, $p=0.027$; Figure 4.2) with larger effect sizes ipsilateral to the seizure focus (Cohen's $d=0.83$ ipsi-lesional; $d=0.47$ contra-lesional). Neocortical FLAIR hyperintensities in TLE were equally present on ipsi- and

Fig. 4.2 Hippocampal FLAIR signal intensity



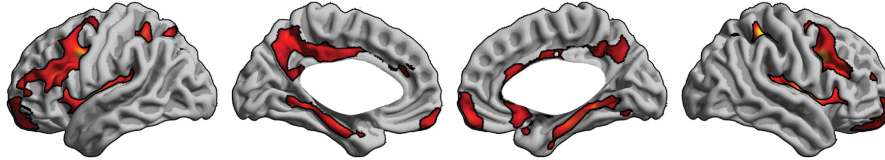
Comparison of FLAIR signal intensity in the ipsi- (A) and contra-lesional (B) hippocampi between TLE patients and controls.

contra-lesional hemispheres. The bilateral topography involved limbic and paralimbic neocortical regions (i.e., parahippocampal, insular, cingulate, and orbitofrontal cortices), together with dorsolateral prefrontal cortex and precuneus (Figure 4.3 (A); $P_{\text{FWE}} < 0.05$). In these regions (Figure 4.4), based on average intensity over the 3 intra-cortical surfaces, we observed moderate-to-large effect sizes ($d = 0.68-0.89$). As assessed using a one-way ANOVA with correction for multiple comparisons, effect sizes were significantly higher at 50% ($p < 0.001$) and 75% ($p < 0.001$) cortical depth surfaces than the surface at 25% cortical thickness. However, there was no significant difference in effect sizes between surfaces at 50% and 75% cortical thickness ($p = 0.14$; Table 4.2). In significant clusters, marked hyperintensity (z score > 1.5) was found in up to 23% of patients. Separately assessing left and right TLE patients confirmed the consistency of FLAIR increases across all significant clusters ($P_{\text{FWE}} < 0.05$). Furthermore, bootstrap reproducibility analysis indicated that the topographic distribution of anomalies was reproducible in up to 70-100% of simulations, suggesting generalizability (Figure 4.5).

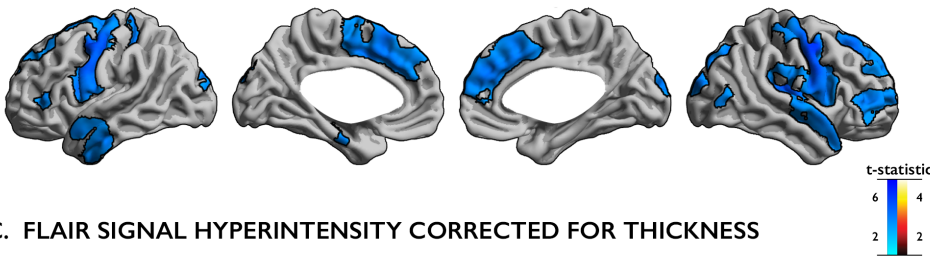
Fig. 4.3 Topography of neocortical FLAIR increases and cortical atrophy in TLE relative to controls

SURFACE-BASED MAPPING OF NEOCORTICAL FLAIR INTENSITY AND THICKNESS

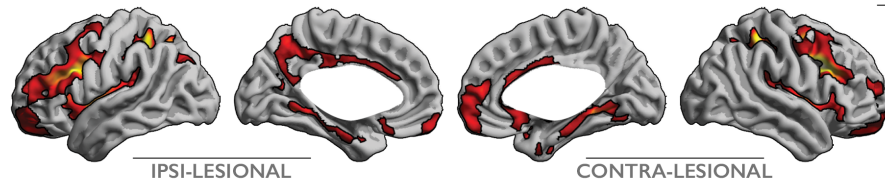
A. FLAIR SIGNAL HYPERINTENSITY IN TLE



B. CORTICAL THINNING IN TLE



C. FLAIR SIGNAL HYPERINTENSITY CORRECTED FOR THICKNESS



A) Topography of neocortical FLAIR increases in TLE. B) Cortical thinning (in blue) in TLE patients vs controls. C) FLAIR increases in TLE after correction of cortical thickness measures at each surface point. Findings have been adjusted for multiple comparisons using random field theory for non-isotropic images (Worsley et al., 1999). In clusters significant at $P_{FWE} < 0.05$, the t-statistics is shown.

4.3.3 Relation to whole-brain topography of cortical thickness

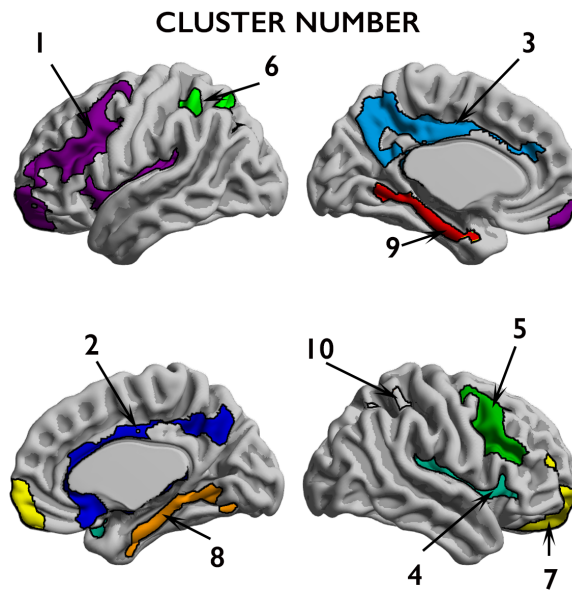
Areas of cortical thinning present in bilateral frontal, temporal, and centro-parietal cortices (Figure 4.3 (B); $P_{FWE} < 0.05$) co-localised only minimally with those displaying FLAIR hyperintensity (Dice overlap index = 9.1%). In fact, repeating the between-group FLAIR comparisons after regressing out vertex-wise cortical thickness revealed virtually identical results with the exception of reduced effects in ipsi-lesional parahippocampus and differences in the contra-lesional precuneus (Figure 4.3 (C); $P_{FWE} < 0.05$).

Table 4.2 Effect sizes in clusters of findings

CLUSTER	INTRA-CORTICAL SURFACE 1 (25%)	INTRA-CORTICAL SURFACE 2 (50%)	INTRA-CORTICAL SURFACE 3 (75%)	AVERAGE OVER SURFACES
1	0.76	0.92	0.76	0.81
2	0.61	0.82	0.82	0.75
3	0.40	0.80	0.72	0.64
4	0.55	0.78	0.67	0.67
5	0.67	0.83	0.66	0.72
6	0.52	0.81	0.71	0.68
7	0.57	0.76	0.64	0.66
8	0.44	0.71	0.82	0.66
9	0.44	0.67	0.75	0.62
10	0.53	0.83	0.62	0.66
Mean	0.55	0.79	0.72	0.69
SD	0.11	0.07	0.07	0.06

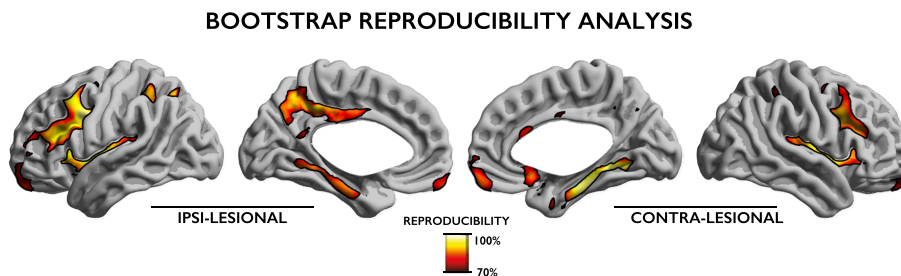
Anatomical location of clusters 1 - 10 visible in Fig. 4.4

Fig. 4.4 Regions of FLAIR hyperintensity in TLE



Clusters of significant FLAIR hyperintensity in TLE after correction for multiple comparisons using random field theory. Clusters are numbered 1 to 10. These numbers correspond to cluster numbers in Table 4.2 where effect sizes at the three intra-cortical surfaces are displayed.

Fig. 4.5 Bootstrap reproducibility



Probability of observing FLAIR hyperintensity in TLE vs controls across 1000 comparisons of groups that were randomly resampled with replacement. Group differences in each iteration were thresholded as in Figure 4.3.

4.3.4 Relation to hippocampal covariance networks

FLAIR intensity covariance networks in controls were remarkably similar for left and right hippocampus, and outlined limbic and paralimbic regions encompassing dorsolateral prefrontal as well as cingulate regions, together with entorhinal, posterior parahippocampal, retrosplenial, and insular cortices (Fig. 4.6 A). We observed a positive correlation between hippocampal FLAIR intensity covariance networks in controls and the topography of group-level FLAIR hyperintensity (Fig. 4.6 A; $r=0.27$, $P<0.001$). This relationship remained unchanged after regressing out geodesic distance from the ipsilateral hippocampus (Fig. 4.6 D), indicating that findings related to topological and not physical proximity ($r=0.28$, $P<0.0001$). In contrast, there was no noteworthy relationship between group differences in FLAIR signal intensity and control hippocampal functional ($r=-0.07$) or morphological ($r=0.06$) networks (Fig. 4.6 B, C), further suggesting that FLAIR alterations are most prominent in regions sharing similar intensity characteristics as the hippocampus. Steiger's test for differences in dependent correlations (Steiger, 1980) indeed showed a stronger association between the topography of FLAIR signal changes in TLE and FLAIR intensity covariance networks compared to those derived from resting-state functional connectivity ($z=81.02$, $P<0.001$) and morphological covariance analysis ($z=48.55$, $p<0.001$).

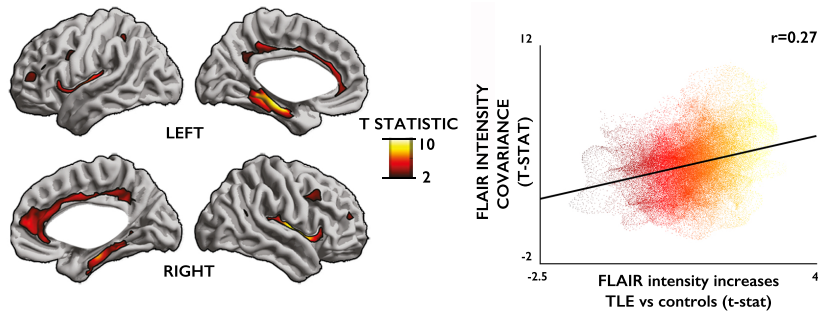
An additional analysis confirmed that FLAIR increases seen in patients specifically related to hippocampal intensity covariance networks. FLAIR intensity covariance analysis in controls was repeated separately seeding from each of the left AAL neocortical parcels, i.e. mean normalized FLAIR intensity of each of the 39 left cortical AAL labels was correlated with the

neocortical intensities at each vertex in the group of controls. Then the t-statistical map of group-level differences in FLAIR between patients and controls was correlated with each of the 39 different AAL network maps. Consistently lower associations between neocortical FLAIR increases and control FLAIR covariance were obtained using these seeds compared to a hippocampal seed (Figure 4.7), supporting specificity for the hippocampus rather than other nodes in the epileptogenic network.

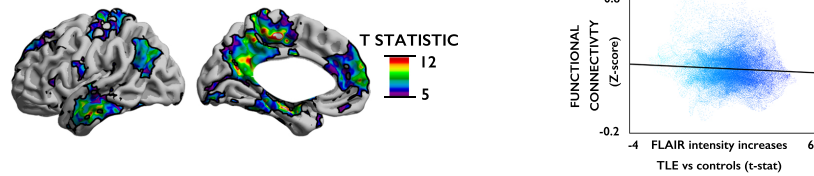
Fig. 4.6 Relationship between FLAIR signal and hippocampal networks.

RELATIONSHIP BETWEEN FLAIR SIGNAL AND HIPPOCAMPAL NETWORKS

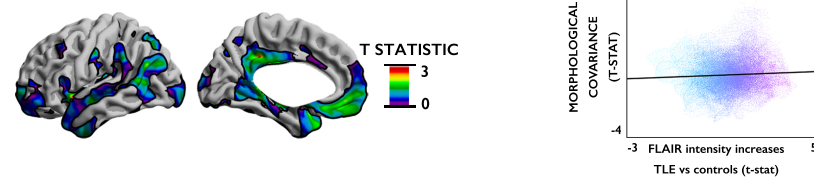
A. HIPPOCAMPAL FLAIR INTENSITY COVARIANCE



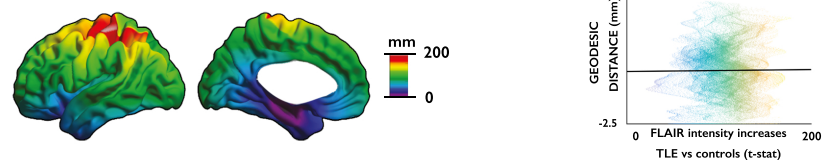
B. HIPPOCAMPAL FUNCTIONAL CONNECTIVITY



C. HIPPOCAMPAL MORPHOLOGICAL COVARIANCE

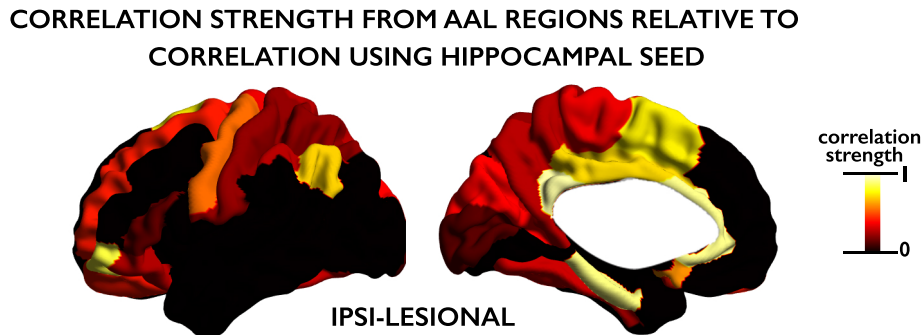


D. GEODESIC DISTANCE FROM HIPPOCAMPUS



Maps display hippocampal FLAIR signal intensity covariance networks to index intracortical tissue similarity (A), resting-state signal correlations to index functional connectivity (B), morphological covariance tapping into maturational coupling (C), and geodesic distance in controls (D). The scatter plots show surface-wide correlation between these networks and the t-statistic of the TLE vs. controls group difference in FLAIR signal.

Fig. 4.7 FLAIR covariance using AAL regions as seeds



Strength of correlation between t-statistic of the TLE-vs-control comparison in cortical FLAIR and the FLAIR covariance map centred on each AAL region in the left hemisphere. Correlation strength for each AAL seed is displayed as a proportion of the (maximal) correlation coefficient that was obtained by relating TLE-vs-control difference map to hippocampal covariance networks (see Figure 4.6 (B); $r=0.27$).

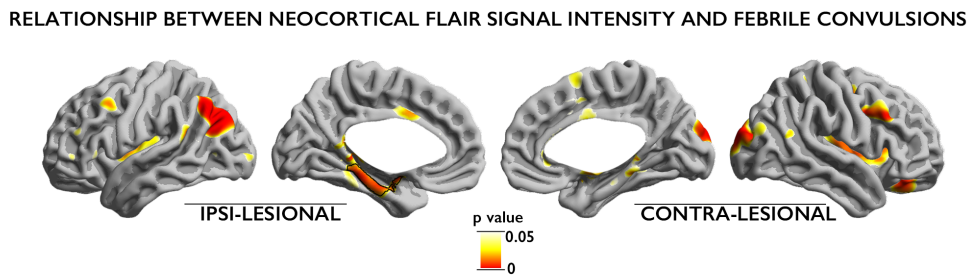
4.3.5 Relation to clinical variables

There were no significant associations between cortical FLAIR and age at seizure onset, duration of epilepsy, or post-surgical seizure freedom ($P_{FWE} > 0.2$). On the other hand, patients with a history of febrile convulsions exhibited more marked FLAIR increases in ipsi-lesional parahippocampal cortex compared to those without ($P_{FWE} < 0.05$, Figure 4.8). It is noteworthy that the spatial distribution of uncorrected whole-brain effects resembled the patient-control differences seen in Figure 4.3, with signal hyperintensities distributed throughout limbic and paralimbic neocortices. Indeed, assessing mean FLAIR signal in clusters of group differences between patients and controls confirmed more marked increases in patients with a history of febrile convulsions ($t=2.61$, $p=0.006$).

4.4 Discussion

Using a surface-based paradigm that samples signal intensity within the cortical mantle, the whole-brain distribution of FLAIR signal in TLE patients was mapped relative to controls. Increased intensities were observed bilaterally in limbic and paralimbic regions, including hippocampal, parahippocampal, insular, cingulate and dorsolateral prefrontal cortices, as well as the orbitofrontal cortex. The topography of FLAIR anomalies was highly similar in left and right TLE patients, and replicable across

Fig. 4.8 Relationship between neocortical FLAIR signal intensity and febrile convulsions.



Map shows FLAIR signal intensity increases in patients with history of febrile convulsions relative to those without. Significant clusters, corrected for multiple comparisons using random field theory at $P_{FWE} < 0.05$ are outlined in black.

thousands of bootstrap simulations, supporting consistency.

Contrary to FLAIR changes, atrophy was primarily observed in frontal and lateral temporal cortices, as previously shown (Bernhardt et al., 2013a; McDonald et al., 2008); moreover, group-level FLAIR findings remained unchanged after correcting for cortical thickness. In agreement with our observations, previous neuroimaging studies found little to no overlap in either the mesiotemporal lobe or neocortex (Bernhardt et al., 2016; Pell et al., 2008), supporting the notion that atrophy and changes in T2-weighted MRI signal reflect different aspects of TLE pathology. While cortical thinning may relate to atrophy, possibly secondary to excitotoxic effects of seizure spread through thalamo-cortical pathways (Bernhardt et al., 2012), FLAIR hypersignal within the cortical ribbon likely signifies alterations in laminar architecture and cell composition. Notably, hippocampal intensity covariance networks observed in controls predicted between-group differences in FLAIR signal, suggesting increased vulnerability of regions with similar intra-cortical tissue composition. In other words, neocortical regions with intensity characteristics similar to the hippocampus were also those displaying FLAIR hyperintensities when comparing TLE patients to healthy controls. These findings, together with the lack of a link between FLAIR anomalies and hippocampal resting-state functional connectivity, morphological covariance, as well as geodesic distance from the hippocampus, further support a shared susceptibility model based on tissue architecture (Alexander-Bloch et al., 2013; Eickhoff et al., 2005). Indeed, regions highlighted by FLAIR covariance and group analyses, referred to as periallocortex, form a transition between

three-layered allocortical limbic areas (such as the hippocampus) and the six-layered isocortex (Zilles, 2004). In the healthy human brain, limbic and paralimbic cortices may appear hypertintense compared to the isocortex on T2-weighted imaging (Hirai et al., 2000). Notably, in monkeys, some of these regions display high glial cell density (Collins et al., 2010), which could contribute to the signal profile. It is thus plausible that differing laminar architecture, as well as cellular composition, drive both FLAIR signal covariance and susceptibility to FLAIR-detectable pathology.

As these TLE patients underwent a selective amygdalo-hippocampectomy, we cannot provide a histopathological verification of our group-level findings. T2-weighted FLAIR signal may be sensitive to several microstructural tissue properties, including iron (Zhou et al., 2001) and myelin (Eriksson et al., 2007), as well as glial cell content. While there is limited evidence for neocortical demyelination (Thom et al., 2000) and decreased iron content in TLE (Zhang et al., 2014), several correlative studies have shown a close association between hippocampal T2 hyperintensity and gliosis (Briellmann et al., 2002; Goubran et al., 2015; Peixoto-Santos et al., 2016). In light of histopathological evidence for neocortical gliosis in similar areas (including the frontal pole and orbitofrontal regions) (Blanc et al., 2011; Margerison and Corsellis, 1966), our findings may thus be compatible with an extensive gliotic process. Long considered a bystander of neuronal damage, evidence from animal models and clinical studies suggest a link between astrogliosis, neuronal excitability and seizure genesis (Devinsky et al., 2013; Vezzani, 2014; Vezzani et al., 2008; Vezzani and Friedman, 2011; Wetherington et al., 2008), an association supported by our results showing more marked FLAIR hyperintensity in patients with a history of febrile convulsions. This is also in line with recent prospective studies documenting visually appreciable hippocampal T2 hyperintensity in a proportion of children following febrile seizures (Lewis et al., 2014). All except one of the patients who developed HS had one affected hippocampus, i.e. unilateral HS. However, interestingly, most of the small subgroup who developed epilepsy did not have temporal lobe epilepsy. Yet, animal models of status epilepticus indicate that chronic glial cell activation extends beyond the hippocampus into the entorhinal and fronto-parietal cortices (Ravizza et al., 2008). Importantly, in pilocarpine-induced status epilepticus, glial alterations (reactive microgliosis and astroglial death) even preceded neuronal damage (Kang

et al., 2006).

Future efforts should be aimed at combining novel MRI contrasts that provide biomarkers of laminar architecture, such as quantitative susceptibility imaging, with ex vivo MRI and immunohistochemistry to precisely understand the cellular basis of signal alterations in epilepsy (Reeves et al., 2015). See supplementary material for a review on the potential of quantitative MR sequences.

Chapter 5

Multimodal surface-based imaging in paediatric temporal lobe epilepsy

5.1 Introduction

Hippocampal sclerosis (HS) is an uncommon aetiology in paediatric epilepsy surgery centres accounting for only 6.5% of surgical resections (Harvey et al., 2008). On histopathology, HS is characterised by cell loss and gliosis with the hippocampal formation (Blümcke et al., 2013; Margerison and Corsellis, 1966), yet post-mortem studies indicate neuronal loss and gliosis is also present in a proportion of patients in the amygdala (Yilmazer-Hanke et al., 2000), entorhinal cortex (Du et al., 1993), temporal neocortex (Thom, 2009) and extra-temporal neocortex (Blanc et al., 2011; Margerison and Corsellis, 1966).

Neuroimaging proffers the possibility to map these cytoarchitectural changes *in vivo*, whilst necessitating careful consideration of the sensitivity and specificity of the sequences and features analysed. Within the hippocampus, volumetric (Bernasconi, 2003; Cendes et al., 1993; Farid et al., 2012; Skirrow et al., 2015), T2 intensity (Briellmann et al., 2002; Goubran et al., 2015; Kubota et al., 2015; Peixoto-Santos et al., 2016), FLAIR intensity (Jafari-Khouzani et al., 2010; Woermann et al., 2001) and advanced shape analyses (Kim et al., 2013) have robustly quantified the pathological anomalies present in TLE. In fact, correlational studies indicate the relationship of atrophy of the hippocampus with neuronal cell loss (Briellmann et al., 2002; Bronen et al., 1991; Goubran et al.,

2015) and T2 signal intensity with glial cell count (Briellmann et al., 2002; Goubran et al., 2015; Peixoto-Santos et al., 2016).

Beyond the hippocampus, there is a body of neuroimaging literature in adults, utilising both volumetric and surface-based methodologies, describing whole-brain changes in grey matter volume (Keller and Roberts, 2008), cortical thickness (Bernhardt et al., 2010; McDonald et al., 2008; Mueller et al., 2009) and T2/FLAIR intensity (Pell et al., 2008)(Adler et al., under review, Chapter 4). However, relative to the large number of studies mapping whole-brain morphology and the distribution of T2 hyperintensity in adults with HS, relatively little is known about extra-hippocampal brain changes in paediatric HS, with one previous voxel-based study demonstrating reductions in grey matter density in medial and lateral temporal as well as posterior cingulate neocortices (Cormack et al., 2005).

In this study, using multimodal imaging to map whole-brain changes both in the hippocampus and neocortex, we document epilepsy-related brain pathology in paediatric HS. We then assess the relationship between these in vivo metrics and clinical factors, such as age of epilepsy onset, duration of epilepsy and history of febrile convulsions.

5.2 Materials & Methods

5.2.1 Participants

A retrospective cohort of patients with radiologically defined hippocampal sclerosis who underwent 3D T1-weighted and FLAIR imaging on the 1.5T MRI scanner at Great Ormond Street Hospital as part of their clinical workup were studied, following permission by the hospital ethical review board. Cases were identified by searching the radiology reports between 2008 and 2015 for a radiological diagnosis of hippocampal sclerosis. Exclusion criteria were patients scanned using a different MRI scanner or protocol. Of the 35 patients identified who met these criteria, 12 further cases were excluded on the basis of poor MR scan quality. The following clinical information from the medical notes was gathered for the 23 remaining patients included in this study: age at epilepsy onset, duration of epilepsy, radiological report, current anticonvulsant medications, history of febrile convulsions and, where applicable, post-surgical histology and

Engel outcome. 21 out of 23 had seizure semiology characteristic of TLE. The 2 remaining patients had non-lateralising and unclear seizure semiology despite visible mesial temporal lobe sclerosis on MRI. A control group of 30 term-born children with no history of any neurological diagnosis were recruited by advertisement.

5.2.2 Neurodevelopment/Cognition

In patients, verbal (VIQ) and performance (PIQ) IQ data from previous neuropsychological assessments performed at GOSH were collected. In patients younger than or equal to seven years ($n=3$), assessments used the Wechsler Preschool and Primary Scale of Intelligence (WPPSI) which has been validated for ages 2:6 to 7:7 years. Whereas, the Wechsler Intelligence Scale for Children (WISC), which has been validated for use between ages 6:0 and 16:11, was used in patients over 7 years old ($n=15$). Cognitive data was available in 18 out of 23 patients. All control participants were assessed using the Wechsler Abbreviated Scale of Intelligence (WASI) ($n=30$).

5.2.3 MR Imaging

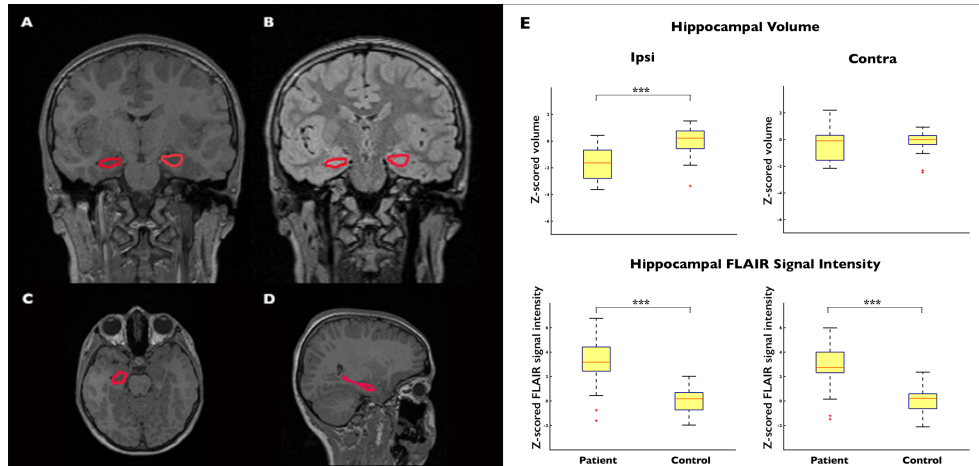
All participants were scanned on a 1.5T Avanto MRI scanner (Siemens, Erlangen, Germany). Three-dimensional data sets were acquired using a T1-weighted 3D-FLASH sequence ($TR = 11$ ms, $TE = 4.94$ ms, $FOV = 256 \times 256$ mm², flip angle = 15°, voxel size = 1x1x1 mm³) and T2-weighted FLAIR sequence ($TR = 6000$ ms, $TE = 353$ ms, $TI = 2200$ ms, $FOV = 256 \times 256$ mm², flip angle = 15°, voxel size = 1x1x1 mm³).

5.2.4 Hippocampal Segmentation

Hippocampal segmentations were created using FSL-FIRST (v.5.0.8; <http://fsl.fmrib.ox.ac.uk/>). In brief, T1-weighted images are initially registered to a standard template. FSL-FIRST uses a Bayesian probabilistic model based on the shape and intensity information from a training set of 336 T1-weighted MRI scans. FSL-FIRST searches through linear combinations of shape modes of variation, from the training set, to find the most likely hippocampal shape given the T1 signal intensities from the image to be segmented (Patenaude et al., 2011). The segmentations were checked in Freeview and manually corrected in cases of overestimation into areas

such as the lateral ventricle or underlying parahippocampal white matter (Figure 5.1 A-D).

Fig. 5.1 Hippocampal atrophy and FLAIR signal intensity



Hippocampal segmentations: coronal section of T1-weighted (A) and FLAIR (B) images; and axial (C) and sagittal (D) T1-weighted sections. (E) Reduced ipsilateral but not contralateral hippocampal volume in patients. Increased FLAIR signal of ipsilateral and contralateral hippocampi in patients.

5.2.5 Cortical Reconstruction

Cortical reconstructions were generated using *FreeSurfer* software v5.3 (Dale et al., 1999; Fischl and Dale, 2000; Fischl et al., 1999). The data is normalized for intensity and RF-bias field inhomogeneities are modeled and removed. The skull and neck are then removed from all of the images using a skull-stripping algorithm (Ségonne et al., 2004). Subsequently, images are classified into grey matter, white matter and cerebrospinal fluid. The hemispheres are separated, tessellated and deformed to create accurate smooth mesh representations of the grey-white matter interface and pial surface, with approximately 150,000 vertices per hemisphere. Within-subject registration of FLAIR scans to T1-weighted images was performed using a boundary-based cost function; the white-matter boundary is mapped to the FLAIR image and the FLAIR intensity is sampled per-vertex either side of the boundary. The difference in intensity between each pair of intensities is then used to calculate the cost function. All of the reconstructions were checked and any inaccuracies were manually corrected by M.B., a MSc student at the Institute of Neurology who was trained on FreeSurfer quality control. I then verified the accuracy of all FreeSurfer reconstructions.

5.2.6 Neocortical Morphological/Intensity Features

Cortical thickness was defined as the mean minimum distance between each vertex on the pial and white matter surfaces, generating a millimeter-scale measure of the thickness of the cortex. Further details of these methods are available in (Fischl and Dale, 2000). **Grey-white matter intensity contrast** was calculated as the ratio of the grey matter signal intensity to the white matter signal intensity (Salat et al., 2009). The grey matter signal intensity was sampled at a distance of 30% of the cortical thickness above the grey-white matter boundary. The white matter signal intensity was sampled 1mm below the grey-white matter boundary. As described in Chapter 2, these are FreeSurfer defaults for calculation of the grey-white contrast. **FLAIR signal intensity** was sampled at 50% of the cortical thickness, to minimise partial volume effects, and normalised by the intensity at the GM/WM boundary. In each participant, per-vertex, FLAIR intensity normalization followed the equation:

$$RI(v) = (I(v) - GMpeak)/(GMpeak - B)$$

Where $RI(v)$ is the relative FLAIR intensity of a vertex, $I(v)$ is the FLAIR signal intensity at this vertex, $GMpeak$ is the mode of the FLAIR intensity histogram at 50% of the cortical thickness, and B is the mode of the intensity histogram at the grey-white matter boundary. This normalization procedure is adapted from a voxel-wise method used in previously studies (Hong et al., 2015, 2014) (Adler et al., under review).

Cortical thickness, grey-white matter intensity contrast and normalized FLAIR intensity features were smoothed using a 10mm FWHM Gaussian diffusion kernel. Finally, individual normalized features were registered to an average space (`fsaverage_sym`) that has an identical number of vertices for each hemisphere (Greve et al., 2013).

5.2.7 Statistical Analysis

Analyses were performed using SurfStat (<http://www.math.mcgill.ca/keith/surfstat/>; (Worsley et al., 2009)) for Matlab (MATLAB 6.1, The MathWorks Inc., Natick, MA, 2000). Features were normalised using a between-subject z-scoring, where each participants per vertex feature was normalised by the mean and standard deviation in the population of

healthy controls. This adjusts for inter-hemispheric differences. Patients were analysed relative to the epileptogenic hemisphere (i.e. ipsi- and contra-lesional to the seizure focus).

a) Hippocampal volumetry and FLAIR signal intensity analysis. Linear models were used to assess between-group differences in hippocampal volume and FLAIR signal intensity using age and intracranial volume as covariates of no interest. Within patients, paired t-tests calculated differences between the affected and unaffected hippocampi. Hippocampal volume and FLAIR signal asymmetry were calculated as follows:

$$Asymmetry = (L - R)/(L + R)$$

where a negative hippocampal volume asymmetry index indicates volume loss of the left hippocampus, whereas a positive hippocampal volume asymmetry index is indicative of atrophy of the right hippocampus. In contradistinction, a positive hippocampal FLAIR asymmetry index indicates FLAIR hyperintensity of the left hippocampus and a negative asymmetry index indicates FLAIR hyperintensity of the right hippocampus.

b) Mapping whole-brain morphometric and intensity changes. Vertex-wise Student's t-tests were used to compare cortical thickness, grey-white matter intensity contrast and normalized FLAIR signal intensity between patients and controls. All analyses were controlled for age. Cohen's d effect sizes were calculated in clusters of findings. Surface-based findings were corrected using random field theory for non-isotropic images (Worsley et al., 1999), controlling the family-wise error (FWE) to be below $P_{FWE} < 0.05$. This is necessary as when surface-based data is projected onto a cortical surface, the different amounts of stretching of the surface alter the original constant FWHM used in the smoothing, making it non-isotropic.

c) Relation to clinical variables. Correlation analyses and t-tests were used to assess the effects of age of epilepsy onset, history of febrile convulsions and duration of epilepsy on MRI morphological and intensity features within the ipsi-lesional hippocampus as well as within clusters of findings established from analysis b.

5.3 Results

5.3.1 Demographics

A total of 23 patients with a radiological diagnosis of HS (14 LTLE, mean±SD age = 10.19±3.45, range = 4.71 - 15.09 years, 7 females; 9 RTLE, mean±SD age = 11.49±3.18, range = 4.55 - 15.08 years, 6 females) and 30 healthy controls (mean age = 14.33±3.01, range = 10.08 - 19.75 years, 13 females) were included. Demographic information for the patients is available in Table 5.1, and for the controls in Table 5.2. The sex of the control group was not significantly different to the TLE group ($X^2 = 1.43$, $p = 0.23$). However, the median age of the control group did differ significantly from the TLE group ($t = 4.15$, $p = 0.001$). In terms of cognition, both verbal (mean±SD 89.28±17.35 patients; 113.13±14.61 controls; $t = 5.1$, $p < 0.001$) and performance (mean±SD 91.89±19.09 patients; 115.73±13.65 controls; $t = 5.04$, $p < 0.001$) were significantly lower in HS patients than controls. Within the patient cohort, mean duration of epilepsy was 7.29±3.77 years and mean age of epilepsy onset was 3.41±3.64 years. At the time of study, 7 out of 23 patients had undergone an anterior temporal lobectomy.

Table 5.1 Paediatric TLE patient demographics

	AGE	SEX	HEMI	ONSET (yr)	DURATION (yr)	FC	VIQ	PIQ	CURRENT AEDS
1	12.09	F	R	0.5	11.59	y	81	86	LVT, TPR
2	11.38	M	L	2	9.38	y	53	55	TPR
3	13.75	F	L	4	9.75	n	108	125	CBZ, LVT
4	7.03	F	L	4.5	2.53	n	112	110	LVT, VPA, OXCBZ
5	11.72	F	R	1.5	10.22	n	83	90	LVT
6	14.29	M	L	12	2.29	n	84	84	LVT, TPR
7	11.95	M	R	7	4.95	n	n.a.	n.a.	None
8	13.57	F	R	0.83	12.74	y	87	86	VPA, OXCBZ
9	12.1	F	R	1.5	10.51	y	65	84	CBZ, TPR
10	8.68	F	L	1.5	7.18	y	87	88	LVT, VPA
11	13.92	F	R	0.92	13	y	108	100	VPA
12	10.06	F	L	0.25	9.81	n	n.a.	n.a.	LVT, VPA
13	4.71	F	L	1	3.71	y	93	79	LVT, CLB, OXCBZ
14	8.53	M	R	1.5	7.03	y	69	77	CBZ, LVT
15	8.01	F	L	1	7.01	y	99	94	VPA, LVT
16	10.21	M	L	3.5	6.71	n	81	92	TPR, LVT
17	14.87	M	L	9	5.87	n	105	109	LTG, CLB, zonisamide, perampanel
18	15.09	F	L	0.75	14.34	n	108	117	OXCBZ, LVT
19	4.55	F	R	0.75	3.8	n	n.a.	n.a.	VPA, LTG
20	6.95	M	L	0.33	6.62	n	45	49	CBZ
21	11.63	M	L	7	4.63	n	98	100	VPA, TPR, LTG
22	5.96	M	L	5	0.96	n	n.a.	n.a.	Midazolam
23	15.08	M	R	12	3.08	n	n.a.	n.a.	LTG, VPA

AGE = age of patient; HEMI = affected hippocampus; ONSET = age of onset of epilepsy; DURATION = duration of epilepsy; FC = history of febrile convulsions; VIQ = verbal IQ; PIQ = performance IQ; CURRENT AEDS = current anti-epileptic drugs; LVT = levetiracetam, CBZ = carbamazepine, OXCBZ = oxcarbazepine, VPA = sodium valproate, CLB = clobazam, LTG = lamotrigine, TPR = topiramate, PNT = phenytoin

Table 5.2 Paediatric control demographics

	AGE	SEX	VIQ	PIQ
1	14.54	M	129	123
2	10.14	M	123	129
3	17.49	M	116	108
4	16.93	M	116	123
5	18.18	F	119	118
6	18.93	F	68	102
7	12.92	M	129	129
8	11.47	F	116	128
9	16.56	M	114	135
10	13.52	F	87	127
11	11.6	M	137	125
12	11.05	F	105	120
13	12.81	M	114	102
14	18.48	M	117	126
15	12.81	F	119	121
16	13.23	M	125	131
17	10.75	F	116	101
18	10.08	F	106	98
19	13.83	M	109	135
20	17.08	F	104	98
21	11.25	M	129	113
22	11.75	M	117	129
23	12.32	M	121	105
24	10.1	M	110	102
25	14.3	M	99	103
26	17.34	F	109	116
27	17.15	F	129	122
28	17.32	M	119	123
29	16.14	F	82	83
30	19.75	M	110	97

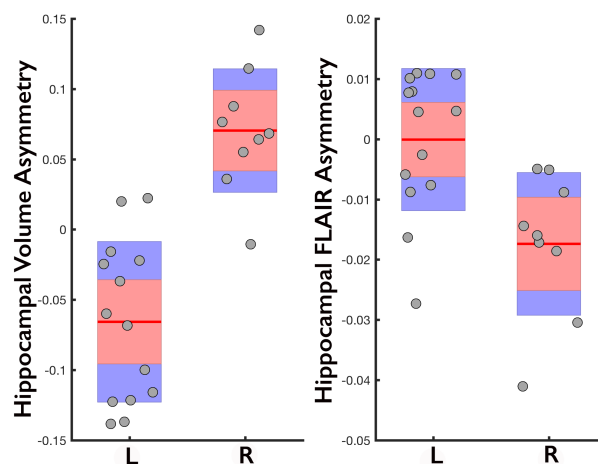
VIQ = verbal IQ; PIQ = performance IQ

5.3.2 Hippocampal Changes

Between-group quantitative analysis of hippocampal volume and normalised FLAIR intensity, with intracranial volume and age as covariates of no interest, revealed atrophy of the ipsi-lesional ($t = 3.41$, $p < 0.001$; Fig. 5.1 E) but not contra-lesional ($t = -0.45$, $p = 0.67$; Fig. 5.1 E) hippocampus and bilateral FLAIR hyperintensities (ipsi-lesional: $t = 7.12$, $p < 0.001$; Fig. 5.1 E; contra-lesional: $t = 6.59$, $p < 0.001$; Fig. 5.1 E) in HS patients. Within patients, paired t-tests indicated significantly more ipsi- compared to contra-lesional hippocampal atrophy ($t = 6.55$, $p < 0.001$) and FLAIR hyperintensity ($t = 3.42$, $p = 0.002$). Hippocampal volume asymmetry indices (Fig. 5.2 A) are able to accurately lateralise

20 out of 23 (87%) patients. Whereas, hippocampal FLAIR signal asymmetry (Fig. 5.2 B) indices are only able to correctly lateralise 17 out of 23 (79%) patients. All patients can be lateralised using either FLAIR or hippocampal volume asymmetries, with 14 out of 23 (61%) patients having both hippocampal volume and FLAIR signal asymmetries that are concordant with the side of the seizure focus. This indicates that the radiological diagnosis of HS bears a close association with quantitative measures of changes on the structural MRI scan.

Fig. 5.2 Hippocampal Asymmetries



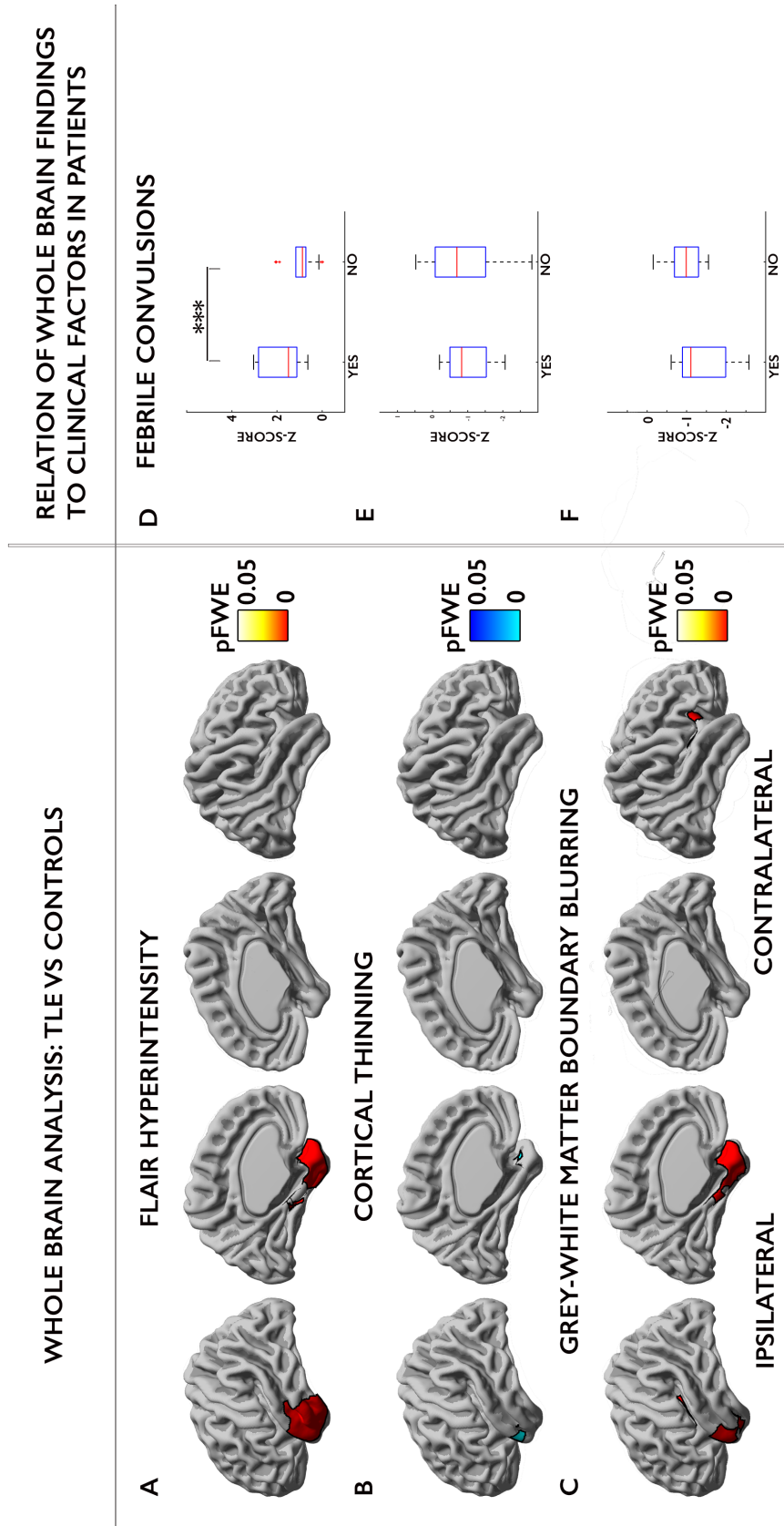
Hippocampal volume asymmetry (left) and FLAIR asymmetry (right) indices. L = LTLE cases; R = RTLE cases. A negative hippocampal volume asymmetry index indicates volume loss of the left hippocampus, whereas a positive hippocampal volume asymmetry index is indicative of atrophy of the right hippocampus. In contradistinction, a positive hippocampal FLAIR asymmetry index indicates FLAIR hyperintensity of the left hippocampus and a negative asymmetry index indicates FLAIR hyperintensity of the right hippocampus.

5.3.3 Topography of Neocortical Changes

Compared to controls, patients showed FLAIR signal hyperintensities (Fig. 5.3 A), cortical atrophy (Fig. 5.3 B) and blurring of the grey-white matter boundary (Fig. 5.3 C) in the ipsi-lesional temporal pole. FLAIR signal hyperintensities and blurring of the grey-white matter boundary were more extensive than cortical thinning. Cohen's *d* effect sizes within clusters of findings were large (Cohen's *d* = 1.49 FLAIR; *d* = 1.09 cortical atrophy; *d* = 2.06 grey-white matter blurring cluster). Visualisation of the *t*-statistic of group differences in FLAIR signal intensity (Fig 5.4) demonstrated a topographic distribution of FLAIR changes involving

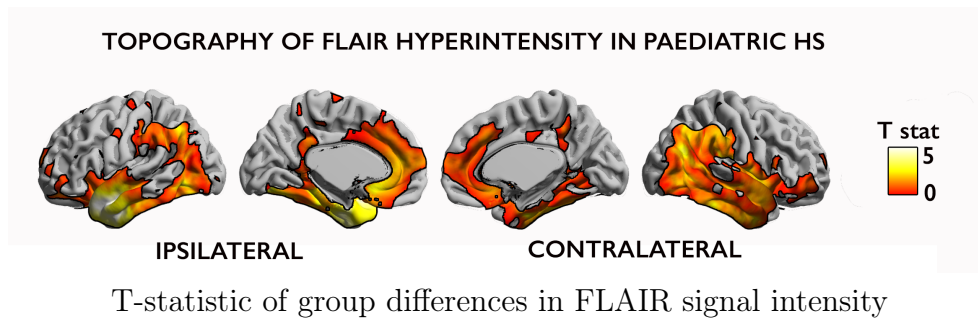
bilateral temporal and cingulate neocortices as well as the insula.

Fig. 5.3 Whole-brain analysis



Topography of FLAIR hyperintensity (A), cortical thinning (B) and grey-white matter boundary blurring (C) in paediatric TLE patients compared to controls. Findings were corrected for multiple comparisons controlling the family-wise error (FWE) to be below $P_{FWE} < 0.05$. Difference in FLAIR hyperintensity (D), cortical thickness (E) and grey-white matter intensity contrast (F) between TLE patients with (yes) and without (no) a history of febrile convulsions.

Fig. 5.4 FLAIR hyperintensity in paediatric HS



5.3.4 Relation to Clinical Variables

In patients, MRI morphological and intensity features within the ipsi-lesional hippocampus or within clusters of neocortical findings were not related to duration of epilepsy or age of epilepsy onset ($p > 0.05$). Although, ipsi-lesional FLAIR signal intensity in the hippocampus was not more pronounced in patients with a history of febrile convulsions; there was increased FLAIR signal intensity in the cluster of neocortical FLAIR signal hyperintensity in the ipsi-lesional temporal lobe ($t = 2.32$, $p = 0.03$; Fig. 5.3 D).

5.4 Discussion

Our quantitative, multimodal framework reveals unilateral hippocampal atrophy and bilateral hippocampal FLAIR hyperintensity in paediatric patients with HS. Hippocampal changes are lateralizing, with more pronounced atrophy and FLAIR signal intensity ipsi- vs- contra-lesional. The surface-based approach, to calculate per-vertex cortical thickness, normalised FLAIR signal intensity and grey-white matter intensity contrast, demonstrates that while paediatric TLE patients did not demonstrate the widespread cortical thinning present in adult cohorts (Bernhardt et al., 2010; Keller and Roberts, 2008; McDonald et al., 2008; Mueller et al., 2009), they nevertheless had morphological and intensity changes in ipsi-lesional temporopolar neocortex. Furthermore, temporopolar FLAIR hyperintensities were more marked in patients with a history of febrile convulsions.

To the best of my knowledge, this is the first study to quantify temporopolar abnormalities in children with HS. The extensive temporopolar FLAIR changes and blurring of the grey-white matter boundary quantified may be revealing subtle ipsi-lesional changes. In adults, HS and temporopolar alterations are well known. A recent study in adults using quantitative FLAIR signal analysis also found temporopolar FLAIR hyperintensity in their series of 5 TLE patients with histologically proven HS (Cardinale et al., 2017). As FLAIR signal intensity in TLE has been correlated with glial cell count (Briellmann et al., 2002; Goubran et al., 2015; Peixoto-Santos et al., 2016) and gliosis has been documented in post-mortem studies (Blanc et al., 2011; Margerison and Corsellis, 1966), FLAIR changes in the temporal neocortex may reflect gliotic changes. However, FLAIR signal is also sensitive to myelin and could reflect alterations in intra-cortical myelin content.

Blurring of the grey-white matter boundary can be seen on visual inspection of T1w MRI scans in 32-66% of adults with TLE and HS (Garbelli et al., 2012) and in 57% of children (Mitchell et al., 2003). It has been postulated to be caused by vasculometabolic changes (Ryvlin et al., 1998), cortical dysplasia (Thom et al., 2001), inflammatory changes (Meiners et al., 1999), increased perivascular spaces (Meiners et al., 1999), abnormal water content (Concha et al., 2009), widespread gliosis (Meiners et al., 1999) as well as myelin loss (Meiners et al., 1999). A seminal work by Garbelli and colleagues relating histopathology to high-field imaging carefully attempted to disentangle these factors and found that blurring was associated with axonal degeneration and reduced axonal numbers in the white matter (Garbelli et al., 2012). Interestingly, they found no difference in blurring between patients with or without subtle cortical dysplasias in the temporal pole. Furthermore, compared to controls, their temporal neocortical specimens did have widespread gliosis. Thus, blurring of the grey-white matter boundary in children with a radiological diagnosis of HS may likely be driven by axonal changes in the underlying subcortical white matter. However, it is also known that dual pathology is exceptionally common in children with HS, with a report of mild to moderate dysplasia being found in 79% of children and adolescents (Mohamed et al., 2001). Of note, 50% of Mohamed et al.,'s cohort had febrile convulsions raising an interesting question as to whether having a malformation of cortical development predisposes to both febrile convulsions and the later development of HS. Thus, the FLAIR changes and

blurring of the grey-white matter boundary found in our cohort of children with HS could be indicative of dual pathology, axonal damage and/or gliotic changes. However, in this study of children with HS from Great Ormond Street Hospital, when analyses were repeated after removing any patients with histologically proven dual pathology or HS secondary to another epilepsy syndrome, the results remained the same. Future work correlating computational anatomy on MRI with histopathology will be required to fully elucidate the underlying aetiology of these findings.

Previous studies in adults have documented widespread neocortical atrophy in patients with TLE (Bernhardt et al., 2010; Keller and Roberts, 2008; McDonald et al., 2008; Mueller et al., 2009). Although, paediatric HS patients do have a cluster of neocortical atrophy in the ipsi-lesional temporal pole, it is much less extensive than the grey-white matter boundary blurring or FLAIR hyperintensities. This dichotomy between adult and paediatric findings may reflect the fact that paediatric HS patients have shorter durations of epilepsy than adult cohorts. Cortical thinning has previously been associated with duration of epilepsy (Bernhardt et al., 2010) and may be related to generalized, seizure-related factors and reflect consequences of the overall disease process. The adult TLE cohort studied in Chapter 4 had a mean duration of epilepsy of 18 years. In contradistinction, this paediatric cohort only has a mean duration of epilepsy of 7 years, and thus the effects of seizure-related excitotoxicity may not be fully established. However, in this paediatric TLE cohort, there is no correlation with duration of epilepsy. Alternatively it is possible that cortical thinning is a relatively subtle change and requires more statistical power to detect. The paediatric cohort was only around 1/3 of the adult TLE sample size. Moreover, during development including adolescence there are widespread changes in cortical composition and connectivity (Whitaker et al., 2016) including in limbic networks (Seidlitz et al., 2017; Vasa et al., 2017). As such, the distributed network of changes seen in adults but not in children might depend on these late-emerging structural connections.

My previous work in adult TLE (Chapter 4) showed a paralimbic distribution of FLAIR hyperintensities and indicated a vulnerability of cortex with similar intracortical tissue composition to FLAIR signal hyperintensities. Although, this paralimbic pattern does not survive correction for multiple comparisons in the paediatric cohort; this bilateral paralim-

bic topographic distribution involving parahippocampal and cingulate cortices as well as the insula is evident (Fig 5.4) supporting the idea that these neocortical areas have a shared vulnerability to pathological changes.

Patients with a history of febrile convulsions have more pronounced FLAIR hyperintensity in the ipsi-lesional temporal pole. This is in line with the results from a prospective imaging study in children that has shown visible T2 hyperintensity in the adjacent ipsi-lesional temporal neocortex following febrile status epilepticus (Shinnar et al., 2012) and suggests a particular vulnerability of the ipsilateral temporal pole to early insults. However, the relationship between febrile seizures and the subsequent development of mesial temporal lobe epilepsy is still unclear (Scott, 2014).

There are several limitations in this study. First, HS is an uncommon aetiology in paediatric epilepsy and as such this study has a modest sample size. This may explain why after correction for multiple comparisons, the paralimbic topography of FLAIR changes found in the adult study (Fig A.1) is not present in the paediatric sample. Collaborations with other paediatric epilepsy centres, so that patients across epilepsy centres can be combined into large well-powered studies would improve this and allow more subtle abnormalities to be captured. Second, as mentioned earlier, it is not possible to disentangle which cytoarchitectural changes (focal cortical dysplasia, gliotic changes, neuronal damage and/or axonal damage) are driving the neuroimaging findings reported in this study. Future work combining multimodal neuroimaging with histopathological verification would be necessary to disentangle which cytoarchitectural changes are driving the neuroimaging findings. Incorporating quantitative MR measures such as T1 mapping, which is sensitive to myelin, iron, calcium and free water, and T2 mapping, sensitive to myelin, iron and gliosis, will also assist in this endeavour (see Supplementary Material 2).

Multimodal structural imaging provides a powerful tool to quantify hippocampal and cortical anomalies in paediatric HS patients. Reduced volume and FLAIR hyperintensity of the affected hippocampus demonstrate the lateralizing capacity of quantitative measurements. However, abnormalities are not limited to mesial temporal structures and extend into the ipsi-lesional temporal pole. This cortex may be particularly vulnerable to early insults such as febrile convulsions.

Chapter 6

Overall Discussion

6.1 Introduction

Epilepsy affects 1% of the paediatric population (Russ et al., 2012) making it one of the most common neurological diseases. For patients with focal epilepsies (such as FCD and TLE), epilepsy surgery, involving the removal of the epileptogenic tissue and disruption of the epileptogenic network, provides a safe treatment. Seizure freedom rates are highly dependent on accurate localisation of brain areas generating the seizures, with one meta-analysis finding seizure freedom rates of 70% when lesions were identified pre-surgically on MRI compared to 46% in MRI negative cases (Télez-Zenteno et al., 2010). Developing tools to improve the detection of lesions on MRI and implementing these tools into the pre-surgical evaluation of patients is therefore integral to improving seizure freedom rates post-operatively.

In focal epilepsies, as well as structural abnormalities associated with the seizure focus there are extra-lesional abnormalities both in adjacent and in more distant neocortex. The most documented extra-lesional pathology is the medial and lateral multi-lobar cortical thinning that is characteristic of adult cohorts with TLE (Bonilha and Keller, 2015). Understanding the topographies of extra-lesional pathology, their biological underpinnings, how they relate to clinical factors, such as seizure semiology, age of epilepsy onset, duration of epilepsy and history of febrile convulsions, as well as whether this extra-lesional pathology affects post-surgical freedom is critical to a more comprehensive understanding of focal epilepsies. It marks a move away from simply considering the focal lesion to an appreciation of the epileptogenic networks and the interplay

between the focal lesion and the rest of the brain.

The body of work presented in this thesis attempts to progress understanding of both lesional and extra-lesional pathology in two forms of focal epilepsy (FCD and TLE). This involved the application of volumetric and surface-based structural MRI analyses as well as advanced machine learning algorithms to clinically acquired data. The focus of the work is on paediatric epilepsy. However, the work included in chapter 4 and supplementary material B is based on adult data from the Montreal Neurological Institute and was completed whilst on a fellowship at the NeuroImaging of Epilepsy Laboratory under the supervision of Professor Andrea Bernasconi, Professor Neda Bernasconi and Professor Boris Bernhardt. Many of the techniques and analyses used in this adult epilepsy work are then applied to paediatric TLE data in chapter 5.

6.2 Lesional pathology

6.2.1 Main Findings

1. **The Doughnut Method** was developed in this thesis as a surface-based post-processing tool to identify local changes in cortical morphology or signal intensity. When applied to paediatric FCD data it was helpful in identifying areas of high variability in cortical thickness, grey-white matter intensity contrast or FLAIR signal. Although sensitive to small FCDs and the boundaries of larger FCDs, many other areas of healthy cortex will also be identified and thus feature maps derived from the Doughnut method must be used in conjunction with other features for lesion identification.
2. **Local Cortical Deformation** is a new measure of cortical folding based on intrinsic curvature that was specifically designed to help identify the subtle focal folding abnormalities associates with FCD lesions. Application of this method to the paediatric FCD data identified folding abnormalities in 41% of this cohort.
3. **Two-stage normalisation of cortical morphological data can help account for developmental trajectories.** Intra-subject z-scoring can account for differences in age between participants.

Subsequent per-vertex z-scoring by the population of matched control subjects can account for regional differences in a feature across the cortical surface.

4. **Automated quantification of lesion characteristics** of paediatric FCDs using surface-based morphometric and intensity analysis revealed that all lesions could be differentiated from healthy cortex (i.e. z score $>\pm 1.5$) by at least one surface-based feature and many by multiple features. These features included cortical thickness, grey-white matter intensity contrast, sulcal depth, local cortical deformation, Doughnut thickness and Doughnut FLAIR intensity.
5. **Heterogeneity of paediatric FCDs.** Kernel density plots of individual FCDs as well as across the entire group demonstrated how variable paediatric FCDs are. They can have low cortical thickness or high values of cortical thickness. They can be hypointense or hyperintense on FLAIR scans. They can be small and at the bottom of sulci or larger and distributed across gyri and sulci. Even within the same histopathological subtype (e.g. FCD Type IIB), some lesions are characterised by abnormally thin cortex and others by abnormally thick cortex.
6. **Discriminatory value of individual surface-based features.** AUC analysis of neural networks trained using only one feature indicated that all surface-based features except curvature have some discriminatory power. This included novel features developed as part of my PhD specifically to characterise radiological characteristics of FCDs as well as established surface-based features that have been used in previous adult FCD studies. The feature with the most discriminatory power was per-vertex interhemispheric FLAIR signal asymmetry.
7. **Automated lesion classification using a neural network was feasible in a cohort of paediatric FCD patients.** 73% of lesions were detected as the top cluster of the neural network output.
8. **Paediatric TLE patients have unilateral hippocampal atrophy.** Volumetric analysis of automated hippocampal segmentations indicated that the hippocampal atrophy seen on conventional visual analysis of MRI scans can be objectively quantified.

9. **Bilateral hippocampal FLAIR signal intensity was found in paediatric HS compared to controls.** However, signal intensity was more elevated in the ipsi- than contra-lesional hippocampus.
10. **Hippocampal volume asymmetry can accurately lateralise 87% of our cohort of paediatric HS patients. Hippocampal FLAIR signal asymmetry can accurately lateralise 79% of paediatric HS patients.**

6.3 Extra-lesional pathology

6.3.1 Main Findings

1. **FLAIR hyperintensity in adults with TLE extends beyond the hippocampus.** The topography of neocortical FLAIR hyperintensity in adults with TLE is bilateral and symmetrical. It involves mainly paralimbic regions such as the parahippocampus, insula and cingulate neocortices. This paralimbic pattern of FLAIR hyperintensity is highly reproducible, as indicated by bootstrap reproducibility analyses.
2. **Cortical thinning in adults with TLE has a different topographical distribution to FLAIR signal hyperintensity.** The topography of neocortical thinning involves medial and lateral frontal and lateral temporal neocortices.
3. **FLAIR signal covariance in healthy controls may provide networks of similar intracortical tissue composition.** Using a hippocampal seed, FLAIR signal covariance analysis reveals a network of paralimbic regions, such as the parahippocampus, insula and cingulate neocortices. These are regions of transitional cortex. As, FLAIR signal is sensitive to a number of microstructural tissue properties including myelin (Eriksson et al., 2007), gliosis (Briellmann et al., 2002), and iron (Zhou et al., 2001), FLAIR signal intensity covariance from the hippocampus may be delineating a network of regions with similar intracortical tissue composition to the hippocampus. This covariance is likely driven by a combination of histological factors that affect FLAIR signal intensity rather than by one factor.

4. **Shared susceptibility model in TLE.** As per-vertex FLAIR signal hyperintensity in patients with TLE significantly correlates with per-vertex FLAIR signal covariance to the hippocampus in healthy controls, areas with similar intracortical tissue composition to the hippocampus are the regions that have FLAIR signal pathology in TLE. This may indicate a shared susceptibility to TLE pathology of regions with similar intra-cortical tissue composition to the hippocampus.
5. **Adult TLE patients with a history of febrile convulsions have increased FLAIR signal hyperintensity in the ipsi-lesional parahippocampus.** The ipsi-lesional parahippocampus and other transitional cortical regions may be particularly vulnerable to early insults such as febrile convulsions.
6. **Surgical outcome is not affected by this extra-lesional pathology.** Neocortical atrophy and FLAIR signal hyperintensity in TLE is not associated with surgical outcome, i.e. the extent of extra-hippocampal abnormalities does not affect chances of seizure freedom after selective amygdalahippocampectomy.
7. **Paediatric HS patients have FLAIR hyperintensities in the ipsi-lesional temporal pole.**
8. **Cortical thinning in paediatric HS patients is limited to a small area in the ipsi-lesional temporal pole.**
9. **There is blurring of the grey-white matter boundary in the ipsi-lesional temporal pole in paediatric HS patients.**
10. **Paediatric HS patients with a history of febrile convulsions have more pronounced FLAIR changes in the ipsi-lesional temporal neocortex.**

6.4 Neurobiological and Clinical Implications

6.4.1 Paediatric FCD

The studies presented in chapters 2 and 3 aimed to address the following questions:

1. Can characteristics of paediatric FCDs be quantified using surface-based structural MRI analysis?
2. Is machine learning capable of automated detection of FCDs in paediatric epilepsy?

This work demonstrates that surface-based analysis of multi-modal MRI can effectively quantify radiological features of paediatric FCDs. Through the development of novel post-processing methods the sensitivity to characterise and delineate malformations of cortical development can be augmented. Multi-modal MRI and the use of a variety of different features capturing different aspects of cortical morphology and MR signal intensity is crucial given the considerable heterogeneity between individual lesions. This heterogeneity is even present within the same histopathological FCD subtype. Moreover, the work presented in this thesis highlights the ability of machine-learning algorithms to find complex patterns in multivariate data, with a trained artificial neural network able to accurately detect 73% of paediatric FCDs as the first cluster and an additional lesion was detected when the top 5 clusters were analysed.

This work supports the incorporation of automated structural MRI-based techniques into the pre-surgical evaluation of children with drug-resistant focal epilepsy. The crucial question is how to translate these findings into a clinical tool that can be used prospectively in the pre-surgical evaluation of children with epilepsy at Great Ormond Street Hospital and in other epilepsy centres.

6.4.2 TLE in adults

The work presented in chapter 4 aimed to address the following questions:

1. Do T2-weighted signal abnormalities extend beyond the hippocampus in adult epilepsy patients with TLE?
2. Is the topography of neocortical pathology related to hippocampal networks?
3. Do any clinical factors influence the extent of neocortical pathology?

This work shows a temporo-limbic topography of FLAIR changes in adults with TLE. The neocortical areas affected are those connected to

the hippocampus in healthy networks of hippocampal FLAIR intensity covariance. As FLAIR signal is sensitive to intra-cortical tissue composition, this indicates a susceptibility of neocortex with similar intra-cortical tissue composition to the hippocampus to FLAIR signal abnormalities. Furthermore, the finding that FLAIR hyperintensities in these temporo-limbic neocortices are more pronounced in patients with a history of febrile convulsions implies a particular susceptibility of these neocortices to early insults. These findings led to the proposal of the shared susceptibility model in TLE, where areas with similar intra-cortical tissue composition to the hippocampus have a shared vulnerability to pathology. Given that post-mortem histopathological studies have found evidence of grey-matter gliosis in similar neocortical regions to those I report (Blanc et al., 2011; Margerison and Corsellis, 1966) and that FLAIR signal is sensitive to gliosis (Briellmann et al., 2002), it is likely that the increased FLAIR signal intensity found in temporo-limbic regions is caused by an extensive gliotic process. Furthermore, although FLAIR signal is also sensitive to iron and myelin, there is limited evidence for neocortical demyelination (Thom et al., 2000) and decreased iron content (Zhang et al., 2014) in TLE.

6.4.3 Paediatric TLE

The paediatric TLE work aimed to address the following questions:

1. Can quantitative analysis of hippocampal volume and FLAIR intensity lateralise paediatric HS patients?
2. Do morphological or MR signal intensity changes extend beyond the hippocampus?
3. Is there a relationship between any clinical factors and neocortical pathology?

This work demonstrates that quantitative analysis of hippocampal volume and FLAIR signal intensity analysis can help lateralise paediatric HS patients. Furthermore, cortical morphological, FLAIR signal intensity and blurring of the grey-white matter boundary are present in the ipsi-lesional temporal lobe. This may stem from dual pathology (i.e. subtle malformations of cortical development in the ipsi-lesional temporal pole) or be due to gliotic or myelin alterations. Further work correlating

temporal neocortical imaging with histopathological findings after temporal resections will be required to disentangle these factors. Moreover, surgical outcome data after paediatric temporal lobe resections is required to determine whether the extent of T2 / FLAIR abnormalities is related to seizure outcome. However, this work putatively lends support for the anterior temporal lobectomy surgical approach rather than a selective amygdalahippocampectomy given the extensive ipsi-lesional temporal neocortical abnormalities.

6.5 Limitations

6.5.1 Clinically acquired paediatric data

All paediatric scans were acquired for clinical purposes. Although this has advantages in terms of the fact that any post-processing tools and analysis can easily be applied in a clinical setting, it also has limitations. Motion artefacts were prevalent in the data and patients had to be excluded if their scans were too affected by head motion to analyse. Furthermore, in order to have relatively homogeneous groups of patients, I had strict inclusion criteria, e.g. patients with a radiological diagnosis of FCD with 3D 1.5T T1 and FLAIR preoperative MRI scans obtained on the same clinical scanner. This resulted in relatively small sample sizes (22 patients in the paediatric FCD cohort and 23 patients in the paediatric TLE cohort). Therefore, findings will need to be validated in large cohorts of patients. To assist in this endeavour all code for the published paediatric FCD study is freely available at <https://github.com/sophieadler/FCDdetection>.

6.5.2 Histopathology

To train a supervised classifier one must first correctly define whether vertices are lesional or not. Establishing the ground-truth upon which this is defined is difficult in the context of FCD. In this thesis, all aetiological diagnoses were based on radiological and clinical findings rather than histopathological diagnoses. However, histopathological verification was available in 50% of paediatric FCD patients. Future efforts should focus on validation of the classifier in histopathologically confirmed cohorts and classifier output should be correlated with Engel outcomes. This will help establish the accuracy of the classifier and the relationship between

classifier defined "lesion" and post-surgical seizure freedom rates, which is integral prior to translating the classifier into clinical practice.

6.5.3 Technical limitations

Another limitation that must be acknowledged is hardware imperfections and biases that increase variance in the intensities of weighted magnetic resonance images. This introduces a lot of non-biological variance. Furthermore, the T1w and FLAIR MR data analysed in this thesis do not provide quantitative maps, they are measured in arbitrary units, which are not comparable across individuals and scanners. As such, the work presented in this thesis is therefore an example of computational anatomy, the automated extraction of morphological features and statistical analysis of grey and white matter maps from MRI images. Normalisation, via intra- and inter-subject z-score transformations, has been utilised in efforts to make the data more comparable across individuals/ However, quantitative MRI, which provides an estimate of the parameters governing the conventional image intensity (Weiskopf et al., 2015), is now available in a clinical setting due to advances in image acquisition.

6.5.4 Accounting for cortical morphometry

When defining cortical thickness it is important to account for curvature given that gyri are thinner than sulci (Wagstyl et al., 2016) and laminar architecture is also affected. For example, layer IV is deeper in sulci than in gyri (Wagstyl et al., under review). To attempt to account for these morphological confounds, in chapter 2, cortical thickness values in lesion were compared to the homotopic region, which should have a similar folding pattern. In chapter 3, mean curvature was included as a feature in the multivariate framework, in order to differentiate gyral and sulcal vertices. However, efforts should be made to account for curvature in future studies in TLE.

6.6 Future perspectives

In conclusion, I have shown that surface-based structural analysis of multi-modal MRI is a powerful technique to study lesional and extra-lesional pathology in drug-resistant epilepsy. It can be used to further neurobiological understanding of the underlying aetiologies and develop

clinical tools to assist in the pre-surgical evaluation of patients.

6.6.1 FCD

One of the aims of future work in the context of malformations of cortical development is the replication of the automated FCD detection work in an independent cohort of patients. Creating freely available, well-documented open-access tools is critical to this. To date, a number of large epilepsy centres worldwide have downloaded our freely available code and are running replication studies on their FCD data. I am in a collaboration with the Cleveland Clinic in Ohio who have run our code on over 60 MRI scans with histopathologically confirmed FCD type IIA and IIB. These include adult and paediatric patients scanned on 3 different scanners in different countries. They are reporting the FCD method I developed to be sensitive to around 80% of lesions. Furthermore, Great Ormond Street Hospital obtained a new 3T MRI scanner during my PhD. Currently around 30 pre-surgical patients with suspected FCDs have been scanned. Future work will involve replication using the 3T data. The development of a clinically useful classifier with high sensitivity and specificity and the ability to generalise over different scanners, different ages, and different FCD subtypes is likely to benefit from multi-centre collaborations pooling MRI scans and sharing ideas and techniques. This will allow machine learning algorithms to be trained and tested on many more subjects improving both the accuracy and generalisability of the classifier.

Another avenue of future work in terms of improving automated detection of FCDs is the continued development of surface-based features and classifiers. The surface-based framework presented in this thesis could easily incorporate features from new quantitative MR maps and data from ultra high-field MRI. Standard structural MRI data, such as T1w and T2w, are able to delineate the brain anatomy but are not specific to tissue property variations. A change in image intensity can be caused by a range of underlying neurobiological processes. Quantitative MRI (qMRI) parameters are specific to tissue structure and biophysical properties at the micrometre scale. These parameters are neuroimaging biomarkers for myelin, water and iron content (Bilgic et al., 2012; Deoni et al., 2015; Schweser et al., 2011), and provide the MRI "fingerprints" (Ma et al.,

2013) of brain tissue microstructure (Weiskopf et al., 2013). By linking brain tissue property changes with image intensity, qMRI may assist understanding of the neurobiological mechanisms underlying a change in morphometry. Future work using qMRI in the context of paediatric epilepsy may assist in both the automated detection of subtle malformations of cortical development as well as for improved understanding of the neurobiological underpinnings of paediatric epilepsies.

In terms of lesion detection, diffusion tensor imaging shows decreased subcortical fiber connectivity in and around the region affected by FCD (Lee et al., 2004) and reduced intra-cellular volume fraction (ICVF) in the lesion area (Winston et al., 2014). These findings are in agreement with altered diffusion measures performed on histology samples (Vargova et al., 2011). FA and MD are altered in the subcortical white matter subjacent to the FCD as well as beyond the MR-visible abnormality (Widjaja et al., 2009). However, alterations in FA and MD distant from the FCD have also been reported (de la Roque et al., 2005; Eriksson et al., 2001) and thus the general consensus is these features are not specific enough for lesion classification. However, they may still be useful in the context of a multivariate framework. ROI studies have estimated the correlation between histology measures and MRI parameters (Reeves et al., 2015). MT, T1, T2 and T2* values are correlated with myelin alteration in the lesion/perilesional areas. FCD type IIA shows decreased T2 and T2* values with respect to the mean values for normal cortex (Reeves et al., 2015).

Cumulatively these studies indicate that qMRI maps are sensitive to histological characteristics of FCDs and provide support for the idea that intra-cortical and subcortical sampling of these maps be useful additional features to include in the multi-modal surface-based classifier.

It is also important to acknowledge the impact that ultra-high field (UHF) strength data may have in the characterization of MRI negative patients. A preliminary study of 7T MR imaging in 21 MRI-negative patients with focal epilepsy, found structural lesions in 29% of patients (De Ciantis et al., 2016). However, there are many technical challenges in acquiring UHF data in a clinical setting, such as signal drop-out. This has implications in terms of applying surface-based post-processing pipelines as the surface reconstructions will be affected by the signal drop-out. One possible solution will be to create the surface reconstructions based on 3T

T1 data and to then co-register UHF data to these surface reconstructions. This may allow delineation and characterization of epileptogenic lesions at a higher spatial resolution.

The ultimate aim is to provide a clinical tool to assist radiologists in the pre-surgical planning of patients with drug-resistant epilepsy due to FCD. However, this surface-based machine learning framework could be applied to other problems both in epilepsy (e.g. the detection of polymicrogyria (PMG) or *in vivo* histopathological subtyping of FCDs (Adler et al., 2017)) or in other neurological disorders (e.g. the detection of grey matter lesions in multiple sclerosis).

6.6.2 TLE

This thesis finds extra-hippocampal FLAIR hyperintensities in both paediatric and adult patients with hippocampal sclerosis. In paediatric HS, correlational studies between FLAIR or T2-weighted signal and quantified histopathological characteristics from the neocortical temporal pole in paediatric HS patients following an anterior temporolobectomy would help disentangle the cytoarchitectural basis of temporal pole pathology. It would also be interesting to determine whether there is a relationship between the extent of T2 changes pre-operatively, the proportion of these abnormalities resected and post-operative seizure freedom. Relating T2 changes to surgical outcome is not restricted to TLE, and could also be used to investigate peri-lesional changes in FCD, DNETs and other focal epilepsies.

To understand the histological basis of the paralimbic FLAIR findings in adults, it would be interesting to conduct a study on post-mortem TLE brains linking MRI with histopathology. This would be able to confirm whether gliosis underpins the FLAIR hyperintensities found. It would also help clarify whether T2 / FLAIR intensity is a biomarker of extra-hippocampal network involvement. The use of quantitative T2 maps would benefit these future studies as T2 mapping has been shown to significantly outperform FLAIR in differentiating sclerotic from healthy hippocampi (Rodionov et al., 2015). Furthermore, histological analysis on resected brain regions has shown that multiple linear regression models using T1 and T2 mapping can accurately predict neuronal loss in hip-

pocampal subfields (Goubran et al., 2015).

Lastly, it would be interesting to understand the impact of extra-lesional pathology on cognition. This would require studies linking specific cognitive functions, such as language, memory and executive function, with structural MR features. This may help improve understanding of the histopathological basis of subtle cognitive deficits.

References

- Adler, S., Lorio, S., Jacques, T. S., Benova, B., and Gunny, R. (2017). Towards in vivo focal cortical dysplasia phenotyping using quantitative MRI. *NeuroImage: Clinical*.
- Adler, S., Wagstyl, K., Gunny, R., Ronan, L., Carmichael, D., Cross, J. H., Fletcher, P. C., and Baldeweg, T. (2016). Novel surface features for automated detection of focal cortical dysplasias in paediatric epilepsy. *NeuroImage: Clinical*, pages 18–27.
- Ahmed, B., Brodley, C. E., Blackmon, K. E., Kuzniecky, R., Barash, G., Carlson, C., Quinn, B. T., Doyle, W., French, J., Devinsky, O., and Thesen, T. (2015). Cortical feature analysis and machine learning improves detection of "MRI-negative" focal cortical dysplasia. *Epilepsy & behavior : E&B*, 48:21–28.
- Alexander, A. L., Hurley, S. A., Samsonov, A. A., Adluru, N., Hosseinbor, A. P., Mossahebi, P., Tromp, D. P. M., Zakszewski, E., and Field, A. S. (2012). Characterization of Cerebral White Matter Properties Using Quantitative Magnetic Resonance Imaging Stains. *dx.doi.org*, 1(6):423–446.
- Alexander-Bloch, A., Raznahan, A., Bullmore, E., and Giedd, J. (2013). The Convergence of Maturational Change and Structural Covariance in Human Cortical Networks. *Journal of Neuroscience*, 33(7):2889–2899.
- Alexander-Bloch, A. F., Reiss, P. T., Rapoport, J., McAdams, H., Giedd, J. N., Bullmore, E. T., and Gogtay, N. (2014). Abnormal Cortical Growth in Schizophrenia Targets Normative Modules of Synchronized Development. *Biological Psychiatry*, 76(6):438–446.
- Ashburner, J. and Friston, K. J. (2000). Voxel-based morphometry—the methods. *NeuroImage*, 11(6 Pt 1):805–821.
- Bancaud, J., Henriksen, o., Rubio-Donnadieu, F., Seino, M., Dreifuss, F. E., and Penry, J. K. (1981). Proposal for revised clinical and electroencephalographic classification of epileptic seizures. From the Commission on Classification and Terminology of the International League Against Epilepsy. *Epilepsia*, 22(4):489–501.
- Barkovich, A. J., Kuzniecky, R. I., Bollen, A. W., and Grant, P. E. (1997). Focal transmantle dysplasia: a specific malformation of cortical development. *Neurology*, 49(4):1148–1152.

- Basser, P. J. and Pierpaoli, C. (2011). Microstructural and physiological features of tissues elucidated by quantitative-diffusion-tensor MRI. *Journal of magnetic resonance*, 213(2):560–570.
- Baulac, S., Ishida, S., Marsan, E., Miquel, C., Biraben, A., Nguyen, D. K., Nordli, D., Cossette, P., Nguyen, S., Lambrecq, V., Vlaicu, M., Daniau, M., Bielle, F., Andermann, E., Andermann, F., Leguern, E., Chassoux, F., and Picard, F. (2015). Familial focal epilepsy with focal cortical dysplasia due to DEPDC5 mutations. *Annals of Neurology*, 77(4):675–683.
- Becker, A. J., Urbach, H., Scheffler, B., Baden, T., Normann, S., Lahl, R., Pannek, H. W., Tuxhorn, I., Elger, C. E., Schramm, J., Wiestler, O. D., and Blumcke, I. (2002). Focal cortical dysplasia of Taylor’s balloon cell type: mutational analysis of the TSC1 gene indicates a pathogenic relationship to tuberous sclerosis. *Annals of Neurology*, 52(1):29–37.
- Beppu, T., Inoue, T., Shibata, Y., Kurose, A., Arai, H., Ogasawara, K., Ogawa, A., Nakamura, S., and Kabasawa, H. (2003). Measurement of fractional anisotropy using diffusion tensor MRI in supratentorial astrocytic tumors. *Journal of Neuro-Oncology*, 63(2):109–116.
- Berg, A. T., Berkovic, S. F., Brodie, M. J., Buchhalter, J., Cross, J. H., van Emde Boas, W., Engel, J., French, J., Glauser, T. A., Mathern, G. W., Moshé, S. L., Nordli, D., Plouin, P., and Scheffer, I. E. (2010). Revised terminology and concepts for organization of seizures and epilepsies: report of the ILAE Commission on Classification and Terminology, 2005-2009. *Epilepsia*, 51(4):676–685.
- Berg, A. T., Langfitt, J. T., Testa, F. M., Levy, S. R., DiMario, F., Westerveld, M., and Kulas, J. (2008). Global cognitive function in children with epilepsy: A community-based study. *Epilepsia*, 49(4):608–614.
- Bernasconi, A., Antel, S. B., Collins, D. L., Bernasconi, N., Olivier, A., Dubeau, F., Pike, G. B., Andermann, F., and Arnold, D. L. (2001). Texture analysis and morphological processing of magnetic resonance imaging assist detection of focal cortical dysplasia in extra-temporal partial epilepsy. *Annals of Neurology*, 49(6):770–775.
- Bernasconi, A., Bernasconi, N., Bernhardt, B. C., and Schrader, D. (2011). Advances in MRI for ‘cryptogenic’ epilepsies. *Nature Reviews Neurology*, 7(2):99–108.
- Bernasconi, N. (2003). Mesial temporal damage in temporal lobe epilepsy: a volumetric MRI study of the hippocampus, amygdala and parahippocampal region. *Brain*, 126(2):462–469.
- Bernhardt, B. C., Bernasconi, A., Liu, M., Hong, S.-J., Caldairou, B., Goubran, M., Guiot, M. C., Hall, J., and Bernasconi, N. (2016). The spectrum of structural and functional imaging abnormalities in temporal lobe epilepsy. *Annals of Neurology*.

- Bernhardt, B. C., Bernasconi, N., Concha, L., and Bernasconi, A. (2010). Cortical thickness analysis in temporal lobe epilepsy: Reproducibility and relation to outcome. *Neurology*, 74(22):1776–1784.
- Bernhardt, B. C., Bernasconi, N., Kim, H., and Bernasconi, A. (2012). Mapping thalamocortical network pathology in temporal lobe epilepsy. *Neurology*, 78(2):129–136.
- Bernhardt, B. C., Hong, S., Bernasconi, A., and Bernasconi, N. (2013a). Imaging structural and functional brain networks in temporal lobe epilepsy. *Frontiers in human neuroscience*, 7:1–14.
- Bernhardt, B. C., Kim, H., and Bernasconi, N. (2013b). Patterns of subregional mesiotemporal disease progression in temporal lobe epilepsy. *Neurology*, 81(21):1840–1847.
- Bernhardt, B. C., Rozen, D. A., Worsley, K. J., Evans, A. C., Bernasconi, N., and Bernasconi, A. (2009a). Thalamo–cortical network pathology in idiopathic generalized epilepsy: Insights from MRI-based morphometric correlation analysis. *NeuroImage*, 46(2):373–381.
- Bernhardt, B. C., Worsley, K. J., Besson, P., Concha, L., Lerch, J. P., Evans, A. C., and Bernasconi, N. (2008). Mapping limbic network organization in temporal lobe epilepsy using morphometric correlations: insights on the relation between mesiotemporal connectivity and cortical atrophy. *NeuroImage*, 42(2):515–524.
- Bernhardt, B. C., Worsley, K. J., Kim, H., Evans, A. C., Bernasconi, A., and Bernasconi, N. (2009b). Longitudinal and cross-sectional analysis of atrophy in pharmaco-resistant temporal lobe epilepsy. *Neurology*, 72(20):1747–1754.
- Besson, P., Andermann, F., Dubeau, F., and Bernasconi, A. (2008a). Small focal cortical dysplasia lesions are located at the bottom of a deep sulcus. *Brain*, 131(Pt 12):3246–3255.
- Besson, P., Bernasconi, N., Colliot, O., Evans, A., and Bernasconi, A. (2008b). Surface-based texture and morphological analysis detects subtle cortical dysplasia. *Medical image computing and computer-assisted intervention : MICCAI ... International Conference on Medical Image Computing and Computer-Assisted Intervention*, 11(Pt 1):645–652.
- Besson, P., Bernasconi, N., Colliot, O., Evans, A., and Bernasconi, A. (2008c). Surface-based texture and morphological analysis detects subtle cortical dysplasia. *Medical image computing and computer-assisted intervention : MICCAI ... International Conference on Medical Image Computing and Computer-Assisted Intervention*, 11(Pt 1):645–652.
- Bettus, G., Guedj, E., Joyeux, F., Confort-Gouny, S., Soulier, E., Laguitton, V., Cozzone, P. J., Chauvel, P., Ranjeva, J.-P., Bartolomei, F., and Guye, M. (2009). Decreased basal fMRI functional connectivity in epileptogenic networks and contralateral compensatory mechanisms. *Human Brain Mapping*, 30(5):1580–1591.

- Bilgic, B., Pfefferbaum, A., Rohlfing, T., Sullivan, E. V., and Adalsteinsson, E. (2012). MRI estimates of brain iron concentration in normal aging using quantitative susceptibility mapping. *NeuroImage*, 59(3):2625–2635.
- Bjørnaes, H., Stabell, K., Henriksen, O., and Løyning, Y. (2001). The effects of refractory epilepsy on intellectual functioning in children and adults. A longitudinal study. *Seizure*, 10(4):250–259.
- Blair, R. D. G. (2012). Temporal lobe epilepsy semiology. *Epilepsy research and treatment*, 2012(1):751510–10.
- Blanc, F., Martinian, L., Liagkouras, I., Catarino, C., Sisodiya, S. M., and Thom, M. (2011). Investigation of widespread neocortical pathology associated with hippocampal sclerosis in epilepsy: a postmortem study. *Epilepsia*, 52(1):10–21.
- Blümcke, I., Thom, M., Aronica, E., Armstrong, D. D., Bartolomei, F., Bernasconi, A., Bernasconi, N., Bien, C. G., Cendes, F., Coras, R., Cross, J. H., Jacques, T. S., Kahane, P., Mathern, G. W., Miyata, H., Moshé, S. L., Oz, B., Ozkara, C., Perucca, E., Sisodiya, S., Wiebe, S., and Spreafico, R. (2013). International consensus classification of hippocampal sclerosis in temporal lobe epilepsy: a Task Force report from the ILAE Commission on Diagnostic Methods. *Epilepsia*, 54(7):1315–1329.
- Blümcke, I., Thom, M., Aronica, E., Armstrong, D. D., Vinters, H. V., Palmini, A., Jacques, T. S., Avanzini, G., Barkovich, A. J., Battaglia, G., Becker, A., Cepeda, C., Cendes, F., Colombo, N., Crino, P., Cross, J. H., Delalande, O., Dubeau, F., Duncan, J., Guerrini, R., Kahane, P., Mathern, G., Najm, I., Ozkara, C., Raybaud, C., Represa, A., Roper, S. N., Salamon, N., Schulze-Bonhage, A., Tassi, L., Vezzani, A., and Spreafico, R. (2010). The clinicopathologic spectrum of focal cortical dysplasias: A consensus classification proposed by an ad hoc Task Force of the ILAE Diagnostic Methods Commission1. *Epilepsia*, 52(1):158–174.
- Bonilha, L. and Keller, S. S. (2015). Quantitative MRI in refractory temporal lobe epilepsy: relationship with surgical outcomes. *Quantitative imaging in medicine and surgery*, 5(2):204–224.
- Bonilha, L., Rorden, C., Appenzeller, S., Carolina Coan, A., Cendes, F., and Min Li, L. (2006). Gray matter atrophy associated with duration of temporal lobe epilepsy. *NeuroImage*, 32(3):1070–1079.
- Bonilha, L., Rorden, C., Halford, J. J., Eckert, M., Appenzeller, S., Cendes, F., and Li, L. M. (2007). Asymmetrical extra-hippocampal grey matter loss related to hippocampal atrophy in patients with medial temporal lobe epilepsy. *Journal of Neurology, Neurosurgery & Psychiatry*, 78(3):286–294.
- Boonyapisit, K., Najm, I., Klem, G., Ying, Z., and Burrier, C. (2003). Epileptogenicity of Focal Malformations Due to Abnormal Cortical Development: Direct Electrographic–Histopathologic Correlations - Boonyapisit - 2003 - Epilepsia - Wiley Online Library. *J Neurochem*.

- Boucher, M., Whitesides, S., and Evans, A. (2009). Depth potential function for folding pattern representation, registration and analysis. *Medical image analysis*, 13(2):203–214.
- Briellmann, R. S., Kalnins, R. M., Berkovic, S. F., and Jackson, G. D. (2002). Hippocampal pathology in refractory temporal lobe epilepsy T2-weighted signal change reflects dentate gliosis. *Neurology*, 58(2):265–271.
- Brodmann, K. (1909). Vergleichende Lokalisationslehre der Groshirnrinde.
- Bronen, R. A., Cheung, G., Charles, J. T., Kim, J. H., Spencer, D. D., Spencer, S. S., Sze, G., and McCarthy, G. (1991). Imaging findings in hippocampal sclerosis: correlation with pathology. *AJNR. American journal of neuroradiology*, 12(5):933–940.
- Bullmore, E. and Sporns, O. (2009). Complex brain networks: graph theoretical analysis of structural and functional systems. *Nature Reviews Neuroscience*, 10(3):186–198.
- Caldairou, B., Bernhardt, B., Kulaga-Yoskovitz, J., Kim, H., Bernasconi, N., and Andrea, B. (2016). A Surface Patch-Based Segmentation Method for Hippocampal Subfields. *MICCAI 2016*.
- Cardinale, F., Francione, S., Gennari, L., Citterio, A., Sberna, M., Tassi, L., Mai, R., Sartori, I., Nobili, L., Cossu, M., Castana, L., Lo Russo, G., and Colombo, N. (2017). SURface-PRojected FLuid-Attenuation-Inversion-Recovery Analysis: A Novel Tool for Advanced Imaging of Epilepsy. *World Neurosurgery*, 98:715–726.e1.
- Carne, R. P., O’Brien, T. J., Kilpatrick, C. J., MacGregor, L. R., Hicks, R. J., Murphy, M. A., Bowden, S. C., Kaye, A. H., and Cook, M. J. (2004). MRI-negative PET-positive temporal lobe epilepsy: a distinct surgically remediable syndrome. *Brain*, 127(Pt 10):2276–2285.
- Castillo, M., Davis, P. C., Takei, Y., and Hoffman, J. C. (1990). Intracranial ganglioglioma: MR, CT, and clinical findings in 18 patients. *American Journal of Roentgenology*, 154(3):607–612.
- Cendes, F., Andermann, F., Dubeau, F., Gloor, P., Evans, A., Jones-Gotman, M., Olivier, A., Andermann, E., Robitaille, Y., and Lopes-Cendes, I. (1993). Early childhood prolonged febrile convulsions, atrophy and sclerosis of mesial structures, and temporal lobe epilepsy: an MRI volumetric study. *Neurology*, 43(6):1083–1087.
- Chao-Gan, Y. and Yu-Feng, Z. (2010). DPARSF: A MATLAB Toolbox for "Pipeline" Data Analysis of Resting-State fMRI. *Frontiers in systems neuroscience*, 4:13.
- Chassoux, F., Rodrigo, S., Semah, F., Beuvon, F., Landre, E., Devaux, B., Turak, B., Mellerio, C., Meder, J.-F., Roux, F.-X., Daumas-Duport, C., Merlet, P., Dulac, O., and Chiron, C. (2010). FDG-PET improves surgical outcome in negative MRI Taylor-type focal cortical dysplasias. *Neurology*, 75(24):2168–2175.

- Chen, H.-H., Chen, C., Hung, S.-C., Liang, S.-Y., Lin, S.-C., Hsu, T.-R., Yeh, T.-C., Yu, H.-Y., Lin, C.-F., Hsu, S. P. C., Liang, M.-L., Yang, T.-F., Chu, L.-S., Lin, Y.-Y., Chang, K.-P., Kwan, S.-Y., Ho, D. M., Wong, T.-T., and Shih, Y.-H. (2014). Cognitive and epilepsy outcomes after epilepsy surgery caused by focal cortical dysplasia in children: early intervention maybe better. *Child's nervous system : ChNS : official journal of the International Society for Pediatric Neurosurgery*, 30(11):1885–1895.
- Coan, A. C., Appenzeller, S., Bonilha, L., Li, L. M., and Cendes, F. (2009). Seizure frequency and lateralization affect progression of atrophy in temporal lobe epilepsy. *Neurology*, 73(11):834–842.
- Collins, C. E., Airey, D. C., Young, N. A., Leitch, D. B., and Kaas, J. H. (2010). Neuron densities vary across and within cortical areas in primates. *Proceedings of the National Academy of Sciences of the United States of America*, 107(36):15927–15932.
- Colliot, O., Bernasconi, N., Khalili, N., Antel, S. B., Naessens, V., and Bernasconi, A. (2006). Individual voxel-based analysis of gray matter in focal cortical dysplasia. *NeuroImage*, 29(1):162–171.
- Colombo, N., Tassi, L., Deleo, F., Citterio, A., Brammerio, M., Mai, R., Sartori, I., Cardinale, F., Lo Russo, G., and Spreafico, R. (2012). Focal cortical dysplasia type IIa and IIb: MRI aspects in 118 cases proven by histopathology. *Neuroradiology*, 54(10):1065–1077.
- Colombo, N., Tassi, L., Galli, C., Citterio, A., Lo Russo, G., Scialfa, G., and Spreafico, R. (2003). Focal cortical dysplasias: MR imaging, histopathologic, and clinical correlations in surgically treated patients with epilepsy. *AJNR. American journal of neuroradiology*, 24(4):724–733.
- Commission (1989). Proposal for revised classification of epilepsies and epileptic syndromes. Commission on Classification and Terminology of the International League Against Epilepsy. *Epilepsia*, 30(4):389–399.
- Concha, L., Beaulieu, C., Collins, D. L., and Gross, D. W. (2009). White-matter diffusion abnormalities in temporal-lobe epilepsy with and without mesial temporal sclerosis. *Journal of Neurology, Neurosurgery & Psychiatry*, 80(3):312–319.
- Concha, L., Beaulieu, C., and Gross, D. W. (2005). Bilateral limbic diffusion abnormalities in unilateral temporal lobe epilepsy. *Annals of Neurology*, 57(2):188–196.
- Concha, L., Kim, H., Bernasconi, A., Bernhardt, B. C., and Bernasconi, N. (2012). Spatial patterns of water diffusion along white matter tracts in temporal lobe epilepsy. *Neurology*, 79(5):455–462.
- Conti, V., Pantaleo, M., Barba, C., Baroni, G., Mei, D., Buccoliero, A. M., Giglio, S., Giordano, F., Baek, S. T., Gleeson, J. G., and Guerrini, R. (2015). Focal dysplasia of the cerebral cortex and infantile spasms associated with somatic 1q21.1-q44 duplication including the AKT3 gene. *Clinical genetics*, 88(3):241–247.

- Coras, R., de Boer, O. J., Armstrong, D., Becker, A., Jacques, T. S., Miyata, H., Thom, M., Vinters, H. V., Spreafico, R., Oz, B., Marucci, G., Pimentel, J., Mühlebner, A., Zamecnik, J., Buccoliero, A. M., Rogerio, F., Streichenberger, N., Arai, N., Bugiani, M., Vogelgesang, S., Macaulay, R., Salon, C., Hans, V., Polivka, M., Giangaspero, F., Fauziah, D., Kim, J.-H., Liu, L., Dandan, W., Gao, J., Lindeboom, B., Blumcke, I., and Aronica, E. (2012). Good interobserver and intraobserver agreement in the evaluation of the new ILAE classification of focal cortical dysplasias. *Epilepsia*, 53(8):1341–1348.
- Cormack, F., Cross, J. H., Isaacs, E., Harkness, W., Wright, I., Vargha-Khadem, F., and Baldeweg, T. (2007). The development of intellectual abilities in pediatric temporal lobe epilepsy. *Epilepsia*, 48(1):201–204.
- Cormack, F., Gadian, D. G., Vargha-Khadem, F., Cross, J. H., Connelly, A., and Baldeweg, T. (2005). Extra-hippocampal grey matter density abnormalities in paediatric mesial temporal sclerosis. *NeuroImage*, 27(3):635–643.
- Cortes, C. and Vapnik, V. (1995). Support-vector networks. *Machine Learning*, 20(3):273–297.
- Costa, R. P., Oliveira, P., Rodrigues, G., Leitao, B., and Dourado, A. (2008). Epileptic seizure classification using neural networks with 14 features. In *International Conference on Knowledge-Based and Intelligent Information and Engineering Systems*, pages 281–288. Springer.
- Crino, P. B. (2009). Focal brain malformations: Seizures, signaling, sequencing. *Epilepsia*, 50(suppl 5):3–8.
- Cross, J. (2002). Epilepsy Surgery in Childhood. *Epilepsia*, pages 1–6.
- Dale, A. M., Fischl, B., and Sereno, M. I. (1999). Cortical surface-based analysis. I. Segmentation and surface reconstruction. *NeuroImage*, 9(2):179–194.
- Damoiseaux, J. S., Rombouts, S. A. R. B., Barkhof, F., Scheltens, P., Stam, C. J., Smith, S. M., and Beckmann, C. F. (2006). Consistent resting-state networks across healthy subjects. *Proceedings of the National Academy of Sciences*, 103(37):13848–13853.
- De Ciantis, A., Barba, C., Tassi, L., Cosottini, M., Tosetti, M., Costagli, M., Bramerio, M., Bartolini, E., Biagi, L., Cossu, M., Pelliccia, V., Symms, M. R., and Guerrini, R. (2016). 7T MRI in focal epilepsy with unrevealing conventional field strength imaging. *Epilepsia*, 57(3):445–454.
- de la Roque, A. D., Oppenheim, C., Chassoux, F., Rodrigo, S., Beuvon, F., Daumas-Duport, C., Devaux, B., and Meder, J.-F. (2005). Diffusion tensor imaging of partial intractable epilepsy. *European Radiology*, 15(2):279–285.
- Deng, H. and Wickham, H. (2011). Density estimation in R. *Electronic publication*.

- Deoni, S. C. L., Dean III, D. C., Remer, J., Dirks, H., and O’Muircheartaigh, J. (2015). Cortical maturation and myelination in healthy toddlers and young children. *NeuroImage*, pages 1–15.
- Devinsky, O., Vezzani, A., Najjar, S., de Lanerolle, N. C., and Rogawski, M. A. (2013). Glia and epilepsy: excitability and inflammation. *Trends in Neurosciences*, 36(3):174–184.
- Dijkstra, E. W. (1959). A note on two problems in connexion with graphs. *Numerische mathematik*, 1(1):269–271.
- Dinse, J., Härtwich, N., Waehnert, M. D., Tardif, C. L., Schäfer, A., Geyer, S., Preim, B., Turner, R., and Bazin, P. L. (2015). A cytoarchitecture-driven myelin model reveals area-specific signatures in human primary and secondary areas using ultra-high resolution in-vivo brain MRI. *NeuroImage*, 114:71–87.
- Du, F., Whetsell, W. O., Abou-Khalil, B., Blumenkopf, B., Lothman, E. W., and Schwarcz, R. (1993). Preferential neuronal loss in layer III of the entorhinal cortex in patients with temporal lobe epilepsy. *Epilepsy Research*, 16(3):223–233.
- Ducharme, S., Albaugh, M. D., Nguyen, T.-V., Hudziak, J. J., Mateos-Pérez, J. M., Labbe, A., Evans, A. C., and Karama, S. (2015). Trajectories of cortical surface area and cortical volume maturation in normal brain development. *Data in brief*, 5:929–938.
- Duncan, J. S., Bartlett, P., and Barker, G. J. (1996). Technique for measuring hippocampal T2 relaxation time. *AJNR. American journal of neuroradiology*, 17(10):1805–1810.
- Duncan, J. S., Winston, G. P., Koepp, M. J., and Ourselin, S. (2016). Brain imaging in the assessment for epilepsy surgery. *The Lancet Neurology*.
- Düzel, E., Schiltz, K., Solbach, T., Peschel, T., Baldeweg, T., Kaufmann, J., Szentkuti, A., and Heinze, H.-J. (2006). Hippocampal atrophy in temporal lobe epilepsy is correlated with limbic systems atrophy. *Journal of Neurology*, 253(3):294–300.
- Ecker, C., Andrews, D., Dell’Acqua, F., Daly, E., Murphy, C., Catani, M., Thiebaut de Schotten, M., Baron-Cohen, S., Lai, M. C., Lombardo, M. V., Bullmore, E. T., Suckling, J., Williams, S., Jones, D. K., Chiocchetti, A., the MRC AIMS Consortium, and Murphy, D. G. M. (2016). Relationship Between Cortical Gyrification, White Matter Connectivity, and Autism Spectrum Disorder. *Cerebral Cortex*, 26(7):3297–3309.
- Ecker, C., Ronan, L., Feng, Y., Daly, E., Murphy, C., Ginestet, C. E., Brammer, M., Fletcher, P. C., Bullmore, E. T., Suckling, J., Baron-Cohen, S., Williams, S., Loth, E., MRC AIMS Consortium, and Murphy, D. G. M. (2013). Intrinsic gray-matter connectivity of the brain in adults with autism spectrum disorder. *Proceedings of the National Academy of Sciences of the United States of America*, 110(32):13222–13227.

- Eickhoff, S., Walters, N. B., Schleicher, A., Kril, J., Egan, G. F., Zilles, K., Watson, J. D. G., and Amunts, K. (2005). High-resolution MRI reflects myeloarchitecture and cytoarchitecture of human cerebral cortex. *Human Brain Mapping*, 24(3):206–215.
- Eltze, C. M., Chong, W. K., Bhate, S., Harding, B., Neville, B. G. R., and Cross, J. H. (2005). Taylor-type Focal Cortical Dysplasia in Infants: Some MRI Lesions Almost Disappear with Maturation of Myelination. *Epilepsia*, 46(12):1988–1992.
- Engel, J. (1996). Introduction to temporal lobe epilepsy. *Epilepsy Research*, 26(1):141–150.
- Engel, J., Jr, Thompson, P. M., Stern, J. M., Staba, R. J., Bragin, A., and Mody, I. (2013). Connectomics and epilepsy. *Current Opinion in Neurology*, 26(2):186–194.
- Engel, J. J. (1993). Outcome with respect to epileptic seizures. *Surgical Treatment of the Epilepsies*, pages 609–621.
- Eriksson, S. H., Free, S. L., Thom, M., Martinian, L., Symms, M. R., Salmenpera, T. M., McEvoy, A. W., Harkness, W., Duncan, J. S., and Sisodiya, S. M. (2007). Correlation of quantitative MRI and neuropathology in epilepsy surgical resection specimens—T2 correlates with neuronal tissue in gray matter. *NeuroImage*, 37(1):48–55.
- Eriksson, S. H., Rugg-Gunn, F. J., Symms, M. R., Barker, G. J., and Duncan, J. S. (2001). Diffusion tensor imaging in patients with epilepsy and malformations of cortical development. *Brain*, 124(3):617–626.
- Evans, A. C. (2013). Networks of anatomical covariance. *NeuroImage*, 80(C):489–504.
- Farid, N., Girard, H. M., Kemmotsu, N., Smith, M. E., Magda, S. W., Lim, W. Y., Lee, R. R., and McDonald, C. R. (2012). Temporal lobe epilepsy: quantitative MR volumetry in detection of hippocampal atrophy. *Radiology*, 264(2):542–550.
- Fauser, S., Schulze-Bonhage, A., Honegger, J., Carmona, H., Huppertz, H.-J., Pantazis, G., Rona, S., Bast, T., Strobl, K., Steinhoff, B. J., Korinthenberg, R., Rating, D., Volk, B., and Zentner, J. (2004). Focal cortical dysplasias: surgical outcome in 67 patients in relation to histological subtypes and dual pathology. *Brain*, 127(11):2406–2418.
- Fauser, S., Sisodiya, S. M., Martinian, L., Thom, M., Gumbinger, C., Huppertz, H.-J., Hader, C., Strobl, K., Steinhoff, B. J., Prinz, M., Zentner, J., and Schulze-Bonhage, A. (2009). Multi-focal occurrence of cortical dysplasia in epilepsy patients. *Brain*, 132(Pt 8):2079–2090.
- Feldman, H. M., Yeatman, J. D., Lee, E. S., Barde, L. H. F., and Gaman-Bean, S. (2010). Diffusion tensor imaging: a review for pediatric researchers and clinicians. *Journal of developmental and behavioral pediatrics : JDBP*, 31(4):346–356.

- Fischl, B. and Dale, A. M. (2000). Measuring the thickness of the human cerebral cortex from magnetic resonance images. *Proceedings of the National Academy of Sciences*, 97(20):11050–11055.
- Fischl, B., Sereno, M. I., and Dale, A. M. (1999). Cortical surface-based analysis. II: Inflation, flattening, and a surface-based coordinate system. *NeuroImage*, 9(2):195–207.
- Fischl, B., van der Kouwe, A., Destrieux, C., Halgren, E., Ségonne, F., Salat, D. H., Busa, E., Seidman, L. J., Goldstein, J., Kennedy, D., Caviness, V., Makris, N., Rosen, B., and Dale, A. M. (2004). Automatically parcellating the human cerebral cortex. *Cerebral Cortex*, 14(1):11–22.
- Fisher, R. S., Acevedo, C., Arzimanoglou, A., Bogacz, A., Cross, J. H., Elger, C. E., Engel, J., Forsgren, L., French, J. A., Glynn, M., Hesdorffer, D. C., Lee, B. I., Mathern, G. W., Moshé, S. L., Perucca, E., Scheffer, I. E., Tomson, T., Watanabe, M., and Wiebe, S. (2014). ILAE official report: a practical clinical definition of epilepsy. *Epilepsia*, 55(4):475–482.
- Fisher, R. S., Cross, J. H., French, J. A., Higurashi, N., Hirsch, E., Jansen, F. E., Lagae, L., Moshé, S. L., Peltola, J., Roulet Perez, E., Scheffer, I. E., and Zuberi, S. M. (2017). Operational classification of seizure types by the International League Against Epilepsy: Position Paper of the ILAE Commission for Classification and Terminology. *Epilepsia*, 58(4):522–530.
- Fjell, A. M., Westlye, L. T., Amlien, I., Espeseth, T., Reinvang, I., Raz, N., Agartz, I., Salat, D. H., Greve, D. N., Fischl, B., Dale, A. M., and Walhovd, K. B. (2009). High Consistency of Regional Cortical Thinning in Aging across Multiple Samples. *Cerebral Cortex*, 19(9):bhn232–2012.
- Focke, N. K., Bonelli, S. B., Yogarajah, M., Scott, C., Symms, M. R., and Duncan, J. S. (2009). Automated normalized FLAIR imaging in MRI-negative patients with refractory focal epilepsy. *Epilepsia*, 50(6):1484–1490.
- Focke, N. K., Symms, M. R., Burdett, J. L., and Duncan, J. S. (2008). Voxel-based analysis of whole brain FLAIR at 3T detects focal cortical dysplasia. *Epilepsia*, 49(5):786–793.
- Fonov, V. S., Evans, A. C., McKinstry, R. C., Almlí, C. R., and Collins, D. L. (2009). Unbiased nonlinear average age-appropriate brain templates from birth to adulthood. *NeuroImage*, 47:S102.
- Garbelli, R., Milesi, G., Medici, V., Villani, F., Didato, G., Deleo, F., D’Incerti, L., Morbin, M., Mazzoleni, G., Giovagnoli, A. R., Parente, A., Zucca, I., Mastropietro, A., and Spreafico, R. (2012). Blurring in patients with temporal lobe epilepsy: clinical, high-field imaging and ultrastructural study. *Brain : a journal of neurology*, 135(Pt 8):2337–2349.

- Garbelli, R., Zucca, I., Milesi, G., Mastropietro, A., D'Incerti, L., Tassi, L., Colombo, N., Marras, C., Villani, F., Minati, L., and Spreafico, R. (2011). Combined 7-T MRI and histopathologic study of normal and dysplastic samples from patients with TLE. *Neurology*, 76(13):1177–1185.
- Gershen, L. D., Zanotti-Fregonara, P., Dustin, I. H., Liow, J.-S., Hirvonen, J., Kreisl, W. C., Jenko, K. J., Inati, S. K., Fujita, M., Morse, C. L., Brouwer, C., Hong, J. S., Pike, V. W., Zoghbi, S. S., Innis, R. B., and Theodore, W. H. (2015). Neuroinflammation in Temporal Lobe Epilepsy Measured Using Positron Emission Tomographic Imaging of Translocator Protein. *JAMA Neurology*, 72(8):882–7.
- Geschwind, N. and Levitsky, W. (1968). Human brain: left-right asymmetries in temporal speech region. *Science (New York, N.Y.)*, 161(3837):186–187.
- Giedd, J. N., Blumenthal, J., Jeffries, N. O., Castellanos, F. X., Liu, H., Zijdenbos, A., Paus, T., Evans, A. C., and Rapoport, J. L. (1999). Brain development during childhood and adolescence: a longitudinal MRI study. *Nature Neuroscience*, 2(10):861–863.
- Giedd, J. N., Raznahan, A., Alexander-Bloch, A., Schmitt, E., Gogtay, N., and Rapoport, J. L. (2015). Child psychiatry branch of the National Institute of Mental Health longitudinal structural magnetic resonance imaging study of human brain development. *Neuropsychopharmacology : official publication of the American College of Neuropsychopharmacology*, 40(1):43–49.
- Giedd, J. N., Vaituzis, a. C., Hamburger, S. D., Lange, N., Rajapakse, J. C., Kaysen, D., Vauss, Y. C., and Rapoport, J. L. (1996). Quantitative MRI of the temporal lobe, amygdala, and hippocampus in normal human development: Ages 4–18 years. *Journal of Comparative Neurology*, 366(2):223–230.
- Glasser, M. F. and Van Essen, D. C. (2011). Mapping human cortical areas in vivo based on myelin content as revealed by T1- and T2-weighted MRI. *The Journal of neuroscience : the official journal of the Society for Neuroscience*, 31(32):11597–11616.
- Gogtay, N., Giedd, J. N., Lusk, L., Hayashi, K. M., Greenstein, D., Vaituzis, a. C., Nugent, T. F., Herman, D. H., Clasen, L. S., Toga, A. W., Rapoport, J. L., and Thompson, P. M. (2004). Dynamic mapping of human cortical development during childhood through early adulthood. *Proceedings of the National Academy of Sciences*, 101(21):8174–8179.
- Gogtay, N., Greenstein, D., Lenane, M., Clasen, L., Sharp, W., Gochman, P., Butler, P., Evans, A., and Rapoport, J. (2007). Cortical brain development in nonpsychotic siblings of patients with childhood-onset schizophrenia. *Archives of General Psychiatry*, 64(7):772–780.
- Goubran, M., Bernhardt, B. C., Cantor-Rivera, D., Lau, J. C., Bliston, C., Hammond, R. R., de Ribaupierre, S., Burneo, J. G., Mirsattari,

- S. M., Steven, D. A., Parrent, A. G., Bernasconi, A., Bernasconi, N., Peters, T. M., and Khan, A. R. (2015). In vivo MRI signatures of hippocampal subfield pathology in intractable epilepsy. *Human Brain Mapping*, 37(3):1103–1119.
- Graham, S. J. and Henkelman, R. M. (1999). Pulsed Magnetization Transfer Imaging: Evaluation of Technique1. *Radiology*, 212(3):903–910.
- Greve, D. N., Van der Haegen, L., Cai, Q., Stufflebeam, S., Sabuncu, M. R., Fischl, B., and Brysbaert, M. (2013). A surface-based analysis of language lateralization and cortical asymmetry. *Journal of cognitive neuroscience*, 25(9):1477–1492.
- Guerrini, R., Duchowny, M., Jayakar, P., Krsek, P., Kahane, P., Tassi, L., Melani, F., Polster, T., Andre, V. M., Cepeda, C., Krueger, D. A., Cross, J. H., Spreafico, R., Cosottini, M., Gotman, J., Chassoux, F., Ryvlin, P., Bartolomei, F., Bernasconi, A., Stefan, H., Miller, I., Devaux, B., Najm, I., Giordano, F., Vonck, K., Barba, C., and Blumcke, I. (2015). Diagnostic methods and treatment options for focal cortical dysplasia. *Epilepsia*, 56(11):1669–1686.
- Guipponi, M., Chentouf, A., Webling, K. E. B., Freimann, K., Crespel, A., Nobile, C., Lemke, J. R., Hansen, J., Dorn, T., Lesca, G., Ryvlin, P., Hirsch, E., Rudolf, G., Rosenberg, D. S., Weber, Y., Becker, F., Helbig, I., Muhle, H., Salzmann, A., Chaouch, M., Oubaiche, M. L., Zigliio, S., Gehrig, C., Santoni, F., Pizzato, M., Langel, U., and Antonarakis, S. E. (2015). Galanin pathogenic mutations in temporal lobe epilepsy. *Human Molecular Genetics*, 24(11):3082–3091.
- Gumbinger, C., Rohsbach, C. B., Schulze-Bonhage, A., Korinthenberg, R., Zentner, J., Häffner, M., and Fauser, S. (2009). Focal cortical dysplasia: a genotype-phenotype analysis of polymorphisms and mutations in the TSC genes. *Epilepsia*, 50(6):1396–1408.
- Gupta, R. K., Rao, S. B., Jain, R., Pal, L., Kumar, R., Venkatesh, S. K., and Rathore, R. K. S. (2001). Differentiation of Calcification from Chronic Hemorrhage with Corrected Gradient Echo Phase Imaging. *Journal of Computer Assisted Tomography*, 25(5):698.
- Harvey, A. S., Cross, J. H., Shinnar, S., Mathern, G. W., Mathern, B. W., and ILAE Pediatric Epilepsy Surgery Survey Taskforce (2008). Defining the spectrum of international practice in pediatric epilepsy surgery patients. *Epilepsia*, 49(1):146–155.
- Hermann, B., Jones, J., Sheth, R., Dow, C., Koehn, M., and Seidenberg, M. (2006a). Children with new-onset epilepsy: neuropsychological status and brain structure. *Brain*, 129(10):2609–2619.
- Hermann, B. P., Dabbs, K., Becker, T., Jones, J. E., Myers y Gutierrez, A., Wendt, G., Koehn, M. A., Sheth, R., and Seidenberg, M. (2010). Brain development in children with new onset epilepsy: A prospective controlled cohort investigation. *Epilepsia*, 51(10):2038–2046.

- Hermann, B. P., Seidenberg, M., Dow, C., Jones, J., Rutecki, P., Bhat-tacharya, A., and Bell, B. (2006b). Cognitive prognosis in chronic temporal lobe epilepsy. *Annals of Neurology*, 60(1):80–87.
- Hill, J., Inder, T., Neil, J., Dierker, D., Harwell, J., and Van Essen, D. (2010). Similar patterns of cortical expansion during human development and evolution. *Proceedings of the National Academy of Sciences*, 107(29):13135–13140.
- Hirai, T., Korogi, Y., Yoshizumi, K., Shigematsu, Y., Sugahara, T., and Takahashi, M. (2000). Limbic lobe of the human brain: evaluation with turbo fluid-attenuated inversion-recovery MR imaging. *Radiology*, 215(2):470–475.
- Hong, S.-J., Bernhardt, B. C., Caldairou, B., Hall, J. A., Guiot, M. C., Schrader, D., Bernasconi, N., and Bernasconi, A. (2017a). Multimodal MRI profiling of focal cortical dysplasia type II. *Neurology*.
- Hong, S.-J., Bernhardt, B. C., Gill, R. S., Bernasconi, N., and Bernasconi, A. (2017b). The spectrum of structural and functional network alterations in malformations of cortical development. *Brain*, 140(8):2133–2143.
- Hong, S. J., Bernhardt, B. C., Schrader, D., Caldairou, B., Bernasconi, A., and Bernasconi, N. (2015). MRI-Based Lesion Profiling of Epileptogenic Cortical Malformations. *MICCAI 2015, Part II, LNCS 9350*, 9350(Chapter 60):501–509.
- Hong, S.-J., Bernhardt, B. C., Schrader, D. S., Bernasconi, N., and Bernasconi, A. (2016). Whole-brain MRI phenotyping in dysplasia-related frontal lobe epilepsy. *Neurology*, 86(7):643–650.
- Hong, S.-J., Kim, H., Schrader, D., Bernasconi, N., Bernhardt, B. C., and Bernasconi, A. (2014). Automated detection of cortical dysplasia type II in MRI-negative epilepsy. *Neurology*, 83(1):48–55.
- House, P. M., Lanz, M., Holst, B., Martens, T., Stodieck, S., and Huppertz, H.-J. (2013). Comparison of morphometric analysis based on T1- and T2-weighted MRI data for visualization of focal cortical dysplasia. *Epilepsy Research*, 106(3):403–409.
- Howard, P., Twycross, R., Shuster, J., Mihalyo, M., Rémi, J., and Wilcock, A. (2011). Anti-epileptic drugs. *Journal of pain and symptom management*, 42(5):788–804.
- Hu, W. H., Zhang, C., Zhang, K., Meng, F. G., and Chen, N. (2013). Selective amygdalohippocampectomy versus anterior temporal lobectomy in the management of mesial temporal lobe epilepsy: a meta-analysis of comparative *J Neurochem*.
- Huppertz, H.-J., Grimm, C., Fauser, S., Kassubek, J., Mader, I., Hochmuth, A., Spreer, J., and Schulze-Bonhage, A. (2005). Enhanced visualization of blurred gray–white matter junctions in focal cortical dysplasia by voxel-based 3D MRI analysis. *Epilepsy Research*, 67(1-2):35–50.

- Huttenlocher, A., Palecek, S. P., Lu, Q., Zhang, W., Mellgren, R. L., Lauffenburger, D. A., Ginsberg, M. H., and Horwitz, A. F. (1997). Regulation of Cell Migration by the Calcium-dependent Protease Calpain. *Journal of Biological Chemistry*, 272(52):32719–32722.
- Huttenlocher, P. R. and Hapke, R. J. (1990). A follow-up study of intractable seizures in childhood. *Annals of Neurology*, 28(5):699–705.
- Ijff, D. m. and Aldenkamp, A. P. (2013). Cognitive side-effects of antiepileptic drugs in children. *Handbook of clinical neurology*, 111:707–718.
- Jafari-Khouzani, K., Elisevich, K., Patel, S., Smith, B., and Soltanian-Zadeh, H. (2010). FLAIR signal and texture analysis for lateralizing mesial temporal lobe epilepsy. *NeuroImage*, 49(2):1559–1571.
- Jansen, L. A., Mirzaa, G. M., Ishak, G. E., O’Roak, B. J., Hiatt, J. B., Roden, W. H., Gunter, S. A., Christian, S. L., Collins, S., Adams, C., Rivière, J.-B., St-Onge, J., Ojemann, J. G., Shendure, J., Hevner, R. F., and Dobyns, W. B. (2015). PI3K/AKT pathway mutations cause a spectrum of brain malformations from megalencephaly to focal cortical dysplasia. *Brain*, 138(6):awv045–1628.
- Johansen-Berg, H. and Behrens, T. (2013). Diffusion MRI: from quantitative measurement to in vivo neuroanatomy.
- Josephson, C. B., Dykeman, J., Fiest, K. M., Liu, X., Sadler, R. M., Jette, N., and Wiebe, S. (2013). Systematic review and meta-analysis of standard vs selective temporal lobe epilepsy surgery. *Neurology*, 80(18):1669–1676.
- Kabat, J. and Król, P. (2012). Focal cortical dysplasia – review. *Polish Journal of Radiology*.
- Kang, T. C., Kim, D. S., Kwak, S. E., Kim, J. E., Won, M. H., Kim, D. W., Choi, S. Y., and Kwon, O. S. (2006). Epileptogenic roles of astroglial death and regeneration in the dentate gyrus of experimental temporal lobe epilepsy. *Glia*, 54(4):258–271.
- Kasperaviciute, D., Catarino, C. B., Matarin, M., Leu, C., Novy, J., Tostevin, A., Leal, B., Hessel, E. V. S., Hallmann, K., Hildebrand, M. S., Dahl, H.-H. M., Ryten, M., Trabzuni, D., Ramasamy, A., Alhusaini, S., Doherty, C. P., Dorn, T., Hansen, J., Krämer, G., Steinhoff, B. J., Zumsteg, D., Duncan, S., Kälviäinen, R. K., Eriksson, K. J., Kantanen, A.-M., Pandolfo, M., Gruber-Sedlmayr, U., Schlachter, K., Reinthaler, E. M., Stogmann, E., Zimprich, F., Théâtre, E., Smith, C., O’Brien, T. J., Meng Tan, K., Petrovski, S., Robbiano, A., Paravidino, R., Zara, F., Striano, P., Sperling, M. R., Buono, R. J., Hakonarson, H., Chaves, J., Costa, P. P., Silva, B. M., da Silva, A. M., de Graan, P. N. E., Koeleman, B. P. C., Becker, A., Schoch, S., von Lehe, M., Reif, P. S., Rosenow, F., Becker, F., Weber, Y., Lerche, H., Rössler, K., Buchfelder, M., Hamer, H. M., Kobow, K., Coras, R., Blumcke, I., Scheffer, I. E., Berkovic, S. F., Weale, M. E., Delanty, N., Depondt, C., Cavalleri, G. L., Kunz, W. S., and Sisodiya, S. M. (2013). Epilepsy, hippocampal

- sclerosis and febrile seizures linked by common genetic variation around SCN1A. *Brain*, 136(10):3140–3150.
- Keller, S. S., Richardson, M. P., O’Muircheartaigh, J., Schoene-Bake, J.-C., Elger, C., and Weber, B. (2015). Morphometric MRI alterations and postoperative seizure control in refractory temporal lobe epilepsy. *Human Brain Mapping*, 36(5):1637–1647.
- Keller, S. S. and Roberts, N. (2008). Voxel-based morphometry of temporal lobe epilepsy: An introduction and review of the literature. *Epilepsia*, 49(5):741–757.
- Keller, S. S., Wiesmann, U. C., Mackay, C. E., Denby, C. E., Webb, J., and Roberts, N. (2002). Voxel based morphometry of grey matter abnormalities in patients with medically intractable temporal lobe epilepsy: effects of side of seizure onset and epilepsy duration. *Journal of Neurology, Neurosurgery & Psychiatry*, 73(6):648–655.
- Kim, D. W., Kim, S., Park, S.-H., Chung, C.-K., and Lee, S. K. (2012). Comparison of MRI features and surgical outcome among the subtypes of focal cortical dysplasia. *Seizure*, 21(10):789–794.
- Kim, H., Mansi, T., and Bernasconi, N. (2013). Disentangling hippocampal shape anomalies in epilepsy. *Frontiers in neurology*, 4:131.
- Kim, J. S., Singh, V., Lee, J. K., Lerch, J., Ad-Dab’bagh, Y., MacDonald, D., Lee, J. M., Kim, S. I., and Evans, A. C. (2005). Automated 3-D extraction and evaluation of the inner and outer cortical surfaces using a Laplacian map and partial volume effect classification. *NeuroImage*, 27(1):210–221.
- Kozlov, M. and Turner, R. (2010). A comparison of Ansoft HFSS and CST microwave studio simulation software for multi-channel coil design and SAR estimation at 7T MRI. *Piers online*.
- Krsek, P., Maton, B., Korman, B., Pacheco-Jacome, E., Jayakar, P., Dunoyer, C., Rey, G., Morrison, G., Ragheb, J., Vinters, H. V., Resnick, T., and Duchowny, M. (2008). Different features of histopathological subtypes of pediatric focal cortical dysplasia. *Annals of Neurology*, 63(6):758–769.
- Kubota, B. Y., Coan, A. C., Yasuda, C. L., and Cendes, F. (2015). T2 hyperintense signal in patients with temporal lobe epilepsy with MRI signs of hippocampal sclerosis and in patients with temporal lobe epilepsy with normal MRI. *Epilepsy & behavior : E&B*, 46:103–108.
- Kudr, M., Krsek, P., Marusic, P., Tomasek, M., Trnka, J., Michalova, K., Jaruskova, M., Sanda, J., Kyncl, M., Zamecnik, J., Rybar, J., Jahodova, A., Mohapl, M., Komarek, V., and Tichy, M. (2013). SISCOM and FDG-PET in patients with non-lesional extratemporal epilepsy: correlation with intracranial EEG, histology, and seizure outcome. *Epileptic disorders : international epilepsy journal with videotape*, 15(1):3–13.

- Kwan, P., Arzimanoglou, A., Berg, A. T., Brodie, M. J., Allen Hauser, W., Mathern, G., Moshé, S. L., Perucca, E., Wiebe, S., and French, J. (2010). Definition of drug resistant epilepsy: Consensus proposal by the ad hoc Task Force of the ILAE Commission on Therapeutic Strategies. *Epilepsia*, 51(6):1069–1077.
- Kwan, P. and Brodie, M. J. (2001). Effectiveness of First Antiepileptic Drug. *Epilepsia*, 42(10):1255–1260.
- Kwan, P., Schachter, S. C., and Brodie, M. J. (2011). Drug-resistant epilepsy. *New England Journal of Medicine*, 365(10):919–926.
- Langkammer, C., Krebs, N., Goessler, W., Scheurer, E., Ebner, F., Yen, K., Fazekas, F., and Ropele, S. (2010). Quantitative MR Imaging of Brain Iron: A Postmortem Validation Study1. *Radiology*, 257(2):455–462.
- Leach, J. L., Greiner, H. M., Miles, L., and Mangano, F. T. (2014a). Imaging spectrum of cortical dysplasia in children. *Seminars in roentgenology*, 49(1):99–111.
- Leach, J. L., Miles, L., Henkel, D. M., Greiner, H. M., Kukreja, M. K., Holland, K. D., Rose, D. F., Zhang, B., and Mangano, F. T. (2014b). Magnetic resonance imaging abnormalities in the resection region correlate with histopathological type, gliosis extent, and postoperative outcome in pediatric cortical dysplasia. *Journal of neurosurgery. Pediatrics*, 14(1):68–80.
- Lee, K. K. and Salamon, N. (2009). [18F] Fluorodeoxyglucose-Positron-Emission Tomography and MR Imaging Coregistration for Presurgical Evaluation of Medically Refractory Epilepsy. *AJNR. American journal of neuroradiology*, 30(10):1811–1816.
- Lee, S.-K., Kim, D. I., Mori, S., Kim, J., Kim, H. D., Heo, K., and Lee, B. I. (2004). Diffusion tensor MRI visualizes decreased subcortical fiber connectivity in focal cortical dysplasia. *NeuroImage*, 22(4):1826–1829.
- Lemieux, L., Salek-Haddadi, A., Josephs, O., Allen, P., Toms, N., Scott, C., Krakow, K., Turner, R., and Fish, D. R. (2001). Event-Related fMRI with Simultaneous and Continuous EEG: Description of the Method and Initial Case Report. *NeuroImage*, 14(3):780–787.
- Lerch, J. P. and Evans, A. C. (2005). Cortical thickness analysis examined through power analysis and a population simulation. *NeuroImage*, 24(1):163–173.
- Lerner, J. T., Salamon, N., Hauptman, J. S., Velasco, T. R., Hemb, M., Wu, J. Y., Sankar, R., Donald Shields, W., Engel Jr, J., Fried, I., Cepeda, C., Andre, V. M., Levine, M. S., Miyata, H., Yong, W. H., Vinters, H. V., and Mathern, G. W. (2009). Assessment and surgical outcomes for mild type I and severe type II cortical dysplasia: A critical review and the UCLA experience. *Epilepsia*, 50(6):1310–1335.

- Lewis, D. V., Shinnar, S., Hesdorffer, D. C., Bagiella, E., Bello, J. A., Chan, S., Xu, Y., MacFall, J., Gomes, W. A., Moshé, S. L., Mathern, G. W., Pellock, J. M., Nordli Jr, D. R., Frank, L. M., Provenzale, J., Shinnar, R. C., Epstein, L. G., Masur, D., Litherland, C., Sun, S., and the FEBSTAT Study Team (2014). Hippocampal sclerosis after febrile status epilepticus: The FEBSTAT study. *Annals of Neurology*, 75(2):178–185.
- Li, G., Wang, L., Shi, F., Lyall, A. E., Lin, W., Gilmore, J. H., and Shen, D. (2014). Mapping longitudinal development of local cortical gyrification in infants from birth to 2 years of age. *The Journal of neuroscience : the official journal of the Society for Neuroscience*, 34(12):4228–4238.
- Lim, J. S., Kim, W.-i., Kang, H. C., Kim, S. H., Park, A. H., Park, E. K., Cho, Y.-W., Kim, S., Kim, H. M., Kim, J. A., Kim, J., Rhee, H., Kang, S.-G., Kim, H. D., Kim, D., Kim, D. S., and Lee, J. H. (2015). Brain somatic mutations in MTOR cause focal cortical dysplasia type II leading to intractable epilepsy. *Nature Medicine*, 21(4):395–400.
- Lin, J. J., Salamon, N., Lee, A. D., Dutton, R. A., Geaga, J. A., Hayashi, K. M., Luders, E., Toga, A. W., Engel, J., and Thompson, P. M. (2007). Reduced neocortical thickness and complexity mapped in mesial temporal lobe epilepsy with hippocampal sclerosis. *Cerebral Cortex*, 17(9):2007–2018.
- Liu, C., Li, W., Johnson, G. A., and Wu, B. (2011). High-field (9.4T) MRI of brain dysmyelination by quantitative mapping of magnetic susceptibility. *NeuroImage*, 56(3):930–938.
- Liu, M., Bernhardt, B. C., Hong, S.-J., Caldairou, B., Bernasconi, A., and Bernasconi, N. (2016). The superficial white matter in temporal lobe epilepsy: a key link between structural and functional network disruptions. *Brain*, page aww167.
- Lorio, S., Kherif, F., Ruef, A., Melie Garcia, L., Frackowiak, R., Ashburner, J., Helms, G., Lutti, A., and Draganski, B. (2016). Neurobiological origin of spurious brain morphological changes: A quantitative MRI study. *Human Brain Mapping*, 37(5):1801–1815.
- Luders, E., Thompson, P. M., Narr, K. L., Toga, A. W., Jancke, L., and Gaser, C. (2006). A curvature-based approach to estimate local gyrification on the cortical surface. *NeuroImage*, 29(4):1224–1230.
- Lutti, A., Dick, F., Sereno, M. I., and Weiskopf, N. (2014). Using high-resolution quantitative mapping of R1 as an index of cortical myelination. *NeuroImage*, 93:176–188.
- Lyttelton, O., Boucher, M., Robbins, S., and Evans, A. (2007). An unbiased iterative group registration template for cortical surface analysis. *NeuroImage*, 34(4):1535–1544.
- Ma, D., Gulani, V., Seiberlich, N., Liu, K., Sunshine, J. L., Duerk, J. L., and Griswold, M. A. (2013). Magnetic resonance fingerprinting. *Nature*, 495(7440):187–192.

- MacAllister, W. S. and Schaffer, S. G. (2007). Neuropsychological deficits in childhood epilepsy syndromes. *Neuropsychology Review*, 17(4):427–444.
- Majores, M., Blumcke, I., Urbach, H., Meroni, A., Hans, V., Holthausen, H., Elger, C. E., Schramm, J., Galli, C., Spreafico, R., Wiestler, O. D., and Becker, A. J. (2005). Distinct Allelic Variants of TSC1 and TSC2 in Epilepsy-Associated Cortical Malformations Without Balloon Cells. *Journal of Neuropathology & Experimental Neurology*, 64(7):629–637.
- Mansouri, A., Fallah, A., McAndrews, M. P., Cohn, M., Mayor, D., Andrade, D., Carlen, P., del Campo, J. M., Tai, P., Wennberg, R. A., and Valiante, T. A. (2014). Neurocognitive and Seizure Outcomes of Selective Amygdalohippocampectomy versus Anterior Temporal Lobectomy for Mesial Temporal Lobe Epilepsy. *Epilepsy research and treatment*, 2014(2):1–8.
- Margerison, J. H. and Corsellis, J. A. (1966). Epilepsy and the temporal lobes. A clinical, electroencephalographic and neuropathological study of the brain in epilepsy, with particular reference to the temporal lobes. *Brain*, 89(3):499–530.
- McDonald, C. R., Hagler, D. J., Ahmadi, M. E., Tecoma, E., Iragui, V., Gharapetian, L., Dale, A. M., and Halgren, E. (2008). Regional neocortical thinning in mesial temporal lobe epilepsy. *Epilepsia*, 49(5):794–803.
- Mechelli, A., Friston, K. J., Frackowiak, R. S., and Price, C. J. (2005). Structural covariance in the human cortex. *The Journal of neuroscience : the official journal of the Society for Neuroscience*, 25(36):8303–8310.
- Meiners, L. C., Witkamp, T. D., de Kort, G. A., van Huffelen, A. C., van der Graaf, Y., Jansen, G. H., van der Grond, J., and van Veen, C. W. (1999). Relevance of temporal lobe white matter changes in hippocampal sclerosis. Magnetic resonance imaging and histology. *Investigative radiology*, 34(1):38–45.
- Mellerio, C., Labeyrie, M.-A., Chassoux, F., Daumas-Duport, C., Landre, E., Turak, B., Roux, F.-X., Meder, J.-F., Devaux, B., and Oppenheim, C. (2012). Optimizing MR imaging detection of type 2 focal cortical dysplasia: best criteria for clinical practice. *AJNR. American journal of neuroradiology*, 33(10):1932–1938.
- Mirzaa, G. M., Campbell, C. D., Solovieff, N., Goold, C. P., Jansen, L. A., Menon, S., Timms, A. E., Conti, V., Biag, J. D., Olds, C., Boyle, E. A., Collins, S., Ishak, G., Poliachik, S. L., Girisha, K. M., Yeung, K.-S., Chung, B. H. Y., Rahikkala, E., Gunter, S. A., McDaniel, S. S., Macmurdo, C. F., Bernstein, J. A., Martin, B., Leary, R. J., Mahan, S., Liu, S., Weaver, M., Dorschner, M. O., Jhangiani, S., Muzny, D. M., Boerwinkle, E., Gibbs, R. A., Lupski, J. R., Shendure, J., Saneto, R. P., Novotny, E. J., Wilson, C. J., Sellers, W. R., Morrissey, M. P., Hevner, R. F., Ojemann, J. G., Guerrini, R., Murphy, L. O., Winckler, W., and Dobyns, W. B. (2016). Association of MTORMutations With Developmental Brain Disorders, Including Megalencephaly, Focal

- Cortical Dysplasia, and Pigmentary Mosaicism. *JAMA Neurology*, 73(7):836–10.
- Mohamed, A., Wyllie, E., Ruggieri, P., Kotagal, P., Babb, T., Hilbig, A., Wylie, C., Ying, Z., Staugaitis, S., Najm, I., Bulacio, J., Foldvary, N., Lüders, H., and Bingaman, W. (2001). Temporal lobe epilepsy due to hippocampal sclerosis in pediatric candidates for epilepsy surgery. *Neurology*, 56(12):1643–1649.
- Mohammadi, S., Carey, D., Dick, F., Diedrichsen, J., Sereno, M. I., Reisert, M., Callaghan, M. F., and Weiskopf, N. (2015). Whole-Brain In-vivo Measurements of the Axonal G-Ratio in a Group of 37 Healthy Volunteers. *Frontiers in neuroscience*, 9(58):441.
- Mueller, S. G., Laxer, K. D., Barakos, J., Cheong, I., Garcia, P., and Weiner, M. W. (2009). Widespread neocortical abnormalities in temporal lobe epilepsy with and without mesial sclerosis. *NeuroImage*, 46(2):353–359.
- Mühlebner, A., Coras, R., Kobow, K., Feucht, M., Czech, T., Stefan, H., Weigel, D., Buchfelder, M., Holthausen, H., Pieper, T., Kudernatsch, M., and Blumcke, I. (2011). Neuropathologic measurements in focal cortical dysplasias: validation of the ILAE 2011 classification system and diagnostic implications for MRI. *Acta neuropathologica*, 123(2):259–272.
- Mühlebner, A., Coras, R., Kobow, K., Feucht, M., Czech, T., Stefan, H., Weigel, D., Buchfelder, M., Holthausen, H., Pieper, T., Kudernatsch, M., and Blümcke, I. (2012). Neuropathologic measurements in focal cortical dysplasias: validation of the ILAE 2011 classification system and diagnostic implications for MRI. *Acta neuropathologica*, 123(2):259–272.
- Neeb, H., Ermer, V., Stocker, T., and Shah, N. J. (2008). Fast quantitative mapping of absolute water content with full brain coverage. *NeuroImage*, 42(3):1094–1109.
- Ngugi, A. K., Bottomley, C., Kleinschmidt, I., Sander, J. W., and Newton, C. R. (2010). Estimation of the burden of active and life-time epilepsy: A meta-analytic approach. *Epilepsia*, 51(5):883–890.
- Nickels, K. C., Wong-Kisiel, L. C., Moseley, B. D., and Wirrell, E. C. (2012). Temporal lobe epilepsy in children. *Epilepsy research and treatment*, 2012:849540.
- Palaniyappan, L. and Liddle, P. (2012). Aberrant cortical gyrification in schizophrenia: a surface-based morphometry study. *Journal of Psychiatry & Neuroscience*, 37(6):399–406.
- Palmini, A., Gambardella, A., Andermann, F., Dubeau, F., da Costa, J. C., Olivier, A., Tampieri, D., Gloor, P., Quesney, F., and Andermann, E. (1995). Intrinsic epileptogenicity of human dysplastic cortex as suggested by corticography and surgical results. *Annals of Neurology*, 37(4):476–487.

- Palmini, A., Najm, I., Avanzini, G., Babb, T., Guerrini, R., Foldvary-Schaefer, N., Jackson, G., Lüders, H. O., Prayson, R., Spreafico, R., and Vinters, H. V. (2004). Terminology and classification of the cortical dysplasias. *Neurology*, 62(6 Suppl 3):S2–8.
- Pardoe, H. R., Berg, A. T., and Jackson, G. D. (2013). Sodium valproate use is associated with reduced parietal lobe thickness and brain volume. *Neurology*, 80(20):1895–1900.
- Parkinson, G. M. (2002). High incidence of language disorder in children with focal epilepsies. *Developmental medicine and child neurology*, 44(8):533–537.
- Patenaude, B., Smith, S. M., Kennedy, D. N., and Jenkinson, M. (2011). A Bayesian model of shape and appearance for subcortical brain segmentation. *NeuroImage*, 56(3):907–922.
- Patnaik, L. M. and Manyam, O. K. (2008). Epileptic EEG detection using neural networks and post-classification. *Computer Methods and Programs in Biomedicine*, 91(2):100–109.
- Peixoto-Santos, J. E., Kandratavicius, L., Velasco, T. R., Assirati, J. A., Carlotti, C. G., Scandiuizzi, R. C., Salmon, C. E. G., Santos, A. C. d., and Leite, J. P. (2016). Individual hippocampal subfield assessment indicates that matrix macromolecules and gliosis are key elements for the increased T2 relaxation time seen in temporal lobe epilepsy. *Epilepsia*, pages 1–11.
- Pell, G. S., Briellmann, R. S., Pardoe, H., Abbott, D. F., and Jackson, G. D. (2008). Composite voxel-based analysis of volume and T2 relaxometry in temporal lobe epilepsy. *NeuroImage*, 39(3):1151–1161.
- Phi, J. H., Paeng, J. C., Lee, H. S., Wang, K.-C., Cho, B.-K., Lee, J.-Y., Park, S.-H., Lee, J., Lee, D. S., and Kim, S.-K. (2010). Evaluation of focal cortical dysplasia and mixed neuronal and glial tumors in pediatric epilepsy patients using 18F-FDG and 11C-methionine pet. *Journal of Nuclear Medicine*, 51(5):728–734.
- Pienaar, R., Fischl, B., Caviness, V., Makris, N., and Grant, P. E. (2008). A methodology for analyzing curvature in the developing brain from preterm to adult. *International Journal of Imaging Systems and Technology*, 18(1):42–68.
- R Core Team (2014). *R: A Language and Environment for Statistical Computing*. R Foundation for Statistical Computing, Vienna, Austria.
- Radhakrishnan, R., Leach, J. L., Mangano, F. T., Gelfand, M. J., Rozhkov, L., Miles, L., and Greiner, H. M. (2016). Prospective detection of cortical dysplasia on clinical MRI in pediatric intractable epilepsy. *Pediatric radiology*, 46(10):1430–1438.
- Rakhade, S. N. and Jensen, F. E. (2009). Epileptogenesis in the immature brain: emerging mechanisms. *Nature Reviews Neurology*, 5(7):380–391.

- Rakic, P. (1988). Specification of cerebral cortical areas. *Science (New York, N.Y.)*, 241(4862):170–176.
- Rathore, C., Dickson, J. C., Teotónio, R., Ell, P., and Duncan, J. S. (2014). The utility of 18F-fluorodeoxyglucose PET (FDG PET) in epilepsy surgery. *Epilepsy Research*, 108(8):1306–1314.
- Ravizza, T., Gagliardi, B., Noé, F., Boer, K., Aronica, E., and Vezzani, A. (2008). Innate and adaptive immunity during epileptogenesis and spontaneous seizures: evidence from experimental models and human temporal lobe epilepsy. *Neurobiology of disease*, 29(1):142–160.
- Raybaud, C., Shroff, M., Rutka, J. T., and Chuang, S. H. (2006). Imaging surgical epilepsy in children. *Child’s nervous system : ChNS : official journal of the International Society for Pediatric Neurosurgery*, 22(8):786–809.
- Raznahan, A., Lee, Y., Stidd, R., Long, R., Greenstein, D., Clasen, L., Addington, A., Gogtay, N., Rapoport, J. L., and Giedd, J. N. (2010). Longitudinally mapping the influence of sex and androgen signaling on the dynamics of human cortical maturation in adolescence. *Proceedings of the National Academy of Sciences of the United States of America*, 107(39):16988–16993.
- Raznahan, A., Shaw, P., Lalonde, F., Stockman, M., Wallace, G. L., Greenstein, D., Clasen, L., Gogtay, N., and Giedd, J. N. (2011). How Does Your Cortex Grow? *Journal of Neuroscience*, 31(19):7174–7177.
- Reeves, C., Tachrount, M., Thomas, D., Michalak, Z., Liu, J., Ellis, M., Diehl, B., Misericocchi, A., McEvoy, A. W., Eriksson, S., Yousry, T., and Thom, M. (2015). Combined Ex Vivo 9.4T MRI and Quantitative Histopathological Study in Normal and Pathological Neocortical Resections in Focal Epilepsy. *Brain Pathology*, 26(3):319–333.
- Régis, J., Tamura, M., Park, M. C., McGonigal, A., Rivière, D., Coulon, O., Bartolomei, F., Girard, N., Figarella-Branger, D., Chauvel, P., and Mangin, J.-F. (2011). Subclinical abnormal gyration pattern, a potential anatomic marker of epileptogenic zone in patients with magnetic resonance imaging-negative frontal lobe epilepsy. *Neurosurgery*, 69(1):80–93– discussion 93–4.
- Reuter, M., Tisdall, M. D., Qureshi, A., Buckner, R. L., van der Kouwe, A. J. W., and Fischl, B. (2015). Head motion during MRI acquisition reduces gray matter volume and thickness estimates. *NeuroImage*, 107:107–115.
- Riney, C. J., Chong, W. K., Clark, C. A., and Cross, J. H. (2012). Voxel based morphometry of FLAIR MRI in children with intractable focal epilepsy: implications for surgical intervention. *European journal of radiology*, 81(6):1299–1305.
- Riney, C. J., Harding, B., Harkness, W. J. F., Scott, R. C., and Cross, J. H. (2006). Hippocampal Sclerosis in Children with Lesional Epilepsy Is Influenced by Age at Seizure Onset. *Epilepsia*, 47(1):159–166.

- Rivière, J.-B., Mirzaa, G. M., O’Roak, B. J., Beddaoui, M., Alcantara, D., Conway, R. L., St-Onge, J., Schwartzentruber, J. A., Gripp, K. W., Nikkel, S. M., Worthylake, T., Sullivan, C. T., Ward, T. R., Butler, H. E., Kramer, N. A., Albrecht, B., Armour, C. M., Armstrong, L., Caluseriu, O., Cytrynbaum, C., Drolet, B. A., Innes, A. M., Lauzon, J. L., Lin, A. E., Mancini, G. M. S., Meschino, W. S., Reggin, J. D., Saggari, A. K., Lerman-Sagie, T., Uyanik, G., Weksberg, R., Zirn, B., Beaulieu, C. L., Consortium, F. o. R. D. G. F. C., Majewski, J., Bulman, D. E., O’Driscoll, M., Shendure, J., Graham Jr, J. M., Boycott, K. M., and Dobyns, W. B. (2012). De novo germline and postzygotic mutations in AKT3, PIK3R2 and PIK3CA cause a spectrum of related megalencephaly syndromes. *Nature Genetics*, 44(8):934–940.
- Robbins, S., Evans, A. C., Collins, D. L., and Whitesides, S. (2004). Tuning and comparing spatial normalization methods. *Medical image analysis*, 8(3):311–323.
- Rodionov, R., Bartlett, P. A., He, C., Vos, S. B., Focke, N. K., Ourselin, S. G., and Duncan, J. S. (2015). T2 mapping outperforms normalised FLAIR in identifying hippocampal sclerosis. *YNICL*, 7(C):788–791.
- Ronan, L., Alhusaini, S., Scanlon, C., Doherty, C. P., Delanty, N., and Fitzsimons, M. (2012). Widespread cortical morphologic changes in juvenile myoclonic epilepsy: Evidence from structural MRI. *Epilepsia*, 53(4):651–658.
- Ronan, L. and Fletcher, P. C. (2014). From genes to folds: a review of cortical gyrification theory. *Brain structure & function*, pages 1–9.
- Ronan, L., Pienaar, R., Williams, G., Bullmore, E., Crow, T. J., Roberts, N., Jones, P. B., Suckling, J., and Fletcher, P. C. (2011). Intrinsic curvature: a marker of millimeter-scale tangential cortico-cortical connectivity? *International Journal of Neural Systems*, 21(5):351–366.
- Rooney, W. D., Johnson, G., Li, X., Cohen, E. R., Kim, S.-G., Ugurbil, K., and Springer, C. S. (2007). Magnetic field and tissue dependencies of human brain longitudinal 1H2O relaxation in vivo. *Magnetic Resonance in Medicine*, 57(2):308–318.
- Rowland, N. C., Englot, D. J., Cage, T. A., Sughrue, M. E., Barbaro, N. M., and Chang, E. F. (2012). A meta-analysis of predictors of seizure freedom in the surgical management of focal cortical dysplasia. *Journal of neurosurgery*, 116(5):1035–1041.
- Rugg-Gunn, F. J., Eriksson, S. H., Symms, M. R., Barker, G. J., and Duncan, J. S. (2001). Diffusion tensor imaging of cryptogenic and acquired partial epilepsies. *Brain*, 124(3):627–636.
- Russ, S. A., Larson, K., and Halfon, N. (2012). A national profile of childhood epilepsy and seizure disorder. *Pediatrics*, 129(2):256–264.
- Ryvlin, P., Bouvard, S., Le Bars, D., De Lamérie, G., Grégoire, M. C., Kahane, P., Froment, J. C., and Mauguière, F. (1998). Clinical utility of flumazenil-PET versus [18F]fluorodeoxyglucose-PET and MRI in

- refractory partial epilepsy. A prospective study in 100 patients. *Brain*, 121 (Pt 11):2067–2081.
- Ryvlin, P., Cross, J. H., and Rheims, S. (2014). Epilepsy surgery in children and adults. *The Lancet Neurology*, 13(11):1114–1126.
- Salamon, N., Kung, J., Shaw, S. J., Koo, J., Koh, S., Wu, J. Y., Lerner, J. T., Sankar, R., Shields, W. D., Engel, J., Fried, I., Miyata, H., Yong, W. H., Vinters, H. V., and Mathern, G. W. (2008). FDG-PET/MRI coregistration improves detection of cortical dysplasia in patients with epilepsy. *Neurology*, 71(20):1594–1601.
- Salat, D. H., Lee, S. Y., van der Kouwe, A. J., Greve, D. N., Fischl, B., and Rosas, H. D. (2009). Age-associated alterations in cortical gray and white matter signal intensity and gray to white matter contrast. *NeuroImage*, 48(1):21–28.
- Schaer, M., Cuadra, M. B., Tamarit, L., Lazeyras, F., Eliez, S., and Thiran, J.-P. (2008). A surface-based approach to quantify local cortical gyrification. *IEEE Transactions on Medical Imaging*, 27(2):161–170.
- Schick, V., Majores, M., Engels, G., Spitoni, S., Koch, A., Elger, C. E., Simon, M., Knobbe, C., Blumcke, I., and Becker, A. J. (2006). Activation of Akt independent of PTEN and CTMP tumor-suppressor gene mutations in epilepsy-associated Taylor-type focal cortical dysplasias. *Acta neuropathologica*, 112(6):715–725.
- Schneider, J. F. and Vergesslich, K. (2007). Maturation of the limbic system revealed by MR FLAIR imaging. *Pediatric radiology*, 37(4):351–355.
- Scholten, L. H., de Reus, M. A., and van den Heuvel, M. P. (2015). Linking contemporary high resolution magnetic resonance imaging to the von Economo legacy: A study on the comparison of MRI cortical thickness and histological measurements of cortical structure. *Human brain mapping*, 36(8):3038–3046.
- Schweser, F., Deistung, A., Lehr, B. W., and Reichenbach, J. R. (2011). Quantitative imaging of intrinsic magnetic tissue properties using MRI signal phase: An approach to in vivo brain iron metabolism? *NeuroImage*, 54(4):2789–2807.
- Scott, R. C. (2014). Consequences of febrile seizures in childhood. *Current Opinion in Pediatrics*, 26(6):662–667.
- Scott, R. C., Gadian, D. G., King, M. D., Chong, W. K., Cox, T. C., Neville, B. G. R., and Connelly, A. (2002). Magnetic resonance imaging findings within 5 days of status epilepticus in childhood. *Brain*, 125(Pt 9):1951–1959.
- Ségonne, F., Dale, A. M., Busa, E., Glessner, M., Salat, D., Hahn, H. K., and Fischl, B. (2004). A hybrid approach to the skull stripping problem in MRI. *NeuroImage*, 22(3):1060–1075.

- Seidlitz, J., Váša, F., Shinn, M., Romero-Garcia, R., Whitaker, K. J., Vértes, P. E., Reardon, P. K., Clasen, L., Messinger, A., Leopold, D. A., Fonagy, P., Dolan, R. J., Jones, P. B., Goodyer, I. M., Raznahan, A., and Bullmore, E. T. (2017). Morphometric similarity networks detect microscale cortical organisation and predict inter-individual cognitive variation. *bioRxiv*.
- Shafee, R., Buckner, R. L., and Fischl, B. (2015). Gray matter myelination of 1555 human brains using partial volume corrected MRI images. *NeuroImage*, 105:473–485.
- Shamshiri, E. A., Tierney, T. M., Centeno, M., St Pier, K., Pressler, R. M., Sharp, D. J., Perani, S., Cross, J. H., and Carmichael, D. W. (2016). Interictal activity is an important contributor to abnormal intrinsic network connectivity in paediatric focal epilepsy. *Human Brain Mapping*, 38(1):221–236.
- Shaw, P., Kabani, N. J., Lerch, J. P., Eckstrand, K., Lenroot, R., Gogtay, N., Greenstein, D., Clasen, L., Evans, A., Rapoport, J. L., Giedd, J. N., and Wise, S. P. (2008). Neurodevelopmental trajectories of the human cerebral cortex. *The Journal of neuroscience : the official journal of the Society for Neuroscience*, 28(14):3586–3594.
- Shinnar, S., Bello, J. A., Chan, S., Hesdorffer, D. C., Lewis, D. V., MacFall, J., Pellock, J. M., Nordli, D. R., Frank, L. M., Moshé, S. L., Gomes, W., Shinnar, R. C., Sun, S., and FEBSTAT Study Team (2012). MRI abnormalities following febrile status epilepticus in children: the FEBSTAT study. *Neurology*, 79(9):871–877.
- Sim, J. C., Scerri, T., Fanjul Fernández, M., Riseley, J. R., Gillies, G., Pope, K., van Roozendaal, H., Heng, J. I., Mandelstam, S. A., McGillivray, G., MacGregor, D., Kannan, L., Maixner, W., Harvey, A. S., Amor, D. J., Delatycki, M. B., Crino, P. B., Bahlo, M., Lockhart, P. J., and Leventer, R. J. (2016). Familial cortical dysplasia caused by mutation in the mammalian target of rapamycin regulator NPRL3. *Annals of Neurology*, 79(1):132–137.
- Skirrow, C., Cross, J. H., Cormack, F., Harkness, W., Vargha-Khadem, F., and Baldeweg, T. (2011). Long-term intellectual outcome after temporal lobe surgery in childhood. *Neurology*, 76(15):1330–1337.
- Skirrow, C., Cross, J. H., Harrison, S., Cormack, F., Harkness, W., Coleman, R., Meierotto, E., Gaiottino, J., Vargha-Khadem, F., and Baldeweg, T. (2015). Temporal lobe surgery in childhood and neuroanatomical predictors of long-term declarative memory outcome. *Brain*, 138(Pt 1):80–93.
- Sled, J. G., Zijdenbos, A. P., and Evans, A. C. (1998). A nonparametric method for automatic correction of intensity nonuniformity in MRI data. *IEEE Transactions on Medical Imaging*, 17(1):87–97.
- Sommer, W. (1880). Erkrankung des Ammonshorns als aetiologisches Moment der Epilepsie. *Archiv für Psychiatrie und Nervenkrankheiten*, 10(3):631–675.

- Song, C., Schwarzkopf, D. S., Kanai, R., and Rees, G. (2015). Neural population tuning links visual cortical anatomy to human visual perception. *Neuron*, 85(3):641–656.
- Sotiropoulos, S. N., Behrens, T. E. J., and Jbabdi, S. (2012). Ball and rackets: Inferring fiber fanning from diffusion-weighted MRI. *NeuroImage*, 60(2):1412–1425.
- Sowell, E. R., Thompson, P. M., Leonard, C. M., Welcome, S. E., Kan, E., and Toga, A. W. (2004). Longitudinal mapping of cortical thickness and brain growth in normal children. *The Journal of neuroscience : the official journal of the Society for Neuroscience*, 24(38):8223–8231.
- Stüber, C., Morawski, M., Schäfer, A., Labadie, C., Wähnert, M., Leuze, C., Streicher, M., Barapatre, N., Reimann, K., Geyer, S., Spemann, D., and Turner, R. (2014). Myelin and iron concentration in the human brain: A quantitative study of MRI contrast. *NeuroImage*, 93:95–106.
- Sun, J., Jia, X., Liu, X., Wu, J., and Li, S. (2015). Application of MSI in MRI-negative focal cortical dysplasia patients with epilepsy. *International journal of clinical and experimental medicine*, 8(10):18427–18433.
- Tanriverdi, T., Olivier, A., Poulin, N., Andermann, F., and Dubeau, F. (2008). Long-term seizure outcome after mesial temporal lobe epilepsy surgery: corticalamygdalohippocampectomy versus selective amygdalohippocampectomy. *Journal of neurosurgery*, 108(3):517–524.
- Tassi, L., Colombo, N., Garbelli, R., Francione, S., Lo Russo, G., Mai, R., Cardinale, F., Cossu, M., Ferrario, A., Galli, C., Bramerio, M., Citterio, A., and Spreafico, R. (2002). Focal cortical dysplasia: neuropathological subtypes, EEG, neuroimaging and surgical outcome. *Brain*, 125(8):1719–1732.
- Tassi, L., Garbelli, R., Colombo, N., Bramerio, M., Lo Russo, G., Deleo, F., Milesi, G., and Spreafico, R. (2010). Type I focal cortical dysplasia: surgical outcome is related to histopathology. *Epileptic disorders : international epilepsy journal with videotape*, 12(3):181–191.
- Taylor, D. C., Falconer, M. A., Bruton, C. J., and Corsellis, J. A. N. (1971). Focal dysplasia of the cerebral cortex in epilepsy. *Journal of Neurology, Neurosurgery & Psychiatry*, 34(4):369–387.
- Téllez-Zenteno, J. F., Ronquillo, L. H., Moien-Afshari, F., and Wiebe, S. (2010). Surgical outcomes in lesional and non-lesional epilepsy: A systematic review and meta-analysis. *Epilepsy Research*, 89(2-3):310–318.
- Thesen, T., Quinn, B. T., Carlson, C., Devinsky, O., DuBois, J., McDonald, C. R., French, J., Leventer, R., Felsovalyi, O., Wang, X., Halgren, E., and Kuzniecky, R. (2011). Detection of Epileptogenic Cortical Malformations with Surface-Based MRI Morphometry. *PLoS One*, 6(2):e16430.

- Thom, M. (2009). Hippocampal Sclerosis: Progress Since Sommer - Thom - 2008 - Brain Pathology - Wiley Online Library. *Brain Pathology*.
- Thom, M. (2014). Review: Hippocampal sclerosis in epilepsy: a neuropathology review. *Neuropathology and applied neurobiology*, 40(5):520–543.
- Thom, M., Eriksson, S., Martinian, L., Caboclo, L. O., McEvoy, A. W., Duncan, J. S., and Sisodiya, S. M. (2009). Temporal lobe sclerosis associated with hippocampal sclerosis in temporal lobe epilepsy: neuropathological features. *Journal of Neuropathology & Experimental Neurology*, 68(8):928–938.
- Thom, M., Holton, J. L., D’Arrigo, C., Griffin, B., Beckett, A., Sisodiya, S., Alexiou, D., and Sander, J. W. (2000). Microdysgenesis with abnormal cortical myelinated fibres in temporal lobe epilepsy: a histopathological study with calbindin D-28-K immunohistochemistry. *Neuropathology and applied neurobiology*, 26(3):251–257.
- Thom, M., Sisodiya, S., Harkness, W., and Scaravilli, F. (2001). Microdysgenesis in temporal lobe epilepsy. A quantitative and immunohistochemical study of white matter neurones. *Brain*, 124(Pt 11):2299–2309.
- Tofts, P. (2005). Concepts: Measurement and MR. In *Quantitative MRI of the brain measuring changes caused by disease*.
- Toga, A. W., Thompson, P. M., and Sowell, E. R. (2006). Mapping brain maturation. *Trends in Neurosciences*, 29(3):148–159.
- Tohka, J., Zijdenbos, A., and Evans, A. (2004). Fast and robust parameter estimation for statistical partial volume models in brain MRI. *NeuroImage*, 23(1):84–97.
- Travis, K., Ford, K., and Jacobs, B. (2005). Regional dendritic variation in neonatal human cortex: a quantitative Golgi study. *Developmental Neuroscience*, 27(5):277–287.
- Trujillo-Ortez, A. and Hernandez-Walls, R. (2003). Levenetest: Levene’s test for homogeneity of variances. A MATLAB file. *Electronic publication*.
- Vargova, L., Homola, A., Cicanic, M., Kuncova, K., Krsek, P., Marusic, P., Sykova, E., and Zamecnik, J. (2011). The diffusion parameters of the extracellular space are altered in focal cortical dysplasias. *Neuroscience Letters*, 499(1):19–23.
- Vasa, F., Seidlitz, J., Romero-Garcia, R., Whitaker, K. J., Rosenthal, G., Vertes, P. E., Shinn, M., Alexander-Bloch, A., Fonagy, P., Dolan, R., Jones, P., Goodyer, I., Sporns, O., and Bullmore, E. T. (2017). Adolescent tuning of association cortex in human structural brain networks. *bioRxiv*.
- Vaughan, D. N., Raffelt, D., Curwood, E., Tsai, M.-H., Tournier, J.-D., Connelly, A., and Jackson, G. D. (2016). Tract-specific atrophy in focal epilepsy: disease, genetics or seizures? *Annals of Neurology*, pages 1–32.

- Vezzani, A. (2014). Epilepsy and inflammation in the brain: overview and pathophysiology. *Epilepsy Currents*, 14(s2):3–7.
- Vezzani, A., Balosso, S., and Ravizza, T. (2008). The role of cytokines in the pathophysiology of epilepsy. *Brain, behavior, and immunity*, 22(6):797–803.
- Vezzani, A. and Friedman, A. (2011). Brain inflammation as a biomarker in epilepsy. *Biomarkers in Medicine*, 5(5):607–614.
- Vingerhoets, G. (2006). Cognitive effects of seizures. *Seizure*, 15(4):221–226.
- Voets, N. L., Beckmann, C. F., Cole, D. M., Hong, S., Bernasconi, A., and Bernasconi, N. (2012). Structural substrates for resting network disruption in temporal lobe epilepsy. *Brain*, 135(Pt 8):2350–2357.
- von Economo, C. B. and Koskinas, G. N. (1925). The cytoarchitectonics of the adult human cortex. Vienna and Berlin.
- Waehnert, M. D., Dinse, J., Schäfer, A., Geyer, S., Bazin, P.-L., Turner, R., and Tardif, C. L. (2016). A subject-specific framework for in vivo myeloarchitectonic analysis using high resolution quantitative MRI. *NeuroImage*, 125:94–107.
- Wagner, J., Weber, B., Urbach, H., Elger, C. E., and Huppertz, H.-J. (2011). Morphometric MRI analysis improves detection of focal cortical dysplasia type II. *Brain*, 134(Pt 10):2844–2854.
- Wagstyl, K., Ronan, L., Goodyer, I. M., and Fletcher, P. C. (2015). Cortical thickness gradients in structural hierarchies. *NeuroImage*, 111:241–250.
- Wagstyl, K., Ronan, L., Whitaker, K. J., Goodyer, I. M., Roberts, N., Crow, T. J., and Fletcher, P. C. (2016). Multiple markers of cortical morphology reveal evidence of supragranular thinning in schizophrenia. *Transl Psychiatry*, 6(4):e780–7.
- Walhovd, K. B., Fjell, A. M., Giedd, J., Dale, A. M., and Brown, T. T. (2017). Through Thick and Thin: a Need to Reconcile Contradictory Results on Trajectories in Human Cortical Development. *Cerebral cortex (New York, N.Y. : 1991)*, 27(2):1472–1481.
- Wang, X., Zhang, C., Wang, Y., Hu, W., Shao, X., Zhang, J.-g., and Zhang, K. (2016). Prognostic factors for seizure outcome in patients with MRI-negative temporal lobe epilepsy: A meta-analysis and systematic review. *Seizure*, 38:54–62.
- Wang, Z. I., Jones, S. E., Jaisani, Z., Najm, I. M., Prayson, R. A., Burgess, R. C., Krishnan, B., Ristic, A., Wong, C. H., Bingaman, W., Gonzalez-Martinez, J. A., and Alexopoulos, A. V. (2015). Voxel-based morphometric magnetic resonance imaging (MRI) postprocessing in MRI-negative epilepsies. *Annals of Neurology*, 77(6):1060–1075.

- Wang, Z. I., Ristic, A. J., Wong, C. H., Jones, S. E., Najm, I. M., Schneider, F., Wang, S., Gonzalez-Martinez, J. A., Bingaman, W., and Alexopoulos, A. V. (2013). Neuroimaging characteristics of MRI-negative orbitofrontal epilepsy with focus on voxel-based morphometric MRI postprocessing. *Epilepsia*, 54(12):2195–2203.
- Wehner, T. and Lüders, H. (2008). Role of neuroimaging in the presurgical evaluation of epilepsy. *Journal of clinical neurology (Seoul, Korea)*, 4(1):1–16.
- Weiskopf, N., Mohammadi, S., Lutti, A., and Callaghan, M. F. (2015). Advances in MRI-based computational neuroanatomy. *Current Opinion in Neurology*, 28(4):313–322.
- Weiskopf, N., Suckling, J., Williams, G., Correia, M. M., Inkster, B., Tait, R., Ooi, C., Bullmore, E. T., and Lutti, A. (2013). Quantitative multi-parameter mapping of R1, PD(*), MT, and R2(*) at 3T: a multi-center validation. *Frontiers in neuroscience*, 7:95.
- Werring, D. J., Clark, C. A., Barker, G. J., Thompson, A. J., and Miller, D. H. (1999). Diffusion tensor imaging of lesions and normal-appearing white matter in multiple sclerosis. *Neurology*, 52(8):1626–1632.
- Wetherington, J., Serrano, G., and Dingledine, R. (2008). Astrocytes in the epileptic brain. *Neuron*, 58(2):168–178.
- Whitaker, K. J., Vértes, P. E., Váša, F., Moutoussis, M., Prabhu, G., Callaghan, M. F., Rittman, T., Tait, R., Inkster, B., Fonagy, P., Dolan, R. J., Jones, P. B., Goodyer, I. M., NSPN Consortium, Bullmore, E. T., Suckling, J., Weiskopf, N., Romero-Garcia, R., Wagstyl, K., and Ooi, C. (2016). Adolescence is associated with genomically patterned consolidation of the hubs of the human brain connectome. *Proceedings of the National Academy of Sciences of the United States of America*, page 201601745.
- Widdess-Walsh, P., Diehl, B., and Najm, I. (2006). Neuroimaging of focal cortical dysplasia. *Journal of neuroimaging : official journal of the American Society of Neuroimaging*, 16(3):185–196.
- Widjaja, E., Zarei Mahmoodabadi, S., Otsubo, H., Snead, O. C., Holowka, S., Bells, S., and Raybaud, C. (2009). Subcortical Alterations in Tissue Microstructure Adjacent to Focal Cortical Dysplasia: Detection at Diffusion-Tensor MR Imaging by Using Magnetoencephalographic Dipole Cluster Localization 1. *Radiology*, 251(1):206–215.
- Winston, G. P., Micallef, C., Symms, M. R., Alexander, D. C., Duncan, J. S., and Zhang, H. (2014). Advanced diffusion imaging sequences could aid assessing patients with focal cortical dysplasia and epilepsy. *Epilepsy Research*, 108(2):336–339.
- Winston, G. P., Yogarajah, M., Symms, M. R., McEvoy, A. W., Micallef, C., and Duncan, J. S. (2011). Diffusion tensor imaging tractography to visualize the relationship of the optic radiation to epileptogenic lesions prior to neurosurgery. *Epilepsia*, 52(8):1430–1438.

- Woermann, F. G., Steiner, H., Barker, G. J., Bartlett, P. A., Elger, C. E., Duncan, J. S., and Symms, M. R. (2001). A fast FLAIR dual-echo technique for hippocampal T2 relaxometry: first experiences in patients with temporal lobe epilepsy. *Journal of magnetic resonance imaging : JMRI*, 13(4):547–552.
- Worsley, K. J., Andermann, M., Koulis, T., MacDonald, D., and Evans, A. C. (1999). Detecting changes in nonisotropic images. *Human Brain Mapping*, 8(2-3):98–101.
- Worsley, K. J., Taylor, J. E., Carbonell, F., Chung, M. K., Duerden, E., Bernhardt, B., Lyttelton, O., Boucher, M., and Evans, A. C. (2009). SurfStat: A Matlab toolbox for the statistical analysis of univariate and multivariate surface and volumetric data using linear mixed effects models and random field theory. *NeuroImage*, Supplement 1(47):S102.
- Yagishita, A., Arai, N., Maehara, T., Shimizu, H., Tokumaru, A. M., and Oda, M. (1997). Focal cortical dysplasia: appearance on MR images. | *Radiology*. *Radiology*, 203(2):553–559.
- Yao, B., LI, T., GELDEREN, P., SHMUELI, K., DEZWART, J., and DUYN, J. (2009). Susceptibility contrast in high field MRI of human brain as a function of tissue iron content. *NeuroImage*, 44(4):1259–1266.
- Yasin, S. A., Ali, A. M., Tata, M., Picker, S. R., Anderson, G. W., Latimer-Bowman, E., Nicholson, S. L., Harkness, W., Cross, J. H., Paine, S. M. L., and Jacques, T. S. (2013). mTOR-dependent abnormalities in autophagy characterize human malformations of cortical development: evidence from focal cortical dysplasia and tuberous sclerosis. *Acta neuropathologica*, 126(2):207–218.
- Yasin, S. A., Latak, K., Becherini, F., Ganapathi, A., Miller, K., Campos, O., Picker, S. R., Bier, N., Smith, M., Thom, M., Anderson, G., Helen Cross, J., Harkness, W., Harding, B., and Jacques, T. S. (2010). Balloon cells in human cortical dysplasia and tuberous sclerosis: isolation of a pathological progenitor-like cell. *Acta neuropathologica*, 120(1):85–96.
- Yilmazer-Hanke, D. M., Wolf, H. K., Schramm, J., Elger, C. E., Wiestler, O. D., and Blumcke, I. (2000). Subregional pathology of the amygdala complex and entorhinal region in surgical specimens from patients with pharmaco-resistant temporal lobe epilepsy. *Journal of Neuropathology & Experimental Neurology*, 59(10):907–920.
- Zhang, D., Henning, T. D., Zou, L. G., Hu, L. B., Wen, L., Feng, X. Y., Dai, S. H., Wang, W. X., Sun, Q. R., and Zhang, Z. G. (2008). Intracranial ganglioglioma: clinicopathological and MRI findings in 16 patients. *Clinical Radiology*, 63(1):80–91.
- Zhang, H., Schneider, T., Wheeler-Kingshott, C. A., and Alexander, D. C. (2012). NODDI: Practical in vivo neurite orientation dispersion and density imaging of the human brain. *NeuroImage*, 61(4):1000–1016.

- Zhang, Z., Liao, W., Bernhardt, B., Wang, Z., Sun, K., Yang, F., Liu, Y., and Lu, G. (2014). Brain iron redistribution in mesial temporal lobe epilepsy: a susceptibility-weighted magnetic resonance imaging study. *BMC Neuroscience*, 15(1):117.
- Zhou, J., Golay, X., van Zijl, P. C., Silvennoinen, M. J., Kauppinen, R., Pekar, J., and Kraut, M. (2001). Inverse T(2) contrast at 1.5 Tesla between gray matter and white matter in the occipital lobe of normal adult human brain. *Magnetic Resonance in Medicine*, 46(2):401–406.
- Zielinski, B. A., Gennatas, E. D., Zhou, J., and Seeley, W. W. (2010). Network-level structural covariance in the developing brain. *Proceedings of the National Academy of Sciences of the United States of America*, 107(42):18191–18196.
- Zielinski, B. A., Prigge, M. B. D., Nielsen, J. A., Froehlich, A. L., Abildskov, T. J., Anderson, J. S., Fletcher, P. T., Zygmont, K. M., Travers, B. G., Lange, N., Alexander, A. L., Bigler, E. D., and Lainhart, J. E. (2014). Longitudinal changes in cortical thickness in autism and typical development. *Brain*, 137(Pt 6):1799–1812.
- Zilles, K. (2004). *Architecture of the Human Cerebral Cortex: Regional and Laminar Organization*. Elsevier Inc., second edition edition.
- Zucca, I., Milesi, G., Medici, V., Tassi, L., Didato, G., Cardinale, F., Tringali, G., Colombo, N., Bramerio, M., D’Incerti, L., Freri, E., Morbin, M., Fugnanesi, V., Figini, M., Spreafico, R., and Garbelli, R. (2016). Type II focal cortical dysplasia: Ex vivo 7T magnetic resonance imaging abnormalities and histopathological comparisons. *Annals of Neurology*, 79(1):42–58.

Supplementary Material A

Towards In Vivo Focal Cortical Dysplasia Phenotyping Using Quantitative MRI

A.1 Abstract

Focal cortical dysplasias (FCDs)¹ are a range of malformations of cortical development each with specific histopathological features. Conventional radiological assessment of standard structural MRI is useful for the localisation of lesions but is unable to accurately predict the histopathological features. Quantitative MRI offers the possibility to probe tissue biophysical properties in vivo and may bridge the gap between radiological assessment and ex-vivo histology. This review will cover histological, genetic and radiological features of FCD following the ILAE classification and will explain how quantitative voxel- and surface-based techniques can characterise these features. We will provide an overview of the quantitative MRI measures available, their link with biophysical properties and finally the potential application of quantitative MRI to the problem of FCD subtyping. Future research linking quantitative MRI to FCD histological properties should improve clinical protocols, allow better characterisation of lesions in vivo and tailored surgical planning to the individual.

¹published in Adler, Lorio et al., (2017) NeuroImage: Clinical

Introduction

Cortical dysplasias are malformations of brain development that are highly epileptogenic. They are a common cause of drug-resistant focal epilepsy in adults and the most common cause in children, the underlying aetiology in 42% of paediatric epilepsy surgery cases (Harvey et al., 2008). Resective surgery is the most effective treatment to eliminate seizures in drug-resistant focal epilepsy population (Fauser et al., 2004), provided there is a well-characterised epileptic focus.

Focal cortical dysplasia (FCD) encompasses a broad spectrum of histopathological and genetic abnormalities. There have been a number of different classification systems but in 2011 the International League Against Epilepsy (ILAE) developed a three-tiered classification system. According to the ILAE, FCD type I has abnormal radial and/or tangential lamination, FCD type II is also associated with aberrant cytology, specifically dysmorphic neurons, and FCD type III occurs alongside another lesion, e.g. hippocampal sclerosis (Blümcke et al., 2010). From the genetic perspective FCD subtypes are characterised by a complex interplay between many signalling molecules involved mostly, but not exclusively, in the mTOR pathway.

Non-invasive subtype classification is crucial for several clinical reasons. First, the epileptogenicity of FCD is related to the histopathological features (Boonyapisit et al., 2003). Second, surgical planning is significantly improved when lesions are identified on pre-operative MRI (Télez-Zenteno et al., 2010) and variability in outcome is seen according to FCD subtypes, with Type I and type IIA having poorer post-surgical outcomes than type IIB (Hong et al., 2015; Mühlebner et al., 2011). This may be explained by the fact that those subtypes often present more diffuse or subtle lesions, with poorly defined boundaries (Blümcke et al., 2010; Hong et al., 2015). The ability to characterise FCD subtypes *in vivo* is therefore clinically relevant as it is informative of post-surgical seizure freedom as well as providing a mechanism for exploring aetiological risk factors and research into cognitive trajectories within specific aetiological subtypes.

Radiological assessments carried out on conventional structural MRI indicate that subtypes may have differentiating MRI features, i.e. they can be distinguished by combinations of morphological and image intensity

features (Blümcke et al., 2010). However, visual definition of histological features on pre-surgical MRI is challenging and often inconclusive (Kim et al., 2012). Two converging areas of imaging research offer the possibility for more specific quantitative measurements of brain structure. The first is computational anatomy, which we define as the automated extraction of morphological features and statistical analysis of grey and white matter maps from MRI images such as T1- and T2- weighted (respectively T1w and T2w), or FLAIR. These morphological features can then be correlated with histopathological and genetic characteristics. The second area is quantitative MRI, which provides an estimate of the parameters governing the conventional image intensity. Standard structural MRI data, such as T1w and T2w, are able to delineate the brain anatomy but are not specific to tissue property variations. A change in image intensity can be caused by a range of underlying neurobiological processes. Quantitative MRI (qMRI) parameters are specific to tissue structure and biophysical properties at the micrometre scale. These parameters are neuroimaging biomarkers for myelin, water and iron content (Bilgic et al., 2012; Deoni et al., 2015; Schweser et al., 2011), and provide the MRI "fingerprints" (Ma et al., 2013) of brain tissue microstructure (Weiskopf et al., 2013). By linking brain tissue property changes with image intensity, qMRI may assist understanding of the neurobiological mechanisms underlying a change in morphometry.

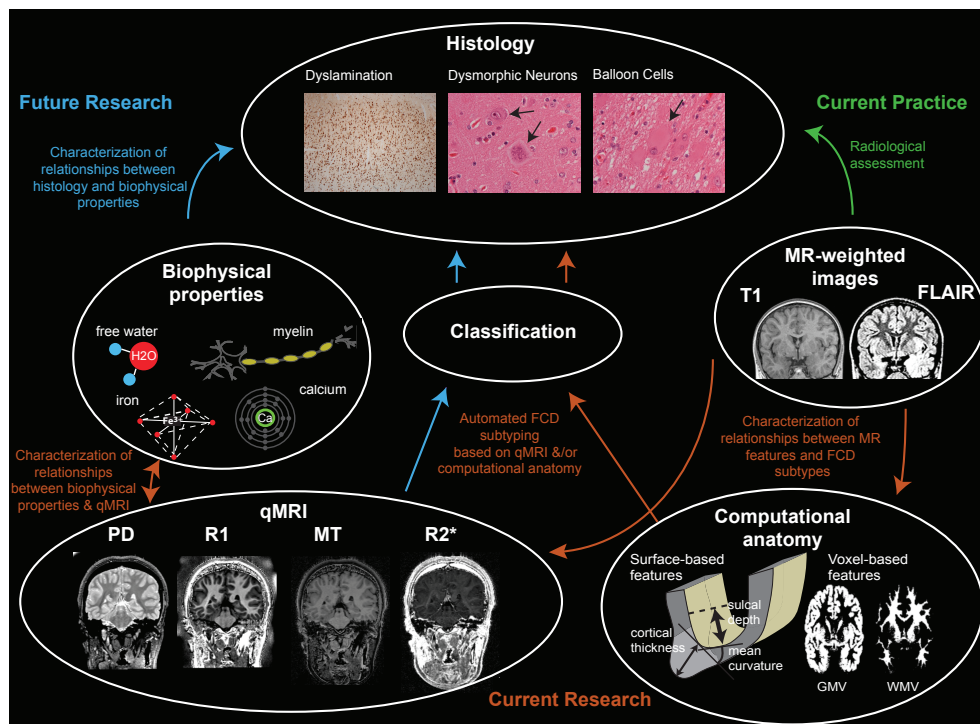
Until recently, qMRI has not been available in a clinical setting due to scan duration and greater complexity in image reconstruction. However, advances in image acquisition now offer the possibility to probe the in vivo tissue microstructure in a clinical setting (Deoni et al., 2015; Weiskopf et al., 2013) with high signal to noise ratio. Furthermore, the increased availability of high field strength (7 Tesla) MRI will enable MRI to be performed at higher resolution and using new contrast mechanisms (Kozlov and Turner, 2010).

Temporal lobe epilepsy is one of the few conditions where qMRI has been routinely used in a clinical setting to differentiate healthy from sclerotic hippocampi as well as to infer histological and connectivity changes in brain areas. T2 mapping has been shown to significantly outperform FLAIR in differentiating sclerotic from healthy hippocampi (Rodionov et al., 2015). Furthermore, histological analysis on resected brain regions has shown that multiple linear regression models using T1

and T2 mapping can accurately predict neuronal loss in hippocampal subfields (Goubran et al., 2015).

The first goal of this review is to report current understanding of histological, genetic and radiological features of FCD lesions. We then investigate the link between those characteristics and the computational anatomy measures reported in the literature. Finally we consider the benefit of using qMRI estimates in the context of FCD subtyping (Figure A.1). Finally, we discuss the need for combinations of computational anatomical features with "in vivo histology" provided by qMRI for non-invasive lesion characterisation.

Fig. A.1 Relationship between histological features, biophysical properties, MR images and quantitative neuroimaging.



Overview of relationship between histological features, biophysical properties, MR images and quantitative neuroimaging. Green arrow indicates current link between MR images and ex vivo histology. Orange arrows indicate areas of current research using computational anatomy based on MR-weighted images for FCD subtyping. Blue arrows indicate future directions to characterise biophysical tissue properties of FCDs using qMRI. qMRI images are sensitive to myelin, iron, calcium and free water content. The qMRI profiles of different FCD subtypes are currently unknown but may offer a technique to probe histology in vivo.

A.2 Histopathology of focal cortical dysplasia

The first detailed descriptions of FCDs were provided by Taylor and colleagues in 1971 (Taylor et al., 1971). The newest classification scheme, provided by the ILAE, has improved inter-observer agreement among expert neuropathologists (Coras et al., 2012). In this review we focus mainly on FCD type I, IIA and IIB (see Table 1).

Table 1. Characteristics of FCD lesion subtypes.

Lesion Subtype	Histology	Genetics	Radiological features
FCD I (A&B)	<p>FCD IA: radial cortical dyslamination (Blumcke et al., 2011)</p> <p>FCD IB: tangential cortical dyslamination (Blumcke et al., 2011)</p>	<ul style="list-style-type: none"> • Variants in DEPDC5 (Baulac et al., 2015) • FCD IB: chromosomal rearrangement in AKT3 (Conti et al., 2015) 	<ul style="list-style-type: none"> • Cortical thinning • Grey/white matter blurring • Signal abnormalities on T1w/T2w imaging • Lobar hypoplasia (Blumcke et al., 2011; Kabat and Król, 2012; Kim et al., 2012; Krsek et al., 2008)
FCD IIA	<p>Dysmorphic neurons (Blumcke et al., 2011)</p>	<ul style="list-style-type: none"> • Variants in NPRL3 (Sim et al., 2016) • Variants in DEPDC5 (Mirzaa et al., 2016) • Variants of TSC2 (Majores et al., 2005) • Mutations of mTOR (Lim et al., 2015; Mirzaa et al., 2016) • Mutation in PI3KCA (Jansen et al., 2015) 	<ul style="list-style-type: none"> • Cortical thickening • Grey/white matter blurring • Signal abnormalities on T1w/T2w imaging • Abnormal gyrification (Kabat and Król, 2012; Krsek et al., 2008)
FCD IIB	<p>Dysmorphic neurons and balloon cells (Blumcke et al., 2011)</p>	<ul style="list-style-type: none"> • Variants of TSC1 (Becker et al., 2002) • Mutations of mTOR (Lim et al., 2015; Mirzaa et al., 2016) • Variant in exon 8 of PTEN (Weiskopf et al., 2013) 	<ul style="list-style-type: none"> • Cortical thickening • Grey/white matter blurring • Signal abnormalities on T1w/T2w imaging • Transmantle sign • Abnormal gyrification (Kim et al., 2012; Mühlebner et al., 2011) (Barkovich et al., 1997)

The table summarises the histological, genetic and radiological features reported to characterise lesion types

FCD Type I

FCD type I is characterised by isolated lesions in the neocortex with radial (type IA) or tangential (type IB) cortical dyslamination, or a mixture of both (type IC).

In FCD type IA the radial cortical dyslamination manifests with prominent microcolumns (Blümcke et al., 2010). A "microcolumn" is defined as at least 8 neurons aligned in a vertical orientation within the cortex (Rakic, 1988). During cortical development, radial units form that consist of cells that originate from progenitor stem cells, share the same birthplace, migrate along the same pathway and reside in the cortex within the same ontogenetic column. The micro-columnar disorganization in FCD type IA is most prominent within layer 3. These lesions are characterised by a thinner neocortex and higher neuronal densities (Mühlebner et al., 2011). Furthermore, the grey- white matter boundary is usually less easily defined due to increased numbers of heterotopic neurons.

In FCD type IB the normal 6-layered composition of the cortex is disrupted. There may be no identifiable layers in the neocortex, or disruptions may be restricted to abnormal layering of layer 2, layer 4, or both (Blümcke et al., 2010).

FCD Type II

In focal cortical dysplasia Type II, in addition to disrupted cortical lamination, there are specific cytologic abnormalities. Both FCD Type IIA and IIB have dysmorphic neurons characterised by increased size, abnormal orientation and abnormal cytoarchitecture with an indistinct border between the grey matter and white matter.

FCD Type IIB is defined by the presence of balloon cells (Blümcke et al., 2010). These cells have large bodies, eosinophilic cytoplasm, which lacks Nissl substance, and have eccentric, sometimes multiple nuclei (Blümcke et al., 2010). They can be located in any layer of the cortex or in the underlying white matter but are frequently found in the subcortical white matter or in superficial cortical layers. The nature of balloon cells is uncertain but a few studies suggest that they are related to progenitor cells (reviewed by Yasin et al. (2010)). Furthermore, they show a defect

in the cellular process of autophagy, which is dependent on overactivity of the serine/threonine kinase, mTOR (Yasin et al., 2013). FCD type IIB lesions also exhibit changes in myelination that are hypothesised to result from aberrant oligodendroglial cell differentiation and reduced neuronal cell densities (Mühlebner et al., 2011).

A.3 Genetics of the focal cortical dysplasias

In recent years, much evidence has cumulated for the common genetic origin of focal epilepsy with FCD (Baulac et al., 2015), with causative pathogenic variants present in the germ line of rare familial cases (see Table 1). An interesting example is the DEPDC5 gene involved both in pathogenesis of a typical genetic epilepsy syndrome (familial focal epilepsy with variable foci - FFEVF) and of FCD (Baulac et al., 2015). DEPDC5 codes for a subunit of GATOR1 complex, an upstream regulator of the mTORC1 protein. In addition, pathogenic variants in the DEPDC5 gene have been identified in a case of hemimegalencephaly with the histological pattern of FCD IIA (Mirzaa et al., 2016). Furthermore, a study of familial cases of histologically confirmed FCD IIA identified germ line pathogenic variants in NPRL3 gene, another mTOR regulator (Sim et al., 2016).

The mTOR pathway has generated great interest in the field of genetic research of various malformations of cortical development, FCD being among them. Indeed, the histological pattern of FCD IIB lesions is identical or closely resembles that of cortical tubers in tuberous sclerosis complex (TSC) and hemimegalencephaly (Majores et al., 2005). Therefore, it has been hypothesised that, given their similarities, these lesions might share a common genetic background. Since pathogenic variants in TSC1 and TSC2 genes have long been known to cause TSC, they have also been studied in FCD lesions, and pathogenic variants of TSC1 gene discovered in FCD IIB brain tissue samples (Becker et al., 2002). Furthermore, interesting allelic variants of TSC2 gene have been observed in FCD IIA samples (Majores et al., 2005), contributing to the evidence for involvement of TSC1 and TSC2 genes, both upstream inhibitors of mTOR signalling. In contrast to these findings, no clear causative pathogenic variants were found for either TSC1 or TSC2 genes in brain tissue samples from a different cohort of FCD patients (Gumbinger et al., 2009). Somatic mutations of mTOR gene itself were discovered in FCD IIA (Lim et al.,

A.4 Radiological identifiers of focal cortical dysplasias

2015; Mirzaa et al., 2016) and FCD IIB (Lim et al., 2015) samples.

Located further upstream of the complex PI3K-AKT-MTOR pathway, the AKT3 and PI3KCA genes contribute to mTOR signalling, and these are primarily involved in severe cortical malformations associated with complex megalencephaly and hemimegalencephaly syndromes (Rivière et al., 2012). As previously mentioned, these malformations may share similar histological features with FCD, and we might expect similar genetic background underlying their formation; indeed, a somatic mutation in PI3KCA was detected in an FCD IIA brain tissue sample (Jansen et al., 2015). In addition, somatic missense variant in exon 8 of PTEN was described in an FCD IIB sample (Schick et al., 2006). Furthermore, a chromosomal rearrangement in the region encompassing the AKT3 gene was identified in the brain tissue sample of a dysplastic frontal lobe, showing the histological pattern of FCD IB (Conti et al., 2015).

The aforementioned examples point to the complex interplay between many signalling molecules involved mostly, but not exclusively, in the mTOR pathway. Further study of these molecules and their interactions is warranted if we aim to understand the complex genetic background of formation of FCD. The intriguing possibility is that the interplay between genetic background and the formation of the cortex may provide defining features that can be measured in vivo using qMRI.

A.4 Radiological identifiers of focal cortical dysplasias

On T1w, T2w and FLAIR MRI scans, FCDs of all types often demonstrate abnormal cortical thickness, an indistinct grey-white matter junction, signal abnormalities in the subcortical white matter and grey matter and irregular cortical folding patterns (Bernasconi et al., 2011; Kabat and Król, 2012). Lesion visibility can change with respect to developing myelination in the brain, the so-called "disappearing" lesion, which may be more obvious on a scan of an unmyelinated brain in infancy but become less distinct later in childhood (Eltze et al., 2005).

FCD Type I

MR features that can assist delineation of these often subtle and difficult to discern lesions include cortical thinning, blurring of the grey-white matter boundary and lobar or sublobar hypoplasia which may be accompanied by atrophy of the white matter (Blümcke et al., 2010; Kabat and Król, 2012; Kim et al., 2012; Krsek et al., 2008; Téllez-Zenteno et al., 2010). The cortical thinning may be linked to altered neuronal density in FCD type I (Blümcke et al., 2010). The white matter changes may be visualised by hypointensities on T1w and hyperintensities on T2w imaging. There are no visually identifiable differences between the MR features of type IA and IB. However, the distribution of these two subtypes across the cortex may be different, with type IA more frequently located in the temporal lobe and IB more frequently located in extra-temporal cortex (Kabat and Król, 2012).

FCD Type II

Radiological MRI features include grey-white matter blurring, cortical thickening, white matter hypointensities on T1w and increased signal intensity on T2w, FLAIR images as well as abnormal gyration patterns, often visible as an asymmetric folding pattern (Blümcke et al., 2010).

Radiological features of FCD type IIB are the same as IIA (Kabat and Król, 2012; Krsek et al., 2008). However, FCD type IIB can also demonstrate the distinguishing transmante sign, a T2w hyperintense signal extending from the subcortical white matter to the lateral ventricle, best seen on FLAIR and proton density images (Barkovich et al., 1997). This is the only MRI feature able to accurately differentiate FCD type IIB (Kim et al., 2012; Mühlebner et al., 2011).

Increased T2w signal intensity present in the white matter of FCD IIB has been related to the demyelination found histologically, which is associated with severe fibre loss and altered myelin sheaths, abnormal cells and sometimes edema (Garbelli et al., 2011; Mühlebner et al., 2011; Zucca et al., 2016).

In light of the above, many radiological features are shared by different FCD subtypes (as shown in Table:1), therefore we are currently not able to

reliably distinguish subtypes on the basis of conventional visual analysis. The remainder of this review will focus on quantitative MRI features, and their incorporation into automated classification algorithms.

A.5 Computational Anatomy

Computerised algorithms can automatically estimate different brain features, such as volume, thickness and shape, relying on the image intensity and tissue contrast to determine anatomical boundaries. Both voxel- and surface- based techniques can be used to extract morphometry and intensity measures from T1w, T2w and FLAIR images to quantify FCD lesion attributes (Guerrini et al., 2015). Voxel- based measures include grey matter and white matter density, also referred to as volume (House et al., 2013; Huppertz et al., 2005) while surface-based features include cortical thickness, sulcal depth, curvature, local gyrification index and intensity sampling (Adler et al., 2016; Ahmed et al., 2015; Hong et al., 2015). These techniques quantify whole-brain structural abnormalities and, with statistical analysis, can assess the clinical utility of group-level patterns to classify the FCD subtype. Using a surface-based technique, the cortical thinning characteristic of FCD type I and cortical thickening and decreased cortical folding complexity in FCD type II were quantified (Hong et al., 2016). However, overall there is a dearth of computational anatomy findings differentiating lesion sub-types. This may be explained by the fact that current measures derived from T1w and T2w data are affected by a mix of tissue properties that may have confounding effects on tissue contrast and hence reduce the sensitivity of computational anatomy measures.

A.6 Quantitative MRI (qMRI)

Anatomical variations detected from structural MRI data (e.g. T1w, T2w, FLAIR) might be due to true morphological alterations or can be the results of changes in MRI contrast due to biophysical processes taking place on the microstructural scale (Lorio et al., 2016; Weiskopf et al., 2013). Quantitative MRI provides measures of parameters that can be used as biomarkers of specific tissue properties (Tofts, 2005).

Here we briefly describe the current range of MRI parameters that can be measured in a clinically relevant timescale (see Table 2). This is limited to MRI features available at mm resolution and therefore excludes MR spectroscopy, which can measure brain metabolites directly typically at a cm scale in the human brain.

T1 relaxation time

T1 relaxation time is mainly affected by myelin and water content (Rooney et al., 2007; Stüber et al., 2014; Waehnert et al., 2016). For this reason many studies have used T1 relaxometry to map the in vivo myeloarchitecture of the cerebral cortex at 3T and 7T, highlighting densely myelinated primary and extra-striate visual areas (Lutti et al., 2014). Previous studies showed high similarity between T1 value changes across cortical layers and myelin histological staining in those brain regions (Lutti et al., 2014; Waehnert et al., 2016). This underlies the sensitivity of qMRI to subtle variations in tissue properties, particularly at high field strength, and highlights the possibility to perform the parcellation of the cerebral cortex from in vivo MRI data (Lutti et al., 2014; Waehnert et al., 2016). This is particularly relevant for FCD where normal cortical layering is perturbed. In addition, FCD provides an opportunity to evaluate the correspondence between MRI derived cortical structure measurements with histological data in surgical patients.

Magnetization transfer (MT)

Another MRI parameter relevant for FCD lesion characterisation is magnetization transfer (MT) imaging. MT specifically targets the exchange of magnetization between protons bound to macromolecules and water protons and is thought to be the MRI biomarker most specific to myelin content (Graham and Henkelman, 1999).

Proton density (PD)

Altered amount of tissue water can be measured using proton density (PD), a parameter sensitive to the density of MRI-visible protons, which are mainly present in tissue water (Tofts, 2005). The non-aqueous protons,

such as the ones bound to macromolecules, are MRI invisible and do not contribute to the PD signal (Neeb et al., 2008).

Transverse relaxation time

T_2 ($=1/R_2$) is the transverse relaxation time, which is related to is related to water mobility, iron deposition, myelin and glial cell count (Briellmann et al., 2002). The effective transverse relaxation parameter that describes the signal decay including main magnetic field inhomogeneities is known as T_2^* . T_2 and T_2^* are related by the following equation:

$$\frac{1}{T_2^*} = \frac{1}{T_2'} + \frac{1}{T_2}$$

where T_2' is the additional relaxation related to the presence of inhomogeneities.

T_2^* is sensitive to local magnetic field perturbations caused by the presence of paramagnetic substances such as iron. Previous studies demonstrated high correlation of the effective transverse relaxation rate R_2^* ($=1/T_2^*$) with iron concentration measured in ferritin-rich structures (Langkammer et al., 2010; Yao et al., 2009). However R_2^* is also sensitive to global sources of field perturbations, such as those from air-water interfaces. Those perturbations cause strong signal changes unrelated to microstructure in basal temporal and frontal brain regions.

Phase-based susceptibility MRI

Phase-based susceptibility MRI provides images sensitive to the local microscopic magnetic agents while removing global sources of magnetic field perturbations increasing their potential specificity to microstructural tissue properties. These techniques can distinguish between paramagnetic haemorrhage and diamagnetic calcification (Gupta et al., 2001). Molecular magnetic dipoles (e.g. ferritin core) aligning to the static magnetic field, increase the local susceptibility depending on dipole strength and concentration, while highly myelinated fibres exhibits the lowest susceptibilities in brain (Langkammer et al., 2010; Liu et al., 2011; Yao et al., 2009).

Diffusion MRI

The MRI signal can be sensitised to the microscopic movement of water self-diffusion, that is the random translational motion of water molecules (Johansen-Berg and Behrens, 2013). In tissue, diffusion is hindered by the semipermeable cell membranes, which couple the diffusivity in extra- and intracellular sub-spaces. Over the last 20 years diffusion has been based on a tensor model of unhindered diffusion allowing for the estimation of diffusion parameters such as fractional anisotropy (FA) and mean diffusivity (MD). FA characterises the directional preference (most preferred / least preferred) of water diffusion in tissue. The presence of highly organised fibres and cell proliferation increase FA, as the water molecules move along the fibre direction (Beppu et al., 2003; Johansen-Berg and Behrens, 2013). Whereas axonal directional dispersion, cellular inflammation and demyelination decrease FA, as water molecules tend to move in all directions (Basser and Pierpaoli, 2011; Johansen-Berg and Behrens, 2013; Werring et al., 1999).

MD reflects the average magnitude of molecular displacement by diffusion. It can be seen as an inverse measure of the membrane density. Brain oedema and demyelination increase MD values, whereas cell proliferation and white matter maturation reduce MD (Alexander et al., 2012; Feldman et al., 2010).

Both FA and MD values are affected by fibre crossings and orientation dispersion, ubiquitous brain features, which confound the relation with other patho-physiological phenomena. This hampers the neurobiological interpretation of signal abnormalities, as they can be due to microstructural changes or can be caused by neural circuitry variations resulting in a modified distribution of the neurite orientation.

Recent improvements in data acquisition and new modelling developments enable to disentangle the effects of fibre crossings and orientation dispersion allowing more specific estimation of diffusion parameters (Zhang et al., 2012). Techniques such as neurite orientation dispersion and density Imaging (NODDI) model different microstructural compartments such as intra-cellular, extra-cellular, and CSF environments (Zhang et al., 2012). The intra-cellular volume fraction represents the space within the membrane of neurites. The signal relative to this environment

is further characterised by neurite orientation, a feature distinguishing highly coherently oriented white matter structures, white matter areas with bending and fanning axons, cortical and subcortical grey matter structures composed by sprawling dendritic processes in all directions (Sotiropoulos et al., 2012; Zhang et al., 2012). The extra-cellular volume fraction represents the space around neurites, where glial cells and cell bodies, in grey matter, are present (Zhang et al., 2012). In this space, the signal is characterised with anisotropic Gaussian diffusion model, as the presence of neurites hinders water molecules diffusion (Zhang et al., 2012). The CSF compartment, referring to the space occupied by cerebrospinal fluid, allows to minimize the confounding effect of CSF- contamination, especially in the periventricular white matter regions (Zhang et al., 2012).

Table 2. Summary of the main tissue properties affecting different MR parameters.

Tissue properties/ bio-physical process						
	Myelin	Iron	Calcium	Free water	Inflammation (glial cell proliferation)	Neuronal density
	References	References	References	References	References	References
T1	↓ (Rooney et al., 2007; Stüber et al., 2014; Wachert et al., 2016)	↓ (Stüber et al., 2014)	↓ (Wehrli, 2013)	↑ (Rooney et al., 2007)		
PD	↓ (Neeb et al., 2008)			↑ (Tofts, 2005)		
MT	↑ (Graham and Henkelman, 1999)			↓ (Tofts, 2005)		
R2*	↑ (Tofts, 2005)	↑ (Haacke et al., 2005; Langkammer et al., 2010; Wehrli, 2013; Yao et al., 2009)		↓ (Haacke et al., 2005)		
R2	↑ (Briellmann et al., 2002)	↑ (Whittall et al., 1997)			↓ (Briellmann et al., 2002)	
χ	↓ (Gupta et al., 2001)	↑ al., 2010; Liu et al., 2011; Yao et al., 2009)	↓ (Schweser et al., 2011)			
FA	↑ (Beppu et al., 2003; Johansen-Berg and Behrens, 2013)				↓ (Werring et al., 1999)	
MD	↓ (Alexander et al., 2012)			↑ (Feldman et al., 2010)		
ICVF	↑ (Jespersen et al., 2010)					↑ (Winston et al., 2014)
IVF				↑ (Zhang et al., 2012)		

The symbol ↑ represents the increase of an MR parameter due to the presence of a specific tissue property/ biophysical process; the symbol ↓ stands for an MR parameter decrease. T1: longitudinal relaxation time; PD: proton density; MT: magnetisation transfer; R2*: effective transverse relaxation rate; χ : susceptibility mapping; FA: fractional anisotropy; MD: mean diffusivity; ICVF: intra-cellular volume fraction, IVF: isotropic volume fraction.

Conclusion on qMRI

qMRI parameters are more specific than standard MRI to biophysical tissue properties changes. However multiple microstructural properties can elicit changes in each parameter's values, limiting its specificity. The combination of multiple quantitative parameters offers an approach to investigate and disentangle the contribution of different tissue properties to the MRI signal, allowing a more detailed characterisation of the whole brain using non-invasive techniques ("in vivo histology") (Dinse et al., 2015; Stüber et al., 2014). For this goal to be realised, determining the multivariate relationship between tissue properties and qMRI parameters is an essential step (Mohammadi et al., 2015). FCD offers a unique opportunity for validation by performing these MRI measurements in the human brain with the subsequent analysis of surgically resected tissue (Figure A.1).

A.7 Quantitative MRI in focal cortical dysplasia detection

In FCD, qMRI has been used in lesion detection as well as region of interest (ROI) studies to histologically characterise and subtype lesions. In terms of lesion detection, diffusion tensor imaging shows decreased subcortical fiber connectivity in and around the region affected by FCD (Lee et al., 2004) and reduced intra-cellular volume fraction (ICVF) in the lesion area (Winston et al., 2014). These findings are in agreement with altered diffusion measures performed on histology samples (Vargova et al., 2011). FA and MD are altered in the subcortical white matter subjacent to the FCD as well as beyond the MR-visible abnormality (Widjaja et al., 2009). However, alterations in FA and MD distant from the FCD have also been reported (de la Roque et al., 2005; Eriksson et al., 2001) and thus the general consensus is these features are not specific enough for lesion classification. Furthermore, changes in diffusion measures/markers have been discovered in other malformations of cortical development as well as in epilepsy patients with normal MRI (Eriksson et al., 2001; Rugg-Gunn et al., 2001). However, future work will be required to evaluate whether more specific diffusion measures such as ICVF provide a greater utility for FCD lesion classification.

A.8 Combinations of qMRI and morphometry measures in FCD

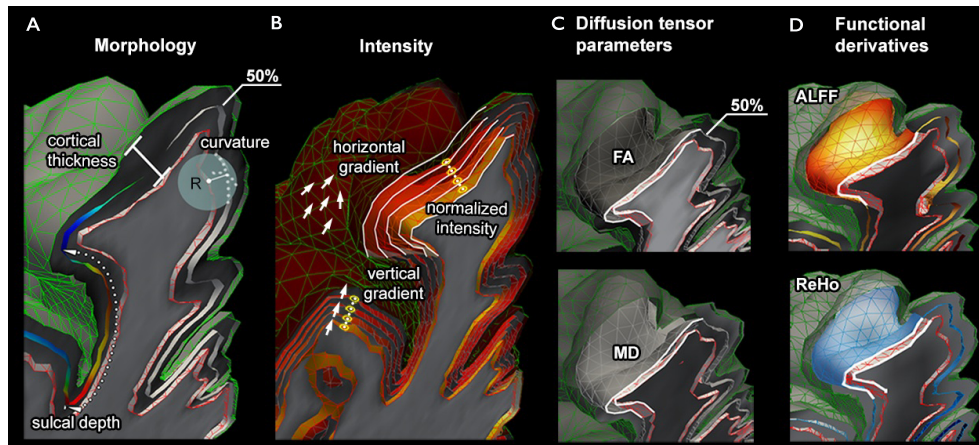
ROI studies have estimated the correlation between histology measures and MRI parameters (Reeves et al., 2015). MT, T1, T2 and T2* values are correlated with myelin alteration in the lesion/perilesional areas. FCD type IIA shows decreased T2 and T2* values with respect to the mean values for normal cortex (Reeves et al., 2015). Overall however, the qMRI signature of FCD subtypes is not yet well defined, mainly due to the lack of quantitative histopathology information as well as incomplete knowledge about the relationship between genetics, histopathology and qMRI parameters (Mühlebner et al., 2011). The existing literature presents data in small patient samples, often limited to a specific diagnosis (i.e. specific subtypes), which increases the chance of bias and hampers generalisation.

A.8 Combinations of qMRI and morphometry measures in FCD

Individual qMRI parameters are unlikely to distinguish subtypes or even detect all FCD lesions, as they are characterised by subtle and overlapping features. As brain structure may be profoundly or subtly affected by the interplay of genetic and histological factors, successful approaches are likely to entail the design of integrated methods to model morphology, intensity and quantitative signals in a multivariate framework.

Hong and colleagues combined quantitative MRI and morphological features in a multivariate analysis using machine learning algorithms (Hong et al., 2015) to classify lesion subtypes (Figure A.2). The study used a surface-based analysis framework for anatomical, diffusion, and functional MRI measures, benefitting from their covariance for improved lesion profiling. Anomalies in type IIB were distributed throughout the cortex and in the subcortical white matter, whereas those in type IIA clustered at the cortico-subcortical interface (Hong et al., 2015). A supervised classifier was reported to predict the FCD subtype with 91% accuracy, exemplifying the ability of combinations of qMRI and computational anatomical metrics to accurately subtype FCD lesions.

Fig. A.2 Computational and quantitative MRI features used by Hong et al.,



A) Morphology features include cortical thickness, curvature and sulcal depth. B) Features include normalized T1 and FLAIR signal intensity sampled at multiple intra- and sub- cortical surfaces, as well as horizontal and vertical intensity gradients. C) Diffusion tensor based features include fractional anisotropy (FA) and mean diffusivity (MD) sampled at 50% cortical depth. D) Resting-state fMRI features include amplitude of local functional fluctuation (ALFF) and regional homogeneity (ReHo). Adapted from "MRI-Based Lesion Profiling of Epileptogenic Cortical Malformations" by Hong et al., 2015. Adapted with permission.

A.9 Conclusions and future directions

The radiological literature regarding FCD subtyping highlights the fact that it is impossible to reliably subtype a lesion based on one MRI feature. However, radiologists are often able to estimate the histopathological subtype with greater than chance accuracy. This suggests that the combination of multiple features may improve accuracy of in vivo classification. Technological advances have shown that it is increasingly possible to map quantitative MRI parameters in clinically feasible scan times. At the same time the correlation between qMRI parameters and tissue microstructure is the subject of intensive investigation. This combined with computational approaches that allow for the comparison of a wide range of imaging features at a local and global level bring the possibility of MRI tissue classification closer to the clinical domain.

FCD is a unique pathology that offers a continuum of tissue organization and distinct changes to neuronal and glial cell types, as well as access to histological classification close to the time point of imaging. Moreover the highly complex structure of the brain is strongly shaped by genetic influences, with several genetic variants underlying differences in

A.9 Conclusions and future directions

lesion subtypes at the individual level (Conti et al., 2015; Jansen et al., 2015; Mirzaa et al., 2016; Sim et al., 2016). On the one hand multivariate analysis of qMRI and computational anatomy seems well placed to characterise FCD lesion type non-invasively while on the other histopathological and genetic analyses of the surgical resections offer the opportunity to validate the sensitivity and specificity of qMRI to tissue properties. The first studies using multivariate analysis for lesion subtyping are now being published. Future studies will need to include multiple quantitative and morphological features in large datasets representative of the entire ILAE classification system. The creation of open source databases of different image modalities and FCD subtypes would facilitate the ability to conduct large-scale studies, create new MR features and test machine learning capabilities. This may open an avenue for new MRI methods to be incorporated into clinical decision making; allowing non-invasive characterisation of the lesion and more individualized surgical planning.

Supplementary Material B

Morphology-corrected metabolic pattern learning: Application to drug-resistant epilepsy

B.1 Abstract

This work presents a fully automated clinical decision support approach based on metabolic neuroimaging data, and evaluates its clinical utility in the assessment of individual patients with drug-resistant focal epilepsy. This framework employs a high-dimensional profiling of neocortical ^{18}F -fluorodeoxyglucose positron emission tomography (FDG-PET) uptake data, sampled along neocortical surface models derived from co-registered magnetic resonance imaging (MRI) data. This approach allows for the mapping of metabolic anomalies in a single patient compared to a reference group, for statistical correction of FDG-PET data by subject-specific variations in cortical morphological parameters, and for the use of surface-based pattern learning for individualized diagnostics. We evaluated our framework in 24 patients with drug-resistant temporal and frontal lobe epilepsy (14 TLE, 10 FLE). Comparing neocortical FDG uptake between both cohorts indicated bilateral temporo-polar and lateral temporal decreases in TLE, whereas FLE patients presented with decreased metabolism in ipsilateral medial prefrontal regions. Findings were reproducible when PET data underwent point-wise correction for variations in morphology. Supervised statistical learning with stratified cross-validation demonstrated high accuracy of FDG-PET data in discriminating between TLE and FLE patients, with morphology-corrected PET outperforming non-corrected PET markers (90% vs 88% accuracy).

This multimodal approach combining cortical metabolism with correction of morphology adequately captures divergent profiles across two common drug-resistant focal epilepsy syndromes, both at the group- and individual-patient level.

B.2 Introduction

Previous studies have suggested clinical utility of ^{18}F -fluorodeoxyglucose positron emission tomography (FDG-PET) in drug-resistant focal epilepsy to unveil metabolic anomalies related to the pathological substrate (Lee and Salamon, 2009; Rathore et al., 2014) and to localize the seizure focus in patients with unremarkable MRI (Carne et al., 2004; Chassoux et al., 2010). Most studies so far have relied on the analysis of FDG-PET in a voxel-based framework, sometimes after the mapping of data to a common stereotaxic space. Recent studies have suggested benefits when data are co-registered to corresponding structural MRI data to guide inter-subject normalization procedures based on anatomical variations (Lerner et al., 2009). Notably, surface-based registration based on patterns of cortical folding improves inter-individual correspondence, while surface-based feature sampling mitigates effects related to partial voluming and morphological variations.

The diagnostic utility of FDG-PET has been mainly assessed visually or via voxel-based analysis. So far, studies have not systematically corrected for morphological confounds, despite the potential of partial volume effects or PET/MRI co-registration errors to disproportionately affect anomalous cortex and sulcal regions. Here, we present a fully automated surface-based metabolic sampling and analysis procedure offering the possibility to correct for cortical thickness. Our approach informed a decision support system for the assessment of drug-resistant epilepsy patients based on supervised pattern learning. We evaluated its utility by assessing how well it would discriminate, at both the group and individual patient level, between two of the most common drug-resistant epilepsy syndromes.

B.3 Materials & Methods

B.3.1 Surface-registration of PET

We linearly co-registered FDG-PET data to corresponding T1-weighted MRI images (Figure B.1). Based on established MRI-based preprocessing applying the Constrained Laplacian Anatomical Segmentation using Proximity algorithm (Kim et al., 2005), we derived geometric models representing the cortical ribbon. FDG-PET voxel values were mapped to vertices of models running at mid-thickness along the cortical mantle using a nearest neighbour interpolation. Data underwent surface-based smoothing using a 20 mm full-width-at-half-maximum Gaussian diffusion kernel, followed by inter-subject registration that aligns individual measurement points based on cortical folding to a hemispheric symmetric surface template (Lyttelton et al., 2007), with folding estimated using the Laplace-Beltrami operator quantifying point-wise deviations from the sphere (Boucher et al., 2009).

B.3.2 Surface-based preprocessing

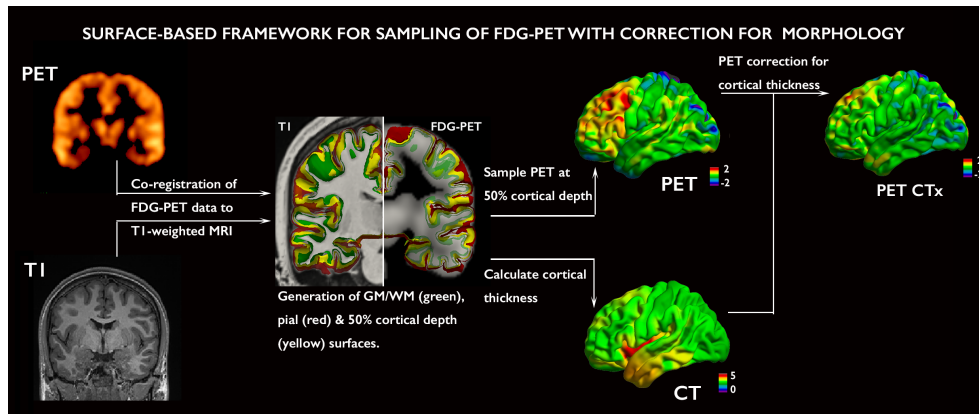
Surface-based PET data were organised as subject specific feature vectors of the size $1 \times k$, with k denoting the number of surface points (henceforth, *vertices*). For a given patient, left/right hemispheric data were sorted relative to the epileptogenic focus (i.e., into ipsi- and contralateral to the focus). In every individual, FDG-PET and thickness data were then normalized using within-subject z-scoring adjusting for overall differences in the mean and standard deviation of cortical PET uptake. Using linear regression, we estimated effects of morphological confounds and control for non-specific markers of age and sex at each cortical measurement point (henceforth, *vertex*).

$$\Psi = \Psi' + \epsilon$$

$$\text{with } \Psi' = \beta_0 + \beta_1 X_1 + \beta_2 X_2 + \beta_3 X_3$$

In the above formula, Ψ represents the vertex-wise PET uptake, β are linear parameter estimates, X_1 is age, X_2 is sex, X_3 is the corresponding cortical thickness measurement and ϵ represents an error term. Normalized PET data can then be estimated for a given subject using: $\Psi_{norm} = \Psi - \Psi'$.

Fig. B.1 Surface sampling of FDG-PET with MRI-informed morphology correction



PET - Positron Emission Tomography; CT - Cortical thickness; PET CTx - Thickness corrected PET.

B.3.3 Group-level statistical inference

Surface-based statistical group analysis was performed using vertex-wise Student's t-tests and Cohen's d effect sizes were computed (Worsley et al., 2009). Surface-based findings were corrected at a family-wise error level of $p_{FWE} < 0.05$, using random field theory for non-isotropic images (Worsley et al., 1999).

B.3.4 Individualised assessment based on supervised learning

Between-group comparisons were complemented by a statistical learning paradigm to automatically diagnose the epilepsy syndrome (i.e., TLE, FLE) in single patients. For feature selection, a vertex-wise t-test between FLE and TLE in the training datasets was performed; this procedure provided a collection of clusters characterising spatial patterns of group-level differences. This data was fed to a support vector machine (SVM) (Cortes and Vapnik, 1995), a supervised statistical learner. In brief, SVM automatically calculates decision boundaries in a high-dimensional feature space based on training data with known label, and particularly considers those training examples that are hard to classify (the so-called support vectors). New data can then be placed into this space and a label is predicted based on the location relative to the hyperplane. Classifier training and performance evaluation was based on stratified 10-fold and 5-fold cross-validations, where the group is subsampled into k subgroups

containing equal numbers of FLE and TLE patients, and one group of patients is classified based on a learner trained on the other cases. The classification was repeated with randomly chosen subgroups 100 times. Permutation testing determined whether classification performance exceeded chance levels through repeated classification with randomly shuffled group labels (TLE, FLE) 1000 times. The percentile position of the actual classifier accuracy (i.e. using the true group labels) within this permutation distribution determined the statistical significance.

B.4 Experiments and Results

B.4.1 Subjects

A consecutive sample of 14 drug-resistant temporal lobe epilepsy (TLE) and 10 frontal lobe epilepsy (FLE) patients referred to the Montreal Neurological Institute (MNI) for presurgical evaluation were studied. All underwent FDG-PET and research-dedicated high-resolution 3T MRI. Demographic and clinical data were obtained through interviews with patients and their relatives. Epilepsy syndrome diagnosis and lateralisation of the seizure focus was determined by a comprehensive evaluation that involved medical history, neurological examination, review of medical records, video-EEG recordings, and clinical MRI. Both patient groups had comparable age, sex, age at seizure, duration of epilepsy, and seizure focus laterality ($P > 0.2$). Most (i.e., 10/14 TLE and 8/10 FLE) patients had been operated at the time of study. Histopathological analysis in all operated TLE patients confirmed the presence of hippocampal sclerosis; all operated FLE patients presented with focal cortical dysplasia type II. All patients showed at least worthwhile seizure outcome after surgery, with 9/18 being completely seizure-free. The local ethics committee approved the study and written informed consent was obtained from all participants.

B.4.2 PET acquisition

Acquisition of ^{18}F FDG scans followed a standard protocol. Subjects were asked to fast for at least 4 hours. Forty-five minutes after injection of 370 MBq of ^{18}F FDG through an arm vein, the patient was placed in the scanner (Siemens HR+, Siemens USA, Knoxville, TN) for a 10-minute

emission acquisition (zoom: 2.5) followed by a 10-minute transmission study using a Germanium-68 line source.

B.4.3 MRI acquisition

MR images were acquired on a 3T Siemens Magnetom TrioTim scanner using a 32-channel head coil. T1-weighted images were acquired using a 3D-MPRAGE sequence (TR=2300 ms, TE=2.98 ms, TI=900 ms, flip angle=9°, FOV=256x256 mm², voxel size=1x1x1 mm³).

B.4.4 PET-MRI processing

a) PET reconstruction and processing. Reconstruction of PET data was carried out based on a filtered back-projection with a Hahn filter with a full-width-at-half-maximum, FWHM, of 6 mm), resulting in approximately 8 mm spatial resolution in the centre of the field of view.

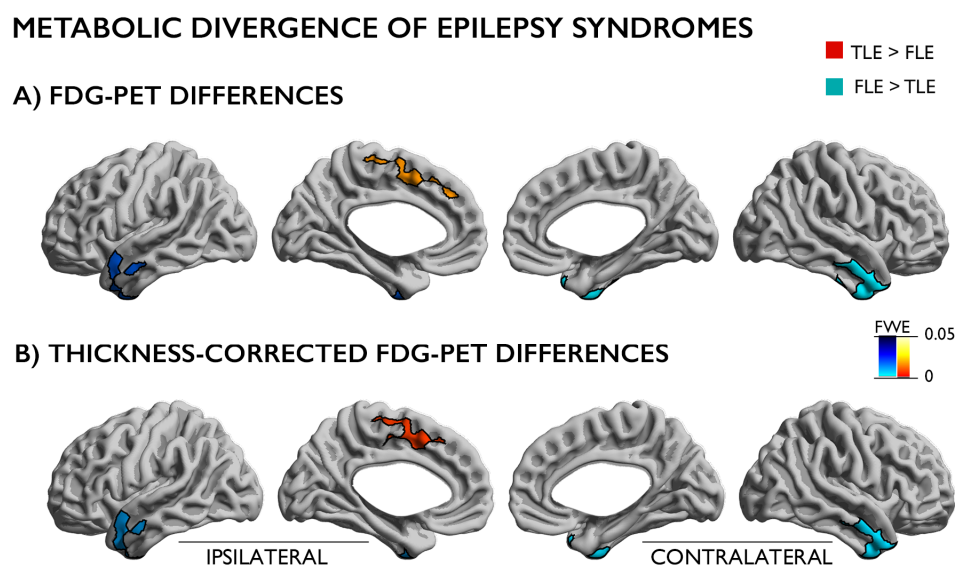
b) MRI processing. Surface representations of the cortical mantle were extracted using automated MRI processing tools developed at the MNI (Kim et al., 2005). In brief, images underwent automated correction for intensity non-uniformity (Sled et al., 1998), intensity standardisation, and linear registration to stereotaxic space based on the hemisphere-symmetric MNI152 template. Stereotaxic images were classified into white matter (WM), grey matter (GM), and cerebro-spinal fluid (CSF). Moreover, they underwent a parallel partial volume classification, which estimates voxel-wise tissue probabilities (Kim et al., 2005; Tohka et al., 2004). The CLASP algorithm (Kim et al., 2005) was applied to generate geometric models of the inner (GM-WM) and outer (GM-CSF) cortical surfaces with 41k vertices per hemisphere. CLASP iteratively warps a triangular mesh to fit the WM-GM boundary. This boundary is expanded along a Laplacian map to model the GM-CSF surface. Cortical thickness was measured as the Euclidean distance between the GM-WM and GM-CSF boundary and this data was smoothed on the tessellated surfaces using a surface-based diffusion kernel with a full-width-at-half-maximum of 20mm. Surface registration (Robbins et al., 2004) aligned individuals based on cortical folding patterns (Lyttelton et al., 2007).

B.5 Results

B.5.1 Group-level results

Comparing cortical surface maps between both epilepsy syndromes demonstrated bilateral temporo-polar and lateral temporal FDG uptake decreases in TLE relative to FLE (pFWE<0.05; $d=2.10$ ipsilateral, $d=2.00$ contralateral; Figure B.2 A). On the other hand, FLE patients showed decreased metabolism in ipsilateral medial prefrontal regions extending to paracentral areas relative to TLE (pFWE<0.05; $d=1.79$; Figure B.2 A). Comparing cortical thickness between both epilepsy cohorts revealed medial frontal thinning in TLE relative to the FLE patients (pFWE<0.05; $d=1.87$). Repeating surface-wide PET comparisons after vertex-wise measures were corrected for corresponding cortical thickness measures yielded virtually identical findings (pFWE<0.05; Figure B.2 B).

Fig. B.2 Metabolic divergence of epilepsy syndromes



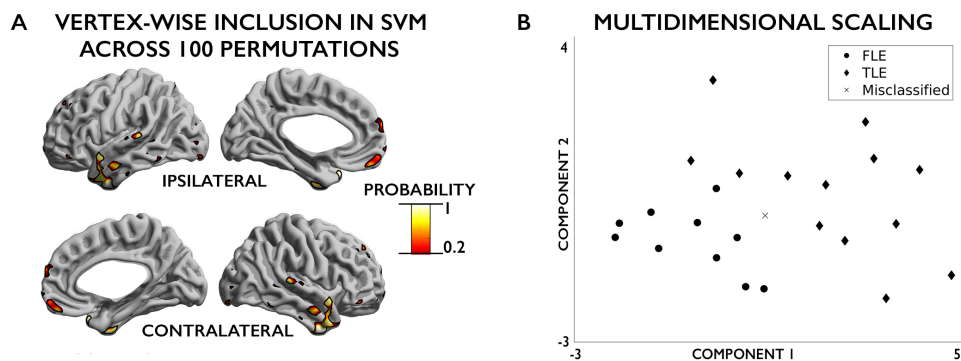
FDG-PET differences (A), and cortical thickness corrected FDG-PET differences (B) between TLE and FLE patients. Findings were corrected for multiple comparisons at a family wise error level (FWE) of 0.05.

B.5.2 Individualised assessments.

The above between-group divergence in cortical metabolism was also seen at the individual patient level (Figure B.3). Indeed, a surface-wide support vector machine trained on cortical FDG-PET maps could discriminate

TLE from FLE patients with high accuracy (mean±SD accuracy=88±6% across 100 10-folds). Performance remained high when using a more conservative cross-validation (84±5% across 100 5-folds). Classification accuracy was better than chance, as indicated by permutation tests, which randomly shuffled the original labels 1000 times and reclassified patients using these 'null' labels (p=0.001, range of permutation-based accuracies=17-87%). A classifier trained on cortical thickness corrected FDG-PET data achieved slightly higher performance (mean±SD accuracy=90±5% across 100 10-folds). Higher performance of morphology-corrected data was also seen when FDG-PET data underwent a prior correction for CSF partial volume effects. Notably, learners trained on PET data or thickness-corrected PET data achieved higher performance than a learner predicting epilepsy syndromes based on cortical thickness alone (mean±SD accuracy=78±6% across 100 10-folds).

Fig. B.3 Individual Classification



A) Feature Selection: probability of vertices being included in SVM based on FDG-PET across 100 permutations. B) Multidimensional scaling (MDS) of selected FDG-PET features in over 90% of permutations, reduced to two components, visualises similarities/dissimilarities between participants. Median accuracy for individual classification is displayed: TLE cases correctly identified = diamond shape; FLE cases correctly identified = circle and misclassified cases = cross.

B.6 Discussion and Conclusion

This work presents a surface-based framework to sample FDG-PET on MRI-derived surfaces, which takes advantage of folding-based inter-subject registration, increased specificity for grey matter signal during feature sampling, and offers the possibility to adjust metabolic data for variations in cortical thickness. This approach was validated in two of the most

common drug-resistant epilepsy syndromes, TLE and FLE. The experiments indicated divergent neocortical metabolic profiles in these patients, with hypometabolism in anterior prefrontal and temporo-limbic areas in TLE and reductions in medial frontal and paracentral areas in FLE.

A supervised classification algorithm based on cortical metabolic profiles achieved high accuracy in discriminating TLE and FLE patients, suggesting that the between-syndrome divergence in neocortical glucose metabolism can also be seen at the level of individual patients. Although accuracy was excellent for both 10- and 5-fold cross-validation schemes, it is of note that the evaluations were based on only a modest patient dataset. To further assess generalisability, future studies in larger cohorts are recommended.

Notably, classifier performance was higher when PET data were used than based on cortical thickness measures, suggesting potentially higher specificity of metabolic patterns than of whole-brain structural alterations. Structural alterations have previously been mapped across several focal epilepsy syndromes, and may not necessarily have spatial correspondence with the putative seizure focus (Bernhardt et al., 2010; Hong et al., 2016). In light of previous studies also showing generally higher degrees of structural changes in patients with long-standing duration of epilepsy (Coan et al., 2009), whole-brain cortical thickness alterations have sometimes been interpreted as being largely reflective of the consequences of drug-resistant epilepsy on whole-brain integrity. Interestingly, small increases in classification performance were observed when correcting the PET data for cortical thickness, possibly related to higher partial volume contamination for thinner areas of cortex.

In sum, this work provides proof-of-concept support that surface-based metabolic pattern learning may offer informative automated decision support in patients with drug-resistant focal epilepsy. In future studies, it will be of interest to evaluate this framework for emerging PET markers as well, including translocator protein imaging that has been shown to be sensitive to inflammatory processes occurring in the proximity of the seizure onset region (Gershen et al., 2015).